# REGULATION OF VASCULAR FUNCTION BY CIRCULATING BLOOD

EDITED BY: Joseph M. Rifkind, Dan E. Berkowitz and Joy G. Mohanty
PUBLISHED IN: Frontiers in Physiology

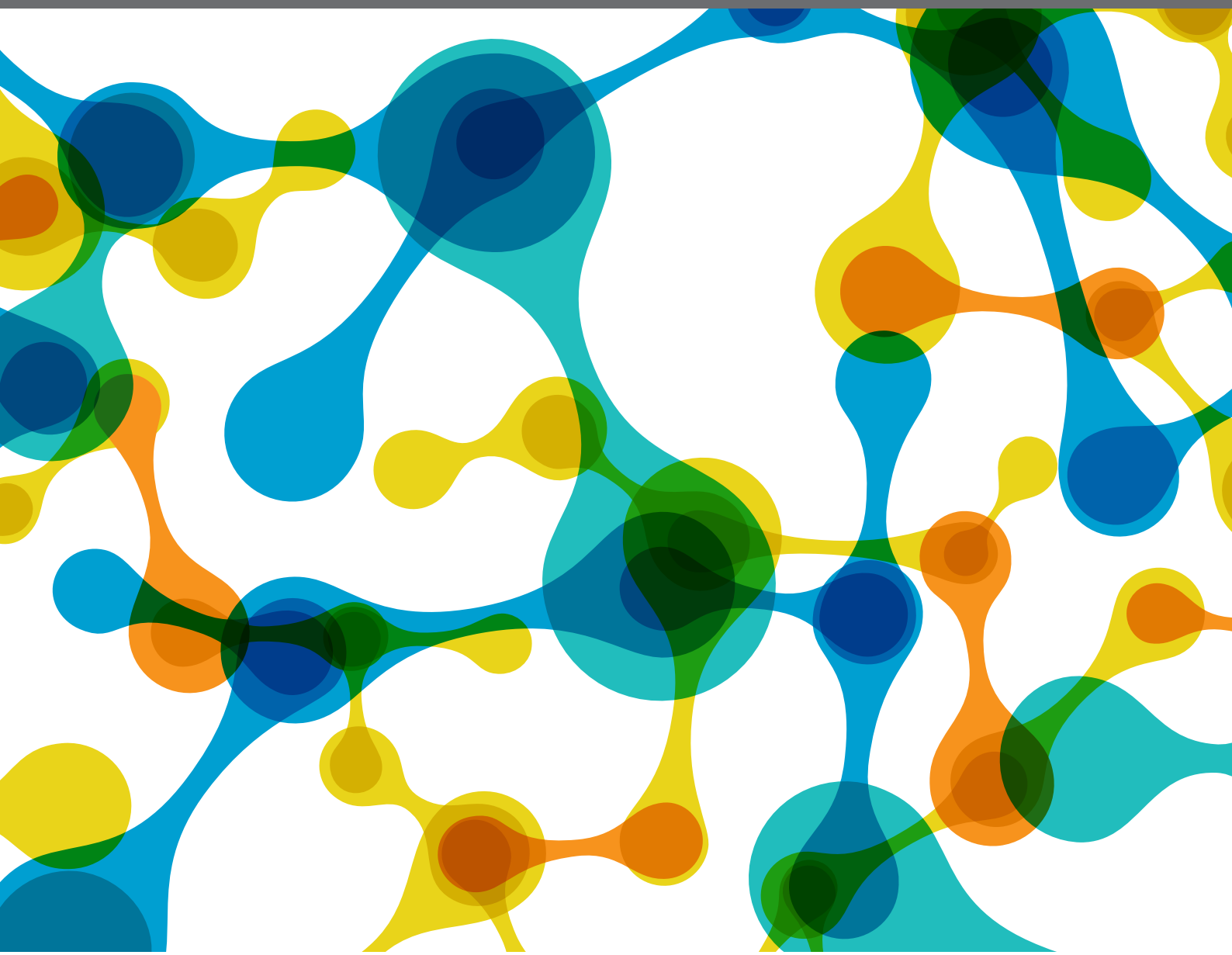

frontiers Research Topics

# frontiers

**Frontiers Copyright Statement**

© Copyright 2007-2019 Frontiers Media SA. All rights reserved.

All content included on this site, such as text, graphics, logos, button icons, images, video/audio clips, downloads, data compilations and software, is the property of or is licensed to Frontiers Media SA ("Frontiers") or its licensees and/or subcontractors. The copyright in the text of individual articles is the property of their respective authors, subject to a license granted to Frontiers.

The compilation of articles constituting this e-book, wherever published, as well as the compilation of all other content on this site, is the exclusive property of Frontiers. For the conditions for downloading and copying of e-books from Frontiers' website, please see the Terms for Website Use. If purchasing Frontiers e-books from other websites or sources, the conditions of the website concerned apply.

Images and graphics not forming part of user-contributed materials may not be downloaded or copied without permission.

Individual articles may be downloaded and reproduced in accordance with the principles of the CC-BY licence subject to any copyright or other notices. They may not be re-sold as an e-book.

As author or other contributor you grant a CC-BY licence to others to reproduce your articles, including any graphics and third-party materials supplied by you, in accordance with the Conditions for Website Use and subject to any copyright notices which you include in connection with your articles and materials.

All copyright, and all rights therein, are protected by national and international copyright laws.

The above represents a summary only. For the full conditions see the Conditions for Authors and the Conditions for Website Use.

ISSN 1664-8714
ISBN 978-2-88945-942-1
DOI 10.3389/978-2-88945-942-1

## About Frontiers

Frontiers is more than just an open-access publisher of scholarly articles: it is a pioneering approach to the world of academia, radically improving the way scholarly research is managed. The grand vision of Frontiers is a world where all people have an equal opportunity to seek, share and generate knowledge. Frontiers provides immediate and permanent online open access to all its publications, but this alone is not enough to realize our grand goals.

## Frontiers Journal Series

The Frontiers Journal Series is a multi-tier and interdisciplinary set of open-access, online journals, promising a paradigm shift from the current review, selection and dissemination processes in academic publishing. All Frontiers journals are driven by researchers for researchers; therefore, they constitute a service to the scholarly community. At the same time, the Frontiers Journal Series operates on a revolutionary invention, the tiered publishing system, initially addressing specific communities of scholars, and gradually climbing up to broader public understanding, thus serving the interests of the lay society, too.

## Dedication to Quality

Each Frontiers article is a landmark of the highest quality, thanks to genuinely collaborative interactions between authors and review editors, who include some of the world's best academicians. Research must be certified by peers before entering a stream of knowledge that may eventually reach the public - and shape society; therefore, Frontiers only applies the most rigorous and unbiased reviews.
Frontiers revolutionizes research publishing by freely delivering the most outstanding research, evaluated with no bias from both the academic and social point of view. By applying the most advanced information technologies, Frontiers is catapulting scholarly publishing into a new generation.

## What are Frontiers Research Topics?

Frontiers Research Topics are very popular trademarks of the Frontiers Journals Series: they are collections of at least ten articles, all centered on a particular subject. With their unique mix of varied contributions from Original Research to Review Articles, Frontiers Research Topics unify the most influential researchers, the latest key findings and historical advances in a hot research area! Find out more on how to host your own Frontiers Research Topic or contribute to one as an author by contacting the Frontiers Editorial Office: researchtopics@frontiersin.org

# REGULATION OF VASCULAR FUNCTION BY CIRCULATING BLOOD

Topic Editors:
**Joseph M. Rifkind,** Johns Hopkins University, United States
**Dan E. Berkowitz,** University of Alabama Birmingham School of Medicine, United States
**Joy G. Mohanty,** National Institute on Aging, United States

**Citation:** Rifkind, J. M., Berkowitz, D. E., Mohanty, J. G., eds. (2019). Regulation of Vascular Function by Circulating Blood. Lausanne: Frontiers Media.
doi: 10.3389/978-2-88945-942-1

# Table of Contents

frontiers in Physiology

EDITORIAL
published: 16 May 2019
doi: 10.3389/fphys.2019.00492

# Editorial: Regulation of Vascular Function by Circulating Blood

*Joseph M. Rifkind*[1]*, *Dan E. Berkowitz*[2] and *Joy G. Mohanty*[3]

[1] Department of Anesthesiology, Johns Hopkins University, Baltimore, MD, United States, [2] Department of Anesthesiology and Perioperative Medicine, University of Alabama Birmingham School of Medicine, Birmingham, AL, United States, [3] Section of Molecular Dynamics, National Institute on Aging, Baltimore, MD, United States

**Keywords: vasculature, endothelial cells, erythrocytes, blood flow, nitric oxide**

## Editorial on the Research Topic

## Regulation of Vascular Function by Circulating Blood

The endothelium, which lines the inner surface of the vasculature, plays a crucial role in vascular function. Endothelial dysfunction results in hypertension, thrombosis, and inflammation that can lead to vascular diseases. Since the endothelium is constantly in contact with the blood and all its components including leukocytes, erythrocytes, and platelets, the flowing blood and the various components of the blood can influence endothelial function. In addition to effects involving individual components of the blood, the flowing blood affects the shear stress that the endothelium experiences, which induce cellular signaling that alters membrane potential and activates kinases. Blood flow, which is essential for the transport of oxygen, carbon dioxide, and other components to and from the tissues involves a cell free layer adjacent to the endothelium in addition to dilatation and constriction which is regulated by interactions with the endothelium. This research topic has investigated the different factors involving the blood, which affect vascular function.

In one study Tripathi et al. discusses autoregulation, which maintains constant blood flow. At low levels of blood pressure, the flow increases when the blood pressure increases. However, above a blood pressure of 70 mmHg autoregulation maintains constant blood flow in peripheral arteries. Three other studies discussed how changes taking place in the vasculature bypass autoregulation that maintains a constant blood flow. In one of these, Chatterjee investigated endothelial mechanotransduction whereby the shear stress and changes in flow patterns are sensed by the endothelium, which results in triggering biochemical signals that alter membrane potential and activate kinases. This process generates oxidant/redox signals that induce inflammation compromising proper vascular function. In a second study, Yalcin et al. discussed the endothelial glycocalyx layer that lines the endothelium. They demonstrated how degradation of the endothelial glycocalyx layer decreased the thickness of the cell free layer, and increased erythrocyte interactions with the vasculature affecting wall shear stress. A third study, Buerk et al. showed how the hypoxic conversion of tissue nitrite into nitric oxide can generate hypoxic vasodilation and improved blood flow. Several other studies (see below) have investigated the generation of NO by erythrocyte nitrite reduction. This study, however, emphasizes the role of the nitrite reduction reaction that occurs in tissues.

The erythrocyte is the dominant component of the blood and is responsible for the transport of oxygen. Several studies investigated how changes in the hemodynamic functionality of erythrocytes affect the interactions of the erythrocytes with the vasculature and how this affects the transport of oxygen through the circulatory system. In one study, Namgung et al. showed how deformability of erythrocytes affect the cell free layer that generally lines the vascular walls facilitating the flow of blood through the microcirculation. It was demonstrated that under physiological conditions RBCs with deformed cells preferentially flow near the vessel wall of small arterioles. In addition, the near wall accumulation of the less deformable cells near the walls of the vessel increases when passing

OPEN ACCESS

***Edited and reviewed by:***
*Gerald A. Meininger,*
*University of Missouri, United States*

***Correspondence:**
*Joseph M. Rifkind*
*jrifkin3@jhmi.edu*

***Specialty section:***
*This article was submitted to Vascular Physiology, a section of the journal Frontiers in Physiology*

***Received:*** *22 October 2018*
***Accepted:*** *08 April 2019*
***Published:*** *16 May 2019*

***Citation:***
*Rifkind JM, Berkowitz DE and Mohanty JG (2019) Editorial: Regulation of Vascular Function by Circulating Blood. Front. Physiol. 10:492. doi: 10.3389/fphys.2019.00492*

by a bifurcation. In a second study, Barshtein et al. investigated transfused blood with impaired hemodynamic functionality. They found that with transfused blood there was a change in skin blood flow and a change in the hemoglobin level indicating that the transfused blood does affect blood flow in the microcirculation.

A number of other studies addressed interactions with the endothelium involving reactions taking place in erythrocytes. In one paper, Helms et al. discussed how the hypoxic vasodilatory effect is at least in part triggered by the release of NO, adenosine triphosphate and S-nitrosothiols from the erythrocyte under hypoxic conditions. They also discussed the effect of cell free hemoglobin generated by cell lysis that scavenges NO leading to vaso-constriction. In a second paper, Rifkind et al. investigated nitric oxide and reactive oxygen species generated by the erythrocyte. They demonstrated that these molecules can be released from the erythrocyte and transferred to the vasculature. Other studies have discussed the erythrocyte production of NO by nitrite reduction and the formation of reactive oxygen species by hemoglobin autoxidation. However, reacting with hemoglobin and antioxidant enzymes in the erythrocyte neutralizes the bulk of these substances. This paper, however, demonstrated that an unusually high affinity of partially oxygenated hemoglobin with band 3 of the erythrocyte membrane, together with a hypoxic enhanced nitrite reduction and hemoglobin autoxidation of this membrane associated partially oxygenated hemoglobin, triggers the release of these substances from the erythrocyte and, under proper conditions, their transfer to the vasculature. In the vasculature, the NO induces a vasodilatory effect and the reactive oxygen species can induce inflammation and other oxidative reactions that impair vasculature function. Namgung et al., as discussed above, showed how altered deformability of the erythrocyte impairs oxygen transport. They, however, did not discuss how erythrocytes with impaired deformability are produced. This is discussed in a third study by Diederich et al. on erythrocyte reactions. This study investigated hypertensive patients and found impaired deformability of erythrocytes and increased reactive oxygen species. They also found that tert-butylhydroperoxide decreased erythrocyte deformability. In addition, they reported that mice deficient in antioxidant/reducing enzymes were affected by tert-butylhydroperoxide to a greater extent than normal mice. They also found that NO did not affect deformability although it did minimize the effect of tert-butylhydroperoxide.

Two additional studies investigated the effects generated by the damage to the erythrocyte. In one paper, Said et al. discussed microparticles formed during erythrocyte maturation and in response to injury. These microparticles promote coagulation, endothelial adhesion, immune modulation and inhibit nitric oxide bioavailability. These changes significantly disturb effective oxygen delivery. In a second paper, Jana et al. investigated the effect of cell free hemoglobin generated during hemolytic episodes in the circulation. The effects were most dramatic for hemoglobins, HbS, and HbE associated with sickle cell disease and beta–thalasemia respectively. These hemoglobins readily undergo oxidation to metHbs as well as ferryl hemoglobin. These proteins damaged the integrity of the endothelial monolayer with a rise in reactive oxygen species, lipid hydroperoxide and increased expression of oxidative stress proteins. In addition, a rise in uncoupled mitochondrial respiration took place.

In reviewing how vascular function is affected by circulating blood, many aspects involving the interactions between the blood and the vasculature were investigated. We started with studies involving autoregulation and how it is generated and maintained. The role of hypoxia in maintaining blood flow by increased generation of NO was also investigated. Since the erythrocyte is responsible for the transport of oxygen, a major part of our review involved the erythrocyte. Several studies investigated hemodynamic functionality under normal conditions and how this can be impaired. In dealing with the erythrocyte, it was also necessary to discuss reactions taking place within the erythrocyte that influence the vasculature as well as effects associated with particles or molecules released from the erythrocyte. These studies provide an important insight into being able to understand the various factors that regulate blood flow and the transport of oxygen and other substances to and from the tissues.

While this review deals with the important role of nitric oxide, the cell free layer and mechanotransduction and how these factors are affected by the erythrocyte, the crucial roles of leukocytes and platelets in affecting vascular function was not addressed. In any future study these need to be addressed.

## AUTHOR CONTRIBUTIONS

JR has written the complete editorial. DB reviewed and approved the manuscript. JM contributed to editing and corrections.

## ACKNOWLEDGMENTS

JR for help in reviewing the manuscript and in the submission. This study was partly sponsored by National Institute on Aging, National Institutes of Health, Baltimore, Maryland, USA.

**Conflict of Interest Statement:** The authors declare that the research was conducted in the absence of any commercial or financial relationships that could be construed as a potential conflict of interest.

*Copyright © 2019 Rifkind, Berkowitz and Mohanty. This is an open-access article distributed under the terms of the Creative Commons Attribution License (CC BY). The use, distribution or reproduction in other forums is permitted, provided the original author(s) and the copyright owner(s) are credited and that the original publication in this journal is cited, in accordance with accepted academic practice. No use, distribution or reproduction is permitted which does not comply with these terms.*

frontiers in Physiology

REVIEW
published: 07 June 2018
doi: 10.3389/fphys.2018.00524

# Endothelial Mechanotransduction, Redox Signaling and the Regulation of Vascular Inflammatory Pathways

*Shampa Chatterjee**

*Department of Physiology, Perelman School of Medicine, Institute for Environmental Medicine, University of Pennsylvania, Philadelphia, PA, United States*

The endothelium that lines the interior of blood vessels is directly exposed to blood flow. The shear stress arising from blood flow is "sensed" by the endothelium and is "transduced" into biochemical signals that eventually control vascular tone and homeostasis. Sensing and transduction of physical forces occur via signaling processes whereby the forces associated with blood flow are *"sensed"* by a mechanotransduction machinery comprising of several endothelial cell elements. Endothelial "*sensing*" involves converting the physical cues into cellular signaling events such as altered membrane potential and activation of kinases, which are "*transmission"* signals that cause oxidant production. Oxidants produced are the "transducers" of the mechanical signals? What is the function of these oxidants/redox signals? Extensive data from various studies indicate that redox signals initiate inflammation signaling pathways which in turn can compromise vascular health. Thus, inflammation, a major response to infection or endotoxins, can also be initiated by the endothelium in response to various flow patterns ranging from aberrant flow to alteration of flow such as cessation or sudden increase in blood flow. Indeed, our work has shown that endothelial mechanotransduction signaling pathways participate in generation of redox signals that affect the oxidant and inflammation status of cells. Our goal in this review article is to summarize the endothelial mechanotransduction pathways that are activated with stop of blood flow and with aberrant flow patterns; in doing so we focus on the complex link between mechanical forces and inflammation on the endothelium. Since this "inflammation susceptible" phenotype is emerging as a trigger for pathologies ranging from atherosclerosis to rejection post-organ transplant, an understanding of the endothelial machinery that triggers these processes is very crucial and timely.

**Keywords: endothelial mechanotransduction, inflammation, redox signals, revascularization, vascular disease**

OPEN ACCESS

***Edited by:***
*Joseph M. Rifkind,*
*Johns Hopkins University,*
*United States*

***Reviewed by:***
*Suowen Xu,*
*University of Rochester, United States*
*Tim Murphy,*
*University of New South Wales,*
*Australia*

***Correspondence:***
*Shampa Chatterjee*
*shampac@pennmedicine.upenn.edu*

***Specialty section:***
*This article was submitted to Vascular Physiology, a section of the journal Frontiers in Physiology*

***Received:*** *23 January 2018*
***Accepted:*** *24 April 2018*
***Published:*** *07 June 2018*

***Citation:***
*Chatterjee S (2018) Endothelial Mechanotransduction, Redox Signaling and the Regulation of Vascular Inflammatory Pathways. Front. Physiol. 9:524. doi: 10.3389/fphys.2018.00524*

## INTRODUCTION

The vascular endothelium serves as an interface between the blood and the tissue. This layer of cells is increasingly recognized as a critical component of vascular health. The endothelial regulation of vasodilation and contraction, of vascular permeability and of inflammation and immune signaling is critical to vascular health which in turn is pivotal to our survival.

Because the endothelial layer lines blood vessels, it can "interact" with the forces arising from the flow of blood (Davies, 2009; Sandoo et al., 2010). Blood flow is associated with tangential shear stress and circumferential wall stretch. In major vessels such as aorta or arteries that are made up of the endothelial lining (intima) and the smooth muscle layer (media and adventitia), the frictional force per unit area from flowing blood, acts on the endothelial cells (ECs) and gives rise to shear stress while the blood pressure exerts a circumferential stretch normal to the vessel wall (Davies, 1993, 1995; Davies et al., 1997). However, microvessels consisting of an endothelial layer only, experience only shear stress. Blood flow in the form of both shear stress and stretch act on the endothelial layer and vessel wall respectively and regulate a number of pathways that participate in maintenance of vascular tone and function. Studies on the effects of shear stress associated with blood flow point to its role on regulating a number of physiological responses (Dewey et al., 1981; Barakat, 1999; Chiu et al., 2007). *In vitro* and *in vivo* studies have shown that these responses range from organization of the vascular tree during the various stages of embryogenesis and development of the fetal circulatory system to adult vascular tone and function (Tardy et al., 1997; Morgan et al., 1998; Topper and Gimbrone, 1999; Matharu et al., 2008). However, disruption of this laminar or regular shear stress (**Figure 1B**) is also a driving factor for the development of several pathologies. These occur when aberrant shear or stop of shear leads to activation of signaling cascades that cause vascular dysfunction, inflammation, and injury.

How does shear stress affect vascular development and function? The answer lies in the endothelium, the layer of cells that are in direct contact with blood flow. Work over the past two decades has demonstrated that the endothelium is equipped with a "sensing" machinery that can "sense" the force associated with blood flow and integrate it across the vasculature in the form of biochemical signals (Chatterjee and Fisher, 2014a,b,b). To date, our knowledge of the "sensing" machinery or mechanosensors is incomplete. Work from several groups including our own (Chien, 2007; Noel et al., 2013) indicate the involvement of several possible candidates that may work separately on in concert. These potential mechanosensors are cell surface and/or cytoplasmic receptors, ion channels, kinases, integrins, and extracellular matrix components (Rizzo et al., 2003; Weinbaum et al., 2003; Ingber, 2006; Wang et al., 2009). Additionally there are multimeric complexes with several mechanosensing moieties that act together to sense alterations in flow (Tzima et al., 2005; Noel et al., 2013). The eventual effect of mechanosensing is a long term adaptive response. In regions of laminar or streamlined blood flow, it maintains vascular tone while in regions where the flow is erratic and turbulent (as shown in **Figure 1A**) it causes onset of inflammation signaling. We found that when blood flow ceases, such as with the presence of a clot, the sudden cessation of shear drives cell proliferation and angiogenesis (Browning et al., 2014).

In this review, we discuss the flow driven mechanosensing pathway and its role in induction and amplification of vascular signaling. In doing so, we focus on the elements of "sensing," and "transduction" that lead to activation of signaling pathways that alter endothelial phenotype (Browning et al., 2014; Chatterjee and Fisher, 2014b; Tao et al., 2016). These pathways that cause production of cellular adhesion molecules (CAMs), pro-inflammatory cytokines as well as activation of pro-inflammatory and angiogenic transcription factors eventually drive endothelial inflammation, vascularization, and remodeling (Browning et al., 2014; Dorland and Huveneers, 2017). Understanding this complex link between mechanical forces of blood flow and inflammation on the endothelium, informs us on the development of pathologies ranging from atherosclerosis to rejection post-organ transplant.

## THE VASCULAR ENDOTHELIUM AS A "SENSOR" OF BLOOD FLOW (SENSING, TRANSDUCTION, TRANSMISSION, RECEPTION, RESPONSE)

The vascular system, a conduit and connector of blood flow across organs, is a network that integrates biochemical and biophysical signals via systemic transport of blood, nutrients and inflammatory, pathogenic moieties across the body. Thus the endothelium that lines the vascular wall serves as an extensive interface where chemical and mechanical stimuli in blood interact directly with a cellular layer and "convey" signals into tissues. In addition, the endothelium is recognized as an initiator and converging site of inflammation, a pivotal event in organ injury. In an adult human, the surface area of the entire endothelium is 3,000 $m^2$ which is equivalent to at least six tennis courts (van Hinsbergh, 2012; Yau et al., 2015). Comprising of one trillion endothelial cells, which weigh more than 100 g, the endothelium can be considered to an extensive and dynamic organ that pervades the entire body. Besides regulating the vasomotor tone, the endothelium controls cellular and nutrient trafficking from the blood into the tissue, maintains homeostasis (i.e., a balance between pro- and anti-coagulant activity of blood and pro-and anti-inflammatory environment in tissues.). To enable its functions, the endothelium must be able to receive "cues" from the local environment in the form of chemotransduction and mechanotransduction. Of note, chemotransduction has been reviewed by us elsewhere (Browning et al., 2012).

At a conceptual level, it is clear that mechanotransduction would involve sensing by the structural components of the cell, its transduction into a biochemical signal, and the effects of this signal on the endothelium and surrounding environment. This is summarized in **Figure 1B** (Chatterjee and Fisher, 2014b) as (a) the **force** of blood flow (b) **sensing** of the force via cellular structures; (c) **transduction** of the force via signaling molecules; (d) **propagation** of the signal and its **reception** by "cellular receptors"; and (e) an eventual physiological **response**.

## SIGNALING WITH FLOW AND ALTERED FLOW (SENSING AND TRANSDUCTION)

The pivotal importance of blood flow in maintenance of vascular health was well recognized as early as the Nineteenth century.

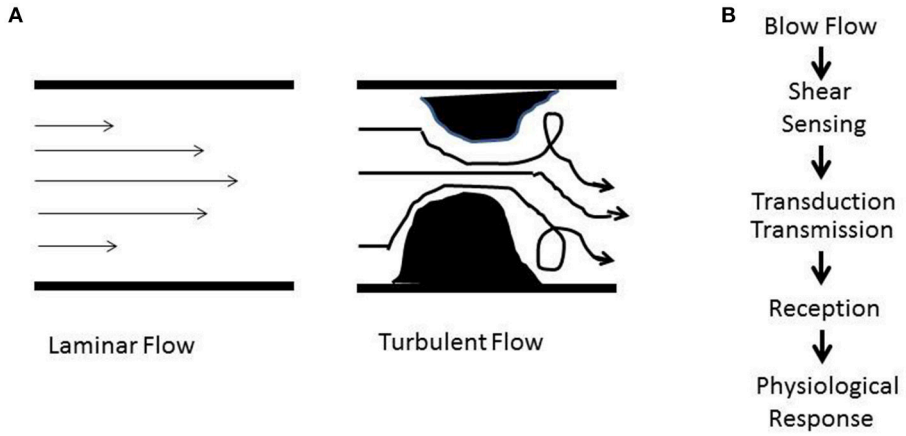


**FIGURE 1 | (A)** Schematic showing patterns of blood flow. The laminar or regular streamlined blood flow is high in the center of the vessel and faces drag or friction along the walls. Obstructive or stasis causes turbulent flow that is characterized by eddies and whirlpools. **(B)** Shear stress induced signaling involves sensing (mechanotransduction), transduction and transmission (ROS, NO), reception (cellular receptors), and physiological response (atherosclerosis, proliferation, angiogenesis, inflammation).

Indeed, Virchow's triad had as its central tenet, three major players that were thought to contribute to thrombosis. These were alteration in blood flow, vascular endothelial injury, and alterations in the constitution of the blood (**Figure 2**; Lowe, 2003). We now know that all these are linked. The normal endothelium under uniform laminar shear stress produces nitric oxide (NO), prostacyclin (PGI2) and tissue plasminogen activator (t-PA) etc., all of which regulate vasoreactivity by controlling the adhesion of platelets, neutrophils etc. (Bagot and Arya, 2008; Aoki et al., 2016). This quiescent endothelial phenotype has been found to change under aberrant flow conditions (Hwang et al., 2003; Johnson et al., 2011). Alterations in shear associated with irregular blood flow such a low shear, eddies, recirculation of flow or by loss of shear can lead to signals that facilitate an activated endothelial phenotype (Hwang et al., 2003) which drives endothelial damage or injury by favoring adhesion of immune cells as well as by infiltration of plasma components such as cholesterol, low density lipoprotein (LDL), and fibrinogen. All these events correlate to increase in blood viscosity. These collective changes can by promoting an atherogenic phenotype eventually lead to thrombosis (Davies, 1995, 2008; Davies et al., 1995).

Thus, the hemodynamics of blood flow, the signaling associated with shear stress as well as the intersection of these signals with risk factors and the effects of underlying genetic control need to be studied for a better understanding of the **blood flow-mechanosignaling-remodeling-disease** paradigm.

At the center of this paradigm is endothelial dysfunction that arises from the loss of equilibrium between pro- and anti-oxidant signaling thereby producing oxidative stress. Oxidative stress or pro-oxidant load arises from redox signals such as reactive oxygen species (ROS) and reactive nitrogen species [RNS such as NO, peroxynitrite (ONOO−), nitrous oxide ($\cdot NO_2$), $N_2O_3$] as well as the activation of pro-inflammatory or pro-angiogenic pathways. Oxidative stress signals triggered by altered

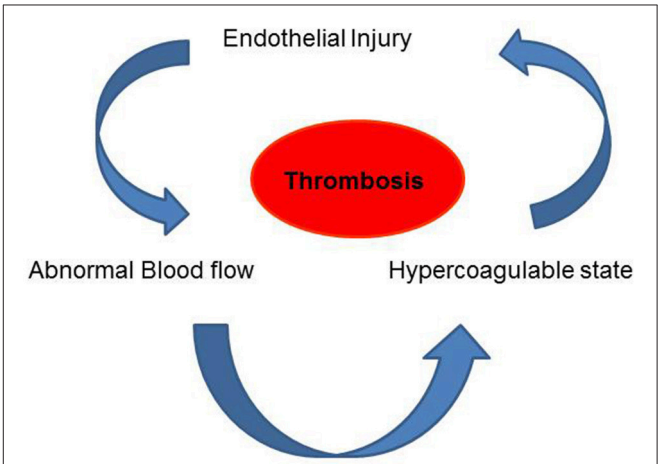


**FIGURE 2 |** Virchow's Triad comprising of blood flow, vascular endothelial injury and the viscosity (constitution) of the blood are the three factors that are thought to contribute to thrombosis.

shear compromise endothelial structure thus driving endothelial dysfunction, the major etiology in diseases of the vasculature (Higashi et al., 2014). In the subsequent sections, we elaborate on the shear signaling initiated with various flow patterns and how these can promote atherosclerosis by either increasing pro-atherogenic or diminishing anti-atherogenic activities (Davies et al., 1995; Dai et al., 2004; Davies, 2008).

The pattern and magnitude of shear stress varies according to the vascular bed and the location of that bed in the vascular tree. In straight vessels, where the flow is laminar i.e., parallel to the vessel, the magnitude of shear stress is directly proportional to the viscosity of blood and inversely proportional to the third power of the (inner) radius of the blood vessel (Equations 1 and 2). Laminar flow maintains vessel function but it is altered flow in the

form of increase, decrease or turbulent/disturbed (recirculating flow or eddies) that leads to signals that drive remodeling and disease.

Shear stress varies according to the vascular bed and species, with magnitude of shear being much higher in mouse vessels as compared to humans (**Table 1**). In arteries, capillaries and veins, the endothelium is exposed to various levels of shear stress ranging from 1 to 70 dyn/cm$^2$. In arteries, shear ranges between 10 and 70 dynes/cm$^2$ while in veins it is ∼1–6 dynes/cm$^2$. Overall in most arteries, shear stress is maintained between 10 and 20 dynes/cm$^2$ (Natarajan et al., 2016).

$$\text{Shear stress in a vessel}\,(\tau) = 4\mu Q/\pi r^3, \qquad (1)$$

**TABLE 1 |** Shear stress in select human blood vessels*.

| Vessel | Shear stress dyn/cm$^2$ |
|---|---|
| Arteries | 10–60 |
| Veins | 1–10 |
| Stenosis in arteries | >100 |
| High Stenosis in arteries | >1,000 |
| Ascending Aorta | 12 |
| Descending Aorta | 5–8 |
| Pulmonary Artery | 5 |
| Small vein | 11 |
| Large vein | 5 |

*Approximate normal values from studies reported by Samet and Lelkes, 1999; Waite and Fine, 2007).

where μ is the blood viscosity, Q the blood flow, π the ratio of the circumference of a circle to its diameter, and r the radius of the blood vessel.

$$\text{Shear Stress in parallel plate chamber}\,(\tau) = 6\mu Q/bh^2 \qquad (2)$$

where μ is the fluid viscosity, Q the blood flow, b is the width of the chamber and h is the distance between plates.

Non-laminar flow implies patterns of disturbed flow that occur at branch points, curvatures of large arteries, and the aortic arch and also with anastomosis/stent insertions as well as surgical manipulations associated with ischemia-reperfusion in procedures such as organ transplantation. These disturbances, in the form of oscillatory flow, retrograde flow and eddies, lead to non-uniform or irregular shear along the vessel wall. At branch points, disturbed flow occurs when high shear stress is impeded thus creating sites of abnormally low and high shear stress (**Figure 3**). This is sensed by the ECs. The resultant signaling causes the activation of a cascade that drives an inflammatory phenotype. This is in the form of a procoagulent surface, production of inflammatory cytokines and cell proliferation. Eventually cell proliferation (of both endothelial and smooth muscle cell) results in remodeling of the blood vessel (Tsao et al., 1996; Dirksen et al., 1998; Nerem et al., 1998; Gimbrone et al., 2000).

Mechanosignaling with shear stress has been well studied using various models of flow *in vitro* and *in situ* (Davies et al., 1995; Albuquerque et al., 2000; Tzima et al., 2005; Chatterjee et al., 2008; Davies, 2008; Rezvan et al., 2011; Chatterjee and Fisher, 2014b). In recent years, *in vivo* models have also been employed to assess the short and long term effects of stop of

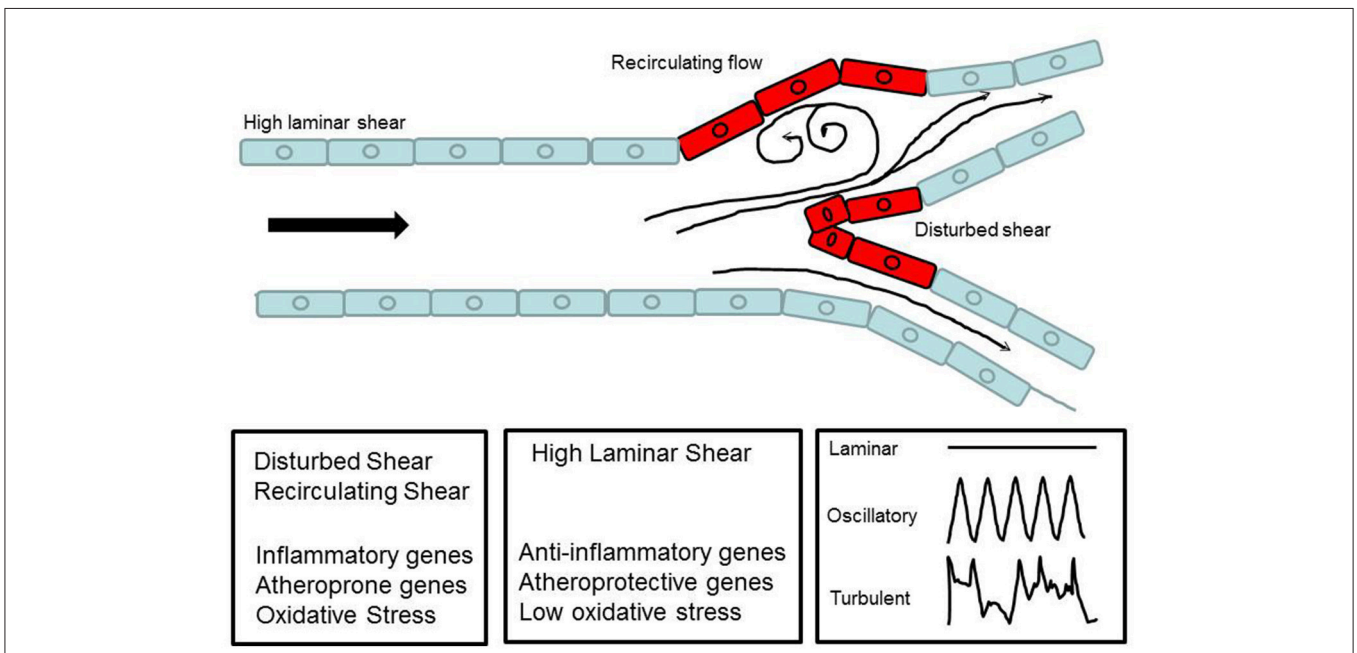


**FIGURE 3 |** Schematic diagram to show laminar flow in a major vessel and disturbed flow at a bifurcation. The diagram illustrates how blood flow forms recirculatory patterns and eddies at the curvatures.

blood flow or disturbed blood flow (Rezvan et al., 2011; Browning et al., 2014). However, most *in vitro* studies have been largely limited to "onset of flow" on ECs in culture. Such models do not accurately represent the *in vivo* state where the ECs are under continuous flow or under turbulent flow. We and others have thus used models with ECs adapted to flow (Chatterjee et al., 2012; Chatterjee and Fisher, 2014b). Yet others have employed models where flow is "stepped up" to create turbulent shear (Kwei et al., 2004). Additionally *in situ* and *in vivo* models have also been employed to evaluate the effects of shear signaling on vascular remodeling and function. Each of these models provides information on shear signaling, but has limitations in that these are confined to representing a particular shear signal, cell type, and vascular bed. Therefore, the findings across all these models need to be integrated in order to inform our knowledge of mechanosignaling. Outlined below are some of the models that have been routinely used in mechanotransduction studies.

## Models of Endothelial Mechanotransduction (Figure 4)

### The Flow Adapted Endothelial Cell (FAEC) as an *in Vitro* Model to Study Mechanotransduction

To monitor the signals activated by altered flow, we devised an *in vitro* flow adapted endothelial cell (FAEC) model whereby cells kept under flow for long periods (24–72 h) were studied (**Figures 4A,B**; Chatterjee et al., 2003, 2006; Tao et al., 2016). We reasoned that adapting ECs to flow for long periods mimics the *in vivo* endothelial bed and stop of flow would closely represent events associated with a blood clot or with organ transplantation (Tao et al., 2016). Our studies have thus evaluated mechanotransduction or mechanosignaling from the point of abrupt stop in shear. Using this *in vitro* stop of flow model, we reported that the earliest event with stop of flow was depolarization of the endothelial cell membrane that occurred due to the closure of a $K_{IR}$ channel (of the 6 family) (Chatterjee et al., 2006, 2012).

### The Isolated Perfused Lung as an *in Situ* Model of Mechanotransduction

Apart from the endothelial layer, the vascular bed is composed of smooth muscle cells and a basement matrix. Thus, mechanosensing events should be investigated in an intact vascular system. For this, our studies to date have used an isolated lung model; use of the intact lung provides a methodological advantage over other organs for "stop of flow" studies, since oxygenation can be maintained via ventilation of lungs (**Figure 4C**). In systemic organs, stop of blood flow would also result in hypoxia and thus mechanosignaling events would be overshadowed by hypoxia signaling. In the lung, stop of flow compromises the mechanical effects of blood flow alone as tissue pO2 values can be kept constant (pO2 *140 mmHg) via ventilation. Indeed there was no decline in ATP levels with stop of blood flow in lungs (Al-Mehdi et al., 1997; Song et al., 2001).

### Onset of Flow Models

Elsewhere, studies on mechanotransduction have used onset of flow models in the form of cone and plate device or parallel plate chambers (**Figure 4D**; Olesen et al., 1988; Franzoni et al., 2016); these studies have reported that the earliest event with onset of flow was endothelial cell membrane hyperpolarization due to the activation or opening of an inwardly rectifying K channel ($K_{IR}$). Although the molecular identity of this channel is not clear, studies seem to indicate that it is a $K_{IR}2.1$ channel (Hoger et al., 2002). Yet others have shown the activation of an outwardly rectifying chloride channel with onset of flow (Gautam et al., 2006).

### Models of Aberrant Flow *in Vitro* and *in Vivo*

Disturbed flow often involves changes in direction of flow (retrograde flow) and *in vitro* models that reproduce these complex flow environments include (a) parallel plate flow chambers with a step at the inlet so as to create eddies downstream of the step (**Figure 4E**; Chiu and Chien, 2011) or with a variation in shear from the entrance (high shear) to the exit (zero shear) (Usami et al., 1993), (b) orbital shakers (Dardik et al., 2005), and (c) cone and plate viscometer. The rotating cone with a small angle creates shear on cells. Underneath the cone there would be an uniform shear field on the cultured cells, while outside the come (with higher centrifugal force) a disturbed flow pattern is created (Spruell and Baker, 2013).

*In vivo* models are

- Ligation and Partial Ligation Model (Rezvan et al., 2011):

  *In vivo* models of turbulent flow involve surgical manipulations in rodents in the form of complete or partial ligating vessels to redirect flow (Korshunov and Berk, 2003; Nam et al., 2009); indeed arteriovenous shunts have been routinely used (Asano et al., 2005). One such model is ligation of the left common carotid artery to increase laminar shear stress in the right carotid artery (**Figure 4F**, left; Alberts-Grill et al., 2012). Another model used by us to mimic stop of flow *in vivo*, is that of complete ligation of the femoral artery (**Figure 4F**, right; Browning et al., 2014).

- Venous Graft Occlusion Model:

  This involves generating an altered shear model in the form of a "high to low shear stress" model by performing an end to end transplantation of the external jugular vein to the common carotid artery (Zou et al., 1998; **Figure 4G**). Such a venous graft model leads to low shear and enhanced intimal thickening (Jiang et al., 2004) and when compared with the contralateral artery (control) is employed to study atherogenesis.

## Signaling With Cessation of Flow

Our group has studied endothelial mechanosignaling from the point of cessation of flow (Chatterjee et al., 2006; Noel et al., 2013). Using both FAECs (adapted to flow at 1–5 dyn/cm$^2$ characteristic of shear in the microvasculature) and isolated lungs, we observed that stop of flow leads to the onset of a signaling cascade, the earliest event of which is the depolarization of the endothelial cell membrane. We observed depolarization by the use of membrane polarity sensitive dyes as well as by measuring membrane currents (patch clamp) (Chatterjee et al., 2006). We discovered that depolarization occurred via a $K_{ATP}$ channel (composed of an inwardly rectifying $K^+$

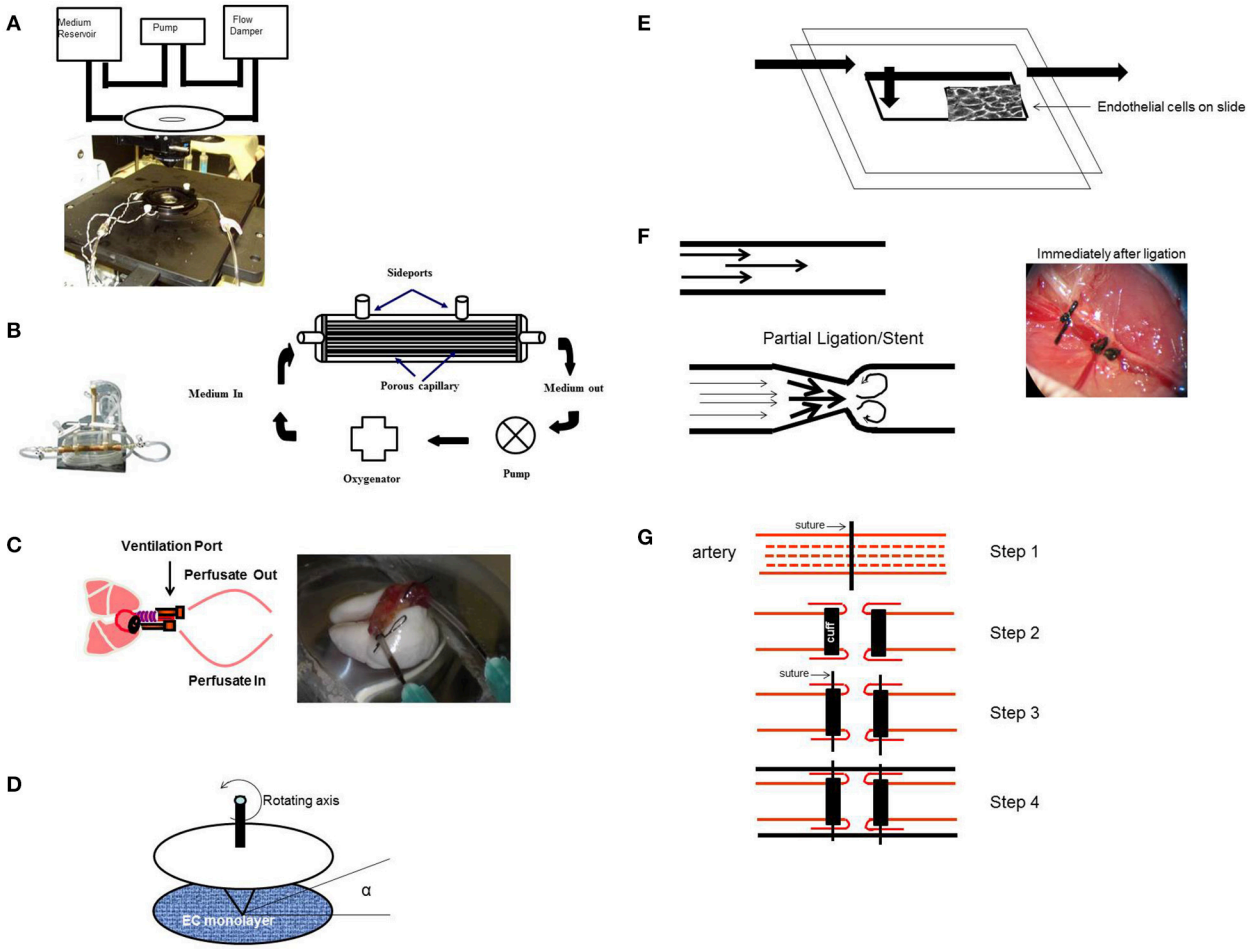


**FIGURE 4 |** Experimental Models (*in vitro* and *in situ*) to study signaling with various patterns of flow. **(A)** *In vitro* flow system (parallel plate chamber) that allows for real time fluorescence microscopy with flow. Endothelial cells grown on coverslips are inserted into the chamber and kept under flow. After 24 h of flow adaptation, various signaling molecules can be monitored by the use of fluorescent dyes (that monitor membrane polarity or ROS production) and real time confocal microscopy. **(B)** Artificial capillary chamber consisting of narrow capillaries (polypropylene) to mimic blood vessels. Endothelial cells seeded into these capillaries and allowed to attach. During this attachment period, cells are fed via perfusion through abluminal ports. For flow adaptation, medium is perfused through luminal ports. **(C)** *In situ* (*ex vivo*) model of altered flow in the lung. Rat or mouse lungs cleared of blood are ventilated and perfused. The lungs are then preperfused with fluorescent dyes, placed on the stage of a microscope, and imaged for ROS, $Ca^{2+}$, or NO, etc. **(D)** Cone-and-plate viscometer recapitulates the blood flow of the arterial system on endothelial cells. **(E)** *In vitro* model of disturbed flow whereby a step at the inlet in a parallel plate chamber can create eddies downstream of the step. **(F)** *In vivo* model of disturbed flow (partial ligation) or stop of flow (ligation) of arteries. Left: ligation or stents would lead to recirculation and eddies. Right: Complete ligation of femoral artery leads to stop of flow as would occur with a clot or thrombus. **(G)** Schema of a bypass graft. First (Step 1) the vessel is sutured and then dissected (Step 2) and cuffs are placed at the end, and segment of the vessel turned outwards to cover the cuff (Step 2). The cuff was kept in place with a suture (Step 3). Finally a vessel segment (vena cava vein) was grafted over the ends (Step 4). The larger diameter of the engrafted vein as compared to that of the smaller vessel, results in lowering of the shear stress in the engrafted vein. Lowered shear can facilitate an atherogenic phenotype [parts of this figure were originally published in Chatterjee et al. (2014), no permission required].

channel of 6 family) that closed in response abrupt cessation of flow. The closure-depolarization event led to activation of a PI3Kinase-Akt pathway that caused assembly of the subunits of the enzyme NADPH oxidase 2 (NOX2) and subsequent production of ROS (Chatterjee et al., 2012). We also observed that depolarization of the endothelial membrane altered its potential from −80 to −60 mV to about −30 to −20 mV, at which potential there was activation of voltage gated calcium channels (VGCC). VGCC facilitates entry of calcium ions into the ECs leading to activation of endothelial nitric oxide synthase (eNOS) and subsequent NO production (Al-Mehdi et al., 2000; **Figure 5**).

Meanwhile, reaction of ROS with NO (generated by both stop and onset of shear) lead to generation of $ONOO^-$ (Pacher et al., 2007; Golub and Pittman, 2014) which can alter endothelial phenotype by disrupting cellular signaling, as well as by inducing the activation of inflammatory pathways, such as NFκB and the mitogen activated protein kinase (MAPK) p38 MAPK. We showed that stop of shear led to activation of transcription factors NFκB and activator protein 1 (AP-1) (Wei et al., 1999, 2001).

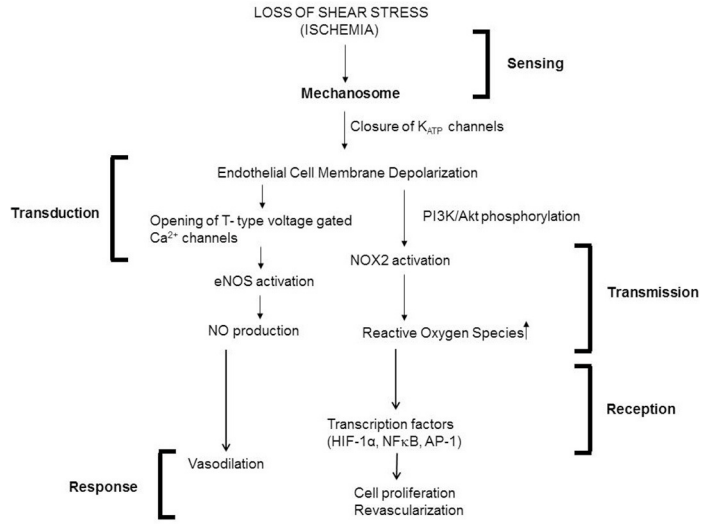


**FIGURE 5 |** Mechanotransduction cascade in pulmonary vascular endothelium with stop of flow following the framework outlined in **Figure 1**. Mechanotransduction by endothelial cells occurs via the mechanosome complex comprising of caveolae-PECAM, VEGFR2 and VE-cadherin resulting in deactivation of KATP channel. This alteration in membrane potential results in activation of NOX2 and eNOS with consequent production of ROS and NO. These mediators result in vasodilation and revascularization probably as a signal to restore the stopped flow (originally published in Chatterjee and Fisher, 2014b, no permission required).

## Signaling With Onset of Flow

Studies on endothelial mechanotransduction from the point of "onset of flow" also showed that the earliest event with start of flow was altered endothelial membrane potential in the form of hyperpolarization. This reportedly occurred via the opening of inwardly rectifying K channels of the 2.1 family (Olesen et al., 1988; Hoger et al., 2002). In other reports, the labs of Martin Schwartz and Eleni Tzima showed that exposing ECs to flow led to the activation of a mechanosensory complex comprising of the platelet endothelial cell adhesion molecule-1/vascular endothelial cadherin/vascular endothelial growth factor receptor 2 (Tzima et al., 2005). This led to conformational activation of integrins which (outside-in integrin activation) activates the transcription factor NFκB via focal adhesion kinase (FAK) dependent phosphorylation. Other reports have shown that similar to stop of flow, ROS is also produced with onset of flow. ROS is well established to activate NFκB via degradation of IκB (Gloire et al., 2006). In general, activation of NFκB facilitates inflammatory activation of the endothelium. With onset of flow both ROS and FAK signaling contributes to NFκB activation (Tzima et al., 2002).

However long term exposure of ECs to laminar flow eventually inhibits the NFκB as well as MAPK pathways. Shear activates the MAPK7 pathway which downregulates inflammatory entities through induction of the anti-inflammatory transcription factors, Kruppel-like factor 2 (KLF2) (Parmar et al., 2006) or KLF4 (Ohnesorge et al., 2010).

## Signaling With Turbulent/Aberrant Flow

Turbulent and disturbed flow occurs in the form of recirculation eddies as well as retrograde or reverse flow at branchings of vessels and at inner curvatures of the aortic arch. In these regions, the endothelium experiences a different magnitude and direction in the flow pattern. Here too endothelial mechanosignaling via shear sensing machinery leads to "activation" of the ECs in the form of generation of redox signals (such as ROS and NO) and activation of pro-inflammatory transcription factors (Davies, 2009). Indeed Passerini et al. (2003) showed that in ECs adapted to flow, reverse flow of low magnitude elevated the expression of inflammatory moieties such as transforming growth factor–beta (TGF-β) and platelet derived growth factor PDGF-B but reduced the production of NO. In porcine arteries, both NO and ROS were found to be produced as a directional response to shear stress; with superoxide production decreasing NO availability during reversed flow (Godbole et al., 2009).

Pro-inflammatory transcription factors such as NFκB and AP-1 lead to high expression of inflammation moieties such as CAMs, monocyte chemotactic protein-1 or MCP-1 (that facilitates monocyte recruitment, adherence, and infiltration into the endothelial layer) (Hsiai et al., 2001, 2003) and growth factors such as vascular endothelial growth factor (VEGF) as well as platelet derived growth factors (PDGF) that increase endothelial proliferation and migration. Studies from the Davies group have shown that disturbed and laminar flow patterns result in different responses on ECs (Davies et al., 1997; Davies, 2008). This leads to preferential localization of atherosclerotic lesions at arterial branches and curvatures while the straight parts of the arterial tree are spared (Davies et al., 2010). However, it needs to be noted that development of atherosclerotic lesions depends of the prevalence of other risk factors in addition to the patterns of blood flow. For instance, in normal adult pigs, regions of turbulent flow show the expression of both atherosclerosis-susceptible (proinflammatory, procoagulant) and atherosclerosis-protective (antioxidant and

anticoagulative) genes (Davies, 2009). Thus although disturbed flow characteristics can predict the possibility of atherosclerosis, the presence of protective genes as well as the absence of risk factors may keep this in check.

Overall, signaling with shear (laminar, turbulent, cessation of shear) involves the activation of several moieties including NFκB, AP-1, MAPK, TGF-β pathways etc. Their (often) paradoxical roles in inflammation, endothelial dysfunction and protection arise due to orchestration and cross talk between various pathways and their intersection with redox signaling molecules on the endothelium. These determine the eventual long term response in the form of inflammation, remodeling, atherosclerosis or maintenance of vascular tone, and vasodilatation.

## The Mechanosensing Machinery in Cells and Tissues

### Tensegrity

The cell as a tensegrity structure: According to this theory the cell with its membrane and cytosolic components acts as a single integrated structure which senses physical forces through tensegrity (tensional-integrity). The load bearing cytoskeletal elements conveys the mechanical stress into the cytoplasm and nucleus (Ingber, 2006). The major cytoskeletal elements in the cell are the actin-myosin machinery which forms filaments, microfilaments microtubules and intermediate filaments. Studies have shown that the cellular response to mechanical stress applied to the cell surface depends on the connectivity or integration of the cell membrane to other cellular structures such as actin, microfilaments, microtubules, and intermediate filaments (Ingber, 2008). The actin filaments associate with myosin filaments, and a mechanical tension is generated that can be distributed throughout the cell as well as to the external extracellular matrix (Ingber, 1993).

### Cytoskeleton

The cytoskeleton is composed of three major types of protein filaments; microtubules, microfilaments and intermediate filaments. This scaffold can "sense" deformation at the cell surface and transmit it as a tension via focal adhesion sites, integrins, cellular junctions, and extracellular matrix (Davies, 2009). These tensional forces are transmitted to other parts of the cell or to the extracellular matrix and other cells.

### Glycocalyx

Shear signaling is also initiated by the direct action of shear on structures on the apical membrane of the endothelium. One such structure is the endothelial glycocalyx, a fibrous net of carbohydrates that protrudes and covers the endothelial membrane. The glycocalyx is composed of heparan sulfate (HS), chondroitin sulfate (CS), and hyaluronic acid (HA). Mechanosensing by glycocalyx occurs via flow-induced tension acting on HS and CS. The biochemical signal triggered is then distributed by the cytoskeletal elements throughout the cell (Fu and Tarbell, 2013).

### Integrins

Integrins are receptors that span across membranes and link cytoskeletal proteins with the endothelial matrix. Shear stress may be transferred by the cytoskeleton to integrins that distribute the force via actin microfilaments, microtubules, and intermediate filaments. This reorganization occurs via activation of focal adhesion kinase and c-Src kinases. The integrin αVβ3 has been reported to be flow sensitive and pretreatment with anti-αVβ3 antibody shows decreased shear induced signaling (Jalali et al., 2001).

### Ion Channels

One of the fastest endothelial responses to shear is activation of flow-sensitive ion channels. Some of these ion channels are candidate flow sensors. Inward rectifying K+ channel (Olesen et al., 1988) and outward rectifying Cl-channel (Barakat et al., 1999) have been reported to be activated by onset of flow. We reported on ATP-sensitive K+ channel (Chatterjee et al., 2006). We observed that this channel was responsive to removal of shear, i.e., it was deactivated by flow cessation. Other mechanosensitive channels ion channels are members of the TRP (Transient Receptor Potential) family such as TRPC1/TRPC3/TRPC6 and TRPV4. Mechanosensing TRPV4 channel facilitates the regulation of vascular growth in tumor ECs (Adapala et al., 2016). Besides conventional ion channels, another family of mechanosensitive ion channels are the Piezo channels, described in the following section.

### Piezo

Piezo channels made up of Piezo proteins 1 and 2 are distinctly different from other mechanosensitive ion channels in that their structure is rather complex and their activation/inactivation kinetics are much more rapid than conventional ion channels. They also transduce very broad and varied kinds of mechanical inputs (Wu et al., 2017). Piezo 1 and 2 which act as mechanotransducers in mammalian cells are extremely large transmembrane proteins (35–40 transmembrane domains) that participate not merely in flow sensing but also in sensory perception, such as pain, touch, hearing etc. (Bagriantsev et al., 2014). Upon mechanical activation, Piezo currents are activated, but they desensitize rapidly as well. In ECs, Piezo1 currents have been reportedly to be activated with flow. In statically cultured ECs, Piezo are localized throughout the cell but under flow, they accumulate along the apical surface and seem to drive endothelial alignment in the direction of flow (Li et al., 2014).

### Platelet-Endothelial Cell Adhesion Molecule (PECAM-1)

PECAM-1 is an adhesion molecule that is expressed along the cell-cell junctions of ECs. It is bound to several other structural moieties, viz integrin αvβ3, vascular endothelial growth factor receptor 2 (VEGFR2) (Tzima et al., 2005). Our work showed that PECAM-1 along with caveolin forms a mechanosensory complex (Noel et al., 2013). Elsewhere PECAM-1 has been reported to form a complex with the tyrosine-specific phospho-transferase Fyn (Chiu et al., 2008). A multimeric complex composed of PECAM-1, vascular endothelial growth factor receptor 2

(VEGFR2), and vascular endothelial cadherin (VE-cadherin) was sufficient to confer responsiveness to shear stress in cells (Tzima et al., 2005). PECAM-1 null mice showed an impaired response to reduction of shear stress in an *in vivo* model of reduced shear achieved by partial carotid artery ligation (Chen and Tzima, 2009; Chen et al., 2010). Isolated lungs from PECAM null mice showed a marked reduction in mechanosignaling (as evidenced by reduced ROS production) with stop of flow compared to wild type (Noel et al., 2013). These observations provide strong evidence for an important role of PECAM in the response of ECs to altered shear stress.

### Caveolae

Caveolae, lipid rich invaginations on the endothelial cell surface, are reported to sense or transduce hemodynamic changes into biochemical signals that regulate vascular function. Caveolin-1, the major coat protein of caveolae, has been reported to show increased expression with increased shear and lack of caveolin-1 affects remodeling with altered blood flow (Yu et al., 2006). Our studies on stop of flow show markedly decreased mechanosignaling in ECs and intact lungs depleted of caveolae by genetic engineering (Noel et al., 2013). It is not clear how caveolae act as mechanosensors but it may be functionally linked to other mechanosensing molecules. We have shown recently that PECAM-1 is co-localized with caveolae as part of the mechanosensing machinery (Noel et al., 2013; Chatterjee and Fisher, 2014b).

### The Mechanosome

The mechanosome (a term that has been previously applied to stress signaling in bone) can be defined as a network of mechanosensors and transducers. Based on our earlier work, we posit that several mechanosensors on the endothelial cell membrane work as a mechanosome, i.e., caveolae, platelet endothelial cell adhesion molecule (PECAM), vascular endothelial growth factor receptor 2 (VEGFR2), vascular endothelial (VE)-cadherin and possibly other elements can sense and transduce shear signaling (Noel et al., 2013; Chatterjee and Fisher, 2014a).

## TRANSCRIPTIONAL REGULATORS OF ENDOTHELIAL MECHANOTRANSDUCTION

Shear stress activates several transcription factors (known as flow-regulated transcriptional factors) that in turn change the expression of a number of genes; the resultant changes in proteins affect endothelial responses, structure and function. Among flow regulated transcriptions factors are those of the Kruppel-like factor family, (KLF2 and KLF4), YAP (an effector of the Hippo signaling pathway), and NFκB (Hamik et al., 2007; Wang et al., 2016). Laminar blood flow which is well established to be atheroprotective and anti-inflammatory is found to induce the expression of KLF2 and KLF4 (Nayak et al., 2011). Once expressed, KLF2 causes increase in eNOS expression, and reduces endothelial permeability. KLF2 and 4 also reduce expression of inflammatory proteins on the endothelium. YAP is also regulated by the mechanical stimuli of shear stress; the resultant tension on the cytoskeletal components facilitates the translocation of YAP between the cytoplasm and nucleus. While unidirectional laminar flow causes nuclear translocation of YAP in a transient manner, disturbed or oscillatory flow facilitates nuclear translocation in a more sustained manner (Wang et al., 2016).

## REDOX SIGNALING IN THE VASCULATURE (ROS, NO) WITH MECHANOTRANSDUCTION

As we have described in an earlier section (**Figure 1B**), the first step in mechanotransduction is "sensing" of shear that occurs via the "mechanosensing machinery." The next step is the transduction and transmission of this signal. Transduction has been reported by us and others (Chatterjee et al., 2012), to occur via kinases and other intermediates and leads to activation of a redox signal.

What are the redox signals generated by the endothelium with altered shear stress? Our work to date shows that stop of flow induced endothelial membrane depolarization is the trigger for activation of a PI3Kinase-Akt pathway. This pathway leads to the assembly of NADPH oxidase 2 and eventual ROS production (**Figure 5**). Elsewhere studies have shown that onset of flow induces endothelial membrane hyperpolarization that presumably causes ROS production, although the exact link has not been explored. We observed that depolarization of the endothelial membrane also led to activation of voltage gated calcium channels (VGCC). These channels that are expressed in ECs *in situ* (Gilbert et al., 2017) are lost when ECs are cultured for several passages. However, keeping cells under flow restored the channel expression (Wei et al., 2004). Our work shows that VGCC facilitates entry of calcium ions into the ECs leading to activation of endothelial nitric oxide synthase (eNOS) and subsequent NO production (Wei et al., 1999; Song et al., 2001; **Figure 5**). NO production has also reported with onset of flow (via transient increase of intracellular calcium; Davis et al., 2001; Sriram et al., 2016). Thus both ROS and NO is also released by the endothelium in response to both onset and cessation of shear stress (blood flow; McAllister and Frangos, 1999; Song et al., 2001).

The predominant source of ROS in the endothelium is NADPH oxidase (NOX). NOX has 7 isoforms (comprising of members NOX1-5 and Duox 1, 2) with NOX2 and 4 (and NOX1 primarily in smooth muscle cells underlying the endothelium) as the most abundant NOX in the vasculature (Pendyala et al., 2009). Work from several groups including ours has shown that NOX2 is localized in caveolar structures that "sense" shear as part of the mechanosome complex; this sensing facilitates NOX2 activation and ROS production (Rizzo et al., 2003; Yang and Rizzo, 2007; Noel et al., 2013).

ROS is a major signaling molecule that "transmits" the mechanosignal of shear stress into a biochemical response. ROS generated by the endothelium is in the form of superoxide ($O_2^{-\cdot}$) and, hydrogen peroxide ($H_2O_2$) which in turn gets converted

to more potent oxidizing species such as hydroxyl radicals and hypochlorous acid (HOCl). The endothelium expresses both NADPH oxidase 2 (NOX2) and 4 (NOX4) which upon activation lead to the production of $O_2^{-\cdot}$ and $H_2O_2$, respectively. $O_2^{-\cdot}$ from NOX2 is produced in response to stop of shear (Chatterjee et al., 2010) but it is generated extracellularly (i.e., outside the endothelial cell membrane); it eventually dismutates to $H_2O_2$, but some of the superoxide directly enters the cells via anion channels (chloride channel 3) (Hawkins et al., 2007). This induces mitochondrial $O_2^{-\cdot}$ generation which plays a role in activating the inflammasome pathway for onset and amplification of inflammation (Rimessi et al., 2016).

NOX4, that generates $H_2O_2$, has been reported to have a protective function. Indeed several studies have shown that mice lacking NOX4 had increased inflammation, hypertrophy of the medial layer in the blood vessels and endothelial dysfunction. Overexpression of NOX4 enhances vasodilation and reduces hypertension (Ray et al., 2011; Morawietz, 2018). This arises primarily from the link between NOX4 and hemeoxygenase-1 (HO-1); when NOX4 is disrupted the reduction in HO-1 leads to loss of activity of the transcription factor Nrf2 (as HO-1 regulates Nrf-2 activation; Schröder et al., 2012). Nrf2 is a well-established regulator of cellular protection against oxidative stress; it achieves this via upregulation of anti-oxidant enzymes. Thus, NOX4 induced Nrf2 activation is protective against endothelial dysfunction.

$O_2^{\cdot-}$ (and its dismutated product) $H_2O_2$ also generates the highly reactive hydroxyl ion and radical (OH– and OH•) via the Haber–Weiss reaction. Both OH– and OH• are very strong oxidizing species and cause oxidative damage to membrane proteins and lipids. In the presence of polymorphonuclear neutrophils (PMN), $H_2O_2$, and chloride generate HOCl, a process that is catalyzed by the PMN specific enzyme myeloperoxidase (MPO). MPO reportedly acts as an NO oxidase. The resultant reduction in NO, increases oxidative stress and exacerbates endothelial dysfunction (Korthuis, 2018).

Besides ROS, NO is the other important signaling molecule that participates in "transmission" of the mechanical signal associated with blood flow. In this, the caveolar structures play a pivotal role. NO is produced primarily via activation of the endothelial nitric oxide synthase (eNOS) that localizes in caveolar structures on the cell membrane. eNOS is activated when it dissociates from caveolin-1. This is followed by its phosphorylation at different serine residues and association with calmodulin (a calcium activating protein). Laminar flow activates eNOS by its dissociation from caveolin and phosphorylation (serine 635 and serine1179) (Fulton et al., 1999). eNOS transcription and expression have also been reported to be laminar shear dependent; indeed a transient increase in eNOS mRNA has been reported with onset of flow although this was found to stabilize with long term exposure to shear stress (Davis et al., 2001; Ishibazawa et al., 2011). Low or turbulent shear stress lead to decrease in eNOS phosphorylation and thus reduction in NO in the vasculature (Malek et al., 1999).

ROS and NO are the transmission signals in the mechanotransduction cascade. Indeed, ROS production is linked to NO generation as ROS can act as a sink for NO resulting in the production of peroxynitrite ($ONOO^{-\cdot}$) that causes endothelial damage, dysfunction and the production of pro-inflammatory cytokines, chemokines, and growth factors. Thus elevated levels of ROS lead to low NO bioavailability, as has been reported in ECs exposed to irregular flow. Reduced bioavailability of NO creates a pro-oxidant milieu resulting in increased oxidative stress. NO regulates the vascular environment by inhibiting proinflammatory cytokines, cell adhesion molecules etc. and by facilitating vasodilation to improve blood flow.

ROS produced by the endothelium leads to activation of transcription factors NFκB, AP-1, and hypoxia inducing factor 1α (HIF-1α), as we reported in our studies using "cessation of shear" models (**Figure 5**). These transcription factors regulate several growth and cell differentiation proteins. Among these are VEGF which was reported by us and others to be upregulated by altered shear (Browning et al., 2014). In our model of stop of blood flow achieved by ligation of the femoral artery, ROS was found to induce HIF-1α activation within minutes of stop of flow prior to hypoxia as monitored by reduction of pO2 values. We found that ROS induced increase in VEGF and HIF-1α are responsible for endothelial growth that drives revascularization with stop of flow (Browning et al., 2014).

Overall the endothelium responds to onset of shear in a manner similar to cessation of shear stress; i.e., the signaling pathways are similar and are activated by a change in shear.

## Mechanosensing and the Regulation of Vascular Inflammatory Signaling

Vascular inflammation necessitates the activation of the endothelium so as to facilitate interaction between the circulating immune cells and the endothelium. The endothelial activation, as we have mentioned earlier, is in the form of increased expression of CAMs and selectins, and in the release of pro-inflammatory cytokines interleukin-4 (IL-4) and 13 (IL-13) and chemokines tumor necrosis factor α (TNFα), IL-1 (Davies, 1993, 2008; Davies et al., 1995). These are signals that lead to recruitment and adherence of leukocytes, PMN and other immune cells to the site of injury; indeed close proximity of immune cells to the endothelium is known to be followed by rolling and adhesion to the endothelial layer aided by adhesion molecules, cytokines etc.

Regions of turbulent flow in the vascular tree show upregulation in the expression of CAMs such as ICAM-1 and VCAM-1 in the endothelium. The integrin-CAM complex increases leukocyte-endothelium adhesion and extravasation into the vascular layer, a key step in development of atherosclerosis. Turbulent shear thus plays is a major role on the development of atherosclerosis at certain locations of the vascular tree.

Under certain conditions, ROS can drive onset of inflammation via upregulation of some inflammatory moieties such as intercellular adhesion molecule (ICAM-1), vascular cell adhesion molecule (VCAM-1), and damage associated molecular patterns (DAMPs) as we have reported in the past (Orndorff et al., 2014; Jungraithmayr et al., 2016; Tao et al., 2016). DAMPs are a class of ligands that are expressed and released

in response to a sterile injury presumably via ROS production. Once expressed DAMPs are released into the circulation where they can bind to their respective receptors on the surface of ECs. In the next section, the ROS-inflammation link in the context of endothelial mechanotransduction will be discussed in detail.

## Mechanotransduction and Vascular Disease

Forces associated with shear are a major determinant for regulation of vessel diameter. As mentioned in earlier sections, atherosclerosis, or the formation of plaques and fibrous caps on vessel walls occurs in those regions of the vascular tree where flow patterns are disturbed. Work over the past decade has shown that endothelial mechanotransduction plays a major role in activating atheroprotective or atherogenic genes based on blood flow patterns.

Under physiological conditions, the endothelial cell-cell barrier is well regulated and vascular permeability is tightly controlled by complex junctional structures, namely adherens junctions (AJ), tight junctions (TJ), and gap junctions (GJ) (Radeva and Waschke, 2017). Under various stimuli these junctions change structurally to regulate permeability. With pathological conditions introduced due to various risk factors as well as in regions of turbulent flow, pro-inflammatory signals activate CAMs and alter AJs (Melchior and Frangos, 2010). Long term shear-induced reorganization of the actin cytoskeleton, to which AJs are linked, can also influence the distribution of these junctions and consequently lead to increased permeability. Indeed regions of turbulent flow show a destabilized endothelial barrier which facilitates penetration of leukocytes, T-lymphocytes, and monocytes/macrophages into the endothelial layer and the arterial intima. Thus increased permeability contributes to the pathogenesis of atherosclerotic vascular disease (Daniel and van Buul, 2013).

Junctional structures (AJ, TJ, GJ) as well as junctional proteins such as occludin and VE-cadherin have also been suggested as potential mechanotransducers that sense the blood flow and contribute to the conversion of mechanical forces to the intracellular signaling (Hahn and Shchwartz, 2009). Low shear has been reported to downregulate expression of junctional proteins such as occludin and to promote its phosphorylation (Conklin et al., 2007) which lead to decreased vascular integrity (DeMaio et al., 2001).

ROS and NO produced as a result of mechanotransduction also play a role in regulating endothelial TJ and permeability. ROS induced inflammatory signals drive PMN recruitment; PMN and inflammatory mediators in turn act on the endothelial junctional proteins and TJs to alter barrier function. ECs exposed to ROS have been reported to show an increased permeability that is directly linked to disruption of TJs due to altered phosphorylation state of junctional adhesion molecules (Rodrigues and Granger, 2015).

ROS induced reduction in endothelial barrier function has also been attributed to an alteration in NO bioavailability. However, NO has been reported as both a negative and a positive modulator of endothelial barrier function (Kubes and Granger, 1992). NO can be protective by limiting the PMN-endothelial cell adhesion. Negative modulation is presumably via NO induced S-nitrosylation of eNOS which inhibits its activity. Inhibition of eNOS increases the permeability of endothelial cell monolayers via formation of stress fibers and disruption of junctional proteins (Durán et al., 2010).

## Mechanotransduction and Revascularization

*In vivo* studies of aberrant flow showed vascular remodeling in terms of thickening of the blood vessels or in terms of driving an "inflammatory" phenotype. In contrast to aberrant shear, our studies with stop of flow models revealed increased proliferation of ECs (Browning et al., 2014) which was abrogated by blocking shear induced signaling either by inhibiting depolarization or by blocking ROS production. We also discovered that cell proliferation was linked to angiogenesis and revascularization. This revascularization that rescued the impeded blood flow was abolished in mice that were administered with agents to block mechanosignaling i.e. to block depolarization or ROS production (NOX2 assembly) and in mice with null of $K_{ATP}$ channel or NOX2 genes. Conditional knockouts (endothelial NOX2 expressors on a null background) showed revascularization indicating that endothelial NOX2 was crucial to the mechanosignaling response (Browning et al., 2014). We thus concluded that endothelial mechanosignaling with stop of flow was an attempt by the vasculature to restore impeded flow via angiogenesis and revascularization (Browning et al., 2014).

## Understanding Mechanotransduction With I/R: Implications in Lung Transplant

The transplant scenario, associated with stop and restart of blood flow represents an altered mechanotransduction paradigm. In most systemic organs, transplant would cause (1) alteration in shear stress and (2) altered oxygen delivery to the organ. This "hypoxia-reoxygenation" signaling overshadows the signaling associated with altered mechanotransduction. Hypoxia-reoxygenation is well established to lead to activation of the xanthine-xanthine oxidase pathway and also the mitochondrial respiratory chain and NADPH oxidase pathway. All of these events result in the formation of oxidants and eventual tissue injury.

Unlike systemic organs, the lung does not obtain its oxygen supply from blood flow; rather alveolar oxygen can keep lung cells "oxygenated" even in the absence of blood flow. Similarly reperfusion of the lung does not increase oxygen supply. Thus pulmonary I/R can be considered to represent a mechanosignaling or mechanotransduction paradigm. Our studies on lung I/R demonstrated that stop and restart of flow caused the production of ROS and led to tissue injury. Since the lung does not become hypoxic with altered blood flow, we investigated the mechanism by which ROS is produced.

What is the fate or effect of the ROS produced in the lungs (or grafts) during ischemia (storage)? Our investigations using murine and human lungs showed that ROS led to production of moieties that triggered the onset of an inflammatory cascade

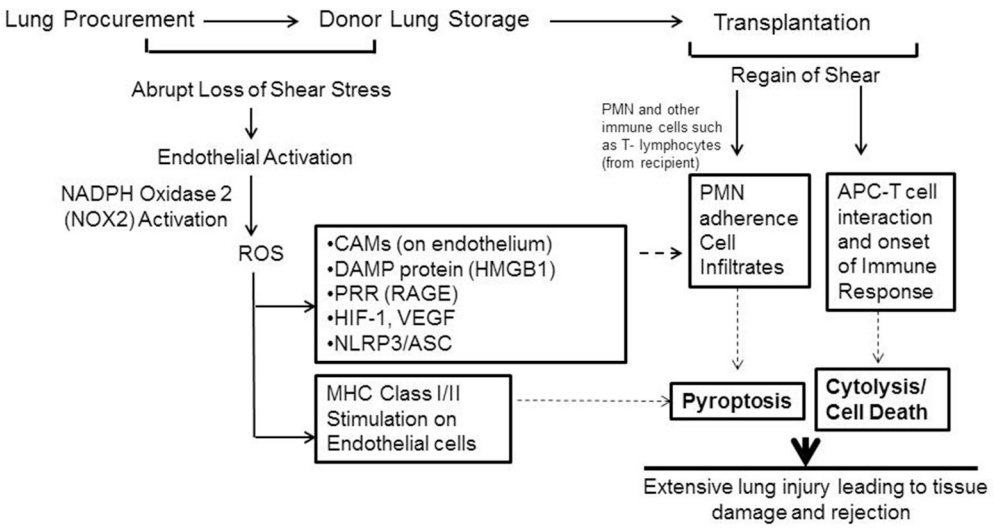


**FIGURE 6 |** Schema showing mechanotransduction induced signaling as would occur with organ storage. ROS activates an inflammation cascade during storage. These predispose the graft to bind to immune cells that influx into it after transplant. ROS can also transform the lung endothelial cells as an antigen presenting cell (APC). The endothelium as APC can "present" donor antigens to the T-lymphocytes that come from the recipient. The APC-T cell interaction leads to cytokine release and cytolysis. (Originally published in Jungraithmayr et al., 2016, permission to reproduce obtained from publisher).

(Jungraithmayr et al., 2016; Tao et al., 2016). Stored or ischemic lungs showed high expression of ICAM-1 and VCAM-1. As we have mentioned earlier, both these moieties facilitate adherence of PMN, macrophages, monocytes etc. to the endothelial layer (**Figure 6**). Additionally the DAMP protein high mobility group box protein (HMGB1) and its receptor RAGE were also upregulated as a function of storage time (Tao et al., 2016). Increase in HMGB1 and are RAGE critical in onset and amplification of inflammation and have been implicated in numerous inflammation pathologies (Wang et al., 1999; Kokkola et al., 2005; Lamkanfi et al., 2010). Indeed the HMGB1–RAGE axis triggers inflammatory cascades by activation of multimeric complexes or inflammasomes (Lamkanfi and Kanneganti, 2010).

Human donor lungs are usually stored under two-thirds inflated conditions prior to transplant and thus continue to be oxygenated; however, if HIF-1α (and thus VEGFA) induction occurred under normoxic conditions of lung storage this would initiate proinflammatory signaling in donor lungs, even in the absence of hypoxia. We also reported on the induction of the HIF1α-VEGF axis in stored or ischemic lungs (Tao et al., 2016) which also participates in driving influx, recruitment and adherence of PMN and other immune cells (**Figure 6**). Furthermore, ROS generated by the endothelium during storage can trigger an adaptive immune response in the form of transformation of lung endothelium as an antigen presenting cell (APC). APCs participate in adaptive immune response by "presenting" donor antigens to the T-lymphocytes from the recipient that enter into the graft after transplant. The activated endothelium of the graft can thus facilitate T cell recruitment and activation; these are well established to lead to cytokine release and cytolysis. The cumulative damage from these events causes injury and onset of rejection post-transplant (Jungraithmayr et al., 2016).

Thus mechanosignaling during lung storage and transplant needs to be minimized in order to reduce graft injury. Toward that end, new strategies advocating for continued perfusion of donor lungs have been adopted. Indeed perfusion of donor lungs is now being increasing employed to (1) prevent damage during storage, (2) preserve the graft over long periods of time, and (3) repair grafts that have been partially damaged so that they may be used for transplantation. We propose that blocking the mechanosignaling cascade by introducing the "perfusion-ventilation" maneuver or by the maintaining of physiological conditions during storage, would maintain graft health. Studies with animal lungs indicate that a relatively low perfusate flow rate can prevent activation of the "loss of shear stress" signaling cascade. Of note, maximal increase in shear signaling occurs with the transition of perfusate flow from 1.8 ml/min to zero (Al-Mehdi et al., 1998).

## SHEAR SIGNALING AND THERAPEUTICS

Our current knowledge on shear stress induced signaling and its role in endothelial integrity and/or in endothelial dysfunction can potentially inform various clinical strategies to protect against shear stress induced endothelial damage. One of the crucial players in shear signaling is ROS; thus delivery of phytopharmaceuticals that can bolster the antioxidant defense can facilitate endothelial protection. For instance, low or abnormal shear induced oxidative stress in ECs can be reduced by the antioxidant resveratrol (Wang et al., 2014). Additionally, the use of agents that drive anti-inflammatory genes or proteins may be employed to reduce endothelial injury arising from abnormal or disturbed shear. Agents such as tannic acid that can increase KLF2 expression on the endothelium can be used to treat atherosclerotic vascular disease (Xu et al., 2017). The protection

conferred on the endothelium by KLF2 is well established and thus other agents that function as KLF2 activators have also been suggested for beneficial cardiovascular effects. Resveratrol (which reportedly induces KLF2 expression) and cholesterol lowering statins (which regulate KLF2 expression) drive an atheroprotective phenotype in the endothelium (Parmar et al., 2005).

## CONCLUSIONS AND FUTURE PERSPECTIVES

Significant advances have been made in recent years toward understanding the various subcellular players and sequence of molecular events that are associated with endothelial mechanotransduction specifically in the context of vascular health and disease. However, the major challenges remain in understanding how mechanosignals integrate at the tissue and organ level across complex cellular environments to generate a biological response. It is also important to analyze and evaluate the collective interaction between mechanosignaling and chemical signals (risk factors etc.) that play a pivotal role in vascular responses to shear.

## AUTHOR CONTRIBUTIONS

The author confirms being the sole contributor of this work and approved it for publication.

## REFERENCES


Adapala, R. K., Thoppil, R. J., Ghosh, K., Cappelli, H. C., Dudley, A. C., Paruchuri, S., et al. (2016). Activation of mechanosensitive ion channel trpv4 normalizes tumor vasculature and improves cancer therapy. *Oncogene* 35, 314–322. doi: 10.1038/onc.2015.83

Alberts-Grill, N., Rezvan, A., Son, D. J., Qiu, H., Kim, C. W., Kemp, M. L., et al. (2012). Dynamic immune cell accumulation during flow-induced atherogenesis in mouse carotid artery: an expanded flow cytometry method. *Arterioscler. Thromb. Vasc. Biol.* 32, 623–632. doi: 10.1161/ATVBAHA.111.242180

Albuquerque, M. L., Waters, C. M., Savla, U., Schnaper, H. W., and Flozak, A. S. (2000). Shear stress enhances human endothelial cell wound closure *in vitro*. *Am. J. Physiol. Heart Circ. Physiol.* 279, H293–H302. doi: 10.1152/ajpheart.2000.279.1.H293

Al-Mehdi, A. B., Song, C., Tozawa, K., and Fisher, A. B. (2000). $Ca2^{+}$- and phosphatidylinositol 3-kinase-dependent nitric oxide generation in lung endothelial cells *in situ* with ischemia. *J. Biol. Chem.* 275, 39807–39810. doi: 10.1074/jbc.C000702200

Al-Mehdi, A. B., Zhao, G., and Fisher, A. B. (1998). Atp-independent membrane depolarization with ischemia in the oxygen-ventilated isolated rat lung. *Am. J. Respir. Cell Mol. Biol.* 18, 653–661. doi: 10.1165/ajrcmb.18.5.2834

Al-Mehdi, A. B., Shuman, H., and Fisher, A. B. (1997). Oxidant generation with k(+)-induced depolarization in the isolated perfused lung. *Free Radic. Biol. Med.* 23, 47–56. doi: 10.1016/S0891-5849(96)00574-6

Aoki, T., Yamamoto, K., Fukuda, M., Shimogonya, Y., Fukuda, S., and Narumiya, S. (2016). Sustained expression of mcp-1 by low wall shear stress loading concomitant with turbulent flow on endothelial cells of intracranial aneurysm. *Acta Neuropathol. Commun.* 4:48. doi: 10.1186/s40478-016-0318-3

Asano, Y., Ichioka, S., Shibata, M., Ando, J., and Nakatsuka, T. (2005). Sprouting from arteriovenous shunt vessels with increased blood flow. *Med. Biol. Eng. Comput.* 43, 126–130. doi: 10.1007/BF02345133

Bagot, C. N., and Arya, R. (2008). Virchow and his triad: a question of attribution. *Br. J. Haematol.* 143, 180–190. doi: 10.1111/j.1365-2141.2008.07323.x

Bagriantsev, S. N., Gracheva, E. O., and Gallagher, P. G. (2014). Piezo proteins: regulators of mechanosensation and other cellular processes. *J. Biol. Chem.* 289, 31673–31681. doi: 10.1074/jbc.R114.612697

Barakat, A. I., Leaver, E. V., Pappone, P. A., and Davies, P. F. (1999). A flow-activated chloride-selective membrane current in vascular endothelial cells. *Circ. Res.* 85, 820–828. doi: 10.1161/01.RES.85.9.820

Barakat, A. I. (1999). Responsiveness of vascular endothelium to shear stress: potential role of ion channels and cellular cytoskeleton (review). *Int. J. Mol. Med.* 4, 323–332. doi: 10.3892/ijmm.4.4.323

Browning, E., Wang, H., Hong, N., Yu, K., Buerk, D. G., DeBolt, K., et al. (2014). Mechanotransduction drives post ischemic revascularization through k(atp) channel closure and production of reactive oxygen species. *Antioxid. Redox Signal.* 20, 872–886. doi: 10.1089/ars.2012.4971

Browning, E. A., Chatterjee, S., and Fisher, A. B. (2012). Stop the flow: a paradigm for cell signaling mediated by reactive oxygen species in the pulmonary endothelium. *Annu. Rev. Physiol.* 74, 403–424. doi: 10.1146/annurev-physiol-020911-153324

Chatterjee, S., Al-Mehdi, A. B., Levitan, I., Stevens, T., and Fisher, A. B. (2003). Shear stress increases expression of a katp channel in rat and bovine pulmonary vascular endothelial cells. *Am. J. Physiol. Cell Physiol.* 285, C959–C967. doi: 10.1152/ajpcell.00511.2002

Chatterjee, S., Browning, E. A., Hong, N., DeBolt, K., Sorokina, E. M., Liu, W., et al. (2012). Membrane depolarization is the trigger for pi3k/akt activation and leads to the generation of ros. *Am. J. Physiol. Heart Circ. Physiol.* 302, H105–H114. doi: 10.1152/ajpheart.00298.2011

Chatterjee, S., Browning, E., Hong, N. K., DeBolt, K., Sorokina, E., Liu, W., et al. (2010). Pi3 kinase/akt activation trigger ros production in a model of pulmonary ischemia. *FASEB J.* 24:796.6.

Chatterjee, S., Chapman, K. E., and Fisher, A. B. (2008). Lung ischemia: a model for endothelial mechanotransduction. *Cell Biochem. Biophys.* 52, 125–138. doi: 10.1007/s12013-008-9030-7

Chatterjee, S., and Fisher, A. B. (2014a). Mechanotransduction: forces, sensors, and redox signaling. *Antioxid. Redox Signal.* 20, 868–871. doi: 10.1089/ars.2013.5753

Chatterjee, S., and Fisher, A. B. (2014b). Mechanotransduction in the endothelium: role of membrane proteins and reactive oxygen species in sensing, transduction, and transmission of the signal with altered blood flow. *Antioxid. Redox Signal.* 20, 899–913. doi: 10.1089/ars.2013.5624

Chatterjee, S., Levitan, I., Wei, Z., and Fisher, A. B. (2006). Katp channels are an important component of the shear-sensing mechanism in the pulmonary microvasculature. *Microcirculation* 13, 633–644. doi: 10.1080/10739680600930255

Chatterjee, S., Nieman, G. F., Christie, J. D., and Fisher, A. B. (2014). Shear stress-related mechanosignaling with lung ischemia: lessons from basic research can inform lung transplantation. *Am. J. Physiol. Lung Cell. Mol. Physiol.* 307, L668–L680. doi: 10.1152/ajplung.00198.2014

Chen, Z., Rubin, J., and Tzima, E. (2010). Role of pecam-1 in arteriogenesis and specification of preexisting collaterals. *Circ. Res.* 107, 1355–1363. doi: 10.1161/CIRCRESAHA.110.229955

Chen, Z., and Tzima, E. (2009). Pecam-1 is necessary for flow-induced vascular remodeling. *Arterioscler. Thromb. Vasc. Biol.* 29, 1067–1073. doi: 10.1161/ATVBAHA.109.186692

Chien, S. (2007). Mechanotransduction and endothelial cell homeostasis: the wisdom of the cell. *Am. J. Physiol. Heart Circul. Physiol.* 292, H1209–H1224. doi: 10.1152/ajpheart.01047.2006

Chiu, J. J., Chen, L. J., Lee, C. I., Lee, P. L., Lee, D. Y., Tsai, M. C., et al. (2007). Mechanisms of induction of endothelial cell e-selectin expression by smooth muscle cells and its inhibition by shear stress. *Blood* 110, 519–528. doi: 10.1182/blood-2006-08-040097

Chiu, J. J., and Chien, S. (2011). Effects of disturbed flow on vascular endothelium: pathophysiological basis and clinical perspectives. *Physiol. Rev.* 91, 327–387. doi: 10.1152/physrev.00047.2009

Chiu, Y. J., McBeath, E., and Fujiwara, K. (2008). Mechanotransduction in an extracted cell model: yn drives stretch- and flow-elicited pecam-1

phosphorylation. *J. Cell Biol.* 182, 753–763. doi: 10.1083/jcb.200801062

Conklin, B. S., Vito, R. P., and Chen, C. (2007). Effect of low shear stress on permeability and occludin expression in porcine artery endothelial cells. *World J. Surg.* 31, 733–743. doi: 10.1007/s00268-006-0735-8

Dai, G., Kaazempur-Mofrad, M. R., Natarajan, S., Zhang, Y., Vaugn, S., Blackman, B. R., et al. (2004). Distinct endothelial phenotypes evoked by arterial waveforms derived from atherosclerosis-susceptible and -resistant regions of human vasculature. *Proc. Natl. Acad. Sci. U.S.A.* 101, 14871–14876. doi: 10.1073/pnas.0406073101

Daniel, A. E., and van Buul, J. D. (2013). Endothelial junction regulation: a prerequisite for leukocytes crossing the vessel wall. *J. Innate Immun.* 5, 324–335. doi: 10.1159/000348828

Dardik, A., Chen, L., Frattini, J., Asada, H., Aziz, F., Kudo, F. A., et al. (2005). Differential effects of orbital and laminar shear stress on endothelial cells. *J. Vasc. Surg.* 41, 869–880. doi: 10.1016/j.jvs.2005.01.020

Davies, P. F., Barbee, K. A., Lal, R., Robotewskyj, A., and Griem, M. L. (1995). Hemodynamics and atherogenesis. Endothelial surface dynamics in flow signal transduction. *Ann. N.Y. Acad. Sci.* 748, 86–102; discussion 102–103. doi: 10.1111/j.1749-6632.1994.tb17310.x

Davies, P. F., Barbee, K. A., Volin, M. V., Robotewskyj, A., Chen, J., Joseph, L., et al. (1997). Spatial relationships in early signaling events of flow-mediated endothelial mechanotransduction. *Annu. Rev. Physiol.* 59, 527–549. doi: 10.1146/annurev.physiol.59.1.527

Davies, P. F., Civelek, M., Fang, Y., Guerraty, M. A., and Passerini, A. G. (2010). Endothelial heterogeneity associated with regional athero-susceptibility and adaptation to disturbed blood flow *in vivo*. *Semin. Thromb. Hemost.* 36, 265–275. doi: 10.1055/s-0030-1253449

Davies, P. F. (1993). Endothelium as a signal transduction interface for flow forces: cell surface dynamics. *Thromb. Haemost.* 70, 124–128.

Davies, P. F. (1995). Flow-mediated endothelial mechanotransduction. *Physiol. Rev.* 75, 519–560. doi: 10.1152/physrev.1995.75.3.519

Davies, P. F. (2008). Endothelial transcriptome profiles *in vivo* in complex arterial flow fields. *Ann. Biomed. Eng.* 36, 563–570. doi: 10.1007/s10439-007-9400-0

Davies, P. F. (2009). Hemodynamic shear stress and the endothelium in cardiovascular pathophysiology. *Nat. Clin. Pract. Cardiovasc. Med.* 6, 16–26. doi: 10.1038/ncpcardio1397

Davis, M. E., Cai, H., Drummond, G. R., and Harrison, D. G. (2001). Shear stress regulates endothelial nitric oxide synthase expression through c-src by divergent signaling pathways. *Circ. Res.* 89, 1073–1080. doi: 10.1161/hh2301.100806

DeMaio, L., Chang, Y. S., Gardner, T. W., Tarbell, J. M., and Antonetti, D. A. (2001). Shear stress regulates occludin content and phosphorylation. *Am. J. Physiol. Heart Circ. Physiol.* 281, H105–H113. doi: 10.1152/ajpheart.2001.281.1.H105

Dewey, C. F. Jr., Bussolari, S. R., Gimbrone, M. A. Jr., and Davies, P. F. (1981). The dynamic response of vascular endothelial cells to fluid shear stress. *J. Biomech. Eng.* 103, 177–185. doi: 10.1115/1.3138276

Dirksen, M. T., van der Wal, A. C., van den Berg, F. M., van der Loos, C. M., and Becker, A. E. (1998). Distribution of inflammatory cells in atherosclerotic plaques relates to the direction of flow. *Circulation* 98, 2000–2003. doi: 10.1161/01.CIR.98.19.2000

Dorland, Y. L., and Huveneers, S. (2017). Cell-cell junctional mechanotransduction in endothelial remodeling. *Cell. Mol. Life Sci.* 74, 279–292. doi: 10.1007/s00018-016-2325-8

Durán, W. N., Breslin, J. W., and Sánchez, F. A. (2010). The no cascade, enos location, and microvascular permeability. *Cardiovasc. Res.* 87, 254–261. doi: 10.1093/cvr/cvq139

Franzoni, M., Cattaneo, I., Ene-Iordache, B., Oldani, A., Righettini, P., and Remuzzi, A. (2016). Design of a cone-and-plate device for controlled realistic shear stress stimulation on endothelial cell monolayers. *Cytotechnology* 68, 1885–1896. doi: 10.1007/s10616-015-9941-2

Fu, B. M., and Tarbell, J. M. (2013). Mechano-sensing and transduction by endothelial surface glycocalyx: composition, structure, and function. *Wiley Interdiscip. Rev. Syst. Biol. Med.* 5, 381–390. doi: 10.1002/wsbm.1211

Fulton, D., Gratton, J. P., McCabe, T. J., Fontana, J., Fujio, Y., Walsh, K., et al. (1999). Regulation of endothelium-derived nitric oxide production by the protein kinase akt. *Nature* 399, 597–601. doi: 10.1038/21218

Gautam, M., Shen, Y., Thirkill, T. L., Douglas, G. C., and Barakat, A. I. (2006). Flow-activated chloride channels in vascular endothelium. Shear stress sensitivity, desensitization dynamics, and physiological implications. *J. Biol. Chem.* 281, 36492–36500. doi: 10.1074/jbc.M605866200

Gilbert, G., Courtois, A., Dubois, M., Cussac, L. A., Ducret, T., Lory, P., et al. (2017). T-type voltage gated calcium channels are involved in endothelium-dependent relaxation of mice pulmonary artery. *Biochem. Pharmacol.* 138, 61–72. doi: 10.1016/j.bcp.2017.04.021

Gimbrone, M. A. Jr., Topper, J. N., Nagel, T., Anderson, K. R., and Garcia-Cardeña, G. (2000). Endothelial dysfunction, hemodynamic forces, and atherogenesis. *Ann. N.Y. Acad. Sci.* 902, 230–239; discussion 239–240. doi: 10.1111/j.1749-6632.2000.tb06318.x

Gloire, G., Legrand-Poels, S., and Piette, J. (2006). Nf-kappab activation by reactive oxygen species: fifteen years later. *Biochem. Pharmacol.* 72, 1493–1505. doi: 10.1016/j.bcp.2006.04.011

Godbole, A. S., Lu, X., Guo, X., and Kassab, G. S. (2009). Nadph oxidase has a directional response to shear stress. *Am. J. Physiol. Heart Circ. Physiol.* 296, H152–H158. doi: 10.1152/ajpheart.01251.2007

Golub, A. S., and Pittman, R. N. (2014). A paradigm shift for local blood flow regulation. *J. Appl. Physiol.* 116, 703–705. doi: 10.1152/japplphysiol.00964.2013

Hahn, C., and Shchwartz, M. A. (2009). Mechanotransduction and endothelial cell homeostasis: the wisdom of the cell. *Nat. Rev. Mol. Cell Biol.* 10, 53–62. doi: 10.1038/nrm2596

Hamik, A., Lin, Z., Kumar, A., Balcells, M., Sinha, S., Katz, J., et al. (2007). Kruppel-like factor 4 regulates endothelial inflammation. *J. Biol. Chem.* 282, 13769–13779. doi: 10.1074/jbc.M700078200

Hawkins, B. J., Madesh, M., Kirkpatrick, C. J., and Fisher, A. B. (2007). Superoxide flux in endothelial cells via the chloride channel-3 mediates intracellular signaling. *Mol. Biol. Cell.* 18, 2002–2012. doi: 10.1091/mbc.e06-09-0830

Higashi, Y., Maruhashi, T., Noma, K., and Kihara, Y. (2014). Oxidative stress and endothelial dysfunction: clinical evidence and therapeutic implications. *Trends Cardiovasc. Med.* 24, 165–169. doi: 10.1016/j.tcm.2013.12.001

Hoger, J. H., Ilyin, V. I., Forsyth, S., and Hoger, A. (2002). Shear stress regulates the endothelial kir2.1 ion channel. *Proc. Natl. Acad. Sci. U.S.A.* 99, 7780–7785. doi: 10.1073/pnas.102184999

Hsiai, T. K., Cho, S. K., Reddy, S., Hama, S., Navab, M., Demer, L. L., et al. (2001). Pulsatile flow regulates monocyte adhesion to oxidized lipid-induced endothelial cells. *Arterioscler. Thromb. Vasc. Biol.* 21, 1770–1776. doi: 10.1161/hq1001.097104

Hsiai, T. K., Cho, S. K., Wong, P. K., Ing, M., Salazar, A., Sevanian, A., et al. (2003). Monocyte recruitment to endothelial cells in response to oscillatory shear stress. *FASEB J.* 17, 1648–1657. doi: 10.1096/fj.02-1064com

Hwang, J., Saha, A., Boo, Y. C., Sorescu, G. P., McNally, J. S., Holland, S. M., et al. (2003). Oscillatory shear stress stimulates endothelial production of o2- from p47phox-dependent nad(p)h oxidases, leading to monocyte adhesion. *J. Biol. Chem.* 278, 47291–47298. doi: 10.1074/jbc.M305150200

Ingber, D. E. (1993). Cellular tensegrity: defining new rules of biological design that govern the cytoskeleton. *J. Cell Sci.* 104, 613–627.

Ingber, D. E. (2006). Cellular mechanotransduction: putting all the pieces together again. *FASEB J.* 20, 811–827. doi: 10.1096/fj.05-5424rev

Ingber, D. E. (2008). Tensegrity-based mechanosensing from macro to micro. *Prog. Biophys. Mol. Biol.* 97, 163–179. doi: 10.1016/j.pbiomolbio.2008.02.005

Ishibazawa, A., Nagaoka, T., Takahashi, T., Yamamoto, K., Kamiya, A., Ando, J., et al. (2011). Effects of shear stress on the gene expressions of endothelial nitric oxide synthase, endothelin-1, and thrombomodulin in human retinal microvascular endothelial cells. *Invest. Ophthalmol. Vis. Sci.* 52, 8496–8504. doi: 10.1167/iovs.11-7686

Jalali, S., del Pozo, M. A., Chen, K., Miao, H., Li, Y., Schwartz, M. A., et al. (2001). Integrin-mediated mechanotransduction requires its dynamic interaction with specific extracellular matrix (ecm) ligands. *Proc. Natl. Acad. Sci. U.S.A.* 98, 1042–1046. doi: 10.1073/pnas.98.3.1042

Jiang, Z., Wu, L., Miller, B. L., Goldman, D. R., Fernandez, C. M., Abouhamze, Z. S., et al. (2004). A novel vein graft model: adaptation to differential flow environments. *Am. J. Physiol. Heart Circ. Physiol.* 286, H240–H245. doi: 10.1152/ajpheart.00760.2003

Johnson, B. D., Mather, K. J., and Wallace, J. P. (2011). Mechanotransduction of shear in the endothelium: basic studies and clinical implications *Vasc. Med.* 16, 365–377. doi: 10.1177/1358863X11422109

Jungraithmayr, W., Gupta, V., Orndorff, R., and Chatterjee, S. (2016). Focusing on donor lung organ storage: implications for inflammation post-transplant. *J. Respir. Res.* 2, 79–84. doi: 10.17554/j.issn.2412-2424.2016.02.23

Kokkola, R., Andersson, A., Mullins, G., Ostberg, T., Treutiger, C. J., Arnold, B., et al. (2005). Rage is the major receptor for the proinflammatory activity of hmgb1 in rodent macrophages. *Scand. J. Immunol.* 61, 1–9. doi: 10.1111/j.0300-9475.2005.01534.x

Korshunov, V. A., and Berk, B. C. (2003). Flow-induced vascular remodeling in the mouse: a model for carotid intima-media thickening. *Arterioscler. Thromb. Vasc. Biol.* 23, 2185–2191. doi: 10.1161/01.ATV.0000103120.06092.14

Korthuis, R. J. (2018). Mechanisms of i/r-induced endothelium-dependent vasodilator dysfunction. *Adv. Pharmacol.* 81, 331–364. doi: 10.1016/bs.apha.2017.08.001

Kubes, P., and Granger, D. N. (1992). Nitric oxide modulates microvascular permeability. *Am. J. Physiol.* 262, H611–H615. doi: 10.1152/ajpheart.1992.262.2.H611

Kwei, S., Stavrakis, G., Takahas, M., Taylor, G., Folkman, M. J., Gimbrone, M. A. Jr., et al. (2004). Early adaptive responses of the vascular wall during venous arterialization in mice. *Am. J. Pathol.* 164, 81–89. doi: 10.1016/S0002-9440(10)63099-4

Lamkanfi, M., and Kanneganti, T. D. (2010). Nlrp3: an immune sensor of cellular stress and infection. *Int. J. Biochem. Cell Biol.* 42, 792–795. doi: 10.1016/j.biocel.2010.01.008

Lamkanfi, M., Sarkar, A., Vande Walle, L., Vitari, A. C., Amer, A. O., Wewers, M. D., et al. (2010). Inflammasome-dependent release of the alarmin hmgb1 in endotoxemia. *J. Immunol.* 185, 4385–4392. doi: 10.4049/jimmunol.1000803

Li, J., Hou, B., Tumova, S., Muraki, K., Bruns, A., Ludlow, M. J., et al. (2014). Piezo1 integration of vascular architecture with physiological force. *Nature* 515, 279–282. doi: 10.1038/nature13701

Lowe, G. D. (2003). Virchow's triad revisited: abnormal flow. *Pathophysiol. Haemost. Thromb.* 33, 455–457. doi: 10.1159/000083845

Malek, A. M., Alper, S. L., and Izumo, S. (1999). Hemodynamic shear stress and its role in atherosclerosis. *JAMA* 282, 2035–2042. doi: 10.1001/jama.282.21.2035

Matharu, N. M., McGettrick, H. M., Salmon, M., Kissane, S., Vohra, R. K., Rainger, G. E., et al. (2008). Inflammatory responses of endothelial cells experiencing reduction in flow after conditioning by shear stress. *J. Cell. Physiol.* 216, 732–741. doi: 10.1002/jcp.21457

McAllister, T. N., and Frangos, J. A. (1999). Steady and transient fluid shear stress stimulate no release in osteoblasts through distinct biochemical pathways. *J. Bone Miner. Res.* 14, 930–936. doi: 10.1359/jbmr.1999.14.6.930

Melchior, B., and Frangos, J. A. (2010). Shear-induced endothelial cell-cell junction inclination. *Am. J. Physiol. Cell Physiol.* 299, C621–C629. doi: 10.1152/ajpcell.00156.2010

Morawietz, H. (2018). Cardiovascular protection by nox4. *Cardiovasc. Res.* 114, 353–355. doi: 10.1093/cvr/cvx252

Morgan, V. L., Graham, T. P. Jr., Roselli, R. J., and Lorenz, C. H. (1998). Alterations in pulmonary artery flow patterns and shear stress determined with three-dimensional phase-contrast magnetic resonance imaging in fontan patients. *J. Thor. Cardiovasc. Surg.* 116, 294–304. doi: 10.1016/S0022-5223(98)70130-8

Nam, D., Ni, C. W., Rezvan, A., Suo, J., Budzyn, K., Llanos, A., et al. (2009). Partial carotid ligation is a model of acutely induced disturbed flow, leading to rapid endothelial dysfunction and atherosclerosis. *Am. J. Physiol. Heart Circ. Physiol.* 297, H1535–H1543. doi: 10.1152/ajpheart.00510.2009

Natarajan, M., Aravindan, N., Sprague, E. A., and Mohan, S. (2016). Hemodynamic flow-induced mechanotransduction signaling influences the radiation response of the vascular endothelium. *Radiat. Res.* 186, 175–188. doi: 10.1667/RR14410.1

Nayak, L., Lin, Z., and Jain, M. K. (2011). "Go with the flow": how kruppel-like factor 2 regulates the vasoprotective effects of shear stress. *Antioxid. Redox Signal.* 15, 1449–1461. doi: 10.1089/ars.2010.3647

Nerem, R. M., Alexander, R. W., Chappell, D. C., Medford, R. M., Varner, S. E., and Taylor, W. R. (1998). The study of the influence of flow on vascular endothelial biology. *Am. J. Med. Sci.* 316, 169–175.

Noel, J., Wang, H., Hong, N., Tao, J. Q., Yu, K., Sorokina, E. M., et al. (2013). Pecam-1 and caveolae form the mechanosensing complex necessary for nox2 activation and angiogenic signaling with stopped flow in pulmonary endothelium. *Am. J. Physiol. Lung Cell. Mol. Physiol.* 305, L805–L818. doi: 10.1152/ajplung.00123.2013

Ohnesorge, N., Viemann, D., Schmidt, N., Czymai, T., Spiering, D., Schmolke, M., et al. (2010). Erk5 activation elicits a vasoprotective endothelial phenotype via induction of kruppel-like factor 4 (klf4). *J. Biol. Chem.* 285, 26199–26210. doi: 10.1074/jbc.M110.103127

Olesen, S. P., Clapham, D. E., and Davies, P. F. (1988). Haemodynamic shear stress activates a k+ current in vascular endothelial cells. *Nature* 331, 168–170. doi: 10.1038/331168a0

Orndorff, R. L., Hong, N., Yu, K., Feinstein, S. I., Zern, B. J., Fisher, A. B., et al. (2014). Nox2 in lung inflammation: quantum dot based *in situ* imaging of nox2-mediated expression of vascular cell adhesion molecule-1. *Am. J. Physiol. Lung Cell. Mol. Physiol.* 306, L260–L268. doi: 10.1152/ajplung.00278.2013

Pacher, P., Beckman, J. S., and Liaudet, L. (2007). Nitric oxide and peroxynitrite in health and disease. *Physiol. Rev.* 87, 315–424. doi: 10.1152/physrev.00029.2006

Parmar, K. M., Larman, H. B., Dai, G., Zhang, Y., Wang, E. T., Moorthy, S. N., et al. (2006). Integration of flow-dependent endothelial phenotypes by kruppel-like factor 2. *J. Clin. Invest.* 116, 49–58. doi: 10.1172/JCI24787

Parmar, K. M., Nambudiri, V., Dai, G., Larman, H. B., Gimbrone, M. A. Jr., and García-Cardeña, G. (2005). Statins exert endothelial atheroprotective effects via the klf2 transcription factor. *J. Biol. Chem.* 280, 26714–26719. doi: 10.1074/jbc.C500144200

Passerini, A. G., Milsted, A., and Rittgers, S. E. (2003). Shear stress magnitude and directionality modulate growth factor gene expression in preconditioned vascular endothelial cells. *J. Vasc. Surg.* 37, 182–190. doi: 10.1067/mva.2003.66

Pendyala, S., Usatyuk, P. V., Gorshkova, I. A., Garcia, J. G., and Natarajan, V. (2009). Regulation of nadph oxidase in vascular endothelium: the role of phospholipases, protein kinases, and cytoskeletal proteins. *Antioxid. Redox Signal.* 11, 841–860. doi: 10.1089/ars.2008.2231

Radeva, M. Y., and Waschke, J. (2017). Mind the gap: mechanisms regulating the endothelial barrier. *Acta Physiol.* 222:e12860. doi: 10.1111/apha.12860

Ray, R., Murdoch, C. E., Wang, M., Santos, C. X., Zhang, M., Alom-Ruiz, S., et al. (2011). Endothelial nox4 nadph oxidase enhances vasodilatation and reduces blood pressure *in vivo*. *Arterioscler. Thromb. Vasc. Biol.* 31, 1368–1376. doi: 10.1161/ATVBAHA.110.219238

Rezvan, A., Ni, C. W., Alberts-Grill, N., and Jo, H. (2011). Animal, *in vitro*, and *ex vivo* models of flow-dependent atherosclerosis: role of oxidative stress. *Antioxid. Redox Signal.* 15, 1433–1448. doi: 10.1089/ars.2010.3365

Rimessi, A., Previati, M., Nigro, F., Wieckowski, M. R., and Pinton, P. (2016). Mitochondrial reactive oxygen species and inflammation: molecular mechanisms, diseases and promising therapies. *Int. J. Biochem. Cell Biol.* 81, 281–293. doi: 10.1016/j.biocel.2016.06.015

Rizzo, V., Morton, C., DePaola, N., Schnitzer, J. E., and Davies, P. F. (2003). Recruitment of endothelial caveolae into mechanotransduction pathways by flow conditioning *in vitro*. *Am. J. Physiol. Heart Circ. Physiol.* 285, H1720–H1729. doi: 10.1152/ajpheart.00344.2002

Rodrigues, S. F., and Granger, D. N. (2015). Blood cells and endothelial barrier function. *Tissue Barriers* 3:e978720. doi: 10.4161/21688370.2014.978720

Sandoo, A., van Zanten, J. J., Metsios, G. S., Carroll, D., and Kitas, G. D. (2010). The endothelium and its role in regulating vascular tone. *Open Cardiovasc. Med. J.* 4, 302–312. doi: 10.2174/1874192401004010302

Schröder, K., Zhang, M., Benkhoff, S., Mieth, A., Pliquett, R., Kosowski, J., et al. (2012). Nox4 is a protective reactive oxygen species generating vascular nadph oxidase. *Circ. Res.* 110, 1217–1225. doi: 10.1161/CIRCRESAHA.112.267054

Samet, M. M., and Lelkes, P. L. (1999). "The hemodynamic environment of the endothelium *in vivo* and its simulation *in vitro*," in *Mechanical Forces and the Endothelium*, ed P. L. Lelkes (Amsterdam: Harwood Academic Publishers), 1–32.

Song, C., Al-Mehdi, A. B., and Fisher, A. B. (2001). An immediate endothelial cell signaling response to lung ischemia. *Am. J. Physiol. Lung Cell Mol. Physiol.* 281, L993–L1000. doi: 10.1152/ajplung.2001.281.4.L993

Spruell, C., and Baker, A. B. (2013). Analysis of a high-throughput cone-and-plate apparatus for the application of defined spatiotemporal flow to cultured cells. *Biotechnol. Bioeng.* 110, 1782–1793. doi: 10.1002/bit.24823

Sriram, K., Laughlin, J. G., Rangamani, P., and Tartakovsky, D. M. (2016). Shear-induced nitric oxide production by endothelial cells. *Biophys. J.* 111, 208–221. doi: 10.1016/j.bpj.2016.05.034

Tao, J. Q., Sorokina, E. M., Vazquez Medina, J. P., Mishra, M. K., Yamada, Y., Satalin, J., et al. (2016). Onset of inflammation with ischemia: implications

for donor lung preservation and transplant survival. *Am. J. Transplant*. 16, 2598–2611. doi: 10.1111/ajt.13794

Tardy, Y., Resnick, N., Nagel, T., Gimbrone, M. A. Jr., and Dewey, C. F. Jr. (1997). Shear stress gradients remodel endothelial monolayers *in vitro* via a cell proliferation-migration-loss cycle. *Arterioscler. Thromb. Vasc. Biol*. 17, 3102–3106. doi: 10.1161/01.ATV.17.11.3102

Topper, J. N., Gimbrone, M. A. Jr. (1999). Blood flow and vascular gene expression: fluid shear stress as a modulator of endothelial phenotype. *Mol. Med. Today* 5, 40–46. doi: 10.1016/S1357-4310(98)01372-0

Tsao, P. S., Buitrago, R., Chan, J. R., and Cooke, J. P. (1996). Fluid flow inhibits endothelial adhesiveness. Nitric oxide and transcriptional regulation of vcam-1. *Circulation* 94, 1682–1689. doi: 10.1161/01.CIR.94.7.1682

Tzima, E., Del Pozo, M. A., Kiosses, W. B., Mohamed, S. A., Li, S., Chien, S., et al. (2002). Activation of rac1 by shear stress in endothelial cells mediates both cytoskeletal reorganization and effects on gene expression. *EMBO J.* 21, 6791–6800. doi: 10.1093/emboj/cdf688

Tzima, E., Irani-Tehrani, M., Kiosses, W. B., Dejana, E., Schultz, D. A., Engelhardt, B., et al. (2005). A mechanosensory complex that mediates the endothelial cell response to fluid shear stress. *Nature* 437, 426–431. doi: 10.1038/nature03952

Usami, S., Chen, H. H., Zhao, Y., Chien, S., and Skalak, R. (1993). Design and construction of a linear shear stress flow chamber. *Ann. Biomed. Eng*. 21, 77–83. doi: 10.1007/BF02368167

van Hinsbergh, V. W. (2012). Endothelium–role in regulation of coagulation and inflammation. *Semin. Immunopathol*. 34, 93–106. doi: 10.1007/s00281-011-0285-5

Waite, L. and Fine, J. (2007). *Applied Biofluid Mechanics*. (New York, NY: McGraw-Hill), 10.

Wang, H., Bloom, O., Zhang, M., Vishnubhakat, J. M., Ombrellino, M., Che, J., et al. (1999). Hmg-1 as a late mediator of endotoxin lethality in mice. *Science* 285, 248–251. doi: 10.1126/science.285.5425.248

Wang, K. C., Yeh, Y. T., Nguyen, P., Limqueco, E., Lopez, J., Thorossian, S., et al. (2016). Flow-dependent yap/taz activities regulate endothelial phenotypes and atherosclerosis. *Proc. Natl. Acad. Sci. U.S.A*. 113, 11525–11530. doi: 10.1073/pnas.1613121113

Wang, N., Tytell, J. D., and Ingber, D. E. (2009). Mechanotransduction at a distance: mechanically coupling the extracellular matrix with the nucleus. *Nat. Rev. Mol. Cell Biol*. 10, 75–82. doi: 10.1038/nrm2594

Wang, Z., Zhang, J., Li, B., Gao, X., Liu, Y., Mao, W., et al. (2014). Resveratrol ameliorates low shear stressinduced oxidative stress by suppressing erk/enosthr495 in endothelial cells. *Mol. Med. Rep*. 10, 1964–1972. doi: 10.3892/mmr.2014.2390

Wei, Z., Al-Mehdi, A. B., and Fisher, A. B. (2001). Signaling pathway for nitric oxide generation with simulated ischemia in flow-adapted endothelial cells. *Am. J. Physiol. Heart Circ. Physiol*. 281, H2226–H2232. doi: 10.1152/ajpheart.2001.281.5.H2226

Wei, Z., Costa, K., Al-Mehdi, A. B., Dodia, C., Muzykantov, V., and Fisher, A. B. (1999). Simulated ischemia in flow-adapted endothelial cells leads to generation of reactive oxygen species and cell signaling. *Circ. Res*. 85, 682–689. doi: 10.1161/01.RES.85.8.682

Wei, Z., Manevich, Y., Al-Mehdi, A. B., Chatterjee, S., and Fisher, A. B. (2004). Ca2+ flux through voltage-gated channels with flow cessation in pulmonary microvascular endothelial cells. *Microcirculation* 11, 517–526. doi: 10.1080/10739680490476367

Weinbaum, S., Zhang, X., Han, Y., Vink, H., and Cowin, S. C. (2003). Mechanotransduction and flow across the endothelial glycocalyx. *Proc. Natl. Acad. Sci. U.S.A*. 100, 7988–7995. doi: 10.1073/pnas.1332808100

Wu, J., Lewis, A. H., and Grandl, J. (2017). Touch, tension, and transduction - the function and regulation of piezo ion channels. *Trends Biochem. Sci*. 42, 57–71. doi: 10.1016/j.tibs.2016.09.004

Xu, Y., Liu, P., Xu, S., Koroleva, M., Zhang, S., Si, S., et al. (2017). Tannic acid as a plant-derived polyphenol exerts vasoprotection via enhancing klf2 expression in endothelial cells. *Sci. Rep*. 7:6686. doi:10.1038/s41598-017-06803-x

Yang, B., and Rizzo, V. (2007). Tnf-alpha potentiates protein-tyrosine nitration through activation of nadph oxidase and enos localized in membrane rafts and caveolae of bovine aortic endothelial cells. *Am. J. Physiol. Heart Circul. Physiol.* 292, H954–H962. doi: 10.1152/ajpheart.00758.2006

Yau, J. W., Teoh, H., and Verma, S. (2015). Endothelial cell control of thrombosis. *BMC Cardiovasc. Disord*. 15:130. doi: 10.1186/s12872-015-0124-z

Yu, J., Bergaya, S., Murata, T., Alp, I. F., Bauer, M. P., Lin, M. I., et al. (2006). Direct evidence for the role of caveolin-1 and caveolae in mechanotransduction and remodeling of blood vessels. *J. Clin. Invest*. 116, 1284–1291. doi: 10.1172/JCI27100

Zou, Y., Dietrich, H., Hu, Y., Metzler, B., Wick, G., and Xu, Q. (1998). Mouse model of venous bypass graft arteriosclerosis. *Am. J. Pathol*. 153, 1301–1310. doi: 10.1016/S0002-9440(10)65675-1

**Conflict of Interest Statement:** The author declares that the research was conducted in the absence of any commercial or financial relationships that could be construed as a potential conflict of interest.

*Copyright © 2018 Chatterjee. This is an open-access article distributed under the terms of the Creative Commons Attribution License (CC BY). The use, distribution or reproduction in other forums is permitted, provided the original author(s) and the copyright owner are credited and that the original publication in this journal is cited, in accordance with accepted academic practice. No use, distribution or reproduction is permitted which does not comply with these terms.*

frontiers in Physiology

HYPOTHESIS AND THEORY
published: 07 June 2018
doi: 10.3389/fphys.2018.00690

# Potential Modulation of Vascular Function by Nitric Oxide and Reactive Oxygen Species Released From Erythrocytes

*Joseph M. Rifkind[1,2]*, Joy G. Mohanty[2], Enika Nagababu[1,2], Maria T. Salgado[2] and Zeling Cao[2]*

*[1] Department of Anesthesiology and Critical Care Medicine, Johns Hopkins University School of Medicine, Baltimore, MD, United States, [2] National Institute on Aging, National Institutes of Health, Baltimore, MD, United States*

The primary role for erythrocytes is oxygen transport that requires the reversible binding of oxygen to hemoglobin. There are, however, secondary reactions whereby the erythrocyte can generate reactive oxygen species (ROS) and nitric oxide (NO). ROS such as superoxide anion and hydrogen peroxide are generated by the autoxidation of hemoglobin. NO can be generated when nitrite reacts with hemoglobin forming an $HbNO^{+}$ intermediate. Both of these reactions are dramatically enhanced under hypoxic conditions. Within the erythrocyte, interactions of NO with hemoglobin and enzymatic reactions that neutralize ROS are expected to prevent the release of any generated NO or ROS. We have, however, demonstrated that partially oxygenated hemoglobin has a distinct conformation that enhances hemoglobin-membrane interactions involving Band 3 protein. Autoxidation of the membrane bound partially oxygenated hemoglobin facilitates the release of ROS from the erythrocyte. NO release is made possible when $HbNO^{+}$, the hemoglobin nitrite-reduced intermediate, which is not neutralized by hemoglobin, is bound to the membrane and releases NO. Some of the released ROS has been shown to be transferred to the vasculature suggesting that some of the released NO may also be transferred to the vasculature. NO is known to have a major effect on the vasculature regulating vascular dilatation. Erythrocyte generated NO may be important when NO production by the vasculature is impaired. Furthermore, the erythrocyte NO released, may play an important role in regulating vascular function under hypoxic conditions when endothelial eNOS is less active. ROS can react with NO and, can thereby modulate the vascular effects of NO. We have also demonstrated an inflammatory response due to erythrocyte ROS. This reflects the ability of ROS to react with various cellular components affecting cellular function.

**Keywords: erythrocytes, vasculature, nitric oxide, reactive oxygen species, superoxide, hypoxia**

OPEN ACCESS

***Edited by:***
*Michael A. Hill,*
*University of Missouri, United States*

***Reviewed by:***
*Brant Isakson,*
*University of Virginia, United States*
*Ulf Simonsen,*
*Aarhus University, Denmark*

****Correspondence:***
*Joseph M. Rifkind*
*jrifkin3@jhmi.edu*

***Specialty section:***
*This article was submitted to Vascular Physiology, a section of the journal Frontiers in Physiology*

***Received:*** *22 December 2017*
***Accepted:*** *17 May 2018*
***Published:*** *07 June 2018*

***Citation:***
*Rifkind JM, Mohanty JG, Nagababu E, Salgado MT and Cao Z (2018) Potential Modulation of Vascular Function by Nitric Oxide and Reactive Oxygen Species Released From Erythrocytes. Front. Physiol. 9:690. doi: 10.3389/fphys.2018.00690*

## INTRODUCTION

The primary role of the erythrocyte is the transport of oxygen through the circulatory system and the delivery of oxygen to the tissues. Effective oxygen transport requires that the erythrocytes contain a major fraction of the required body oxygen and come into intimate contact with all the tissues of the body. The close contact of erythrocytes in the capillaries to the body tissues opens up

the possibility that compounds produced by secondary reactions involving hemoglobin can also be transferred to the tissues and thereby influence the proper function of the organism.

One of these secondary reactions of hemoglobin involves its autoxidation (**Figure 1**) resulting in the reduction of oxygen to superoxide (Levy et al., 1991). Hemoglobin is relatively stable but does slowly undergo autoxidation. This reaction, which is very slow for fully oxygenated hemoglobin, is increased by several orders of magnitude for partially oxygenated hemoglobin (Abugo and Rifkind, 1994; Balagopalakrishna et al., 1996). Reactions of superoxide generate other reactive oxygen species (ROS) including hydrogen peroxide (**Figure 1**) and hydroxyl radicals (Nagababu et al., 2003a; Nagababu and Rifkind, 2004). These ROS are a potential source of damage to the vasculature (**Figure 1**) (Rifkind et al., 2003; Taniyama and Griendling, 2003). ROS by reacting with nitric oxide (NO) impair endothelial dependent vasorelaxation, which has a major effect on blood flow and oxygen delivery. Other established effects of ROS on the vasculature include an inflammatory response (Huertas et al., 2013), the increased expression of adhesion molecules like the vascular adhesion molecule (VCAM-1) and the intracellular adhesion molecule (ICAM-1), which result in monocyte adhesion contributing to atherosclerotic lesion formation (Dimmeler and Zeiher, 2000). In addition, ROS induce proliferation and migration of endothelial cells, mediate lymphocyte-activated tubulogenesis and mediate angiogenic growth factors like VEGF, all of which contribute to vascular remodeling (Staiculescu et al., 2014).

An additional secondary reaction associated with hemoglobin involves the production of NO (**Figure 2**) by the reaction of deoxygenated heme groups with nitrite (Cosby et al., 2003; Nagababu et al., 2003b). Nitrite is produced in the circulation when NO released by the endothelium reacts with oxygen (Liu et al., 1998). This nitrite can be taken up by the erythrocyte and the vasculature. Nitrite in the vascular wall can be converted into NO under hypoxic conditions (Kleinbongard et al., 2006; Dalsgaard et al., 2007; Li et al., 2008; Aamand et al., 2009). In the erythrocyte, NO can also be generated by the hypoxic reaction of nitrite with deoxygenated hemoglobin (**Figure 2**). Another source of erythrocyte NO involves erythrocyte NO synthase (Kleinbongard et al., 2006). These pools of NO, if transmitted to the vasculature (**Figure 2**) can play a role in regulating dilatation and vascular tone (Ignarro et al., 1999).

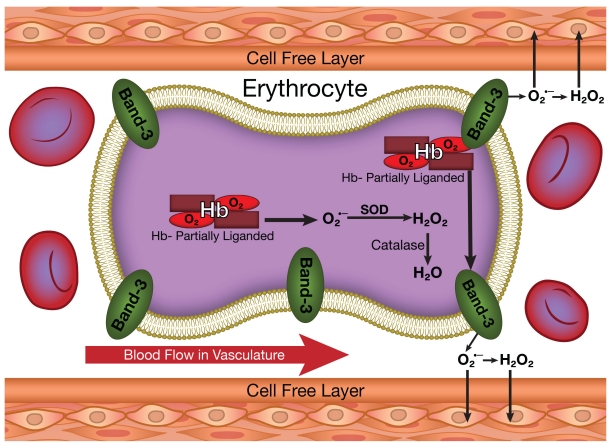


**FIGURE 1 |** The production of superoxide and other ROS in erythrocytes and their potential transfer to the vasculature.

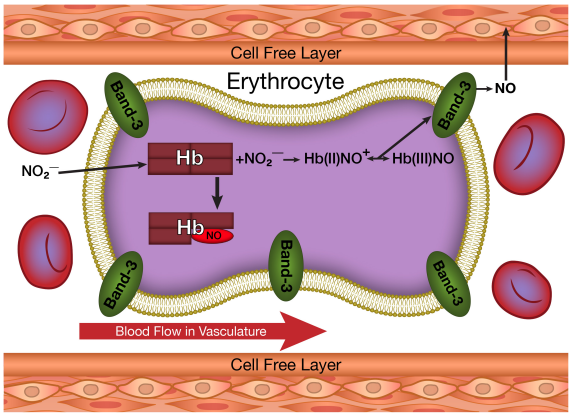


**FIGURE 2 |** The production of NO from nitrite taken up by erythrocytes and its potential transfer to the vasculature.

Despite the potential vascular effects of both ROS and NO, cytoplasmic reactions within the erythrocyte are expected to completely neutralize any ROS (**Figure 1**) or NO (**Figure 2**) formed in the erythrocyte. Superoxide dismutase reacts with any superoxide formed, while catalase and glutathione peroxidase react with any hydrogen peroxide formed (Nagababu et al., 2003a). NO has a very high affinity for deoxygenated hemoglobin chains (Lancaster, 1994) and readily reacts with the oxygenated chains (Kelm et al., 1997). Therefore, the erythrocyte is not expected to be a source for vascular ROS or NO.

We have, however, demonstrated that significant amounts of ROS generated by hemoglobin autoxidation can be released from the erythrocyte, despite the high levels of erythrocyte antioxidants. This release was explained by a unique conformation for partially liganded hemoglobin formed under hypoxic conditions. This conformational change both increases the rate of autoxidation of oxygenated hemoglobin producing superoxide (Abugo and Rifkind, 1994) and enhances the binding of the partially liganded hemoglobin to the membrane band 3 (Cao et al., 2009) facilitating the release of the produced superoxide from the erythrocyte without being scavenged by erythrocyte antioxidant enzymes.

The direct formation of NO when nitrite reacts with deoxygenated hemoglobin would result in the immediate neutralization of the NO by reactions with hemoglobin (see above). We, however, found that the reaction of nitrite with deoxyhemoglobin produces two hemoglobin associated intermediates prior to the formation of NO (Salgado et al., 2009) The same conformational change for partially liganded hemoglobin that enhances the binding of partially oxygenated hemoglobin to the membrane facilitating the release of superoxide (ROS) also increases the affinity of the nitrite-reacted

hemoglobin for band 3 on the erythrocyte membrane and enhances the formation of NO from one of these nitrite-reacted hemoglobin intermediates (Salgado et al., 2015). These reactions facilitate the release of NO from the erythrocyte.

Once released from the erythrocyte, possible effects of ROS and NO on the vasculature and other cells in the circulation need to be considered.

## THE REACTION OF NITRITE WITH DEOXYHEMOGLOBIN

The initial reaction in the erythrocyte involves the binding of nitrite to the hemoglobin deoxygenated hemes. This complex is then converted to an intermediate (Salgado et al., 2009) $Hb(II)NO^+$. This intermediate can share an electron with the heme iron and the beta–93 thiol group producing a hybrid intermediate with properties of $Hb(II)NO^+$, Hb(III)NO and ·SHb(II)NO (Salgado et al., 2011). The electron delocalization produces a relatively stable complex that retains the nitrite in a form that is not neutralized by irreversible reactions with hemoglobin. This complex can under proper conditions release NO. The Hb(III)NO can directly release NO and the $Hb(II)NO^+$ can release NO by a nucleophilic reaction involving the distal histidine in the same way that oxyhemoglobin releases superoxide (Salgado et al., 2015). These reactions provide a pool of hemoglobin that can potentially release NO.

Since the reaction with nitrite occurs with hemoglobin that is appreciably deoxygenated, the nitrite-reacted-hemoglobin has the same properties as partially liganded hemoglobin. Therefore, it has an increased affinity for band 3 of the erythrocyte membrane. This results in a pathway for releasing NO from the erythrocyte when nitrite reacts with deoxygenated hemoglobin that is analogous to the pathway for the release of ROS from partially oxygenated hemoglobin.

## THE DISTINCT HEMOGLOBIN CONFORMATIONAL CHANGE FOR PARTIALLY LIGANDED HEMOGLOBIN THAT FACILITATES THE RELEASE OF ROS AND NO FROM THE ERYTHROCYTE

### The Involvement of Ligand Induced Fluctuations

Hemoglobin consists of four subunits, two α-chains and two β-chains. Oxygen binds to the distal side of the heme groups with a histidine bound directly to the opposite proximal side of the heme. The four subunits are arranged tetragonally with two distinct interfaces between the α and β chains, the $\alpha_1\beta_1$ and $\alpha_1\beta_2$ interfaces.

The structural studies of hemoglobin have focused on the distinct properties of fully oxygenated (R-state) hemoglobin (Shaanan, 1983) and fully deoxygenated (T-state) hemoglobin (Fermi et al., 1984), with cooperativity explained by the cooperative structural changes detected by X-ray diffraction studies that take place when the T-state converts to the R-state (Perutz, 1970; Shaanan, 1983; Fermi et al., 1984). The structural changes detected by X-ray studies primarily involve the proximal side of the heme that undergoes an altered configuration when oxygen is bound. These changes are transmitted to the $\alpha_1\beta_2$ interface, which undergoes a rearrangement that alters the quaternary conformation from that of the T-state to that of the R-state. It is this quaternary change in conformation that is considered responsible for the cooperative binding of oxygen, which results in the efficient transfer of oxygen to the tissues. Although other studies have suggested other conformational states for hemoglobin (Makino and Sugita, 1982; Smith et al., 1987; Perrella et al., 1990), these have also focused on the proximal side of the heme and the $\alpha_1\beta_2$ interface.

We have, however, demonstrated alterations in the conformation of hemoglobin that involve perturbations of the distal pocket that are transmitted across the $\alpha_1\beta_1$ interface to other subunits (Levy et al., 1992). These changes were originally demonstrated using valency hybrids where some subunits had Fe(II) hemes that bind oxygen and carbon monoxide, while other subunits had Fe(III) hemes that do not bind oxygen or carbon monoxide but can undergo configurational changes that are readily detected by electron paramagnetic resonance. Oxygen and carbon monoxide, which can both bind to the Fe(II) subunits, have different configurations when bound resulting in distinctly different interactions with the distal heme pocket. When the oxygen in the Fe(II) chains were replaced by carbon monoxide, these distal pocket changes were found to be transmitted to the Fe(III) subunit across the $\alpha_1\beta_1$ interface. Unlike the perturbations of the $\alpha_1\beta_2$ interface involved in the T to R quaternary conformational change, the $\alpha_1\beta_1$ interface does not undergo any noticeable structural changes. Instead, we are dealing with fluctuations transmitted through the interface from one subunit to another. These primarily dynamic changes are not readily detected by X-ray diffraction studies.

### Dynamic Coupling Between Subunits in Partially Oxygenated Hemoglobin

Our initial studies involved R-state valency hybrids where perturbations were induced by replacing oxygen with carbon monoxide. The demonstration that changes induced in the distal pocket by different ligands are transmitted across the $\alpha_1\beta_1$ interface implies closely coupled dynamic interactions between subunits. This same coupling would be expected to induce changes in T-state hemoglobin, with a more closely knit distal pocket, when oxygen is initially bound to deoxygenated hemoglobin producing partially oxygenated hemoglobin. This predicts that partially liganded hemoglobin, where one of the two subunits linked by the $\alpha_1\beta_1$ interface has a ligand and the other chain is unliganded, should result in perturbations in the ligand pocket that should be transmitted between subunits.

This process was originally demonstrated in studies involving the changes in the rates of hemoglobin autoxidation as

a function of the partial pressure of oxygen (Abugo and Rifkind, 1994; Balagopalakrishna et al., 1996). We, thus, found a dramatic increase in the rate of autoxidation for partially oxygenated hemoglobin (Abugo and Rifkind, 1994). This was interpreted in terms of a dramatic increase in fluctuations in the subunit with oxygen present as a result of the absence of a ligand in the coupled subunit. These increased fluctuations facilitate a nucleophilic interaction of the distal histidine with the bound oxygen resulting in the production of superoxide (**Figure 1**) (Balagopalakrishna et al., 1996).

More recently an analogous process was postulated to explain the release of NO from hemoglobin when deoxyhemoglobin (deoxyHb) reacts with nitrite (Nagababu et al., 2003b; Salgado et al., 2015). The initial reaction of nitrite with deoxyHb produces a hybrid intermediate with properties of $Hb(II)NO^+$, Hb(III)NO and ·SHb(II)NO (Salgado et al., 2009, 2011). The unique properties found for partially oxygenated hemoglobin are expected to be similar to those of any partially liganded hemoglobin. The hybrid intermediate produced when low levels of nitrite react with deoxyHb, is a partially liganded hemoglobin with a heme reacted with nitrite instead of oxygen. The same nucleophilic displacement reaction, which transfers an electron from the Fe(II) heme to the bound oxygen producing superoxide, will transfer an electron from the Fe(II) heme to the bound $NO^+$ producing NO (Salgado et al., 2015). This reaction is expected to result in the release of NO from hemoglobin (**Figure 2**) in the same way that autoxidation results in the release of ROS (**Figure 1**). The Fe(III)NO component of the hybrid intermediate has a very low affinity for the NO bound and will also release NO.

## Changes in the $\alpha_1\beta_1$ Interface Increase Membrane Affinity of Hemoglobin

The superoxide and NO released from hemoglobin would be expected to be neutralized by antioxidant enzymes (superoxide dismutase) and irreversible reactions with hemoglobin, respectively. We have, however, found that ROS generated in the erythrocyte can be transferred to the vasculature (Kiefmann et al., 2008). Such a transfer would have to involve the ROS from the erythrocyte membrane avoiding neutralization by the cytosolic antioxidant enzymes. A role for hemoglobin binding to band 3 of the erythrocyte membrane was further confirmed by the finding that blocking the band 3 binding site inhibits the transfer of ROS to the vasculature (Huertas et al., 2013).

Our studies with nitrite-reacted hemoglobin have demonstrated that partially liganded hemoglobin (in this case the nitrite-reacted deoxygenated hemoglobin) has a higher affinity for the erythrocyte membrane (presumably band 3) than deoxyhemoglobin, known to have a higher affinity than oxyhemoglobin (Cao et al., 2009; Salgado et al., 2015). We have, thus, shown that when erythrocytes are deoxygenated, the low levels of nitrite-reacted hemoglobin present are in large part associated with the limited membrane binding sites. This occurs even though there is a very large excess of deoxygenated hemoglobin not reacted with nitrite (Salgado et al., 2015). To rule out a specific effect involving nitrite reacted hemoglobin, we found that the affinity of nitrite reacted hemoglobin for the membrane was appreciably reduced when the sample was oxygenated. These results indicate that the increased affinity is associated with a partially liganded hemoglobin state irrespective of the ligand bound to the hemoglobin

This increased membrane-band 3 affinity for partially liganded hemoglobin can be attributed to the same increased fluctuations across the $\alpha_1\beta_1$ interface (Levy et al., 1992) that have been shown to increase the release of ROS and NO. The hemoglobin interfaces are involved in the binding of hemoglobin to the erythrocyte membrane band 3 (Chetrite and Cassoly, 1985). Interface interactions have been attributed to the significant increase in membrane affinity for T-state deoxyHb relative to R-state oxyhemoglobin (oxyHb). The increased fluctuations being transmitted across the $\alpha_1\beta_1$ interface for partially liganded hemoglobin can also affect the hemoglobin membrane-band 3 interactions. Such an interaction would explain the enhanced affinity of partially liganded hemoglobin for band 3 of the erythrocyte membrane (Salgado et al., 2015). We can, therefore, conclude that the same conformational change responsible for the enhanced formation of superoxide and NO from partially liganded hemoglobin, also results in a dramatic increase in the affinity of hemoglobin for the erythrocyte membrane (**Figure 3**).

## The Release of Superoxide and NO From Erythrocytes

As indicated above the erythrocyte cytoplasmic antioxidants and hemoglobin react with any ROS or NO released from hemoglobin. However, the dramatic increase in binding of partially oxygenated hemoglobin and nitrite-reacted hemoglobin to the membrane (**Figure 3**) results in a significant fraction of any released superoxide or NO diffusing out of the erythrocyte without being neutralized (**Figures 1**, **2**). The same conformational change enhances the formation of superoxide and NO (see above). For the NO reaction, by a determination

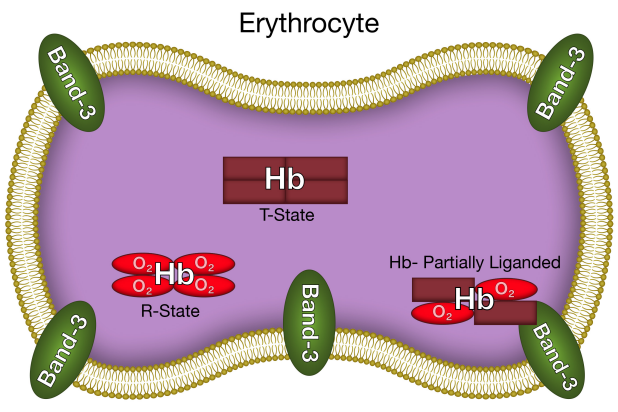


**FIGURE 3 |** The altered hemoglobin conformation of partially liganded hemoglobin that results in enhanced binding to the erythrocyte membrane.

of the NO in the gas phase above a solution of nitrite reacted hemoglobin, we have actually shown, that the altered interface fluctuations involved in binding hemoglobin to the membrane further enhances the nucleophilic displacement that enhances the release of NO from the erythrocyte (Salgado et al., 2015).

The unique conformation of partially liganded hemoglobin, involving fluctuations transmitted across the $\alpha_1\beta_1$ interface between adjacent subunits increase band 3 membrane interactions of hemoglobin (**Figure 3**) and nucleophilic interactions of the distal histidine with ligands bound to the ferrous heme (**Figures 1**, **2**). These changes provide a mechanism for the release of NO and ROS from the erythrocyte.

## TRANSFER OF REACTIVE ROS AND NO FROM THE ERYTHROCYTE TO THE VASCULATURE

It was demonstrated that under hypoxic conditions, the conformation of partially liganded hemoglobin facilitates the release of ROS and/or NO from the erythrocyte (see above). For ROS, we have demonstrated that the released ROS is transferred into capillary venules (Huertas et al., 2013; Kiefmann et al., 2008). Whether the transfer is due to diffusion across the narrow cell free layer present in capillaries (Ng et al., 2015) or a transient adherence of hypoxic erythrocytes to the vasculature is being investigated. It has further been demonstrated that this transfer induces an inflammatory response (Huertas et al., 2013) that can modulate vascular function.

Nitric oxide released from the erythrocyte can interact with platelets in the circulation inhibiting platelet activation (Wang et al., 1998). The resultant inhibition of platelet adhesion to the vascular endothelium can affect vascular function. It has also been reported that NO generated in the erythrocyte can dilate small mesenteric arteries (Ulker et al., 2013) suggesting that under certain conditions the highly reactive NO released from erythrocytes can interact directly with the vasculature.

These findings are supported by a computational study utilizing a multicellular model to simulate the transport of NO generated by nitrite from erythrocytes to the vasculature and the smooth muscle cells in arterioles (Chen et al., 2008). In this model, free diffusion of NO released in the cells provided only 0.04 pM NO in the smooth muscle cells, which is not expected to cause any vasodilatation. However, a membrane associated mechanism that protects NO bioactivity and facilitates its export out of the erythrocyte increases the level of NO that can react with the smooth muscle cells by 3 orders of magnitude to $\sim$ 43 pM and can cause vasodilatation. This dramatic increase took into account the diffusion of released NO back into the erythrocyte, where it can be scavenged by hemoglobin. Our studies involving the release of NO from hemoglobin bound to band 3 of the erythrocyte membrane reflects such a membrane-associated mechanism and is consistent with potential effects on the vasculature. The study by Liu et al. (2007) that concluded that NO generated in the erythrocyte cannot exert any physiological effects were limited to free diffusion of NO released in the cell with very high membrane permeability. Under such conditions interactions with the erythrocyte membrane were eliminated. Experiments are being planned to confirm the transfer of NO from the erythrocyte to the vasculature in the same way that we were able to show that ROS are transferred from the erythrocyte to the vasculature.

## CONCLUSION

A completely new perspective in our understanding of interactions between erythrocytes and the vasculature is provided by these studies. A distinct conformation of hemoglobin under hypoxic conditions provides a mechanism for the release of NO and ROS from the erythrocytes (**Figure 3**). Furthermore, at least in arterioles and narrow capillaries, these molecules can potentially be transferred to the vasculature (**Figures 1**, **2**).

For ROS, this transfer into the vasculature under hypoxic conditions has been demonstrated (Kiefmann et al., 2008). Additional studies are required to demonstrate that NO released into the lumen from the erythrocyte can diffuse into the smooth muscle cells of arterioles to induce vasodilatation.

We are also investigating a possible role for erythrocyte adherence to the vasculature. Such adherence that is involved in many pathological conditions (Setty and Stuart, 1996) provides a mechanism for increasing the time the erythrocyte is in contact with the endothelium. Such an interaction would also be expected to increase the transfer of both NO and ROS to the vasculature.

For the release of ROS and transfer of ROS to the vasculature, hemoglobin must be partially oxygenated (**Figure 1**). However, the hemoglobin conformation that triggers membrane binding and the potential transfer of NO utilizes a partially liganded hemoglobin involving the nitrite reacted intermediate and does not require an oxygen bound to the hemoglobin (**Figure 2**). This process is therefore able to deliver NO to the vasculature even under very low partial pressures of oxygen where NO synthase is unable to generate NO. The transfer of NO from the erythrocyte to the vasculature can, therefore, play an important role in regulating vascular function when an impaired vasculature and/or reduced levels of oxygen limit the production of NO.

## AUTHOR CONTRIBUTIONS

JR was responsible for all the research that led to this hypothesis originally as section chief of Molecular Dynamics at the National Institute on Aging. While at Johns Hopkins these ideas were finalized and the manuscript was written. JM was responsible for the figures and the bibliography. He also helped formulate the hypothesis and write the manuscript. EN played a major role in our understanding of the formation of nitric oxide and reactive oxygen species by erythrocytes. MS performed crucial experiments on the formation and release of nitric oxide formed in erythrocytes due to the reaction of nitrite with deoxyhemoglobin. ZC did crucial experiments

involving the association of partially oxygenated hemoglobin and nitrite reacted hemoglobin with the erythrocyte membrane. This binding is what facilitates the release of nitric oxide and reactive oxygen species from the erythrocyte.

## FUNDING

This research was supported (in part) by the Intramural Research Program of the NIH, National Institute on Aging.

## REFERENCES


Aamand, R., Dalsgaard, T., Jensen, F. B., Simonsen, U., Roepstorff, A., and Fago, A. (2009). Generation of nitric oxide from nitrite by carbonic anhydrase: a possible link between metabolic activity and vasodilation. *Am. J. Physiol. Heart Circ. Physiol.* 297, H2068–H2074. doi: 10.1152/ajpheart.00525.2009

Abugo, O. O., and Rifkind, J. M. (1994). Oxidation of hemoglobin and the enhancement produced by nitroblue tetrazolium. *J. Biol. Chem.* 269, 24845–24853.

Balagopalakrishna, C., Manoharan, P. T., Abugo, O. O., and Rifkind, J. M. (1996). Production of superoxide from hemoglobin-bound oxygen under hypoxic conditions. *Biochemistry* 35, 6393–6398. doi: 10.1021/bi952875+

Cao, Z., Bell, J. B., Mohanty, J. G., Nagababu, E., and Rifkind, J. M. (2009). Nitrite enhances RBC hypoxic ATP synthesis and the release of ATP into the vasculature: a new mechanism for nitrite-induced vasodilation. *Am. J. Physiol. Heart Circ. Physiol.* 297, H1494–H1503. doi: 10.1152/ajpheart.01233.2008

Chen, K., Pittman, R. N., and Popel, A. S. (2008). Nitric oxide in the vasculature: where does it come from and where does it go? A quantitative perspective. *Antioxid. Redox Signal.* 10, 1185–1198. doi: 10.1089/ars.2007.1959

Chetrite, G., and Cassoly, R. (1985). Affinity of hemoglobin for the cytoplasmic fragment of human erythrocyte membrane band 3. Equilibrium measurements at physiological pH using matrix-bound proteins: the effects of ionic strength, deoxygenation and of 2,3-diphosphoglycerate. *J. Mol. Biol.* 185, 639–644.

Cosby, K., Partovi, K. S., Crawford, J. H., Patel, R. P., Reiter, C. D., Martyr, S., et al. (2003). Nitrite reduction to nitric oxide by deoxyhemoglobin vasodilates the human circulation. *Nat. Med.* 9, 1498–1505. doi: 10.1038/nm954

Dalsgaard, T., Simonsen, U., and Fago, A. (2007). Nitrite-dependent vasodilation is facilitated by hypoxia and is independent of known NO-generating nitrite reductase activities. *Am. J. Physiol. Heart Circ. Physiol.* 292, H3072–H3078. doi: 10.1152/ajpheart.01298.2006

Dimmeler, S., and Zeiher, A. M. (2000). Reactive oxygen species and vascular cell apoptosis in response to angiotensin II and pro-atherosclerotic factors. *Regul. Pept.* 90, 19–25. doi: 10.1016/S0167-0115(00)00105-1

Fermi, G., Perutz, M. F., Shaanan, B., and Fourme, R. (1984). The crystal structure of human deoxyhaemoglobin at 1.74 A resolution. *J. Mol. Biol.* 175, 159–174. doi: 10.1016/0022-2836(84)90472-8

Huertas, A., Das, S. R., Emin, M., Sun, L., Rifkind, J. M., Bhattacharya, J., et al. (2013). Erythrocytes induce proinflammatory endothelial activation in hypoxia. *Am. J. Respir. Cell Mol. Biol.* 48, 78–86. doi: 10.1165/rcmb.2011-0402OC

Ignarro, L. J., Cirino, G., Casini, A., and Napoli, C. (1999). Nitric oxide as a signaling molecule in the vascular system: an overview. *J. Cardiovasc. Pharmacol.* 34, 879–886. doi: 10.1097/00005344-199912000-00016

Kelm, M., Dahmann, R., Wink, D., and Feelisch, M. (1997). The nitric oxide/superoxide assay. Insights into the biological chemistry of the NO/O-2. interaction. *J. Biol. Chem.* 272, 9922–9932. doi: 10.1074/jbc.272.15.9922

Kiefmann, R., Rifkind, J. M., Nagababu, E., and Bhattacharya, J. (2008). Red blood cells induce hypoxic lung inflammation. *Blood* 111, 5205–5214. doi: 10.1182/blood-2007-09-113902

Kleinbongard, P., Schulz, R., Rassaf, T., Lauer, T., Dejam, A., Jax, T., et al. (2006). Red blood cells express a functional endothelial nitric oxide synthase. *Blood* 107, 2943–2951. doi: 10.1182/blood-2005-10-3992

Lancaster, J. R. Jr. (1994). Simulation of the diffusion and reaction of endogenously produced nitric oxide. *Proc. Natl. Acad. Sci. U.S.A.* 91, 8137–8141. doi: 10.1073/pnas.91.17.8137

Levy, A., Abugo, O., Franks, M., and Rifkind, J. M. (1991). Evidence that autoxidation of oxyhemoglobin involves the displacement of oxygen as a superoxide radical. *J. Inorg. Biochem.* 43:327. doi: 10.1016/0162-0134(91)84314-Y

Levy, A., Sharma, V. S., Zhang, L., and Rifkind, J. M. (1992). A new mode for heme-heme interactions in hemoglobin associated with distal perturbations. *Biophys. J.* 61, 750–755. doi: 10.1016/S0006-3495(92)81879-9

Li, H., Cui, H., Kundu, T. K., Alzawahra, W., and Zweier, J. L. (2008). Nitric oxide production from nitrite occurs primarily in tissues not in the blood: critical role of xanthine oxidase and aldehyde oxidase. *J. Biol. Chem.* 283, 17855–17863. doi: 10.1074/jbc.M801785200

Liu, X., Miller, M. J., Joshi, M. S., Sadowska-Krowicka, H., and Clark, D. A. (1998). Diffusion-limited reaction of free nitric oxide with erythrocytes. *J. Biol. Chem.* 273, 18709–18713. doi: 10.1074/jbc.273.30.18709

Liu, X., Yan, Q., Baskerville, K. L., and Zweier, J. L. (2007). Estimation of nitric oxide concentration in blood for different rates of generation. Evidence that intravascular nitric oxide levels are too low to exert physiological effects. *J. Biol. Chem.* 282, 8831–8836. doi: 10.1074/jbc.M611684200

Makino, N., and Sugita, Y. (1982). The structure of partially oxygenated hemoglobin. A highly reactive intermediate toward a sulfhydryl titrant. *J. Biol. Chem.* 257, 163–168.

Nagababu, E., Chrest, F. J., and Rifkind, J. M. (2003a). Hydrogen-peroxide-induced heme degradation in red blood cells: the protective roles of catalase and glutathione peroxidase. *Biochim. Biophys. Acta* 1620, 211–217.

Nagababu, E., Ramasamy, S., Abernethy, D. R., and Rifkind, J. M. (2003b). Active nitric oxide produced in the red cell under hypoxic conditions by deoxyhemoglobin-mediated nitrite reduction. *J. Biol. Chem.* 278, 46349–46356.

Nagababu, E., and Rifkind, J. M. (2004). Heme degradation by reactive oxygen species. *Antioxid. Redox Signal.* 6, 967–978. doi: 10.1089/ars.2004.6.967

Ng, Y. C., Namgung, B., and Kim, S. (2015). Two-dimensional transient model for prediction of arteriolar NO/O2 modulation by spatiotemporal variations in cell-free layer width. *Microvasc. Res.* 97, 88–97. doi: 10.1016/j.mvr.2014.08.010

Perrella, M., Benazzi, L., Shea, M. A., and Ackers, G. K. (1990). Subunit hybridization studies of partially ligated cyanomethemoglobins using a cryogenic method. Evidence for three allosteric states. *Biophys. Chem.* 35, 97–103. doi: 10.1016/0301-4622(90)80064-E

Perutz, M. F. (1970). Stereochemistry of cooperative effects in haemoglobin. *Nature* 228, 726–739. doi: 10.1038/228726a0

Rifkind, J. M., Nagababu, E., Ramasamy, S., and Ravi, L. B. (2003). Hemoglobin redox reactions and oxidative stress. *Redox Rep.* 8, 234–237. doi: 10.1179/135100003225002817

Salgado, M. T., Cao, Z., Nagababu, E., Mohanty, J. G., and Rifkind, J. M. (2015). Red blood cell membrane-facilitated release of nitrite-derived nitric oxide bioactivity. *Biochemistry* 54, 6712–6723. doi: 10.1021/acs.biochem.5b00643

Salgado, M. T., Nagababu, E., and Rifkind, J. M. (2009). Quantification of intermediates formed during the reduction of nitrite by deoxyhemoglobin. *J. Biol. Chem.* 284, 12710–12718. doi: 10.1074/jbc.M808647200

Salgado, M. T., Ramasamy, S., Tsuneshige, A., Manoharan, P. T., and Rifkind, J. M. (2011). A new paramagnetic intermediate formed during the reaction of nitrite with deoxyhemoglobin. *J. Am. Chem. Soc.* 133, 13010–13022. doi: 10.1021/ja1115088

Setty, B. N., and Stuart, M. J. (1996). Vascular cell adhesion molecule-1 is involved in mediating hypoxia-induced sickle red blood cell adherence to endothelium: potential role in sickle cell disease. *Blood* 88, 2311–2320.

Shaanan, B. (1983). Structure of human oxyhaemoglobin at 2.1 A resolution. *J. Mol. Biol.* 171, 31–59. doi: 10.1016/S0022-2836(83)80313-1

Smith, F. R., Gingrich, D., Hoffman, B. M., and Ackers, G. K. (1987). Three-state combinatorial switching in hemoglobin tetramers: comparison between functional energetics and molecular structures. *Proc. Natl. Acad. Sci. U.S.A.* 84, 7089–7093. doi: 10.1073/pnas.84.20.7089

Staiculescu, M. C., Foote, C., Meininger, G. A., and Martinez-Lemus, L. A. (2014). The role of reactive oxygen species in microvascular remodeling. *Int. J. Mol. Sci.* 15, 23792–23835. doi: 10.3390/ijms151223792

Taniyama, Y., and Griendling, K. K. (2003). Reactive oxygen species in the vasculature: molecular and cellular mechanisms. *Hypertension* 42, 1075–1081. doi: 10.1161/01.HYP.0000100443.09293.4F

Ulker, P., Gunduz, F., Meiselman, H. J., and Baskurt, O. K. (2013). Nitric oxide generated by red blood cells following exposure to shear stress dilates isolated small mesenteric arteries under hypoxic conditions. *Clin. Hemorheol. Microcirc.* 54, 357–369. doi: 10.3233/CH-2012-1618

Wang, G. R., Zhu, Y., Halushka, P. V., Lincoln, T. M., and Mendelsohn, M. E. (1998). Mechanism of platelet inhibition by nitric oxide: *in vivo* phosphorylation of thromboxane receptor by cyclic GMP-dependent protein kinase. *Proc. Natl. Acad. Sci. U.S.A.* 95, 4888–4893. doi: 10.1073/pnas.95.9.4888

**Conflict of Interest Statement:** The authors declare that the research was conducted in the absence of any commercial or financial relationships that could be construed as a potential conflict of interest.

*Copyright © 2018 Rifkind, Mohanty, Nagababu, Salgado and Cao. This is an open-access article distributed under the terms of the Creative Commons Attribution License (CC BY). The use, distribution or reproduction in other forums is permitted, provided the original author(s) and the copyright owner are credited and that the original publication in this journal is cited, in accordance with accepted academic practice. No use, distribution or reproduction is permitted which does not comply with these terms.*

frontiers in Physiology

ORIGINAL RESEARCH
published: 11 May 2018
doi: 10.3389/fphys.2018.00332

# On the Effects of Reactive Oxygen Species and Nitric Oxide on Red Blood Cell Deformability

*Lukas Diederich[1], Tatsiana Suvorava[1], Roberto Sansone[1], T. C. Stevenson Keller IV[1,2], Frederik Barbarino[1], Thomas R. Sutton[3], Christian M. Kramer[1], Wiebke Lückstädt[1], Brant E. Isakson[2], Holger Gohlke[4], Martin Feelisch[3], Malte Kelm[1,5] and Miriam M. Cortese-Krott[1]**

[1] Cardiovascular Research Laboratory, Division of Cardiology, Pneumology and Vascular Medicine, Medical Faculty, Heinrich-Heine-University Düsseldorf, Düsseldorf, Germany, [2] Department of Molecular Physiology and Biological Physics, Robert M. Berne Cardiovascular Research Center, University of Virginia, Charlottesville, VA, United States, [3] Clinical & Experimental Sciences, Faculty of Medicine, University of Southampton, Southampton, United Kingdom, [4] Faculty of Mathematics and Natural Sciences, Institute for Pharmaceutical and Medicinal Chemistry, Heinrich-Heine-University Düsseldorf, Düsseldorf, Germany, [5] Medical Faculty, Cardiovascular Research Institute Düsseldorf, Heinrich-Heine-University Düsseldorf, Düsseldorf, Germany

OPEN ACCESS

**Edited by:**
Joseph M. Rifkind,
Johns Hopkins University,
United States

**Reviewed by:**
Sanjay Khandelwal,
Duke University, United States
Pingnian He,
Pennsylvania State University,
United States
Anna Bogdanova,
Universität Zürich, Switzerland

***Correspondence:**
Miriam M. Cortese-Krott
miriam.cortese@uni-duesseldorf.de

**Specialty section:**
This article was submitted to Vascular Physiology, a section of the journal Frontiers in Physiology

**Received:** 30 October 2017
**Accepted:** 16 March 2018
**Published:** 11 May 2018

**Citation:**
Diederich L, Suvorava T, Sansone R, Keller TCS IV, Barbarino F, Sutton TR, Kramer CM, Lückstädt W, Isakson BE, Gohlke H, Feelisch M, Kelm M and Cortese-Krott MM (2018) On the Effects of Reactive Oxygen Species and Nitric Oxide on Red Blood Cell Deformability. Front. Physiol. 9:332. doi: 10.3389/fphys.2018.00332

The main function of red blood cells (RBCs) is the transport of respiratory gases along the vascular tree. To fulfill their task, RBCs are able to elastically deform in response to mechanical forces and, pass through the narrow vessels of the microcirculation. Decreased RBC deformability was observed in pathological conditions linked to increased oxidative stress or decreased nitric oxide (NO) bioavailability, like hypertension. Treatments with oxidants and with NO were shown to affect RBC deformability *ex vivo*, but the mechanisms underpinning these effects are unknown. In this study we investigate whether changes in intracellular redox status/oxidative stress or nitrosation reactions induced by reactive oxygen species (ROS) or NO may affect RBC deformability. In a case-control study comparing RBCs from healthy and hypertensive participants, we found that RBC deformability was decreased, and levels of ROS were increased in RBCs from hypertensive patients as compared to RBCs from aged-matched healthy controls, while NO levels in RBCs were not significantly different. To study the effects of oxidants on RBC redox state and deformability, RBCs from healthy volunteers were treated with increasing concentrations of *tert*-butylhydroperoxide (*t*-BuOOH). We found that high concentrations of *t*-BuOOH ($\geq$ 1 mM) significantly decreased the GSH/GSSG ratio in RBCs, decreased RBC deformability and increased blood bulk viscosity. Moreover, RBCs from Nrf2 knockout (KO) mice, a strain genetically deficient in a number of antioxidant/reducing enzymes, were more susceptible to *t*-BuOOH-induced impairment in RBC deformability as compared to wild type (WT) mice. To study the role of NO in RBC deformability we treated RBC suspensions from human volunteers with NO donors and nitrosothiols and analyzed deformability of RBCs from mice lacking the endothelial NO synthase (eNOS). We found that NO donors induced S-nitrosation of the cytoskeletal protein spectrin, but did not affect human RBC deformability or blood bulk viscosity; moreover, under unstressed conditions RBCs from eNOS KO mice showed

fully preserved RBC deformability as compared to WT mice. Pre-treatment of human RBCs with nitrosothiols rescued *t*-BuOOH-mediated loss of RBC deformability. Taken together, these findings suggest that NO does not affect RBC deformability *per se*, but preserves RBC deformability in conditions of oxidative stress.

**Keywords: erythrocytes, thiols, non-canonical function, mechanotransduction, RBC deformability, nitric oxide synthase, reactive oxygen species**

## INTRODUCTION

The biochemical, biophysical, and mechanical properties of RBCs, as well as their structural characteristics are optimized for their function. RBCs carry a very high (supersaturated) concentration of hemoglobin (equivalent to 10 mM heme), which is kept in the reduced $Fe^{2+}$/oxygen binding state by a battery of antioxidant and reducing enzymes (Kuhn et al., 2017). In addition, the peculiar cytoskeleton, which is mainly composed of hexagonal aligned units of spectrin, confers stability, flexibility, and elasticity of the cells. The distribution and biophysical characteristics of the cytoskeletal proteins (mainly spectrin) are responsible for their typical biconcave "donut-like" shape. RBC shape and deformability allow the cells to dynamically adapt to changes in hydrodynamic forces along the vascular tree, and to squeeze through capillaries smaller than their own diameter at rest (Kuhn et al., 2017).

RBC deformability was found to be decreased in several disease states associated with oxidative stress and endothelial dysfunction and/or impaired nitric oxide (NO) bioavailability, such as hypertension and diabetes (Cicco and Pirrelli, 1999; Cicco et al., 1999a,b, 2001; Turchetti et al., 1999; Vetrugno et al., 2004; Radosinska and Vrbjar, 2016; Lee et al., 2017). Interestingly, a linear relationship between deformability and RBC oxidative stress has been documented in studies involving sickle cell disease patients (Barodka et al., 2014a). In disease states, reactive oxygen species (ROS)-mediated damage of RBC membrane components is thought to increase erythrocyte membrane rigidity and fragility, resulting in intravascular hemolysis, release of hemoglobin into the plasma, and systemic NO scavenging. In spite of the clinical significance of these phenomena the biological chemistry and biochemistry of the processes that control physiological RBC deformability in health and disease, and the underlying signaling pathways remain poorly characterized.

There is compelling evidence that treatment of RBCs with thiol-reactive molecules such as diamide or oxidants such as peroxides not only strongly impair RBC deformability (Fischer et al., 1978; Corry et al., 1980), but also change RBC shape (Becker et al., 1986; Mcgough and Josephs, 1990), suggesting an important role of intracellular redox status in control of RBC deformability and structural characteristics. In contrast, treatment with NO donors was shown to improve RBC deformability (Bor-Kucukatay et al., 2003; Grau et al., 2013; Riccio et al., 2015), while treatment with nitric oxide synthase (NOS) inhibitors impaired RBC deformability (Bor-Kucukatay et al., 2003; Grau et al., 2013, 2015). *S*-nitrosation of intracellular proteins such as hemoglobin or spectrin (Grau et al., 2015) and/or activation of soluble guanylate cyclase (sGC) (Bor-Kucukatay et al., 2003) have all been proposed to be involved in these effects. However, these findings are not without controversy. Recent studies have shown that treatment of human RBCs with the NO donors DEA/NO, sodium nitroprusside, and NO synthase (NOS) substrate L-arginine did not improve deformability of RBCs (Barodka et al., 2014b; Belanger et al., 2015). Similarly, neither NOS inhibition nor inhibition of sGC in RBCs affect their deformability (Barodka et al., 2014b; Cortese-Krott et al., 2017). The reasons for these discrepancies are unknown.

In this work, we investigated whether and how changes in intracellular redox status of RBCs, NO, and nitrosation reactions affect RBC deformability. According to previous studies referred to above (Sandhagen et al., 1990; Vaya et al., 1992; Cicco and Pirrelli, 1999; Cicco et al., 1999a,b, 2001; Radosinska and Vrbjar, 2016), we found that hypertensive patients show decreased RBC deformability; interestingly, this was accompanied by an increase in intracellular ROS levels, with unchanged intracellular NO levels. In *ex vivo* experiments carried out with isolated RBCs, we found that changes in intracellular redox status provoked by an oxidant challenge with high concentrations of *t*-BuOOH decreases RBC deformability and increases blood viscosity. Although treatment with NO donors did not significantly affect RBC deformability *per se*, it protected RBCs from adverse changes induced by oxidants. Preserving the antioxidant capacity of RBCs would therefore seem to be of fundamental importance not only to protect membrane integrity and avoid hemolysis, but also to maintain RBC deformability in response to hydrodynamic forces.

## MATERIALS AND METHODS

### Materials and Stock Solutions

Unless not indicated otherwise, all chemicals were purchased by Sigma Aldrich (Darmstadt, Germany) and were of the highest purity available. MilliQ quality water was used to prepare all home-made solutions (Millipore, Darmstadt, Germany), Hank's balanced salt solution with $Ca^{2+}$ ($HBSS^{+}$)(1.26 mM $CaCl_2$, 0.49 mM $MgCl_2$ x $6H_2O$, 0.41 $MgSO_4$ x $7H_2O$, 5.33 mM KCl, 0.44 $KH_2PO_4$, 4.12 $NaHCO_3$, 137.93 mM NaCl, 0.34 mM $Na_2HPO_4$, 5.56 mM D-glucose) was purchased by Life technologies. Working solutions of *tert*-butylhydroperoxide (*t*-BuOOH) were prepared by diluting 1 M stock in $HBSS^{+}$. Stock solutions of 2-(N,N-diethylamino)-diazenolate-2-oxide (DEA/NO) (50 mM) were prepared in 10 mM NaOH and kept on ice until use. Stock solutions of nitrosated cysteine (CysNO) were prepared as described (Cortese-Krott et al., 2012a).

Briefly, 200 mM stock solution of nitrite (VWR, Darmstadt, Germany) and acidified L-cysteine hydrochloride were mixed in equal part, equilibrated to neutral pH, kept on ice in the dark until use and diluted to final concentrations in $HBSS^+$.

## Human Study and Collection of Human Blood Samples

For *ex vivo* analyses, young (20–40 years old), healthy volunteers were recruited and gave written informed consent to participate before enrollment (ClinicalTrials.gov Identifier: NCT02272530). To analyze the effects of hypertension on RBC function, study participants (40–60 years old, average age 50.6 ± 6.9 years for hypertensive subjects and 47.8 ± 5.5 years for healthy subjects) were recruited from the outpatient clinic of the Department of Cardiology, Pneumology and Angiology, University Hospital Düsseldorf. The study was approved by the ethics committee of the Heinrich-Heine-University (HHU) of Düsseldorf, and registered in the coordination center for clinical trials of HHU (KKS, registration ID 201307443). Both studies were conducted in accordance with the Declaration of Helsinki. Clinical protocol and patients' characteristics are described in the Supplemental Information (Table S1).

## Determination of Intracellular ROS by Flow Cytometry

For determination of ROS in RBCs, blood was collected from the antecubital vein of human donors into tubes containing heparin (5000 I.U.), kept on ice and processed within 2 h. Blood was diluted 1:500 with ice cold Dulbecco's phosphate buffered solution (PBS) to reach a final RBC concentration of $\sim 4 \times 10^5$ RBC/μL and divided into 1 ml aliquots. Aliquots were treated for 30 min either with 20 μM diclorofluoresceine diacetate (DCF-DA, Invitrogen, Germany) to assess ROS, or with 20 μM Thiol Tracker (TT, Invitrogen) to assess free thiols, or 10 μM 4-amino-5-methylamino-2′,7′-difluorofluorescein-diacetate (DAF-FM, Invitrogen) to assess NO levels, washed, and analyzed in a FACS BD FACSCanto II flow cytometer (BD Bioscience, Heidelberg, Germany) as described (Cortese-Krott et al., 2012a).

## Collection of Blood From Nrf2 KO, eNOS KO, and WT Mice

All mouse experiments were approved by the LANUV (State Agency for Nature, Environment and Consumer Protection) and conducted in agreement with the German "Tierschutzgesetz" and the "Guide for the Care and Use of Laboratory Animals" of the US National Research Council. The mouse strains used in this study were wildtype C57BL/6J (WT) (Janvier, France), Nrf2 knockout (Nrf2 KO) (BRC No. 01390); kindly provided by Rinken (Koyadai, Tsukuba, Ibaraki, Japan) and endothelial NOS knockout (eNOS KO) (Godecke et al., 1998). Mouse whole blood was drawn in anesthetized mice by cardiac puncture using heparin as anticoagulant.

## Determination of Shear-Induced Elongation of RBCs by Ektacytometry

For determination of shear-induced elongation of RBCs, 25 μL of whole blood or RBC pellet (as indicated in the figure legends) were added to 5 mL pre-warmed (37°C) high viscosity PVP solution (RR Mechatronics, Hoorn, The Netherlands) to yield a cell suspension behaving closely to a Newtonian liquid. Using the laser optical rotational red cell analyzer (Lorrca, RR Mechatronics), the elongation index (EI) was measured at a range of different shear stresses (0.30–50 Pa), as indicated in the figures. For *Lineweaver-Burk* transformation, the reciprocal values for the deformability index were plotted against the reciprocal values of the respective shear stress. After linear regression, maximal deformability ($EI_{max}$) and half maximal shear stress ($SS_{1/2max}$) were calculated as described previously (Baskurt and Meiselman, 2013).

## Determination of Whole Blood Bulk Viscosity by Low Shear Viscosimetry

Whole blood viscosity measurements were conducted using the LS300 viscometer (proRheo, Althengstett, Germany) as described by Ruef et al. (2014). Briefly 1 mL of treated whole blood suspension was measured at 37°C for a range of different shear rates (0.5–150 1/s).

## RBC Isolation

Human and mouse RBC isolation was carried out as described before (Cortese-Krott et al., 2017). Briefly, human whole blood anticoagulated with heparin was transferred into a 20 ml syringe and centrifuged at 800 g for 10 min at 4°C; plasma and buffy coat were aspirated from the top and RBCs were eluted from the bottom of the syringe. The RBC pellet was washed three times with $HBSS^+$ by centrifugation at 300 g, for 10 min at 4°C. RBC pellets were kept on ice or equilibrated in pre-warmed $HBSS^+$ at 37°C at a cell concentration of 40% hematocrit (hct) on a rolling plate until used for experiments, as indicated below. Mouse RBCs were separated similarly to human RBCs except the centrifugation steps were carried out in Eppendorf tubes.

## Determination of GSH and GSSG in RBCs by Liquid Chromatography/Mass Spectrometry

A defined volume (100 μL) of RBC pellet was lysed and protein precipitated in a solution containing 5% sulfosalicylic acid (SSA) and 10 mM N-ethylmaleimide (NEM) in double distilled water (ratio 1:5). After addition of the internal standard (2 mM glutathione ethylester), cell lysis was completed in an ultrasonic bath for 20 s. Afterwards, samples were centrifuged for 10 min, 10,000 g, and at 4°C. Cell pellets were washed once with the same volume buffer used before, centrifuged with the configurations used in the last step, and both supernatants were merged. To separate analytes, a gradient elution on a Zorbax Eclipse Plus C18 RRHD 2.1× 50 mm 1.8 μm (Agilent) was chosen with 0.1% formic acid in double distilled water (A) and acetonitrile (B) (0–2 min: 99% A, 1% B; 2–7 min: 99% A, B 1%→1% A, 99% B; 7–12 min: 1% A, 99% B; 12–12.1 min: 1% A, 99% B→99%

A, 1% B, 12.1–16 min 99% A, 1% B) on a 1290 Infinity UPLC system (Agilent, Waldbronn, Germany) and analyzed in an Agilent 6550 iFunnel Accurate-Mass Quadrupole Time-of-Flight Mass Spectrometer (Q-TOF MS). Ionization source was set to positive mode with the configurations: gas temperature 220°C, drying gas 12 l/min, nebulizer 35 psig, sheath gas temperature 330°C, sheath gas flow 11 l/min, Vcapillary 2500 V, nozzle voltage 1000 V, fragmentor 30 V. Data were analyzed using an Agilent MassHunter Workstation Software (Agilent).

## Effects of *t*-BuOOH on GSH/GSSG Levels in Human RBCs

To analyze the effects of *t*-BuOOH on glutathione (GSH) and glutathione-disulfide (GSSG) levels in human RBCs, washed human RBC suspensions at 40% hct were incubated for 10 min at 37°C with increasing concentrations of *t*-BuOOH (1 nM−10 mM, as indicated in the figure legend), then centrifuged at 300 g for 5 min at 4°C, put on ice, and used immediately for GSH and GSSG determination. We decided to measure reduced and oxidized glutathione since the use of the half redox potential has been criticized as being less relevant in cell physiological processes (Flohe, 2013).

## Effects of *t*-BuOOH and NO Donors on RBC Deformability and Bulk Blood Viscosity

To analyze the effects of *t*-BuOOH on both shear induced elongation and bulk blood viscosity in parallel, whole blood of each sample was split into 1 mL aliquots, and blood samples were incubated by addition of 100 μL *t*-BuOOH working solutions to reach the concentrations corresponding to 3, 5, and 7 mM *t*-BuOOH. Incubation times from 10 min at 37°C were followed by measurements of deformability (see section Determination of Shear-Induced Elongation of RBCs by Ektacytometry) and viscosity (see section Determination of Whole Blood Bulk Viscosity by Low Shear Viscosimetry) under the same experimental conditions. To examine the effects of *t*-BuOOH on RBCs from Nrf2 KO mice and WT mice, RBC pellets were diluted at 0.8% hct in $HBSS^+$, and treated for 20 min with *t*-BuOOH at room temperature (RT). Cells were pelleted by centrifugation (800 g, 4°C, 10 min) and washed with $HBSS^+$ and deformability measured as described in section Determination of Shear-Induced Elongation of RBCs by Ektacytometry. To test the effects of NO under conditions used by previous studies (see Table S8), RBC suspensions in $HBSS^+$ buffer (see section Determination of Shear-Induced Elongation of RBCs by Ektacytometry) at 1.6% hct were treated with DEA/NO (0–200 μM) and incubated for 10 min at 37°C, pelleted by centrifugation at 800 g for 10 min, and suspended in buffer before analysis. To determine the effects of nitrosothiols, RBC suspensions in $HBSS^+$ (see section RBC Isolation) at 25% hct were treated with CysNO as indicated for 10 min at 37°C and pelleted by centrifugation at 800 g for 10 min and re-suspended in $HBSS^+$ before analysis. In a further series of experiments, samples were treated with CysNO as indicated for 10 min at 37°C, washed two times with 4 volumes of $HBSS^+$ buffer by centrifugation for 5 min at 800 g at 4°C, and then treated with 3 mM *t*-BuOOH for 10 min at 37°C. Cells were pelleted by centrifugation (800 g, 4°C, 10 min) and re-suspended in $HBSS^+$ before analysis. In addition, these experiments were carried out in reversal with *t*-BuOOH incubation first and CysNO second.

## Detection of Spectrin Nitrosation by Biotin Switch Assay

RBC suspensions were prepared by diluting 500 μL of washed RBCs in PBS (137 mM NaCl, 2.7 mM KCl, 10 mM $Na_2HPO_4$, 1.8 mM $KH_2PO_4$, pH = 7.4) containing diethylenetriaminepentaacetic acid (1 μM) and incubated with $10^{-9}$-$10^{-2}$ M concentrations of CysNO for 30 min at RT. CysNO was subsequently removed by ultrafiltration using Pall Nanosep 10 kDA MWCO spin columns. RBCs were re-suspended in lysis buffer with protease inhibitors [150 mM $NH_4Cl$, cOmplete ULTRA Tablets (Roche), in $H_2O$]. After protein determination by Lowry (DC Protein Assay, Bio-Rad, München, Germany), a biotin switch assay was carried out to determine the extent of S-nitrosation. The assay was performed according to manufacturer's protocol using a concentration of 0.8 mg/mL protein (*S*-Nitrosylated Protein Detection Kit, Cayman, Ann Arbor, USA). Samples were loaded onto a 7% Nupage Novex Tris/Acetate precast gel, and a Western blot was performed as described elsewhere (Cortese-Krott et al., 2017). Membranes were incubated with a primary mouse anti-spectrin antibody (1:1000) from Sigma Aldrich at 4°C overnight, followed by parallel assessment of spectrin and biotin signals on the same nitrocellulose membrane using anti-mouse Cy3-coupled antibodies (Thermo Fisher) and strepdavidin- coupled to the Cy5 fluorophore (Thermo-Fisher).

## Statistics

All data were analyzed by using GraphPad Prism PC software (version 6.01; Graph Pad, La Jolla, CA, USA), and are expressed as means ± S.E.M. of n individual samples as stated in Results and Figure legends. Statistical comparisons between groups were performed by one-way or two-way ANOVA as required by experimental setting, followed by an appropriate multiple comparison *post-hoc* test (Dunnet's or Sidak's) or *t*-test as indicated in the figure legend. Comparison of data from hypertensive subjects with aged-matched controls was carried out by non-parametric Mann-Whitney-*U*-testing. $P < 0.05$ was considered statistically significant.

# RESULTS

## RBCs From Hypertensive Patients Have Decreased Deformability and Increased Intracellular ROS Levels

The bulk of data on the effects of pathological conditions on RBC deformability show that RBCs of patients with hypertension have significantly decreased RBC deformability (Sandhagen et al., 1990; Vaya et al., 1992; Cicco and Pirrelli, 1999; Cicco et al., 1999a,b, 2001; Turchetti et al., 1999; Vetrugno et al., 2004; Radosinska and Vrbjar, 2016). Hypertension is a complex

condition, which is accompanied by endothelial dysfunction and reduced NO bioavailability. A characterization of RBC deformability in relation to redox status/NO levels in RBCs of hypertensive patients was never carried out before. Therefore, we carried out an observational study where RBCs from hypertensive patients were compared with RBCs from aged matched individuals without hypertension (see supplemental information Table S1 for patient characteristics). We measured RBC characteristics including RBC deformability, ROS levels, NO levels, and total free thiol levels.

We found that RBCs from patients with hypertension showed significantly decreased shear-induced elongation, as assessed by ektacytometry in a LORCA; in fact, we found that the EI was decreased at low shear rates (1.73 Pa: healthy 0.275 ± 0.022, hypertension: 0.2568 ± 0.007; $p = 0.056$; Table S2) and at 2.68 Pa (**Figure 1A**), while no difference was detectable at higher shear rates. The data were analyzed using the Lineweaver-Burk transformation (Baskurt and Meiselman, 2013) by plotting the reciprocal values of EI against the reciprocal shear stress ($r^2_{\text{hypertension}} = 0.91$, $r^2_{\text{healthy}} = 0.83$). We found that $SS_{1/2max}$ and $EI_{max}$ were not significantly different in hypertensive subjects as compared to age-matched controls (Table S2).

We also found a significant increase of intracellular levels of ROS (assessed by intracellular DCF fluorescence by flow cytometry) in RBCs from hypertensive patients as compared to age-matched controls (**Figure 1B**). However, RBCs from patients with hypertension showed no changes in total (high molecular weight and low molecular weight) "free"/reduced thiol levels in RBCs; these were analyzed by intracellular fluorescence of a Thiol Tracker® (TT), which reacts with "free"/reduced intracellular sulfhydryl (-SH) groups (Table S1). Likewise, the levels of NO metabolites in RBCs measured by intracellular DAF fluorescence (Cortese-Krott et al., 2012a,b) as well as intracellular nitrite concentrations were similar in both study groups (Table S1). Taken together, these data demonstrate that RBCs from hypertensive patients have decreased EI at low shear stresses and increased intracellular ROS, while intracellular NO levels and total free thiol levels were preserved.

## Oxidative Stress Induced by Treatment With *tert*-Butylhydroperoxide Decreases Redox Reserve (Total GSH) and Impairs RBC Deformability and Whole Blood Viscosity

Oxidation of cytoskeletal proteins in RBCs were shown to induce changes in RBC shape and membrane elasticity. To verify that ROS cause changes in RBC deformability, we tested the effect of a prototypical pharmacological oxidative challenge *t*-BuOOH on intracellular redox state and RBC deformability. This treatment was found to induce oxidation of the cytoskeletal protein spectrin (Lii and Hung, 1997) and hemoglobin (Gorbunov et al., 1997). To analyze intracellular redox changes in RBCs following treatment with *t*-BuOOH, we measured intracellular concentrations of reduced glutathione ("free GSH") and oxidized glutathione (GSSG) and calculated the concentration of total GSH (GSH + 2 * GSSG; indicative of the antioxidant reserve) and the molar ratio (GSH/GSSG), which is indicative of the redox state of the cell. Treatment with concentrations of *t*-BuOOH higher than 3 mM decreased free intracellular GSH levels in a concentration-dependent fashion (starting at levels >100 μM), while GSSG levels simultaneously increased (**Figure 2A**). The ratios of GSH and GSSG were stable at low concentrations of *t*-BuOOH, but began to decrease and started to drop with a *t*-BuOOH concentration of $10^{-6}$ M (**Figure 2B**), as a result of depletion of reduced GSH and increase of GSSG at high *t*-BuOOH concentrations. This is in accordance with previous studies showing that high non-physiological concentrations of *t*-BuOOH are needed to induce oxidative stress in RBCs (Trotta et al., 1983; Rice-Evans et al., 1985; Lii and Hung, 1997).

To evaluate whether those redox changes induced by *t*-BuOOH influence RBC deformability, we treated blood samples with increasing concentrations of *t*-BuOOH and measured both shear-induced elongation (by using a LORCA) as well as "bulk" blood viscosity (by using a low shear viscosimeter). *t*-BuOOH in concentrations of < 3 mM did not affect any of the parameters of RBC deformability while significantly decreasing EI at discrete shear stresses at concentrations ≥ 3 mM (**Figure 2C**). However, $EI_{max}$ and $SS_{1/2max}$ (calculated according to Lineweaver-Burk transformation) were not significantly different from control. It is important to point out that in these experiments at high concentrations of *t*-BuOOH the linearity of the Lineweaver-Burk relationship was lost (Table S3), indicating that this transformation method is not applicable in the described experimental conditions.

Assessments of bulk blood viscosity by low shear viscosimetry revealed that *t*-BuOOH in concentrations of 5 mM and 7 mM significantly increased blood viscosity (**Figure 2D**). By comparing changes in EI and whole blood viscosity assessed at the same shear rates we found that *t*-BuOOH-induced decrease of deformability corresponded to a simultaneous increase in bulk viscosity, and that both parameters were dependent on the concentration of *t*-BuOOH (**Figure 2E**). We can exclude membrane damage as we did not detect any increases of hemolysis induced by all applied treatments (Table S3).

Taken together, these data indicate that *t*-BuOOH induces changes in shear-induced elongation of RBCs and affects the overall rheological properties of RBCs in whole blood. Interestingly, those events appear to occur only at *t*-BuOOH concentrations that fully consumed the antioxidant capacity (total GSH) and redox reserve (GSH/GSSG ratio) in RBCs.

## Effects of *t*-BuOOH on RBC Deformability in Nrf2 KO Mice

Next we analyzed the effects of *t*-BuOOH on RBCs from Nrf2 KO mice. This mouse strain was chosen, because lack of Nrf2 induces deficiency of a number of antioxidant/reducing enzymes (Suzuki and Yamamoto, 2015) and may serve as a model for increased susceptibility to oxidative damage. This strain showed increased susceptibility to oxidative challenges (Rangasamy et al., 2005), as well as decreased levels of total GSH in heart and aortic tissue (Erkens et al., 2015). However, the impact of oxidative stress on RBC deformability has been

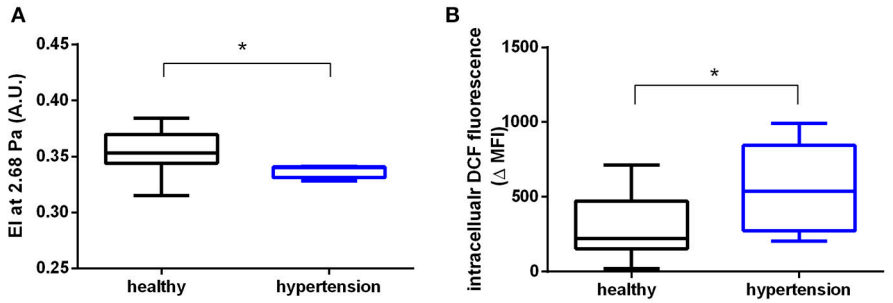


**FIGURE 1 |** RBCs from patients with hypertension display decreased RBC deformability and increased ROS levels. **(A)** Decreased elongation index (EI) measured in RBCs of hypertensive ($n = 4$) and healthy ($n = 9$) participants at a shear stress of 2.68 Pa. *Mann-Whitney-*U* test, $p < 0.05$. **(B)** Increased levels of ROS in RBCs of hypertensive participants ($n = 9$) measured as intracellular dichlorofluorescein (DCF) fluorescence values and compared to healthy controls ($n = 11$) (MFI, median fluorescence intensity; ΔMFI = MFI of loaded RBCs—MFI unloaded RBCs) *Mann-Whitney-*U* test, $p < 0.05$. All ektacytometric measurements were carried out from whole blood diluted in PVP solution and measured in a range of shear stresses of 0.3–10 Pa.

never investigated so far. Unexpectedly, RBCs from Nrf2 KO mice did not show any significant differences in redox reserve (total intracellular GSH); instead we found a compensatory decrease in oxidized GSH (GSSG), which in the absence of any changes in free GSH levels translates into an improved 1.3-fold GSH/GSSG ratio (redox reserve) as shown in **Figure 3A** and **Table 1**. Accordingly to our hypothesis that redox state is one of the major determinants of RBC deformability, there were no differences in deformability of RBCs at baseline (**Figure 3B**) between Nrf2 KO and WT mice. However, when RBCs were challenged with high concetrations of *t*-BuOOH, clear differences in RBC deformability became apparent. Specifically, treatment of RBCs from Nrf2 KO mice with 50 or 100 μM *t*-BuOOH induced a significant impairment of deformability of RBCs from Nrf2 KO mice at both low and high range of shear stresses (**Figures 3C,D**) and significantly decreased $EI_{max}$ as compared to WT (Table S4). These findings suggest that the compensatory increase in the GSH/GSSG ratio of RBCs from Nrf2 KO seen under resting conditions is not enough to protect RBCs from oxidant-induced impairment of RBC deformability, and are indicative of impaired resilience against oxidants of Nrf2 KO RBCs as compared to WT mice.

## RBC Deformability Is Not Affected by Endogenously Produced or Exogenously Applied NO

Another determinant of RBC deformability described in literature is both exogenously applied or endogenously produced NO by red cell eNOS. Both endogenously and exogenously applied NO have been described to affect RBC deformability *ex vivo*, assessed either as RBC filterability or as shear-induced deformation by ektacytometry (Korbut and Gryglewski, 1993; Bor-Kucukatay et al., 2003; Kleinbongard et al., 2006; Grau et al., 2013). These data stand in contrast to more recent data showing no effects of sodium nitroprusside (Barodka et al., 2014b), or NO donors or NOS inhibitors on RBC deformability determined by ektacytometry (Belanger et al., 2015), calling for a careful reassessment of those earlier findings.

Therefore, to analyze the effects of NO on RBC deformability in our experimental setting, RBCs were exposed to increasing concentrations of the NO donor DEA/NO. DEA/NO was chosen because it is well known to spontaneously release NO in a controlled and predictable manner (differently from sodium nitroprusside, which needs to be metabolized in cells and releases also $O_2^-$) (Feelisch, 1998). In our hands, the incubation of RBCs with the spontaneous NO donor DEA/NO (1–100 μM) did not significantly influence deformability indices over the whole range of shear stresses analyzed (**Figure 4A**). Lineweaver-Burk transformations of this data (**Figure 4B**) followed by calculation of $EI_{max}$ and $SS_{1/2max}$ (Table S5) resulted in values not significantly different from control conditions at concentrations ranging from 1 to 100 μM. Instead, treatment with the highest concentration of DEA/NO (200 μM) decreased RBC deformability significantly (**Figure 4A**). These data indicate that exposure of RBCs to exogenous NO does not influence RBC deformability in a beneficial manner.

It is well-established that RBCs carry a functional eNOS (Kleinbongard et al., 2006; Cortese-Krott et al., 2012b) and, according to published data by Bor-Kucukatay *et al*. RBC eNOS-derived NO is able to improve RBC deformability (Bor-Kucukatay et al., 2003). To examine the effects of endogenously produced NO in RBCs, we compared RBC deformability of global eNOS KO mice with RBC deformability of WT mice and found that genetic deficiency for eNOS had no effect on RBC deformability. This was evidenced by essentially superimposable deformability curves measured at discrete shear stresses in WT and eNOS KO (**Figure 4C**) and virtually identical calculated values for $EI_{max}$ and $SS_{1/2max}$ after Lineweaver-Burk transformation (**Figure 4D**, Table S6). Likewise, the levels of GSH and GSSG or their ratios were not different between eNOS KO and WT strains (**Table 1**). Therefore, RBC deformability is neither affected by treatment with NO donors nor by endogenous NO formation/synthesis by red cell eNOS.

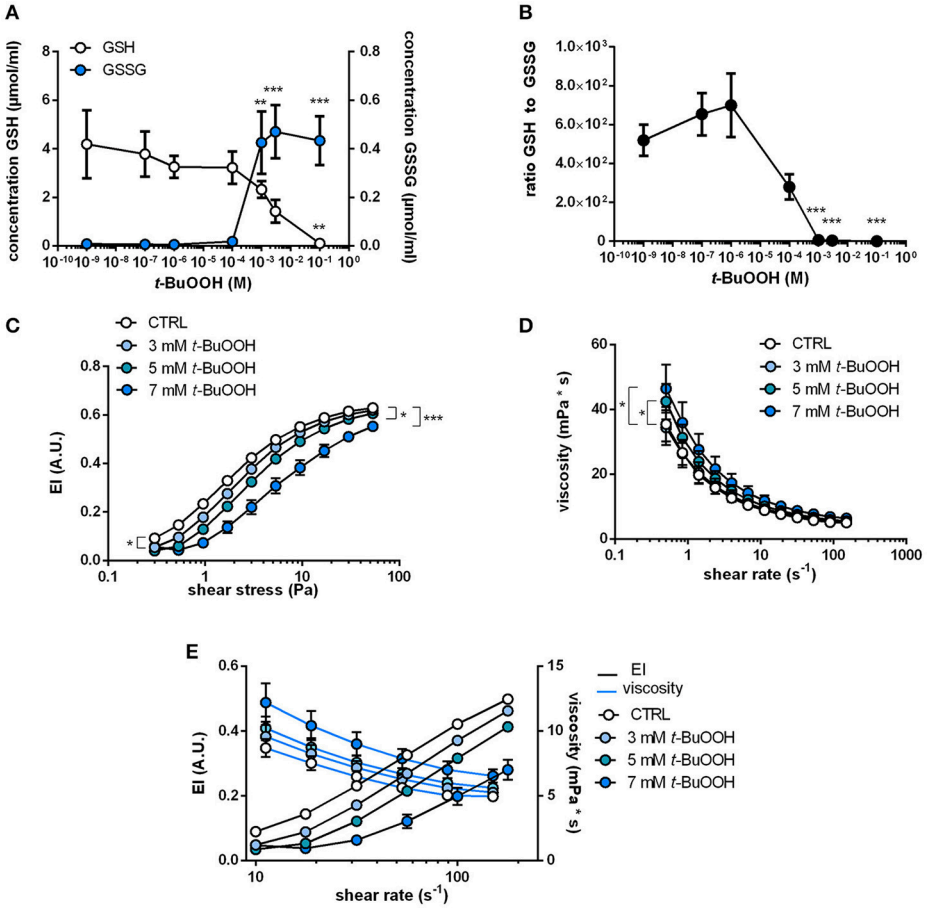


**FIGURE 2 |** Changes in intracellular redox state by treatment with *t*-BuOOH decrease RBC deformability and increase blood viscosity in a concentration-dependent fashion. **(A)** Changes in intracellular GSH and GSSG levels upon treatment of RBCs with different concentrations of *t*-BuOOH (0 M, $10^{-9}$ M, $10^{-7}$ M, $10^{-6}$ M, $10^{-4}$ M, $10^{-3}$ M, $3 \times 10^{-3}$ M, $10^{-1}$ M). Free/reduced GSH levels decreased with a simultaneous increase of GSSG, the oxidized form of glutathione ($n = 4$). GSH: one-way RM ANOVA $p = 0.0218$, $^{**}p < 0.01$, Dunett's test vs. untreated control. GSSG: one-way RM ANOVA $p < 0.0001$, $^{**}p < 0.01$, $^{***}p < 0.001$, Dunett's test vs. untreated control. **(B)** Ratio of free/reduced GSH and GSSG calculated from the values in **(A)**. One-way RM ANOVA $p < 0.0001$, $^{***}p < 0.001$, Dunett's test vs. untreated control. **(C)** Relationship between elongation index (EI) and applied shear stress (0.30–53.33 Pa) of whole blood samples treated with increasing concentrations of *t*-BuOOH (3–7 mM) showing that *t*-BuOOH impairs RBC deformability in a concentration-dependent fashion ($n = 6$). Two-way RM ANOVA $p < 0.001$ and Dunett's test vs. untreated control; $^{*}p \leq 0.05$, $^{***}p < 0.001$ (statistically significant for 3 mM from shear stresses between 0.3 and 9.48 Pa; for 5 and 7 mM over the whole range of shear stresses). **(D)** Analysis of blood viscosity of the same samples described in **(C)** over a range of different shear rates ($n = 6$). Two-way ANOVA $p = 0.0004$ and Dunett's test vs. untreated control, $^{*}p \leq 0.05$ (for 5 mM statistically significant from shear rates between 0.5 and 3.98 $s^{-1}$ and for 7 mM from shear rates between 0.5 and 11.22 $s^{-1}$). **(E)** Comparison of changes in viscosity and EI at matching shear rates show inverse relationship between the two parameters.

## Treatment With *S*-Nitrosothiols Leads to Nitrosation of Cytoskeletal Proteins and Rescues From *t*-BuOOH-Mediated Damage

There is evidence for a role of nitrosation of critical thiols in the cytoskeletal protein spectrin in the regulation of RBC deformability (Grau et al., 2013). To study whether *S*-nitrosation reactions impact RBC deformability, we incubated RBCs with the nitrosothiol CysNO. We found that 1 mM CysNO indeed increases *S*-nitrosation of the cytoskeletal protein spectrin, as determined by biotin switch assay and Western blotting (**Figure 5A**; Figure S4). However, similar to what we observed with the NO donor DEA/NO, the treatment of RBCs with CysNO at concentrations ranging from 0.001 to 1000 µM did neither affect EI, $EI_{max}$, and $SS_{1/2max}$, nor bulk viscosity beneficially in CysNO-treated RBCs compared to untreated cells (**Figure 5B**, Figure S2, Table S7). Similar to what we observed for 200 µM DEA/NO, also high concentrations of CysNO (50,000 µM) decreased RBC deformability significantly (**Figure 5B**).

To analyze the effects of CysNO on *t*-BuOOH-induced impairment of RBCs deformability, we pre-incubated RBCs with CysNO, washed them, and afterwards treated them with *t*-BuOOH. The deformability curves showed that pre-treatment with CysNO at concentrations between 1 and 1000 µM significantly improved RBC deformability (**Figure 5C**). These effects were especially profound with high shear stresses as

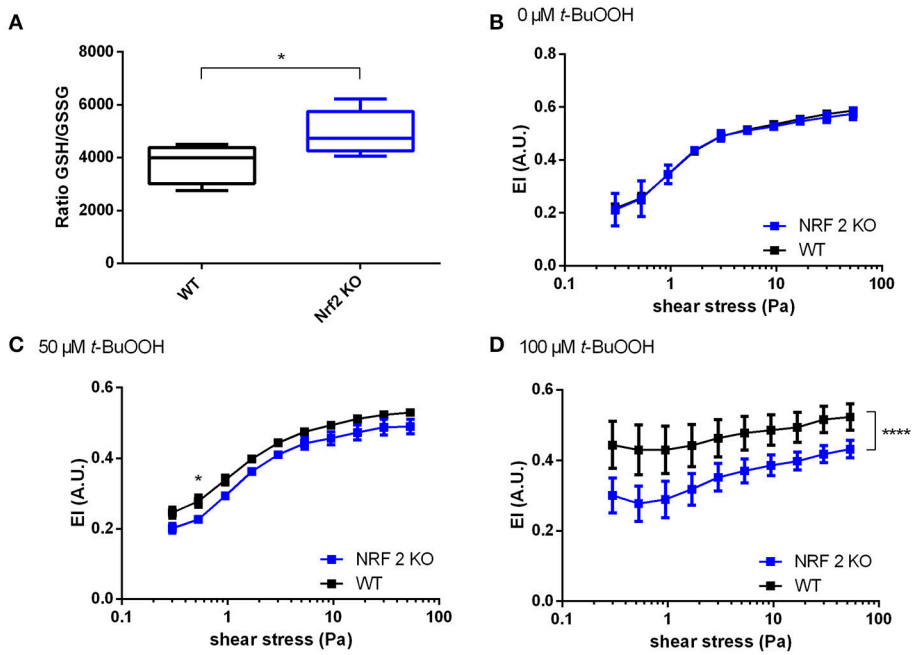


**FIGURE 3 |** Increased susceptibility of RBCs from Nrf2 KO mice to *t*-BuOOH-induced impairment of deformability. **(A)** The ratio of GSH/GSSG in Nrf2 KO is increased as compared to WT mice ($n = 5$),*$p < 0.05$ student's *t*-test. **(B)** No difference exists between RBC deformability curves in wild type (WT) mice and Nrf2 KO mice as determined by ektacytometric analysis of RBC pellet two-way RM ANOVA $p = 0.4497$. **(C)** RBCs from Nrf2 KO mice show a significant decrease of EI values after treatment with 50 µM *t*-BuOOH to WT controls ($n = 6$). Two-way ANOVA $p = 0.0341$ and Sidak's test; *$p \leq 0.05$, **(D)** RBCs from Nrf2 KO mice show a significant decrease of EI values after treatment with 100 µM *t*-BuOOH as compared to WT controls ($n = 6$). Two-way ANOVA $p = 0.0095$ and Sidak's test; ****$p < 0.0001$ over the whole range of shear stresses. All ektacytometric measurements were carried out from washed RBC diluted in PVP and measured in a range of shear stresses of 0.3–53.33 Pa.

demonstrated by increase in EI (**Figure 5C**), while $EI_{max}$ and $SS_{1/2max}$ were not significantly different (Table S7). Interestingly, treatment with CysNO after *t*-BuOOH incubation resulted in comparable protection of RBC deformability (**Figure 5D**).

Taken together, treatment of RBCs with nitrosothiols led to *S*-nitrosation of the cytoskeletal protein spectrin but did not affect RBC deformability *per se*, as assessed by measurements of shear-dependent elongation and bulk viscosity. However, nitrosothiols protected RBCs against *t*-BuOOH-mediated impairment of RBC deformability.

## DISCUSSION

Studying the molecular mechanisms controlling RBC deformability is of fundamental importance to understand physiology and pathophysiology of RBCs. Oxidative modifications of the RBC cytoskeleton were shown to decrease deformability (Sinha et al., 2015). In addition, NO was proposed to participate in the regulation of RBC deformability (Bor-Kucukatay et al., 2003; Grau et al., 2013), but these findings were not reproduced by other laboratories (Barodka et al., 2014b; Belanger et al., 2015; Cortese-Krott et al., 2017).

In this work, we investigated if and how changes in intracellular redox status, levels of ROS, NO metabolites, and nitrosation reactions may affect RBC deformability. We found that: (1) in hypertensive patients decreased RBC deformability was accompanied by an increase in intracellular ROS levels, with unchanged intracellular NO levels and total free thiols; (2) treatment with high concentrations of *t*-BuOOH provoked changes of intracellular redox state, induced changes in RBC deformability and increased blood viscosity; (3) effects of high concentrations of *t*-BuOOH on RBC deformability were more pronounced in RBCs from mice lacking the Nrf2-dependent antioxidant response; (4) neither NO administration by NO donors nor nitrosothiols nor the lack of eNOS in eNOS KO mice induced changes in RBC deformability; (5) treatment with a nitrosothiol rescued RBCs from adverse changes induced by high concentrations of *t*-BuOOH.

Taken together, these findings suggest that NO itself does not affect RBC deformability *per se*, but preserves RBC deformability in conditions of oxidative stress. The mechanisms linking NO-mediated biochemical pathways and modifications regulating RBC deformability induced by ROS need to be identified in future studies.

### Relationship Between Intracellular Redox State and Mechanical Properties of RBCs

The deformability of RBCs is defined as the ability of RBCs to change their shape in response to external hydrodynamic forces, which are exerted on the cells. Intrinsic determinants

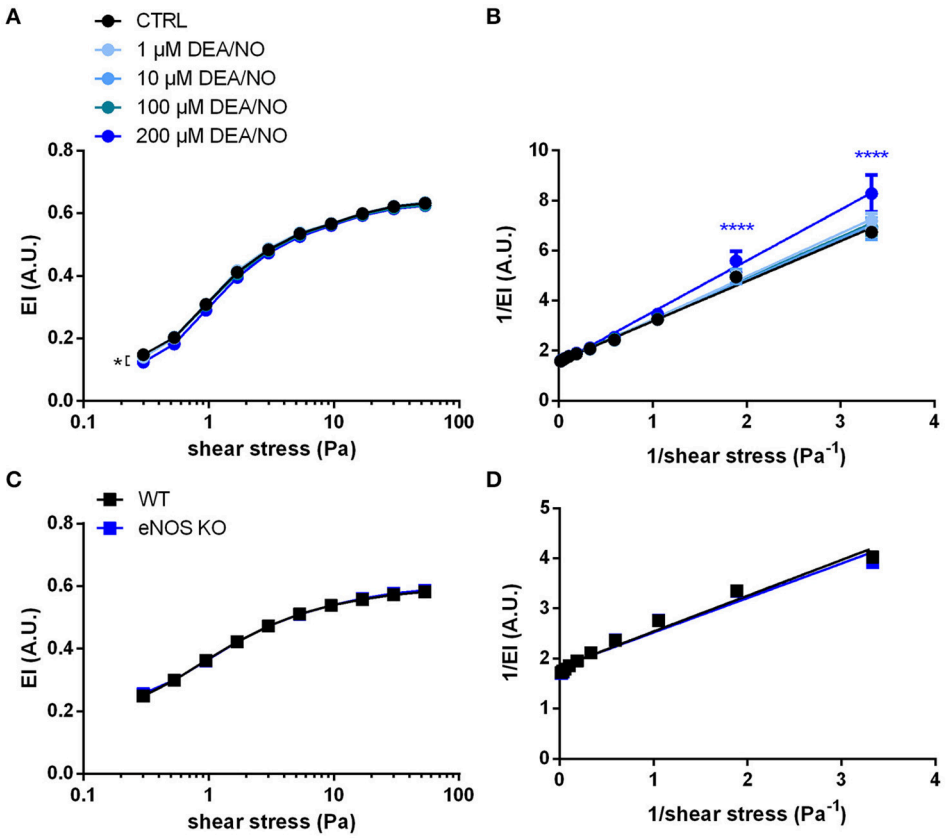


**FIGURE 4 |** NO does not influence RBC deformability measured by ektacytometry: **(A)** Treatment with the NO donor DEA/NO did not affect EI; the highest concentration (200 µM DEA/NO) significantly decreased RBC deformability. Two-way RM ANOVA $p < 0.0001$ and Dunnett's test vs. untreated control, $^{*}p \leq 0.05$ (statistically significant for 200 µM DEA/NO in the range of shear stresses between 0.3–5.3 and 30–53.33 Pa). **(B)** The Lineweaver–Burk transformation resulted in linear regression curves that are not significantly different from each other ($n = 6$). Two-way ANOVA $p = 0.0015$ and Dunnett's test vs. untreated control, $^{****}p < 0.0001$. **(C)** Deformability curves of RBCs from eNOS KO mice do not differ from that of WT mice. Two-way ANOVA $p = 0.4725$. **(D)** Lineweaver-Burk transformation of curves in C do not show any significant difference ($n = 6$). Two-way ANOVA $p = 0.6029$ All ektacytometric measurements were carried out from washed RBCs diluted in PVP solution and measured in a range of shear stresses of 0.3–53.33 Pa.

**TABLE 1 |** GSH content and redox state in RBCs from eNOS KO, Nrf2 KO, and WT mice.

| | RBC eNOS KO | RBC Nrf2 KO | RBC WT |
|---|---|---|---|
| GSH (nM) | $3.76*10^6 \pm 0.26*10^6$ | $3.77*10^6 \pm 0.14*10^6$ | $3.93*10^6 \pm 0.23*10^6$ |
| GSSG (nM) | 946.0 ± 161.3 | 781.5 ± 68.6 | 1057.7 ± 46.4 |
| Total GSH (nM) | $3.76*10^6 \pm 0.26*10^6$ | $3.77*10^6 \pm 0.14*10^6$ | $3.94*10^6 \pm 0.23*10^6$ |
| GSH/GSSG | 3974.6 | 4821.5 | 3718.3 |

*Intracellular reduced/"free" GSH, oxidized GSH (GSH disulfide), total GSH (calculated by GSH and GSH disulfide levels), and ratio of GSH to GSH disulfide measured in RBCs by mass spectroscopy.*

of RBC deformability are (1.) the geometry of the cells (i.e., the relationship between surface area and cellular volume), (2.) intracellular viscosity, and (3.) the elastic properties of the membrane/membrane viscosity (Chien, 1987; Mohandas and Gallagher, 2008). These three parameters can be seen as species-unspecific, which enabled us to compare human and murine RBCs. RBC deformability measurements have been carried out by analyzing stress-strain relationships; i.e., by applying a deforming force (on the whole cell or on a small portion of the membrane) and analyzing the resulting cell deformation by direct microscopic observation or by indirect estimations, such as analyzing changes in light diffraction pattern during ellipsoidal deformation (ektacytometry) or changes in bulk viscosity.

Under these conditions, the overall deformation of RBCs depends on both intrinsic properties of the RBC (geometry, intracellular viscosity, membrane viscosity) and on extracellular bulk viscosity; in turn the latter depends on a variety of factors, including cell concentration, plasma/medium viscosity, hydrodynamic forces, cell aggregation, and cell-cell interactions (Chien, 1987). Thus, depending on the forces applied and the experimental setup used for the assessment, each system induces changes in RBC shape that are more or less influenced by changes in cell geometry, intracellular viscosity, or extracellular medium composition in a different way.

This is particularly relevant if the biological chemistry and biochemistry of changes in RBC cell deformability by oxidants

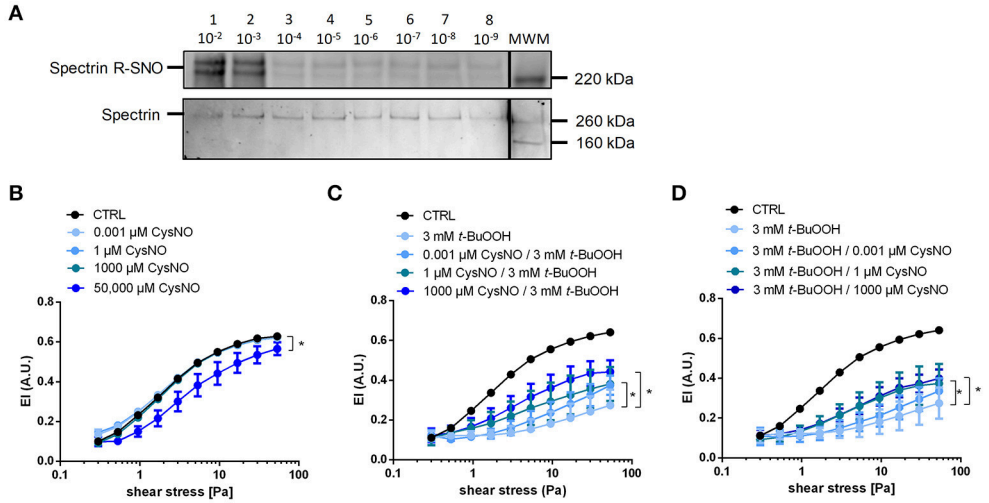


**FIGURE 5 |** Treatment with CysNO leads to *S*-nitrosation of spectrin and protects RBCs from *t*-BuOOH-induced impairment of RBC deformability. **(A)** *S*-nitrosation of spectrin following treatment of RBC suspension with $10^{-9}$ to $10^{-2}$ M CysNO for 30 min as assessed by biotin switch assay (upper lane). Total spectrin, on the same membrane determined by Western blot. Each lane is labeled with the treatment concentration of CysNO. Lane MWM is the corresponding molecular weight marker (for whole images of whole membrane please refer to Figure S4). **(B)** Increasing concentrations of CysNO did not affect RBC deformability, except at the highest concentration (50,000 µM CysNO). Two-way RM ANOVA $p = 0.0059$ and Dunnett's test vs. untreated control, $^*p \leq 0.05$ (for 50,000 µM statistically significant over a range of shear stresses from 0.53 to 53.33 Pa). **(C)** Pre-incubation of RBCs with different concentrations of nitrosating agent CysNO significantly rescued RBC deformability after treatment with 3 mM *t*-BuOOH ($n = 5$). Two-way RM ANOVA $p < 0.0003$ and Tukey's test; $^*p \leq 0.05$ vs. 3 mM *t*-BuOOH (statistically significant for 1 µM CysNO pre-incubation in the shear stresses from 5.33 to 53.33 Pa and for 1000 µM CysNO pre-incubation in the shear stress range from 3 to 53.33 Pa). **(D)** Post-incubation of RBCs with different concentrations of nitrosating agent CysNO significantly rescued RBC deformability after treatment with 3 mM *t*-BuOOH ($n = 5$). Two-way RM ANOVA $p < 0.0003$ and Tukey's test; $^*p \leq 0.05$ vs. 3 mM *t*-BuOOH (statistically significant for 1 µM CysNO and 1000 µM CysNO in the range of shear stresses from 5.33 to 53.33 Pa). Deformability index of RBC pellets measured in a range of shear stresses of 0.3–53.33 Pa.

or NO metabolites are investigated in a system as complex as the RBCs (and may help to explain some of the discrepancies found in the literature regarding the role of NO and oxidant in RBC deformability, as discussed in detail below in paragraph section Protective Effects of Treatment With Nitrosothiols on *t*-BuOOH-Induced Decrease of RBC Deformability).

In our study, RBC deformability was measured, first as changes in cell elongation in response to shear stress in diluted cell suspensions in a highly viscous PVP medium (by LORCA), and second as changes in bulk viscosity of RBC suspensions at physiological hct in response to a range of shear rates. In the LORCA measurements, the deforming force ($\tau$) is dependent on the two components shear rate ($\gamma$) and medium viscosity ($\eta_o$) and is defined as "bulk shear stress" and expressed in Pa.

$$\tau = \gamma \times \eta_o. \quad (1)$$

In the LORCA the highly viscous, Newtonian medium is the PVP solution ($\eta_o$), and therefore the degree of RBC deformation is mainly determined by the intrinsic viscosity parameters of the RBC, i.e., intracellular viscosity ($\eta_i$) and membrane viscosity ($\eta_m$); parameters such as cell geometry, or cell adhesion play a minor or non-existent role in ektacytometric measurements (Chien, 1987).

In the LAS300 low-shear viscosimeter measurements are carried out using whole blood; here the blood itself behaves like a highly concentrated cell suspension analogous to a highly viscous artificial medium, with the difference of being a non-Newtonian fluid. Therefore, in low-shear viscosimetry shear induced deformation depends on both intrinsic and extrinsic erythrocyte properties, including intracellular viscosity ($\eta_i$) and membrane viscosity ($\eta_m$) (like in ektacytometry), but also cell volume, cell-cell interactions and blood plasma viscosity (Musielak, 2009).

Intracellular viscosity ($\eta_i$) is mainly dependent on the concentration and physicochemical properties of hemoglobin (Mohandas et al., 1980; Chen and Kaul, 1994), while membrane viscosity $\eta_m$ depends on the elasticity of the spectrin cytoskeleton and its interactions with transmembrane proteins and/or hemoglobin. Therefore, according to these measurement principles described above, changes in RBC deformability assessed by LORCA (or similar methods measuring stress-induced elongation) as a consequence of oxidative stress are likely resulting from changes of the structure/integrity and concentration of hemoglobin and/or of cytoskeletal proteins like spectrin (Corry et al., 1980; Chen and Kaul, 1994; Kiefer and Snyder, 2000; Mandal et al., 2002).

To induce oxidative stress in RBCs, RBCs were treated with high non-physiological concentrations of *t*-BuOOH. The conditions chosen for the experiments were based on previous data/findings showing that millimolar concentrations of *t*-BuOOH are needed to induce changes on RBC deformability (Corry et al., 1980; Trotta et al., 1983). Based on this published observations, we carried out experiments to carefully characterize the effects of increasing concentrations of *t*-BuOOH ranging from $10^{-9}$ to$10^{-1}$ M on intracellular redox status (assessed

as GSH/GSSG ratio), as well as RBC membrane integrity and hemolysis. Here, we found that only the concentrations of *t*-BuOOH, which decreased the intracellular GSH/GSSG ratio, significantly affected shear-induced elongation and bulk blood viscosity (**Figure 2**). Our findings are in agreement with previous results demonstrating that only high millimolar concentrations of *t*-BuOOH induce hemoglobin oxidation and changes in viscosity of hemoglobin solutions, membrane lipid peroxidation (Trotta et al., 1983), as well as oxidative modifications of cytoskeletal proteins (including crosslinking). Interestingly, oxidants are also known to promote crosslinking of hemoglobin to cytoskeletal proteins (Nagababu et al., 2010), probably further contributing to an impairment of RBC deformability.

This protection may be afforded by both exceptionally high concentrations of intracellular antioxidant systems and a highly efficient reducing capacity that allows rapid recycling of oxidized low-molecular weight constituents, such as glutathione and/or ascorbate (Kuhn et al., 2017). In fact, as also shown here by analyzing RBCs from Nrf2 KO mice, the antioxidant capacity in RBCs is linked to the susceptibility to oxidative damage. In Nrf2 KO mice, the levels of antioxidant and detoxifying enzymes are significantly decreased (Suzuki and Yamamoto, 2015), and Nrf2 KO mice are more sensitive to oxidative damage. Therefore, we expected Nrf2 KO mice to be more susceptible to oxidative stress of high concetrations of *t*-BuOOH.

In fact, we found that RBC of Nrf2 KO mice showed an increased susceptibility to *t*-BuOOH-induced impairment of RBC deformability. Specifically, the effects of *t*-BuOOH on the elongation curves of Nrf2 KO RBCs were significant already at lower concentrations of the peroxide as compared to WT RBCs. In contrast, in untreated cells (at baseline) RBCs from Nrf2 KO mice showed fully preserved antioxidant reserve (total GSH levels), and increased GSH/GSSG ratio in RBCs. This is in contrast to what we and others observed in other organs (aorta, heart) of these mice, where a decrease in total GSH and expression of GSH synthesizing enzymes was observed (Enomoto et al., 2001; Erkens et al., 2015). Therefore, although RBCs of Nrf2 KO mice are able to compensate for genetic deficiency of antioxidant enzymes by increase of total GSH in the RBCs, they are more susceptible to *t*-BuOOH-induced impairment of RBC deformability.

In the present study we were specifically interested in seeing how oxidative stress resulting from an acute challenge with of an oxidant leads to a drop in GSH/GSSG ratio and affects RBC deformability. As pointed out before, the concentrations of *t*-BuOOH needed to induce such changes were in the millimolar range, and therefore 10 to 1,000-folds higher as compared to physiological peroxide concentrations. Experimental setups analyzing the effects treatments with lower concentrations of peroxide may provide further information on how RBCs cope with oxidative stress induced by physiological concentrations of oxidants produced by vascular or blood cells, or due to the presence of xenobiotics in the circulation. Although the concentrations of *t*-BuOOH applied were very high, we did not observe significant membrane damage and hemolysis in our samples (Figure S3). According to previously published data (Trotta et al., 1983), even higher concentrations of peroxide ($H_2O_2$ or *t*-BuOOH) were required to induce hemolysis, further emphasizing the exceptional high antioxidant reserve capacity of RBCs.

This peculiarly high redox buffering capacity of RBCs is likely due to the need of keeping hemoglobin (Hb) in a reduced-$Fe^{2+}$, oxygen-binding form to function as efficient $O_2$ delivery system. Interestingly, the major source of ROS in RBCs is thought to be Hb itself through the autoxidation reaction of Hb (Kuhn et al., 2017). Moreover, redox dysregulation, due to genetic deficiency of enzymes providing redox equivalents (such as GAPDH) or antioxidant/detoxifying enzymes (such as glutathione peroxidase) is associated with increased membrane fragility and intravascular hemolysis, and hemolytic anemia (Kuhn et al., 2017).

Taken together, these results demonstrate that changes in the intracellular redox reserve (total GSH) of RBCs may profoundly affect their intrinsic RBC flexibility prior to the loss of membrane integrity and hemolysis.

## Protective Effects of Treatment With Nitrosothiols on *t*-BuOOH-Induced Decrease of RBC Deformability

There is a large amount of literature describing the effects of oxidants, alkylating agents, $Ca^{2+}/Ca^{2+}$ ionophore, NO donors and nitrosothiols, as well as NOS inhibitors, and the sGC inhibitor ODQ on RBC deformability (Fischer et al., 1978; Corry et al., 1980; Mesquita et al., 2001; Bor-Kucukatay et al., 2003; Barodka et al., 2014b). However, especially in the case of NO donors and inhibitors of the eNOS/sGC pathway, some of these effects could not be reproduced by other laboratories including ours (Barodka et al., 2014b; Belanger et al., 2015; Cortese-Krott et al., 2017).

The effects of NO on RBC deformability were attributed to the ability of NO donors (Bor-Kucukatay et al., 2003; Riccio et al., 2015) or eNOS-derived NO (Grau et al., 2013) to induce nitrosation reactions of intracellular proteins, including hemoglobin (Riccio et al., 2015) and the cytoskeletal protein spectrin (Grau et al., 2013). We found that neither treatment with NO donors nor nitrosothiols affected RBC deformability and blood viscosity under the conditions applied in this study.

These data are in striking contrast to previously published results (Bor-Kucukatay et al., 2000, 2003; Grau et al., 2013), but are supported by recent findings of two independent groups showing no effects of different NO donors on deformability of human RBCs (Barodka et al., 2014b; Belanger et al., 2015) as assessed by a microfluidic ektacytometric technique (Barodka et al., 2014b), or by osmotic gradient ektacytometry (Belanger et al., 2015). Accordingly, using RBCs from eNOS KO mice, we could not confirm the role of red cell eNOS in regulating RBC deformability (assessed by ektacytometry). Accordingly, treatment with the NOS inhibitor ETU *in vitro* or *in vivo* did not affect RBC deformability in WT (Figure S1).

We were unable to identify any methodological difference in the ektacytometric measurements that might explain these discrepancies (please refer to Table S8 for a comparison of the experimental setups). In previous publications, it was shown

that NOS inhibition changed human RBC filterability (Bor-Kucukatay et al., 2000; Kleinbongard et al., 2006), which is dependent on both, RBC deformability and aggregability (Chien, 1987). In chicken, we have found that treatment of RBCs with a NOS inhibitor decreased RBC deformability and RBC velocity in the microcirculatory system of the chorioallantoic membrane (Horn et al., 2011). However, chicken RBCs are nucleated, and their eNOS-dependent effects might be different from the effects in mammalian, an anuclear RBCs.

Nitrosation of critical thiols was suggested as one of the possible molecular mechanisms underlying the NO-dependent changes of RBC deformability. Nitrosation of the cytoskeletal protein spectrin was proposed to be involved in the control of RBC deformability determined by LORCA (Grau et al., 2013). Likewise, in another study, treatment with NO donors was suggested as a way "to load" RBCs with nitroso-species, including *S*-nitrosohemoglobin (i.e., NO bound to Cys93 in the beta chain of hemoglobin), increased RBC deformability (again assessed by LORCA), and proposed to improve oxygen delivery to the tissues (Riccio et al., 2015). We here confirmed that treatment with the nitrosothiol CysNO induced intracellular nitrosation of the cytoskeletal protein spectrin, as demonstrated before (Grau et al., 2013). However treatment with CysNO alone did not affect RBC deformability or blood viscosity. Instead, we observed that treatment using CysNO protected RBCs against *t*-BuOOH-induced impairment of RBC deformability Similarly Barodka *et al.* and Belanger *et al.* showed a protective effect of sodium nitroprusside on RBC deformability in response to $Ca^{2+}$-stress induced by treatment with $Ca^{2+}$/Ca ionophore (Barodka et al., 2014b; Belanger et al., 2015).

Taking into consideration the well-known effects of oxidants and thiol reactive molecules such as *N*-methylmaleimide and glutaraldehyde on RBC deformability (Fischer et al., 1978; Haest et al., 1980), it is tempting to speculate that nitrosation of critical thiols by CysNO or sodium nitroprusside may protect intracellular proteins from oxidation and/or cross-linking reactions. Other mechanisms by which CysNO may preserve RBC deformability are also possible. It was proposed that nitrosylation of hemoglobin (i.e., formation of a NO-Hb complex centered on the heme iron) may protect against toxicity of *t*-BuOOH in the K562 erythroid cell line, as assessed by EPR (Gorbunov et al., 1997); the authors of this work proposed that the nitrosylated-heme complex is more difficult to oxidize by *t*-BuOOH. Formation of methemoglobin (Trotta et al., 1983) was also proposed to protect RBCs from *t*-BuOOH-induced oxidative degradation of Hb and lipid peroxidation. Another possibility is that treatment of RBCs with nitrosating agents loads RBCs with both high molecular weight and low molecular weight nitroso-species, allowing a more efficient detoxification of the oxidant. Another conclusion based on these findings may be that RBCs from eNOS KO mice might be more susceptible to oxidative stress, as they lack eNOS-derived NO formation. However, it is important to point out that the expression levels of eNOS and the amount of NO released in RBCs are very low as measured and discussed by us (Cortese-Krott et al., 2012b; Cortese-Krott and Kelm, 2014). In general, it is important to take into consideration that the current experimental data do neither allow us to explain the biochemistry nor the molecular mechanisms underlying the effects of oxidants and the protective effects of nitrosothiols or sodium nitroprusside on shear-induced elongation. Therefore, these considerations should be seen as speculative.

## What Are the Mechanisms Responsible for Decrease of RBC Deformability in Hypertensive Patients?

This study started with the observation that RBCs from patients with hypertension show decreased RBC deformability and concomitant increase in ROS, while their NO levels in RBCs were unchanged. According to the findings presented here, changes in ROS levels as well as EI in RBCs from hypertensive patients may reflect oxidative modifications of intracellular proteins (hemoglobin, spectrin), which should be investigated in future studies.

Endothelial dysfunction of hypertensive patients (demonstrated here by a decrease in FMD) is not reflected by decreases of NO levels (DAF-FM) or $NO_2^-/NO_3^-$ levels in RBCs, nor does it correlate with RBC deformability. Similarly, in eNOS KO mice, which have increased blood pressure and decreased NO bioavailability (Godecke et al., 1998), RBC deformability is fully preserved. This indicates that decreased NO bioavailability of RBCs or hypertensive state are not major determinants of RBC deformability, but rather the levels of ROS and the intracellular redox state impact RBC deformability.

Although the findings presented in this study clearly indicate that increases in ROS in RBCs seems to be a plausible cause of loss in RBC deformability, as observed in hypertensive patients, there are some important limitations of this study that need to be considered. Hypertension is a complex disease with many influencing factors. For example, patients in our study were smokers or had a history of smoking (1 smoker and 4 ex-smoking individuals of 9 hypertensive individuals; compared to 1 smoker and 3 ex-smoking individuals of 11 normotensive controls). Smoking may increase systemic oxidative stress. In the cohorts, we did not collect information on systemic redox state (levels of thiols, oxidant and antioxidant levels in plasma), such changes may lead to the changes of redox state observed in RBCs from hypertensive patients and therefore is not a cause of hypertensive disease.

Taken together, translational and clinical studies should be focused on understanding the molecular mechanisms and the pathophysiological consequences of decreased RBC deformability in hypertension.

## Summary and Future Directions

RBCs were considered for a long time as simple "bags" packed with hemoglobin circulating in the blood for the only purposes of gas exchange and maintenance of acid/base equilibria; however evidence is now accumulating that RBC function is far more complex and highly regulated. Importantly, in contrast to the common knowledge that NO directly affects RBC deformability, this study shows that neither eNOS-dependent NO formation nor NO donors affected RBC deformability *per se*; instead, we found that treatment with nitrosothiols contributes to preserve their resilience to intracellular oxidative modifications and loss of membrane flexibility.

More insights on the chemical, biochemical, and biophysical interactions regulating the mechanical properties of RBCs (which include intracellular viscosity largely dependent on Hb, elasticity and plasticity of the cytoskeletal network regulated by protein-protein interactions, and the fluidity of the membrane) will shed further light on the molecular mechanisms of these effects.

Such future studies should include experimental observations of *ex vivo* and *in vivo* behavior of RBCs, experimental identification and verification of specific redox switches involved therein, as well as computer-aided multiscale modeling approaches of RBCs (from the atomistic level of RBC proteins to RBC rheological behavior in flow conditions along the vascular tree), accompanied by studies analyzing the role of redox changes in tissue perfusion *in vivo*. These integrative studies will hopefully provide a link between cell elastic behavior, its physiological role *in vivo* and significances of changes in RBC deformability observed in hypertension and other pathologies.

## AUTHOR CONTRIBUTIONS

LD planned and executed experiments, analyzed data, and drafted the manuscript. TS provided conceptual and intellectual input, drafted, and critically revised the manuscript. RS coordinated the human study, recruited patients, collected blood samples, measured FMD, and critically revised the manuscript; TK, FB, TRS, CK, and WL planned and executed experiments and revised the manuscript. BEI, HG, MF, and MK made substantial contribution in interpretation of the work, and critically revised the work. MC-K designed and coordinated the work and wrote the paper. All authors have given their final approval of the version of the manuscript to be published.

## FUNDING

We are grateful to the German Research Council Foundation (DFG CO 1305/2-1, IRTG 1902 TP09 to MC-K, MK, and BEI, and CO 1305/3-1/GO 1367/3-1 to MC-K and HG), to the Forschungskommission of the Universitätsklinikum Düsseldorf (9772646 to TS), NIH HL088554 to BEI, NIH 5T32GM007055 to TK, and the Susanne-Bunnenberg-Stiftung of the Düsseldorf Heart Center (to MK) for financial support. LD and TK are Scholars of DFG IRTG1902 (TP09 to MC-K, MK, and BEI); CK is a Scholar of DFG SFB1116 TP06 (to MC-K and MK). FB is a Scholar of the SPP 1710 (to MC-K and HG). TRS and MF acknowledge the support of the Faculty of Medicine, University of Southampton and the Biomedical Research Centre, University Hospital Southampton NHS Foundation Trust.

## ACKNOWLEDGMENTS

We thank Stefanie Becher, Franziska Strigl, Maximilian Ziegler, and Sivatharsini Thasian-Sivarajah for the excellent help with the experiments.

## SUPPLEMENTARY MATERIAL

The Supplementary Material for this article can be found online at: https://www.frontiersin.org/articles/10.3389/fphys.2018.00332/full#supplementary-material

## REFERENCES

Barodka, V. M., Nagababu, E., Mohanty, J. G., Nyhan, D., Berkowitz, D. E., Rifkind, J. M., et al. (2014a). New insights provided by a comparison of impaired deformability with erythrocyte oxidative stress for sickle cell disease. *Blood Cells Mol. Dis.* 52, 230–235. doi: 10.1016/j.bcmd.2013.10.004

Barodka, V., Mohanty, J. G., Mustafa, A. K., Santhanam, L., Nyhan, A., Bhunia, A. K., et al. (2014b). Nitroprusside inhibits calcium-induced impairment of red blood cell deformability. *Transfusion* 54, 434–444. doi: 10.1111/trf.12291

Baskurt, O. K., and Meiselman, H. J. (2013). Data reduction methods for ektacytometry in clinical hemorheology. *Clin. Hemorheol. Microcirc.* 54, 99–107. doi: 10.3233/CH-2012-1616

Becker, P. S., Cohen, C. M., and Lux, S. E. (1986). The effect of mild diamide oxidation on the structure and function of human erythrocyte spectrin. *J. Biol. Chem.* 261, 4620–4628.

Belanger, A. M., Keggi, C., Kanias, T., Gladwin, M. T., and Kim-Shapiro, D. B. (2015). Effects of nitric oxide and its congeners on sickle red blood cell deformability. *Transfusion* 55, 2464–2472. doi: 10.1111/trf.13134

Bor-Kucukatay, M., Wenby, R. B., Meiselman, H. J., and Baskurt, O. K. (2003). Effects of nitric oxide on red blood cell deformability. *Am. J. Physiol. Heart Circ. Physiol.* 284, H1577–1584. doi: 10.1152/ajpheart.00665.2002

Bor-Kucukatay, M., Yalcin, O., Gokalp, O., Kipmen-Korgun, D., Yesilkaya, A., Baykal, A., et al. (2000). Red blood cell rheological alterations in hypertension induced by chronic inhibition of nitric oxide synthesis in rats. *Clin. Hemorheol. Microcirc.* 22, 267–275.

Chen, D., and Kaul, D. K. (1994). Rheologic and hemodynamic characteristics of red cells of mouse, rat and human. *Biorheology* 31, 103–113. doi: 10.3233/BIR-1994-31109

Chien, S. (1987). Red cell deformability and its relevance to blood flow. *Annu. Rev. Physiol.* 49, 177–192.

Cicco, G., Carbonara, M. C., Stingi, G. D., and Pirrelli, A. (2001). Cytosolic calcium and hemorheological patterns during arterial hypertension. *Clin. Hemorheol. Microcirc.* 24, 25–31.

Cicco, G., Dolce, E., Vicenti, P., Stingi, G. D., Tarallo, M. S., and Pirrelli, A. (1999a). Hemorheological aspects in hypertensive menopausal smoker women treated with female hormones. *Clin. Hemorheol. Microcirc.* 21, 343–347.

Cicco, G., and Pirrelli, A. (1999). Red blood cell (RBC) deformability, RBC aggregability and tissue oxygenation in hypertension. *Clin. Hemorheol. Microcirc.* 21, 169–177.

Cicco, G., Vicenti, P., Stingi, G. D., Tarallo, and Pirrelli, A. (1999b). Hemorheology in complicated hypertension. *Clin. Hemorheol. Microcirc.* 21, 315–319.

Corry, W. D., Meiselman, H. J., and Hochstein, P. (1980). t-Butyl hydroperoxide-induced changes in the physicochemical properties of human erythrocytes. *Biochim. Biophys. Acta* 597, 224–234. doi: 10.1016/0005-2736(80)90101-7

Cortese-Krott, M. M., Evathia, M., Kamer, C. M., Lückstädt, W., Yang, J., Wolff, G., et al. (2017). Identification of a soluble guanylate cyclase in red blood cells: preserved activity in patients with coronary artery disease. *Redox Biol.* 14, 328-337. doi: 10.1016/j.redox.2017.08.020

Cortese-Krott, M. M., and Kelm, M. (2014). Endothelial nitric oxide synthase in red blood cells: key to a new erythrocrine function? *Redox Biol.* 2, 251–258. doi: 10.1016/j.redox.2013.12.027

Cortese-Krott, M. M., Rodriguez-Mateos, A., Kuhnle, G. G., Brown, G., Feelisch, M., and Kelm, M. (2012a). A multilevel analytical approach for detection and visualization of intracellular NO production and nitrosation events using diaminofluoresceins. *Free Radic. Biol. Med.* 53, 2146–2158. doi: 10.1016/j.freeradbiomed.2012.09.008

Cortese-Krott, M. M., Rodriguez-Mateos, A., Sansone, R., Kuhnle, G. G., Thasian-Sivarajah, S., Krenz, T., et al. (2012b). Human red blood cells at work: identification and visualization of erythrocytic eNOS activity in health and disease. *Blood* 120, 4229–4237. doi: 10.1182/blood-2012-07-442277

Enomoto, A., Itoh, K., Nagayoshi, E., Haruta, J., Kimura, T., O'connor, T., et al. (2001). High sensitivity of Nrf2 knockout mice to acetaminophen hepatotoxicity associated with decreased expression of ARE-regulated drug metabolizing enzymes and antioxidant genes. *Toxicol. Sci.* 59, 169–177. doi: 10.1093/toxsci/59.1.169

Erkens, R., Kramer, C. M., Luckstadt, W., Panknin, C., Krause, L., Weidenbach, M., et al. (2015). Left ventricular diastolic dysfunction in Nrf2 knock out mice is associated with cardiac hypertrophy, decreased expression of SERCA2a, and preserved endothelial function. *Free Radic. Biol. Med.* 89, 906–917. doi: 10.1016/j.freeradbiomed.2015.10.409

Feelisch, M. (1998). The use of nitric oxide donors in pharmacological studies. *Naunyn Schmiedebergs. Arch. Pharmacol.* 358, 113–122. doi: 10.1007/PL00005231

Fischer, T. M., Haest, C. W., Stohr, M., Kamp, D., and Deuticke, B. (1978). Selective alteration of erythrocyte deformabiliby by SH-reagents: evidence for an involvement of spectrin in membrane shear elasticity. *Biochim. Biophys. Acta* 510, 270–282. doi: 10.1016/0005-2736(78)90027-5

Flohe, L. (2013). The fairytale of the GSSG/GSH redox potential. *Biochim. Biophys. Acta* 1830, 3139–3142. doi: 10.1016/j.bbagen.2012.10.020

Godecke, A., Decking, U. K., Ding, Z., Hirchenhain, J., Bidmon, H. J., Godecke, S., et al. (1998). Coronary hemodynamics in endothelial NO synthase knockout mice. *Circ. Res.* 82, 186–194. doi: 10.1161/01.RES.82.2.186

Gorbunov, N. V., Yalowich, J. C., Gaddam, A., Thampatty, P., Ritov, V. B., Kisin, E. R., et al. (1997). Nitric oxide prevents oxidative damage produced by tert-butyl hydroperoxide in erythroleukemia cells via nitrosylation of heme and non-heme iron. Electron paramagnetic resonance evidence. *J. Biol. Chem.* 272, 12328–12341. doi: 10.1074/jbc.272.19.12328

Grau, M., Mozar, A., Charlot, K., Lamarre, Y., Weyel, L., Suhr, F., et al. (2015). High red blood cell nitric oxide synthase activation is not associated with improved vascular function and red blood cell deformability in sickle cell anaemia. *Br. J. Haematol.* 168, 728–736. doi: 10.1111/bjh.13185

Grau, M., Pauly, S., Ali, J., Walpurgis, K., Thevis, M., Bloch, W., et al. (2013). RBC-NOS-dependent S-nitrosylation of cytoskeletal proteins improves RBC deformability. *PLoS ONE* 8:e56759. doi: 10.1371/journal.pone.0056759

Haest, C. W., Driessen, G. K., Kamp, D., Heidtmann, H., Fischer, T. M., and Stohr-Liesen, M. (1980). Is "deformability" a parameter for the rate of elimination of erythrocytes from the circulation? *Pflugers Arch.* 388, 69–73.

Horn, P., Cortese-Krott, M. M., Keymel, S., Kumara, I., Burghoff, S., Schrader, J., et al. (2011). Nitric oxide influences red blood cell velocity independently of changes in the vascular tone. *Free Radic. Res.* 45, 653–661. doi: 10.3109/10715762.2011.574288

Kiefer, C. R., and Snyder, L. M. (2000). Oxidation and erythrocyte senescence. *Curr. Opin. Hematol.* 7, 113–116. doi: 10.1097/00062752-200003000-00007

Kleinbongard, P., Schulz, R., Rassaf, T., Lauer, T., Dejam, A., Jax, T., et al. (2006). Red blood cells express a functional endothelial nitric oxide synthase. *Blood* 107, 2943–2951. doi: 10.1182/blood-2005-10-3992

Korbut, R., and Gryglewski, R. J. (1993). Nitric oxide from polymorphonuclear leukocytes modulates red blood cell deformability *in vitro*. *Eur. J. Pharmacol.* 234, 17–22. doi: 10.1016/0014-2999(93)90700-R

Kuhn, V., Diederich, L., Keller, T. C. S. T., Kramer, C. M., Luckstadt, W., Panknin, C., et al. (2017). Red blood cell function and dysfunction: redox regulation, nitric oxide metabolism, Anemia. *Antioxid. Redox Signal.* 26, 718–742. doi: 10.1089/ars.2016.6954

Lee, S., Park, H., Kim, K., Sohn, Y., Jang, S., and Park, Y. (2017). Refractive index tomograms and dynamic membrane fluctuations of red blood cells from patients with diabetes mellitus. *Sci. Rep.* 7:1039. doi: 10.1038/s41598-017-01036-4

Lii, C. K., and Hung, C. N. (1997). Protein thiol modifications of human red blood cells treated with t-butyl hydroperoxide. *Biochim. Biophys. Acta* 1336, 147–156. doi: 10.1016/S0304-4165(97)00020-2

Mandal, D., Moitra, P. K., Saha, S., and Basu, J. (2002). Caspase 3 regulates phosphatidylserine externalization and phagocytosis of oxidatively stressed erythrocytes. *FEBS Lett.* 513, 184–188. doi: 10.1016/S0014-5793(02)02294-9

Mcgough, A. M., and Josephs, R. (1990). On the structure of erythrocyte spectrin in partially expanded membrane skeletons. *Proc. Natl. Acad. Sci. U.S.A.* 87, 5208–5212. doi: 10.1073/pnas.87.13.5208

Mesquita, R., Pires, I., Saldanha, C., and Martins-Silva, J. (2001). Effects of acetylcholine and spermineNONOate on erythrocyte hemorheologic and oxygen carrying properties. *Clin. Hemorheol. Microcirc.* 25, 153–163.

Mohandas, N., Clark, M. R., Jacobs, M. S., and Shohet, S. B. (1980). Analysis of factors regulating erythrocyte deformability. *J. Clin. Invest.* 66, 563–573. doi: 10.1172/JCI109888

Mohandas, N., and Gallagher, P. G. (2008). Red cell membrane: past, present, and future. *Blood* 112, 3939–3948. doi: 10.1182/blood-2008-07-161166

Musielak, M. (2009). Red blood cell-deformability measurement: review of techniques. *Clin. Hemorheol. Microcirc.* 42, 47–64. doi: 10.3233/CH-2009-1187

Nagababu, E., Mohanty, J. G., Bhamidipaty, S., Ostera, G. R., and Rifkind, J. M. (2010). Role of the membrane in the formation of heme degradation products in red blood cells. *Life Sci.* 86, 133–138. doi: 10.1016/j.lfs.2009.11.015

Radosinska, J., and Vrbjar, N. (2016). The role of red blood cell deformability and Na,K-ATPase function in selected risk factors of cardiovascular diseases in humans: focus on hypertension, diabetes mellitus and hypercholesterolemia. *Physiol. Res.* 65 (Suppl. 1), S43–S54.

Rangasamy, T., Guo, J., Mitzner, W. A., Roman, J., Singh, A., Fryer, A. D., et al. (2005). Disruption of Nrf2 enhances susceptibility to severe airway inflammation and asthma in mice. *J. Exp. Med.* 202, 47–59. doi: 10.1084/jem.20050538

Riccio, D. A., Zhu, H., Foster, M. W., Huang, B., Hofmann, C. L., Palmer, G. M., et al. (2015). Renitrosylation of banked human red blood cells improves deformability and reduces adhesivity. *Transfusion* 55, 2452–2463. doi: 10.1111/trf.13189

Rice-Evans, C., Baysal, E., Pashby, D. P., and Hochstein, P. (1985). t-butyl hydroperoxide-induced perturbations of human erythrocytes as a model for oxidant stress. *Biochim. Biophys. Acta* 815, 426–432. doi: 10.1016/0005-2736(85)90370-0

Ruef, P., Gehm, J., Gehm, L., Felbinger, C., Poschl, J., and Kuss, N. (2014). The new low shear viscosimeter LS300 for determination of viscosities of Newtonian and non-Newtonian fluids. *Gen. Physiol. Biophys.* 33, 281–284. doi: 10.4149/gpb_2014011

Sandhagen, B., Frithz, G., Waern, U., and Ronquist, G. (1990). Increased whole blood viscosity combined with decreased erythrocyte fluidity in untreated patients with essential hypertension. *J. Intern. Med.* 228, 623–626. doi: 10.1111/j.1365-2796.1990.tb00289.x

Sinha, A., Chu, T. T., Dao, M., and Chandramohanadas, R. (2015). Single-cell evaluation of red blood cell bio-mechanical and nano-structural alterations upon chemically induced oxidative stress. *Sci. Rep.* 5:9768. doi: 10.1038/srep09768

Suzuki, T., and Yamamoto, M. (2015). Molecular basis of the Keap1-Nrf2 system. *Free Radic. Biol. Med.* 88, 93–100. doi: 10.1016/j.freeradbiomed.2015.06.006

Trotta, R. J., Sullivan, S. G., and Stern, A. (1983). Lipid peroxidation and haemoglobin degradation in red blood cells exposed to t-butyl hydroperoxide. The relative roles of haem- and glutathione-dependent decomposition of t-butyl hydroperoxide and membrane lipid hydroperoxides in lipid peroxidation and haemolysis. *Biochem. J.* 212, 759–772. doi: 10.1042/bj2120759

Turchetti, V., Bellini, M. A., Guerrini, M., and Forconi, S. (1999). Evaluation of hemorheological parameters and red cell morphology in hypertension. *Clin. Hemorheol. Microcirc.* 21, 285–289.

Vaya, A., Martinez, M., Garcia, J., Labios, M., and Aznar, J. (1992). Hemorheological alterations in mild essential hypertension. *Thromb. Res.* 66, 223–229. doi: 10.1016/0049-3848(92)90192-D

Vetrugno, M., Cicco, G., Cantatore, F., Arnese, L., Delle Noci, N., and Sborgia, C. (2004). Red blood cell deformability, aggregability and cytosolic calcium concentration in normal tension glaucoma. *Clin. Hemorheol. Microcirc.* 31, 295–302.

**Conflict of Interest Statement:** The authors declare that the research was conducted in the absence of any commercial or financial relationships that could be construed as a potential conflict of interest.

*Copyright © 2018 Diederich, Suvorava, Sansone, Keller, Barbarino, Sutton, Kramer, Lückstädt, Isakson, Gohlke, Feelisch, Kelm and Cortese-Krott. This is an open-access article distributed under the terms of the Creative Commons Attribution License (CC BY). The use, distribution or reproduction in other forums is permitted, provided the original author(s) and the copyright owner are credited and that the original publication in this journal is cited, in accordance with accepted academic practice. No use, distribution or reproduction is permitted which does not comply with these terms.*

frontiers in Physiology

ORIGINAL RESEARCH
published: 16 March 2018
doi: 10.3389/fphys.2018.00168

# Implications Enzymatic Degradation of the Endothelial Glycocalyx on the Microvascular Hemodynamics and the Arteriolar Red Cell Free Layer of the Rat Cremaster Muscle

*Ozlem Yalcin*[1,2], *Vivek P. Jani*[2], *Paul C. Johnson*[2] *and Pedro Cabrales*[2]*

[1] *Koç University School of Medicine, Sariyer, Istanbul, Turkey,* [2] *Department of Bioengineering, University of California, San Diego, San Diego, La Jolla, CA, United States*

The endothelial glycocalyx is a complex network of glycoproteins, proteoglycans, and glycosaminoglycans; it lines the vascular endothelial cells facing the lumen of blood vessels forming the endothelial glycocalyx layer (EGL). This study aims to investigate the microvascular hemodynamics implications of the EGL by quantifying changes in blood flow hydrodynamics post-enzymatic degradation of the glycocalyx layer. High-speed intravital microscopy videos of small arteries (around 35 μm) of the rat cremaster muscle were recorded at various time points after enzymatic degradation of the EGL. The thickness of the cell free layer (CFL), blood flow velocity profiles, and volumetric flow rates were quantified. Hydrodynamic effects of the presence of the EGL were observed in the differences between the thickness of CFL in microvessels with an intact EGL and glass tubes of similar diameters. Maximal changes in the thickness of CFL were observed 40 min post-enzymatic degradation of the EGL. Analysis of the frequency distribution of the thickness of CFL allows for estimation of the thickness of the endothelial surface layer (ESL), the plasma layer, and the glycocalyx. Peak flow, maximum velocity, and mean velocity were found to statistically increase by 24, 27, and 25%, respectively, after enzymatic degradation of the glycocalyx. The change in peak-to-peak maximum velocity and mean velocity were found to statistically increase by 39 and 32%, respectively, after 40 min post-enzymatic degradation of the EGL. The bluntness of blood flow velocity profiles was found to be reduced post-degradation of the EGL, as the exclusion volume occupied by the EGL increased the effective volume impermeable to RBCs in microvessels. This study presents the effects of the EGL on microvascular hemodynamics. Enzymatic degradation of the EGL resulted in a decrease in the thickness of CFL, an increase in blood velocity, blood flow, and decrease of the bluntness of the blood flow velocity profile in small arterioles. In summary, the EGL functions as a molecular sieve to solute transport and as a lubrication layer to protect the endothelium from red blood cell (RBC) motion near the vessel wall, determining wall shear stress.

**Keywords: cell free layer, endothelial glycocalyx, endothelial surface layer, plasma layer, enzymatic degradation, blood flow, shear stress, microcirculation**

OPEN ACCESS

***Edited by:***
*Joseph M. Rifkind, Johns Hopkins University, United States*

***Reviewed by:***
*Alun Hughes, University College London, United Kingdom*
*Sangho Kim, National University of Singapore, Singapore*

***Correspondence:**
*Pedro Cabrales*
*pcabrales@ucsd.edu*

***Specialty section:***
*This article was submitted to Vascular Physiology, a section of the journal Frontiers in Physiology*

***Received:*** *17 August 2017*
***Accepted:*** *20 February 2018*
***Published:*** *16 March 2018*

***Citation:***
*Yalcin O, Jani VP, Johnson PC and Cabrales P (2018) Implications Enzymatic Degradation of the Endothelial Glycocalyx on the Microvascular Hemodynamics and the Arteriolar Red Cell Free Layer of the Rat Cremaster Muscle. Front. Physiol. 9:168. doi: 10.3389/fphys.2018.00168*

## INTRODUCTION

Blood is a multiphase fluid, consisting of red blood cells (RBCs), plasma, proteins, and electrolyte, with nearly 45% of blood volume occupied by RBCs. Consequently, the resistance to blood flow and blood apparent viscosity are largely dependent on the shear stress experienced by RBCs (Zhang et al., 2009). Hydrodynamic forces during blood flow force RBC migration away from the vessel wall, generating a RBC depleted zone near the vessel wall, or cell free layer (CFL), and a RBC packed core near the center of the blood vessel (Cokelet and Goldsmith, 1991). The formation of the CFL in flowing blood is an important hemodynamic feature of blood flow in the microcirculation. The CFL corresponds to a low viscosity zone, which acts as a lubricating hydrodynamic layer, reducing resistance to flow between the central core of RBCs and the vessel wall (Reinke et al., 1987; Zhang et al., 2009). The thickness of the CFL is proportional to the yield stress of the flowing fluid and depends on the hematocrit (Hct), RBC aggregation, vessel geometry, the migration forces driving the RBCs to away from the vessel wall, and the endothelial glycocalyx.

The endothelial cells lining the luminal side of blood vessels are covered with membrane-bound macromolecules, glycoproteins, and proteoglycans known as the endothelial glycocalyx. The polyanionic nature of the glycocalyx is a consequence of the glycoproteins, bearing acidic oligoasaccharides and terminal sialic acids (SAs) and the proteoglycans, with their glycosaminoglycan (GAG) side chains, that compose it. As such, under physiological conditions the glycocalyx is negatively charged. Association of the polyanionic components of the endothelial glycocalyx layer (EGL) with blood-borne molecules results in an extended endothelial surface layer (ESL) that arises from the EGL (Adamson and Clough, 1992; Pries et al., 2000). Enzymes and their inhibitors, growth factors, plasma proteins, cytokines, cations, and water, all associate with this matrix of biopolyelectrolytes (Bernfield et al., 1999; Osterloh et al., 2002). In addition to glycoproteins, proteoglycans and GAGs, the EGL mainly consists of keratan sulfate, chondroitin sulfate, dermatan sulfate, heparan sulfate, and hyaluronan. The EGL provides selective vasoprotective barrier properties of the vascular wall against vascular leakage, platelet, and leukocyte adhesion (Nieuwdorp et al., 2005). In intact blood vessels, the glycocalyx has an important role in a wide range of physiological processes including increasing vascular permeability, sensing shear stress, and impeding leukocyte and platelet adhesion to the vessel wall (Nieuwdorp et al., 2005; Weinbaum et al., 2007). *In vivo* observations have reported a structure named the ESL, which includes the glycocalyx and other plasma proteins attached to the glycocalyx (Pries et al., 2000). The ESL thickness has been reported to be approximately range from 0.5 μm to over 1 μm (Weinbaum et al., 2007). In general, reports suggest that the ESL thickness varies in different regions of the vascular network (Becker et al., 2010). It is well known that an ESL exists but *in vivo* thickness of the layer is controversial because of the different values from the different techniques in the literature.

This study was conducted to evaluate the effect of the EGL on microvascular blood flow in small arterioles using the rat cremaster muscle preparation. The endothelial glycocalyx was enzymatically degraded by enzymatic degradation via systemic infusion of enzymes to cleave specific GAGs (heparinase, chondroitinase, and hyaluronidase). The degradation of the EGL did not produce major changes in the main systemic parameters of the studied animals. We evaluated the hypothesis that as the EGL determines CFL dynamics, blood flow, and shear rates, it consequently affects blood apparent viscosity. By degrading the EGL, we investigate *in vivo* the non-Newtonian relationship between shear rate and shear stress of blood flow in microvessels to establish the implications of the EGL on vascular resistance. Responses to changes in the integrity of the EGL were studied for individual arterioles using intravital microscopy and capturing high-speed video recordings to measure the CFL thickness and blood flow velocity. *In vivo* blood flow measurements were combined with CFL thickness assessment with sufficient spatial and temporal resolution.

## MATERIALS AND METHODS

### Animal Model and Tissue Preparation

Sprague-Dawley rats (Harlan Laboratories, Livermore, CA) weighing 150–185 g were used to perform the studies. Experiments were approved by the Institutional Animal Care and Use Committee at University of California San Diego and conducted in accordance with the Guide for the Care and Use of Laboratory Animals (National Research Council Committee US, 2010). The cremaster muscle model, for which the complete surgical preparation is elsewhere described in detail, was used for observation of the microcirculation (Baez, 1973). Briefly, 60 mg/kg pentobarbital sodium was injected ip for anesthesia of rats. Throughout the experiment, additional anesthesia was administered as needed. Blood withdrawals and pressure measurements were obtained from the catheterized femoral artery. Catheterization of the right jugular vein was utilized for fluid and anesthesia administration. The animal was positioned on a stage where the cremaster muscle was gently lifted and secured by sutures on a temperature controlled plexiglass pedestal (Physitemp Instruments, Inc. Clifton, NJ). Plastic film was used to cover the exposed muscle (Saran, Dow Corning, Indianapolis, IN). Arteriole responsiveness to a physiological stimulus was tested by topically applying adenosine ($10^{-4}$ M) mixed with suffusate under the polyvinyl film. The experimental procedures were started after 20–30 min after the adenosine was washed away. Non-reactive vessels or vessels not recovering baseline diameter within this time period were excluded from study. Similarly, at the end of the study, adenosine ($10^{-4}$ M) was reapplied and non-reactive vessels, or vessels that had not recovered their diameter prior adenosine application 20 min after washing it, were excluded from study. At the end of the experiment, animals were euthanized.

### Intravital Microscopy

The experimental setup consisted of an intravital microscope (Olympus-BX51WI) equipped with a matching long working

distance condenser (NA = 0.8, Thorlabs, Newton, NJ). Two magnifications of 2X and 1.5X were installed between the objective (40X, LUMPFL-WIR, NA = 0.8; Olympus) and the high-speed camera, providing a total magnification of 1200X with an equivalent resulting pixel size of 0.125 μm relative to the object plane. A mercury arc lamp (100 W, Walker Instruments, Scottsdale, AZ) was used to illuminate the tissue. A 400-nm interference filter (Spectra Physics, no. 59820) was placed above the condenser in the light path to maximize contrast between blood and the surrounding tissue. A high-speed video camera (Fastcam 1024 PCI, Photron USA), equipped with a one-megapixel chip was used for video recording. Additionally, all videos were recorded between 2,000 and 3,000 frames per second and the camera shutter speed was optimized to obtain the highest quality image possible.

## Experimental Protocol

As blood rheology is strongly influenced by hematocrit (Hct), the systemic Hct of all animals included in the study was standardized to 40% Hct via hemodilution when needed. Hemodilution was accomplished by concurrent withdrawal of blood from the arterial catheter and infusion of 5% wt/v human serum albumin solution (ABO Pharmaceuticals, San Diego, CA) using the venous catheter. Vessel diameter was continuously monitored, and video recordings for velocity measurements were collected at selected time points.

## Microvascular Diameter and Cell Free Layer (CFL) Thickness

The analysis of intensity along a video raster line across the vessel was used to determine the vessel diameter (D), RBC column width, and CFL thickness. Detailed information of the algorithm has been previously described (Kim et al., 2006). The CFL thickness was approximated as the distance between the outer edge of the RBC core and the vessel wall. CFL analysis was performed on both sides of the vessel using a sequence of 1,600 consecutive video frames. Diameter and CFL were measured over a 0.8 s time. Vessel diameter was averaged over this period, and only diameters with standard deviation close to zero were used. Diameter measurements with high standard deviation were discarded and repeated, as diameters were not expected to change over this short period. CFL temporal variation (TV) was defined as the standard deviation of the CFL measurements in an entire image sequence divided by the time elapsed (Kim et al., 2007).

## Blood Velocity Profiles

The instantaneous blood flow velocities at different points along the radial direction of the micro-vessel were determined from velocity profiles measured using 2D cross correlation. Briefly, images are segmented (10 × 10 pixels), and the displacement of each segment relative to the subsequent image is calculated based on the maximum correlation coefficient, from which cross correlation coefficients are calculated. Velocity was calculated as the longitudinal displacement multiplied by the frame rate (2,000 fps). This approach provides a spatial velocity profile for every set of two consecutive frames and allows for a range of velocity measurements between 0.3 and 250 mm/s. Mean velocity was calculated as the arithmetic mean of the velocity profile. Blood flow (Q) was calculated assuming Poiseuille's flow, as:

$$Q = \frac{\pi D^4 V}{4} \tag{1}$$

where D is the vessel diameter, and V is the mean blood flow velocity.

## Enzymatic Degradation of the Endothelial Glycocalyx

Enzymatic degradation of the glycocalyx in the cremaster muscle is achieved by systemic infusion of specific enzyme cocktail. Specific GAGs were cleaved by the enzymes heparinase III (50 U/mL), chondroitinase ABC (10 U/mL) and hyaluronidase (3,000 U/mL) and were given in bolus doses via the femoral catheter (Cabrales et al., 2007). CFL recordings were made at 5, 20, 40, and 60 min after enzyme treatment and for a sham group at the same timepoints. This treatment was selected as it is reported not to produce any significant changes in the main systemic parameters of the studied animals.

## Estimation of the Endothelial Glycocalyx Thickness

EGL thickness was estimated by subtracting the 99% confidence interval of the CFL in a glass tube, in which only fluid hydrodynamic forces from the 99% confidence interval measured *in vivo*. As the CFL is the sum of the effects of the EGL and the fluid hydrodynamic forces, subtraction of the two distributions will yield an approximation of the thickness of the endothelial glycocalyx. However, because the glycocalyx itself has hydrodynamic forces associated with its presence, it is impossible to exactly determine the thickness of the glycocalyx utilizing this methodology.

## Velocity Profiles

Velocity profiles were determined via auto-correlation of high-speed intravital microscopy videos before and after enzymatic degradation of the endothelial glycocalyx, and results were fit to the following model:

$$\upsilon\,(r) = \upsilon_{max}\left(1 - \left|\frac{r}{R}\right|^K\right) \tag{2}$$

where v(r) is the spatial velocity profile, vmax is the maximum velocity of the profile, R is the radius of the vessel, and K is the blunting coefficient. Least squared fits were determined using the MATLAB Curve Fitting Toolbox (Mathworks, 2017).

## Statistical Analysis

Results are presented as mean ± standard deviation. All statistical calculations and graphics were performed with a commercially available software package (Prism 7.0, GraphPad). To test the normality of the distributions, the D'Agostino and Pearson Normality test was used. Group's comparisons were performed for diameter and CFL thickness data utilizing both ordinary one-way ANOVA. In this case, the assumption of normality in the ANOVA test-statistic was validated via the non-parameterized

Geisser Greenhouse test to test for sphericity. As the sphericity metric for all comparisons approached 1, it can be concluded that the ANOVA test statistic is Gaussian, even though the original distributions for CFL thickness were non-Gaussian. Pair-wise comparisons for velocity and flow data were performed with a Mann-Whitney *U*-Test. Variance comparisons were performed utilizing the *F*-test. For all tests, $P < 0.05$ was accepted as statistically significant. Histograms and cumulative distribution functions (CDFs) of the CFL were numerically determined and analyzed at different time points. The maximum likelihood of the CFL thickness was approximated as the inflection point of the CDF. Ninety nine confidence intervals are presented from the point at which $P = 0.01$ to the maximum likelihood determined from the CDF. A Bland Altman analysis was utilized to analyze variations in CFL thickness over time as compared to a glass tube:

$$S(x, y) = \left(\frac{S_1 + S_2}{2}, S_1 - S_2\right) \tag{3}$$

Where $S_1$ is the thickness of the CFL at baseline and after enzymatic degradation, and $S_2$ is the thickness of the CFL in a glass tube. All animals passed the Grubbs' test, ensuring that all the measured values at baseline were within a similar population ($P < 0.05$).

## RESULTS

A total of 27 animals ($n = 27$) were entered into the study, two or three arteries were selected in each animal. After application of the systemic and vessel reactivity inclusion criteria, data from 20 animals ($n = 20$) were in included in the results. We found no significant differences in the systemic parameters, confirming that the EGL degradation only had microvascular effects without causing systemic hemodynamic disturbance. Additionally, **Table 1** presents the thickness of the CFL after enzymatic treatment and in a Control group over time. As demonstrated in the sham group variations in the CFL thickness were within ±5% of that at baseline, while the CFL thickness decreased by 11.4% 40 min after enzymatic treatment. These results provide sufficient evidence that changes in the thickness of the CFL were likely due to enzymatic treatment and not due to spontaneous variations.

### CFL Analysis for a Single Blood Vessel

Initial arteriole diameter was 34–36 μm and maximally decreased to 32–33 μm 20 min after enzymatic degradation of the glycocalyx. No change in diameter was detected in the Control group overtime relative to baseline. The maximal change in diameter measured was < 5% from baseline diameter at 20 min after enzymatic degradation of the glycocalyx. The reduction in diameter increases the fraction of the radius of the arterioles occupied by the CFL from 5.8 to 6.1%. Image analysis of high-speed intravital microscopy videos recorded for a single arteriole was quantified in terms of the CFL thickness at different time points after infusion of the enzyme cocktail (**Figure 1**). Thickness of the CFL is presented in **Figure 1A**. The CFL thickness was found to be statistically different from baseline at all-time points. The median value of the CFL thickness decreased to 86% of that at baseline at 40 min after enzymatic degradation of the glycocalyx. Distributions of the CFL thickness were also found to deviate from a standard Gaussian to a right-skewed distribution, indicative of the vessel wall acting as a physical boundary to blood flow as the distributions failed the Kolmogorov-Smirnov and the D'Agostino and Pearson Normality Test, $P < 0.001$ (**Figures 1B,C**). Differences in the variances of the distributions were also found to be statistically significant. The 99% confidence interval of the CFL thickness is presented in **Figure 1D**. The cumulative fractions of the CFL over time compared to baseline are presented in **Figure 2**. The 99% confidence interval of the CFL was found to decrease from $\delta \in [1.50\,\mu m, 2.25\,\mu m]$ to a low of $\delta \in [0.50\mu m, 1.75\mu m]$ at a time of 40 min, where $\delta$ is the thickness of the CFL. Additionally, thickness of the CFL increased between 40 and 60 min to $\delta \in [1.50\,\mu m, 2.25\,\mu m]$, indicating recovery of the endothelial glycocalyx.

### CFL Analysis From Multiple Blood Vessels

Changes in vascular tone for all the 46 arterioles (ranging from 30 to 36 μm) from 20 different animals were not statistically significant at the different time points compared to baseline. The thickness of the CFL for the 46 arterioles is presented in **Figure 3A**. Similar to the analysis of a single vessel, there were statistically differences in the CFL thickness over all time points compared to baseline. The CFL thickness does not fit a Gaussian (normal) distribution, indicating random variation, as the distributions failed the D'Agostino and Pearson Normality Test, $P < 0.001$. The distribution of the CFL thickness was observed to be right-skewed, which is due to the vessel wall acting as a physical barrier to the thickness of the CFL (**Figures 3B,C**). The 99% confidence interval of the CFL thickness for 46 arterioles is presented in **Figure 3D**. The cumulative fractions of the CFL over time compared to baseline are showed in **Figure 4**. The 99% confidence interval of the CFL was found to decrease from $\delta \in [1.00\,\mu m, 2.25\mu m]$ to a low of $\delta \in [0.50\mu m, 1.75\mu m]$ at a time of 40 min. Additionally, thickness of the CFL increased between 40 and 60 min to of $\delta \in [1.00\mu m, 2.75\mu m]$. For reference, the

**TABLE 1 |** Thickness of the CFL after enzymatic treatment and control groups.

| | Baseline | 5 min | 20 min | 40 min | 60 min |
|---|---|---|---|---|---|
| Control (% change from BL) | 2.04 ± 0.01 μm (0.0%) | 2.13 ± 0.01 μm (+4.6%) | 2.11 ± 0.01 μm (+3.4%) | 2.06 ± 0.02 μm (+0.8%) | 1.98 ± 0.01 μm (−3.1%) |
| Enzyme treatment (% change from BL) | 2.76 ± 0.02 μm (0.0%) | 2.93 ± 0.02 μm (+7.8%) | 2.50 ± 0.01 μm (−5.8%) | 2.42 ± 0.02 μm (−11.4%) | 3.22 ± 0.02 μm (+18.4%) |

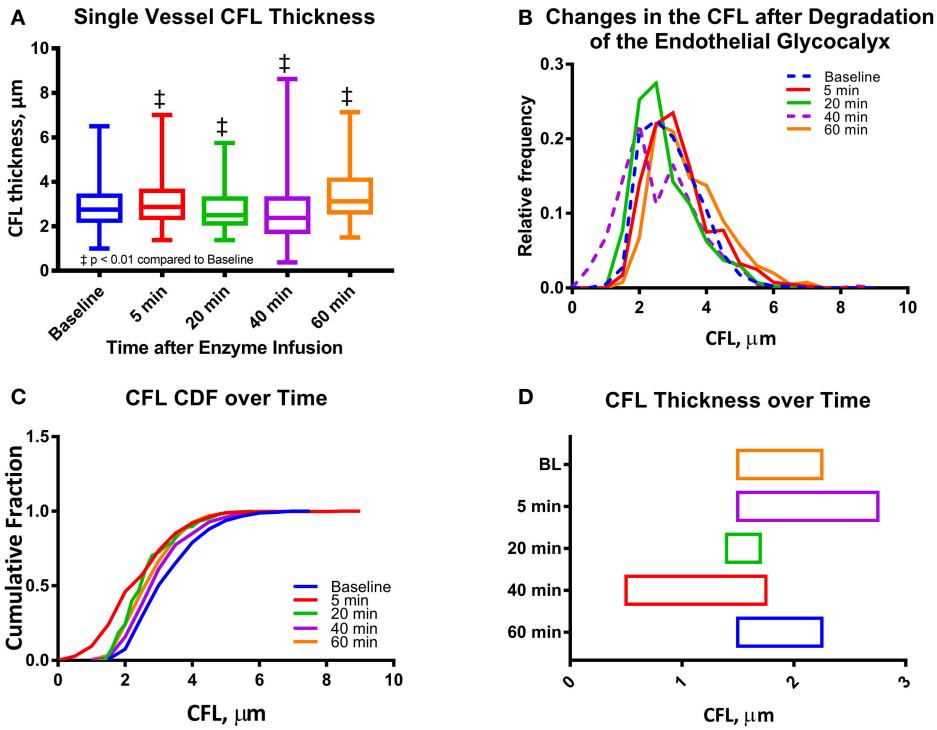


**FIGURE 1 |** Single microvessel CFL thickness during enzymatic degradation of the EGL: **(A)** CFL thickness over time after enzyme infusion. The changes in the mean CFL were found to be statistically significant ($^{\ddagger}P < 0.05$) at all-time points. **(B)** Histograms of CFL thickness over time after enzyme infusion. **(C)** Cumulative distribution functions (CDF) of CFL thickness over time after enzyme infusion. **(D)** One tailed 99% confidence interval of CFL over time after infusion. The left hand bound was determined as the point on the CDF at which $P < 0.01$, and the right hand bound was determined as the inflection point of the CDF (see **Supplemental Figure 1**). ($^{\ddagger}P < 0.05$) compared to baseline.

thickness of the CFL in a glass tube was measured and the 99% confidence interval was found to be $\delta \in [0.50\mu m, 1.75\mu m]$. In addition, the size of the 99% confidence interval of the CFL was found the statistically larger than that at baseline via the *F*-test, indicating unequal spatial recovery of the EGL after enzymatic degradation.

## EGL Thickness

Glycocalyx thickness was found to be approximately 0.50 ± 0.02 µm and was found to degrade to 0.25 ± 0.02 µm 20 min after infusion of the enzyme cocktail (**Figures 3A**, **4**).

## Variances in CFL Thickness Over Time

Variations in the CFL thickness over time before and after enzymatic degradation of the CFL are shown in **Figure 5A** and compared to those in a glass tube of equal diameter in **Figure 5B** via a Bland-Altman plot. The mean deviation of the CFL from that of a glass tube statistically decreased after enzymatic degradation of the EGL. The size of the 95% confidence interval did not change after degradation of the EGL. The negative end of the 95% confidence interval changed, while the positive end remained constant, determined by the presence of the vessel wall. Comparing the variance of the CFL thickness from the blood vessel to the glass tube before and after enzymatic degradation of the glycocalyx, shows that degradation of glycocalyx increases the difference in the CFL between the blood vessel and the glass tube. The positive end of the difference remained unaltered, because it is indicative of the vessel wall, whereas the negative boundary of the difference shows the increased erratic variations in the CFL of the blood vessel after the degradation of the glycocalyx.

## Blood Flow and Blood Velocity Over Time

Max blood flow, max blood velocity, and mean velocity were found to statistically increase by 24, 27, and 25%, respectively, after enzymatic degradation of the EGL. Additionally, the change in peak-to-peak max velocity and peak-to-peak mean velocity between were found to statistically increase by 39 and 32%, respectively, after enzymatic degradation of the EGL. However, the increase in the change in peak-to-peak flow was not found to be statistically significant after degradation of the EGL. Results are summarized in **Figures 6**, **7A,B**.

## Velocity Profiles After Enzymatic Degradation of the EGL

Velocity profiles before and after degradation of the EGL are presented in **Figures 7C,D**. During systole, the blunting coefficient decreased from 4.1 ± 0.4 to 3.5 ± 0.7 after enzymatic degradation of the EGL. Similarly, during diastole, the blunting coefficient decreased from 3.1 ± 0.6 to 2.2 ± 0.6 after enzymatic degradation of the EGL. Thus degradation of the EGL decreased microvessel blood velocity bluntness and a shift toward Poiseuille flow.

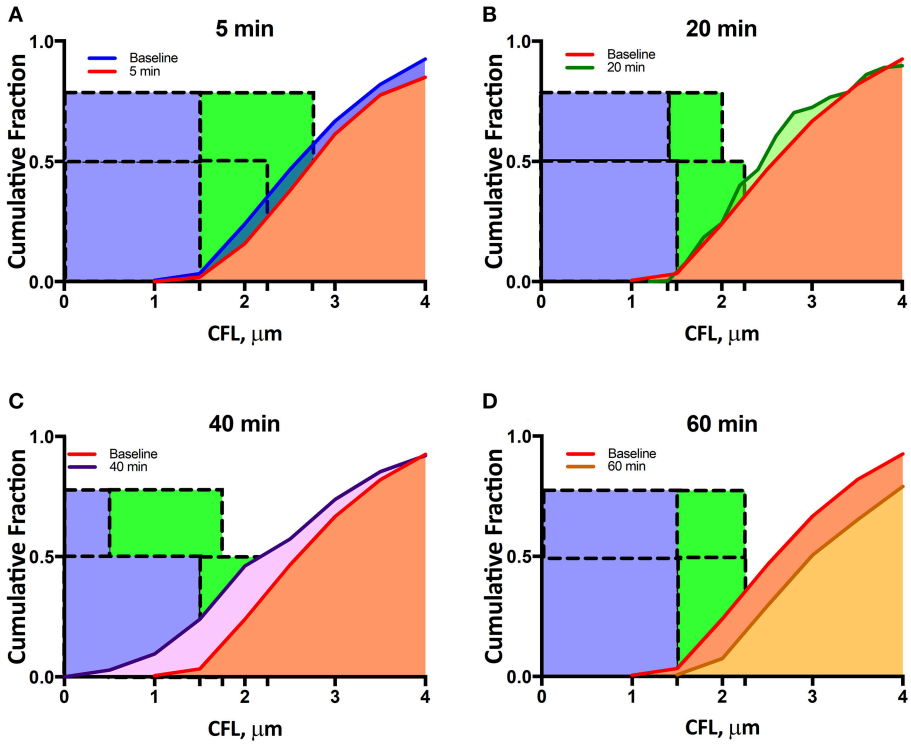


**FIGURE 2 |** Single microvessel cumulative distribution function during enzymatic degradation of the EGL: CDFs at baseline and at **(A)** 5 min, **(B)** 20 min, **(C)** 40 min, and **(D)** 60 min after enzyme infusion. The blue bonding box represents the portion of the CFL influenced by the glycocalyx and its associated hydrodynamic forces, and the green bounding box represents the one-tailed 99% confidence interval of the CFL thickness (see **Supplemental Figure 2**).

## DISCUSSION

The principle finding of this study is that enzymatic degradation of the EGL resulted in a statistically decrease in the CFL thickness, as well as a statistical increase in max blood flow, and max and mean blood velocity. Enzymatic degradation of the EGL also decreased the blunting of the blood velocity profile in arterioles, indicating a shift toward Poiseuille flow. Previous studies have posed models to explain the hydrodynamic and physical forces associated with the EGL (Pries et al., 1990, 1997; Secomb et al., 1998; Long et al., 2004; Weinbaum et al., 2007). Our study provides *in vivo* validation of the hydrodynamic effects of the EGL on blood flow. Changes in the thickness of the CFL during enzymatic degradation compared to the CFL thickness in glass tubes confirms the physical presence of the glycocalyx and the hydrodynamic lubricating layer it produces, and allows for estimation of the apparent thickness (0.5 μm). Literature and mathematical models describe the effects of enzymatic degradation of the EGL on microvascular blood flow as the balance between two opposing forces. As the glycocalyx is a physical barrier to blood flow, it decreases the effective diameter, or the diameter accessible to blood flow, of the lumen. In this schema, degradation of the EGL increases the effective diameter of the lumen, thus decreasing vascular resistance and consequently decreasing blood flow. However, the anionic character of the glycocalyx imparted to it by the glycoproteins and glycosaminoglycans that constitute it are a source of electrical forces that effectively increase the apparent viscosity of blood by forcing negatively charged RBCs toward the center of the lumen, known as the electro-viscous effect. In this schema, degradation of the EGL will decrease the apparent viscosity of blood, increasing blood flow. The effects of the EGL on microvascular blood flow are a summation of both phenomena. As observed in this study, in the case of a 34 μm, blood flow was found to increase with enzymatic degradation of the EGL, indicating that electro-viscous effects are more dominant for arterioles of this size. The thickness of the EGL and ESL are a small fraction of the arteriole lumen diameter, which increases as the arteriole diameter decreases. Therefore, degradation or damages in the EGL have different effects on microvascular blood flow depending on the arteriole diameter, as the electro-viscous effect of the EGL on blood flow becomes less significant in smaller arterioles. The small changes in diameter induced by the enzymatic degradation of the EGL are not responsible for the changes in the CFL thickness or the hemodynamics measured in the study; although, the vasoconstriction induced by the degradation of the EGL is a confounding effect that overestimates the fraction of the arteriole lumen occupied EGL.

The analyzed video recordings determined arteriolar blood flow using spatial cross-correlation analysis, which allows for

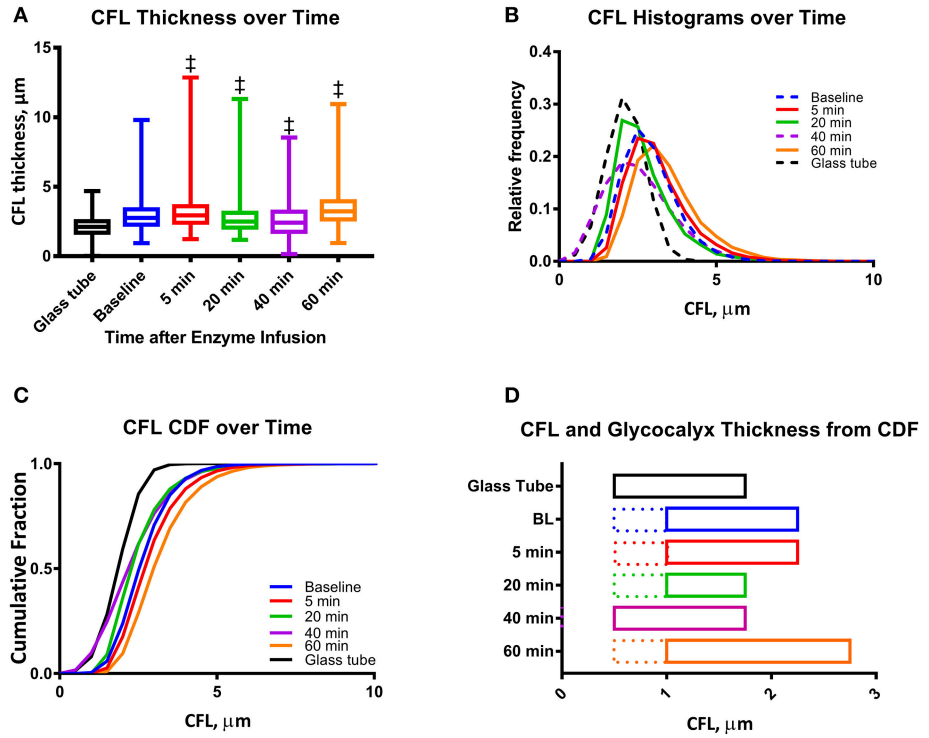


**FIGURE 3 |** Mean CFL thickness during enzymatic degradation of the EGL: **(A)** CFL thickness over time after enzyme infusion. The changes in the mean CFL were found to be statistically significant ($^{\ddagger}P < 0.05$) at all-time points. **(B)** Histograms of CFL thickness over time after enzyme infusion. For individual histograms, see **Supplemental Figure 2**. **(C)** Cumulative distribution functions (CDF) of CFL thickness over time after enzyme infusion. **(D)** One tailed 99% confidence interval of CFL over time after infusion. The left hand bound was determined as the point on the CDF at which $P < 0.01$, and the right hand bound was determined as the inflection point of the CDF (see **Supplemental Figure 1**). The thickness of the EGL (indicated as dotted line) was approximated by correcting the CFL distributions with that measured for a glass tube, in which only fluid hydrodynamic forces are present. ($^{\ddagger}P < 0.05$) compared to baseline.

measurements of blood flow velocities up to 40 mm/s with a precision that ranges between 0.5 and 1 µm (Ortiz et al., 2014) Arteriolar diameters exhibited minimal variations during the experiments after enzyme treatment. As such, arteriolar blood flow velocity was used to estimate relative changes in network flow resistance. Enzymatic degradation of the EGL decreases the plug flow behavior of the blood velocity profile shifting toward pipe flow behavior, as demonstrated by the decreasing magnitude of the blunting coefficient (**Figures 7C,D**). These results are once again in accordance with the electro-viscous effects produced by the EGL as the electrical forces present in the CFL invalidate the no-slip boundary condition that defines pipe flow. As degradation of the EGL decreases the magnitude of the electrical forces present in the CFL, pipe flow is observed after degradation of the glycocalyx, as the no-slip boundary condition is now valid. This paradigm can also be explained with respect to a classical fluid dynamics model posed by Damiano et al. in which the presence of the EGL promotes Darcy flow in the CFL by increasing the velocity gradients in the plasma interface, thus increasing viscous drag forces in the CFL (Damiano, 1998; Weinbaum et al., 2003). In addition to providing a mechanism for the mechanotransductive behavior, the presence of Darcy flow in the CFL invalidates the no-slip condition, necessary for pipe flow (Weinbaum et al., 2003; Tarbell and Shi, 2013). The EGL is thought to behave as a porous material with a high hydraulic resistance, and consequently plasma velocity through the EGL is very limited; although RBCs essentially slide over the EGL. Thus, degradation of the EGL could increase vascular resistance via preventing RBCs from gliding over the vessel wall.

Enzymatic degradation of the glycocalyx directly affects the ESL, the active composite of bound plasma constituents attached to the EGL. The ESL *per se* influences blood cell-vessel wall interactions, affects blood rheology, and determines solute transport out of the vessel lumen. The ESL function has been suggested to safeguard the fragile EGL from fluid shear stress and from direct physical interactions with blood cells (Secomb et al., 2001). Increased endothelial shear increases nitric oxide (NO) production, dilating vessels and reducing shear stress (Jacob et al., 2007). Additionally, it has been observed that under shear stress, human umbilical vein endothelial cells double the hyaluronic acid in the endothelial glycocalyx, suggesting a secondary mechanism by which the vascular endothelium responds to shear stress (Gouverneur et al., 2006). As the EGL is exposed to the shear stress of the plasma layer, a function of both the shear rate at the surface of the glycocalyx and the plasma viscosity, the surface of the ESL is exposed to the

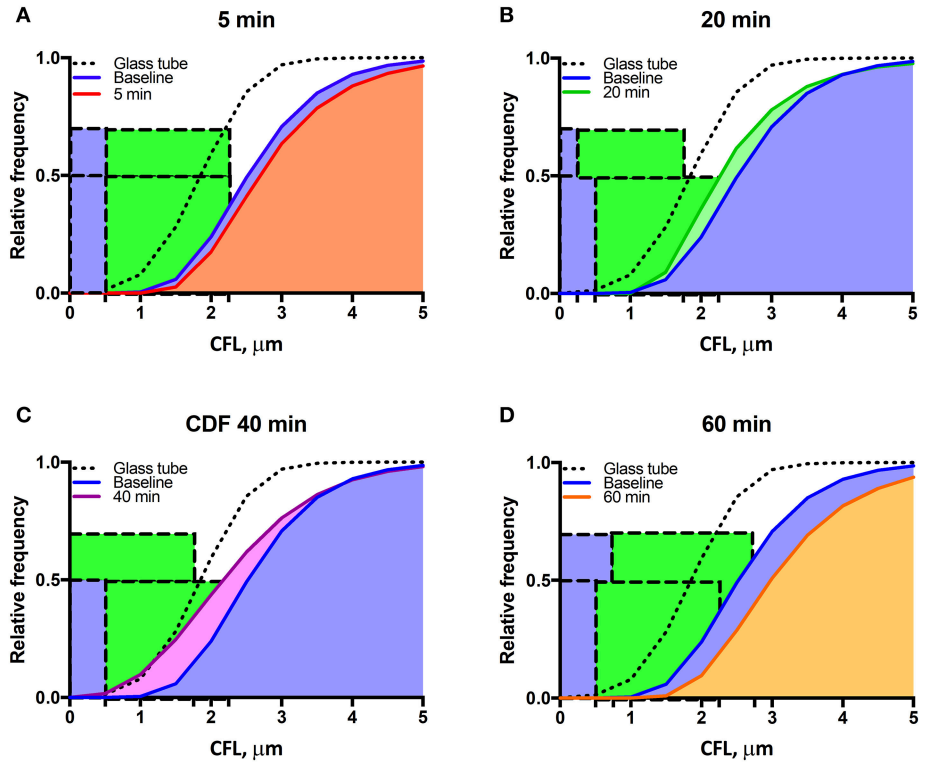


**FIGURE 4 |** Mean cumulative distribution function during enzymatic degradation of the EGL: CDFs at baseline and at **(A)** 5 min, **(B)** 20 min, **(C)** 40 min, and **(D)** 60 min after enzyme infusion. The blue bonding box represents the approximated thickness of the glycocalyx, and the green bounding box represents the one-tailed 99% confidence interval of the CFL thickness.

shear stress of the adjacent whole blood. The resultant effect on the signal transduction pathways of the endothelium could then be combined effects of fluid shear stress on both layers. Previous studies on relationship between the ESL in capillaries and flowing blood demonstrate that the ESL can be highly deformable (Long et al., 2004). However, the finite resistance to compression of the ESL prevents direct plasma shear stress to be generated by blood flow on endothelial cells by decreasing plasma fluid movement within the ESL (Pries et al., 2000). The plasma shear stress cannot be transmitted to the ESL as a fluid shear stress; rather, the ESL transfers its shear strain to the structures forming the ESL (Secomb et al., 2001). Enzymatically degrading the EGL impairs transduction of plasma fluid shear stress and solid shear stress in the ESL, which are both potential mechanisms of endothelial shear stress mechanotransduction (Florian et al., 2003). Therefore, endothelial cell surface shear stress transmitted to through the ESL, or plasma fluid shear stress within the ESL, remain plausible as the mechanism of blood flow mediated mechanotransduction by endothelial cells.

In addition, in capillaries, the ESL creates a large repulsive forces that supports the movement of RBCs by acting as a lubrication layer, which reduces capillary blood flow resistance (Secomb et al., 1998; Feng and Weinbaum, 2000). This observation highlights the role of the EGL in microvascular perfusion. Pathophysiological degradation of the EGL would increase capillary blood flow resistance by decreasing the thickness of the lubrication layer provided by the EGL. Recent studies have demonstrated that in chronically obese subjects, diabetic subjects, and subjects with coronary microvascular disease, the EGL is found to be thinner as compared to healthy subjects, resulting in impaired vasomotor activity, increased vascular permeability, and decreased perfusion. Additional studies have demonstrated marked improvement in perfusion in animal models with coronary microvascular disease by increasing recovery of the glycocalyx with metformin and sulodexide (van Haare et al., 2017). Therefore, as the ESL and the glycocalyx decrease capillary blood flow resistance, it seems plausible that pathophysiological degradation of the EGL may play a role in decreased perfusion associated with obesity and related pathophysiologies and influence further progression of these pathophysiologies (van Haare et al., 2017).

Various approaches have been used directly visualize or estimate the EGL due to the increased recognition of its functional importance. Groups have labeled the glycocalyx with specific markers that attach to one or more of its components, making them fluorescent or detectable (Vink and Duling, 1996). This demonstrates the presence of the EGE, or its components, but it does not establish the thickness of the EGL. Unfortunately,

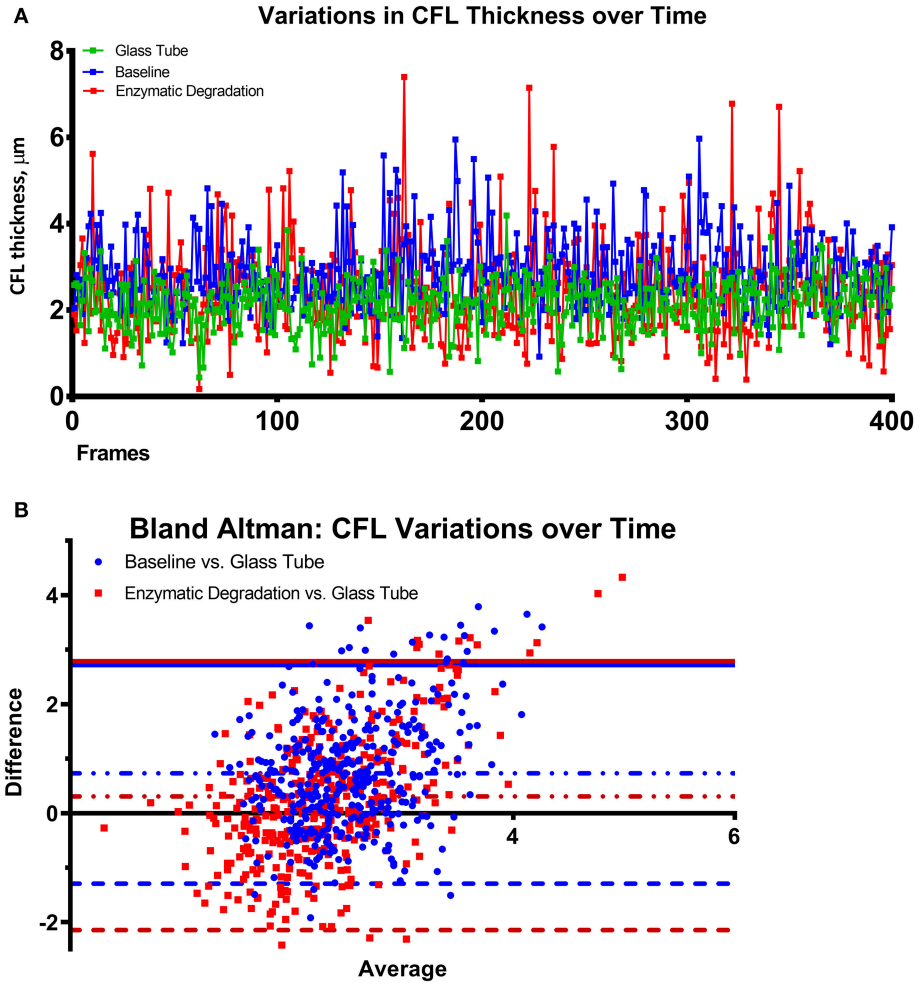


**FIGURE 5 |** Thickness of the CFL over time after enzymatic degradation of the EGL. **(A)** Fluctuations in the thickness of the CFL over time in a glass tube, at baseline, and after enzymatic degradation of the glycocalyx. **(B)** Bland Altman plots comparing the difference of the CFL thickness vs. a glass tube at baseline and after enzymatic degradation of the glycocalyx. The 95% confidence interval of the difference between the CFL of the blood vessels are illustrated with lines. The solid line indicates the positive end of the difference between the CFL of the blood vessels and the glass tube, which remained unaltered as it is determined by the vessel wall. The dotted line indicates the negative boundary of the difference between the CFL of the blood vessels and the glass tube, illustrates the increased erratic variations in the CFL of the blood vessel after the glycocalyx degradation.

the EGL is easily disturbed and very vulnerable to dehydration. Consequently, the EGL dimension is easily underestimated; early studies estimated EGL thickness to be approximated 20 nm in capillaries using transmission electron microscopy (TEM) (Luft, 1966). Other attempts using TEM reported the EGL to be around 40 nm (Ueda et al., 2004). These early estimations did not conform to experimental and theoretical estimation however, suggesting that the EGL should be nearer 1 μm (Klitzman and Duling, 1979; Vink and Duling, 1996). The thickness of the EGL remains controversial, as resent studies with fluorescent labeling and high-resolution fluorescent micro-particle image velocimetry suggest that the GGL is around 0.5 μm in post-capillary venules of the rat mesenteric and the mouse cremaster muscle, both using intravital microscopy (Smith et al., 2003; Gao and Lipowsky, 2010). Recently, new imaging protocols using fluorescently tagged antibodies to heparan sulfate and hyaluronan has revealed a much thicker EGL, over 4.0 μm in the mouse common carotid artery (Megens et al., 2007), 2.2 μm in the mouse internal carotid artery (van den Berg et al., 2009), and 2.5 μm in the external carotid artery (Reitsma et al., 2011). Most recently, cryo-TEM, which avoids the dehydration artifacts of early TEM, has suggested that the thickness of the EGL is of the order of 10 μm on cultured endothelial cells *in vitro* (Ebong et al., 2011). Therefore, the thickness of the EGL measured from our method is in good agreement with both the classical method for measurement of the EGL and other indirect methods (Weinbaum et al., 2007). The approach used in this manuscript to estimate the EGL based on the hydrodynamic implications that the presence of the EGL has in the thickness of the CLF relative to glass tubes of similar

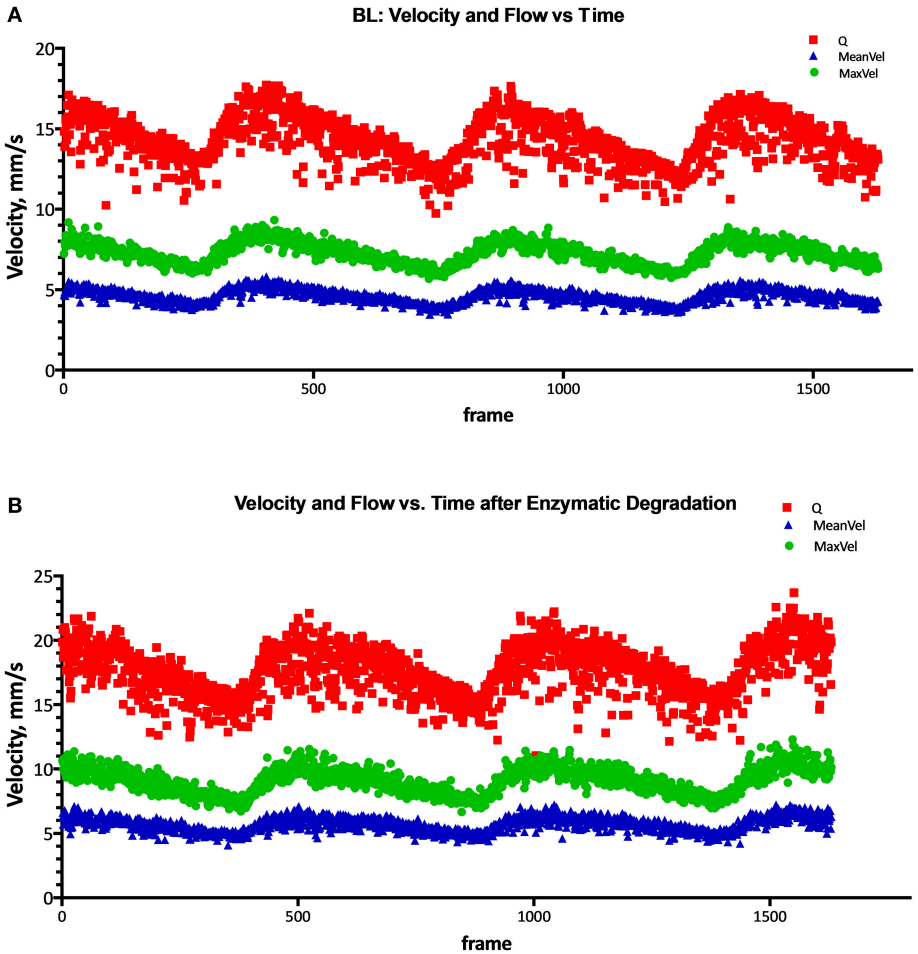


**FIGURE 6 |** Flow, mean velocity, and peak velocity after degradation of the EGL. Flow (Q), mean velocity ($V_{mean}$), and peak max velocity ($V_{max}$) at **(A)** Baseline, and **(B)** after enzymatic degradation of the glycocalyx.

diameters. The estimation of the EGL presented in here could differ from the physical thickness of the EGL; although it corresponds to the functional hydrodynamic layer that affect blood flow and exchanges between the flowing blood and the tissues.

The EGL affects blood apparent viscosity in microvessel via the CFL thickness, which is the region with much lower viscosity than the lumen core heavily populated with pack RBCs. Variations in the thickness of the CFL are a consequence of both the Fahraeus effect and the Fahraeus–Lindqvist effect (Fåhraeus, 1929). In the microvasculature (<40 μm), the CFL thickness is significant percentage of the microvessel tube diameter, resulting in smaller microvessels having a lower relative apparent viscosity compared to larger vessels (>40 μm). The effects of the EGL with respect to the Fahraeus effect have an impact on oxygen flux to tissues and NO scavenging by hemoglobin in the RBCs, as the EGL contributes to the separation of RBCs from the vascular endothelium. The separation of blood flow between the vessel lumen core, rich of RBCs, and the endothelium, by the CFL zones affects oxygen delivery and NO consumption by RBCs. Computational models for oxygen and NO transport indicate that the CFL determines resistance to diffusion of oxygen and NO to and from RBCs (Lamkin-Kennard et al., 2004; Ng et al., 2015). In addition, the CFL thickness becomes more important for controlling and enhancing oxygen release and NO bioavailability to both the surrounding tissue and the vascular wall in microvessels with diameters of 30 μm or less (Lamkin-Kennard et al., 2004). The glycocalyx might have additional effects in NO transport, as it modulates vessel wall shear stress-dependent NO production by the endothelium.

The blood flow velocity profiles appear to be a function of the CFL thickness, and therefore in the vessel wall shear stress on the endothelium walls. The thickness of the CFL and its variability is demonstrated by fluctuations in pressure about the mean, as quantified by the standard deviation of the pressure wave. Consequently, changes in CFL thickness counteract changes in blood flow; as CFL thickness increases, volumetric blood flow rate decreases. Volumetric blood flow rate also decreases as the correlation length decreases and/or the standard deviation of

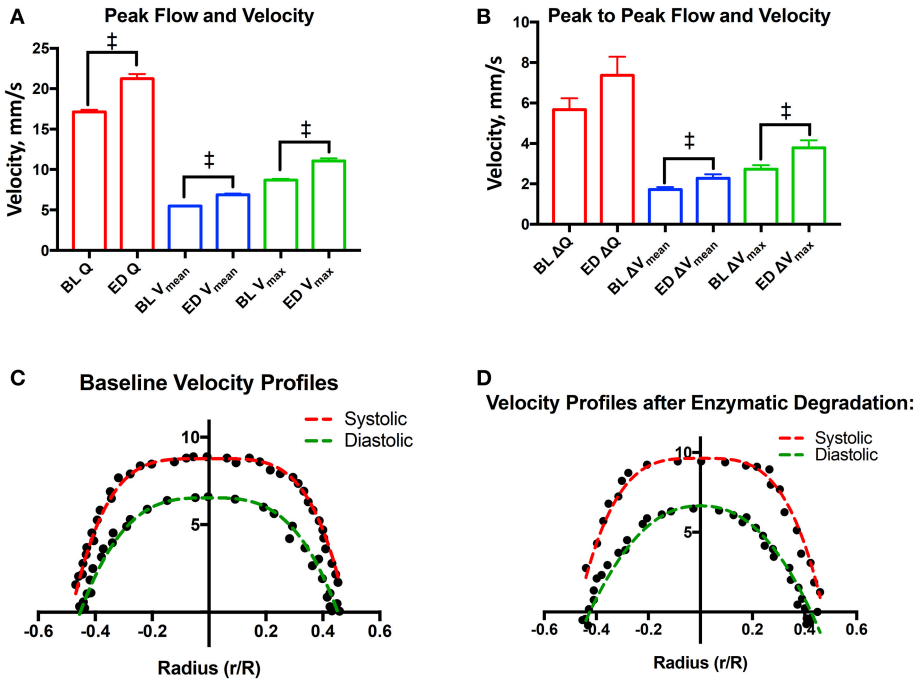


**FIGURE 7 |** Velocity profiles after degradation of the EGL: **(A)** Systolic flow, mean velocity, and peak velocity after degradation of the glycocalyx ($^{\ddagger}P < 0.05$). **(B)** Changes in flow (Q), mean velocity ($V_{mean}$), and max peak velocity ($V_{max}$) between systole and diastole after degradation of the glycocalyx ($^{\ddagger}P < 0.05$). **(C)** Baseline velocity profiles during systole and diastole. Results were fit to the model, $\upsilon\,(r) = V_{max}\left(1 - \left|\frac{r}{R}\right|^{K}\right)$. During systole, $V_{max} = 8.8 \pm 0.2$, $R = 0.48 \pm 0.01$, and $K = 4.1 \pm 0.4$. During diastole $V_{max} = 6.5 \pm 0.4$, $R = 0.45 \pm 0.01$, and $K = 3.1 \pm 0.6$. **(D)** Velocity profiles during systole and diastole after enzymatic degradation of the glycocalyx. Results were fit to the model, $\upsilon\,(r) = V_{max}\left(1 - \left|\frac{r}{R}\right|^{K}\right)$. During systole, $V_{max} = 9.6 \pm 0.5$, $R = 0.47 \pm 0.01$, and $K = 3.4 \pm 0.7$. During diastole $V_{max} = 6.7 \pm 0.7$, $R = 0.43 \pm 0.01$, and $K = 2.2 \pm 0.6$. ($^{\ddagger}P < 0.05$) compared to baseline.

the amplitude increases. The mean shear rate can also increase with fluctuations in the endothelium and the CFL. Increasing or decreasing fluctuations in the endothelium can also extend the entrance length (the length through which the flow regime is not fully-developed, and shear stress statistics are constant). Thus, blood viscosity, estimated from *in vivo* experiments by Poiseuille's law, depends not only on the rheological properties of blood, but also by the statistical parameters that quantify endothelium roughness.

The distribution of plasma and RBCs at the vascular wall has traditionally been attributed to the Fahraeus effect and axial migration of red cells (Fåhraeus, 1929). However, it is now well established that ESL also importantly affect this distribution (Pries et al., 2000). The ESL significantly restricts the approach of RBCs and plasma to the vascular wall (Kim et al., 2007). This study was conducted to evaluate the effects of the effects of enzymatic degradation of the EGL on blood flow via preparation of the rat cremaster muscle. We evaluated the hypothesis that enzymatic degradation of the EGL resulted in variations and reductions of the CFL, increased randomness of blood flow, and variations in the observed microhemodynamics. By measuring the change in the thickness of the CFL over time after degradation as well as the probability distribution of RBCs as a function of distance, it is possible to establish a relationship between the micro hemodynamic properties of blood flow and the EGL. Recent studies have demonstrated that the glycocalyx influences homogenous flow distribution in the microcirculation (McClatchey et al., 2016). In addition, many recent studies have implicated the alterations in the mechanotransductive effects of the EGL under different pathophysiological conditions, including inflammation, diabetes, and atherosclerosis (Harrison et al., 2006). As such, future studies should investigate changes in the hemodynamics under these pathophysiological conditions that result due to alterations in the EGL utilizing *in vivo* models.

## CONCLUSION

These results demonstrate that enzymatic degradation of the EGL results in a statistically significant increase in flow and mean velocity as well as a decrease in the bluntness of the velocity profile in the microcirculation. In addition to providing *in vivo* validation of many mathematical models that explain the hydrodynamic effects of the EGL, these results suggest that the EGL is responsible for alterations in blood flow in microvessels via both the electrical and hydrodynamic fluid forces that it produces. Future studies should investigate the changes in hydrodynamics associated with pathophysiological alterations in the EGL.

## AUTHOR CONTRIBUTIONS

All authors listed have made a substantial, direct and intellectual contribution to the work, and approved it for publication.

## FUNDING

This work was supported by NIH grants from the Heart Lung and Blood Institute, P01-HL11090, R01HL126945, and R01-HL138116.

## SUPPLEMENTARY MATERIAL

The Supplementary Material for this article can be found online at: https://www.frontiersin.org/articles/10.3389/fphys.2018.00168/full#supplementary-material

**Supplemental Figure 1 |** Numerical differences of the cumulative distribution function of the CFL thickness. To determine the inflection point of the CDF, the second numerical difference of order 4 was determined, and the bisection method was used to determine the root of the second derivative.

**Supplemental Figure 2 |** Mean histograms of the thickness of the CDF. Histograms of the thickness of the CDF during **(A)** Baseline, and **(B)** 40 min after enzyme infusion.

## REFERENCES


Adamson, R. H., and Clough, G. (1992). Plasma proteins modify the endothelial cell glycocalyx of frog mesenteric microvessels. *J. Physiol.* 445, 473–486. doi: 10.1113/jphysiol.1992.sp018934

Baez, S. (1973). An open cremaster muscle preparation for the study of blood vessels by *in vivo* microscopy. *Microvasc. Res.* 5, 384–394. doi: 10.1016/0026-2862(73)90054-X

Becker, B. F., Chappell, D., and Jacob, M. (2010). Endothelial glycocalyx and coronary vascular permeability: the fringe benefit. *Basic Res. Cardiol.* 105, 687–701. doi: 10.1007/s00395-010-0118-z

Bernfield, M., Götte, M., Park, P. W., Reizes, O., Fitzgerald, M. L., Lincecum, J., et al. (1999). Functions of cell surface heparan sulfate proteoglycans. *Annu. Rev. Biochem.* 68, 729–777. doi: 10.1146/annurev.biochem.68.1.729

Cabrales, P., Vázquez, B. Y., Tsai, A. G., and Intaglietta, M. (2007). Microvascular and capillary perfusion following glycocalyx degradation. *J. Appl. Physiol.* 102, 2251–2259. doi: 10.1152/japplphysiol.01155.2006

Cokelet, G. R., and Goldsmith, H. L. (1991). Decreased hydrodynamic resistance in the two-phase flow of blood through small vertical tubes at low flow rates. *Circ. Res.* 68, 1–17. doi: 10.1161/01.RES.68.1.1

Damiano, E. (1998). "Blood flow in microvessels lined with a poroelastic wall layer," in *Poromechanics*, eds J. F. Thimus, Y. Abousleiman, A. H. D. Cheng, O. Coussy, and E. Detourna (Rotterdam: Balkema), 403–408.

Ebong, E. E., Macaluso, F. P., Spray, D. C., and Tarbell, J. M. (2011). Imaging the endothelial glycocalyx *in vitro* by rapid freezing/freeze substitution transmission electron microscopy. *Arterioscler. Thromb. Vasc. Biol.* 31, 1908–1915. doi: 10.1161/ATVBAHA.111.225268

Fåhraeus, R. (1929). The suspension stability of the blood. *Physiol. Rev.* 9, 241–274. doi: 10.1152/physrev.1929.9.2.241

Feng, J., and Weinbaum, S. (2000). Lubrication theory in highly compressible porous media: the mechanics of skiing, from red cells to humans. *J. Fluid Mech.* 422, 281–317. doi: 10.1017/S0022112000001725

Florian, J. A., Kosky, J. R., Ainslie, K., Pang, Z., Dull, R. O., and Tarbell, J. M. (2003). Heparan sulfate proteoglycan is a mechanosensor on endothelial cells. *Circ. Res.* 93, e136–e42. doi: 10.1161/01.RES.0000101744.47866.D5

Gao, L., and Lipowsky, H. H. (2010). Composition of the endothelial glycocalyx and its relation to its thickness and diffusion of small solutes. *Microvasc. Res.* 80, 394–401. doi: 10.1016/j.mvr.2010.06.005

Gouverneur, M., Spaan, J. A., Pannekoek, H., Fontijn, R. D., and Vink, H. (2006). Fluid shear stress stimulates incorporation of hyaluronan into endothelial cell glycocalyx. *Am. J. Phys. Heart Circ. Physiol.* 290, H458–H462. doi: 10.1152/ajpheart.00592.2005

Harrison, D. G., Widder, J., Grumbach, I., Chen, W., Weber, M., and Searles, C. (2006). Endothelial mechanotransduction, nitric oxide and vascular inflammation. *J. Intern. Med.* 259, 351–363. doi: 10.1111/j.1365-2796.2006.01621.x

Jacob, M., Rehm, M., Loetsch, M., Paul, J. O., Bruegger, D., Welsch, U., et al. (2007). The endothelial glycocalyx prefers albumin for evoking shear stress-induced, nitric oxide-mediated coronary dilatation. *J. Vasc. Res.* 44, 435–443. doi: 10.1159/000104871

Kim, S., Kong, R. L., Popel, A. S., Intaglietta, M., and Johnson, P. C. (2006). A computer-based method for determination of the cell-free layer width in microcirculation. *Microcirculation* 13, 199–207. doi: 10.1080/10739680600556878

Kim, S., Kong, R. L., Popel, A. S., Intaglietta, M., and Johnson, P. C. (2007). Temporal and spatial variations of cell-free layer width in arterioles. *Am. J. Phys. Heart Circ. Physiol.* 293, H1526–H1535. doi: 10.1152/ajpheart.01090.2006

Klitzman, B., and Duling, B. R. (1979). Microvascular hematocrit and red cell flow in resting and contracting striated muscle. *Am. J. Physiol. Heart Circ. Physiol.* 237, H481–H490. doi: 10.1152/ajpheart.1979.237.4.H481

Lamkin-Kennard, K. A., Jaron, D., and Buerk, D. G. (2004). Impact of the Fåhraeus effect on NO and $O_2$ biotransport: a computer model. *Microcirculation* 11, 337–349. doi: 10.1080/10739680490437496

Long, D. S., Smith, M. L., Pries, A. R., Ley, K., and Damiano, E. R. (2004). Microviscometry reveals reduced blood viscosity and altered shear rate and shear stress profiles in microvessels after hemodilution. *Proc. Natl. Acad. Sci. U.S.A.* 101, 10060–10065. doi: 10.1073/pnas.0402937101

Luft, J. H. (1966). Fine structures of capillary and endocapillary layer as revealed by ruthenium red. *Fed. Proc.* 25, 1773–1783.

Mathworks (2017). *MATLAB*. Natick, MA. Available online at: https://www.mathworks.com/products/matlab.html

McClatchey, P. M., Schafer, M., Hunter, K. S., and Reusch, J. E. (2016). The endothelial glycocalyx promotes homogenous blood flow distribution within the microvasculature. *Am. J. Phys. Heart Circ. Physiol.* 311, H168–H176. doi: 10.1152/ajpheart.00132.2016

Megens, R. T., Reitsma, S., Schiffers, P. H., Hilgers, R. H, De Mey, J. G., Slaaf, D. W., et al. (2007). Two-photon microscopy of vital murine elastic and muscular arteries. *J. Vasc. Res.* 44, 87–98. doi: 10.1159/000098259

National Research Council Committee US (2010). *Guide for the Care and Use of Laboratory Animals*. Washington, DC: National Academies Press.

Ng, Y. C., Namgung, B., and Kim, S. (2015). Two-dimensional transient model for prediction of arteriolar NO/O2 modulation by spatiotemporal variations in cell-free layer width. *Microvasc. Res.* 97, 88–97. doi: 10.1016/j.mvr.2014.08.010

Nieuwdorp, M., Meuwese, M. C., Vink, H., Hoekstra, J. B., Kastelein, J. J., and Stroes, E. S. (2005). The endothelial glycocalyx: a potential barrier between health and vascular disease. *Curr. Opin. Lipidol.* 16, 507–511. doi: 10.1097/01.mol.0000181325.08926.9c

Ortiz, D., Briceño, J. C., and Cabrales, P. (2014). Microhemodynamic parameters quantification from intravital microscopy videos. *Physiol. Meas.* 35, 351–367. doi: 10.1088/0967-3334/35/3/351

Osterloh, K., Ewert, U., and Pries, A. R. (2002). Interaction of albumin with the endothelial cell surface. *Am. J. Phys. Heart Circ. Physiol.* 283, H398–H405. doi: 10.1152/ajpheart.00558.2001

Pries, A. R., Secomb, T. W., Gaehtgens, P., and Gross, J. F. (1990). Blood flow in microvascular networks. Experiments and simulation. *Circ. Res.* 67, 826–834. doi: 10.1161/01.RES.67.4.826

Pries, A. R., Secomb, T. W., Jacobs, H., Sperandio, M., Osterloh, K., and Gaehtgens, P. (1997). Microvascular blood flow resistance: role of endothelial surface layer. *Am. J. Phys. Heart Circ. Physiol.* 273, H2272–H2279. doi: 10.1152/ajpheart.1997.273.5.H2272

Pries, A. R., Secomb, T. W., and Gaehtgens, P. (2000). The endothelial surface layer. *Pflügers Arch.* 440, 653–666. doi: 10.1007/s004240000307

Reinke, W., Gaehtgens, P., and Johnson, P. (1987). Blood viscosity in small tubes: effect of shear rate, aggregation, and sedimentation. *Am. J. Physiol. Heart Circ. Physiol.* 253, H540–H547. doi: 10.1152/ajpheart.1987.253.3.H540

Reitsma, S., oude Egbrink, M. G., Vink, H., Van Den Berg, B. M., Passos, V. L., Engels, W., et al. (2011). Endothelial glycocalyx structure in the intact carotid artery: a two-photon laser scanning microscopy study. *J. Vasc. Res.* 48, 297–306. doi: 10.1159/000322176

Secomb, T. W., Hsu, R., and Pries, A. R. (1998). A model for red blood cell motion in glycocalyx-lined capillaries. *Am. J. Physiol. Heart Circ. Physiol.* 274, H1016–H1022. doi: 10.1152/ajpheart.1998.274.3.H1016

Secomb, T. W., Hsu, R., and Pries, A. R. (2001). Effect of the endothelial surface layer on transmission of fluid shear stress to endothelial cells. *Biorheology* 38, 143–150.

Smith, M. L., Long, D. S., Damiano, E. R., and Ley, K. (2003). Near-wall μ-PIV reveals a hydrodynamically relevant endothelial surface layer in venules *in vivo*. *Biophys. J.* 85, 637–645. doi: 10.1016/S0006-3495(03)74507-X

Tarbell, J. M., and Shi, Z. D. (2013). Effect of the glycocalyx layer on transmission of interstitial flow shear stress to embedded cells. *Biomech. Model. Mechanobiol.* 12, 111–121. doi: 10.1007/s10237-012-0385-8

Ueda, A., Shimomura, M., Ikeda, M., Yamaguchi, R., and Tanishita, K. (2004). Effect of glycocalyx on shear-dependent albumin uptake in endothelial cells. *Am. J. Phys. Heart Circ. Physiol.* 287, H2287–H2294. doi: 10.1152/ajpheart.00808.2003

van den Berg, B. M., Spaan, J. A., and Vink, H. (2009). Impaired glycocalyx barrier properties contribute to enhanced intimal low-density lipoprotein accumulation at the carotid artery bifurcation in mice. *Pflügers Arch. Eur. J. Physiol.* 457, 1199–1206. doi: 10.1007/s00424-008-0590-6

van Haare, J., Kooi, M. E.,van Teeffelen, J. W., Vink, H., Slenter, J., Cobelens, H., et al. (2017). Metformin and sulodexide restore cardiac microvascular perfusion capacity in diet-induced obese rats. *Cardiovasc. Diabetol.* 16:47. doi: 10.1186/s12933-017-0525-7

Vink, H., and Duling, B. R. (1996). Identification of distinct luminal domains for macromolecules, erythrocytes, and leukocytes within mammalian capillaries. *Circ. Res.* 79, 581–589. doi: 10.1161/01.RES.79.3.581

Weinbaum, S., Tarbell, J. M., and Damiano, E. R. (2007). The structure and function of the endothelial glycocalyx layer. *Annu. Rev. Biomed. Eng.* 9, 121–167. doi: 10.1146/annurev.bioeng.9.060906.151959

Weinbaum, S., Zhang, X., Han, Y., Vink, H., and Cowin, S. C. (2003). Mechanotransduction and flow across the endothelial glycocalyx. *Proc. Natl. Acad. Sci. U.S.A.* 100, 7988–7995. doi: 10.1073/pnas.1332808100

Zhang, J., Johnson, P. C., and Popel, A. S. (2009). Effects of erythrocyte deformability and aggregation on the cell free layer and apparent viscosity of microscopic blood flows. *Microvasc. Res.* 77, 265–272. doi: 10.1016/j.mvr.2009.01.010

**Conflict of Interest Statement:** The authors declare that the research was conducted in the absence of any commercial or financial relationships that could be construed as a potential conflict of interest.

*Copyright © 2018 Yalcin, Jani, Johnson and Cabrales. This is an open-access article distributed under the terms of the Creative Commons Attribution License (CC BY). The use, distribution or reproduction in other forums is permitted, provided the original author(s) and the copyright owner are credited and that the original publication in this journal is cited, in accordance with accepted academic practice. No use, distribution or reproduction is permitted which does not comply with these terms.*

frontiers in Physiology

REVIEW
published: 22 February 2018
doi: 10.3389/fphys.2018.00125

# Erythrocytes and Vascular Function: Oxygen and Nitric Oxide

*Christine C. Helms*[1]*, *Mark T. Gladwin*[2,3] *and Daniel B. Kim-Shapiro*[4,5]

[1] Physics Department, University of Richmond, Richmond, VA, United States, [2] Heart, Lung, Blood and Vascular Medicine Institute, University of Pittsburgh, Pittsburgh, PA, United States, [3] Division of Pulmonary, Allergy, and Critical Care Medicine, Department of Medicine, University of Pittsburgh, Pittsburgh, PA, United States, [4] Physics Department, Wake Forest University, Winston-Salem, NC, United States, [5] Translational Science Center, Wake Forest University, Winston-Salem, NC, United States

Erythrocytes regulate vascular function through the modulation of oxygen delivery and the scavenging and generation of nitric oxide (NO). First, hemoglobin inside the red blood cell binds oxygen in the lungs and delivers it to tissues throughout the body in an allosterically regulated process, modulated by oxygen, carbon dioxide and proton concentrations. The vasculature responds to low oxygen tensions through vasodilation, further recruiting blood flow and oxygen carrying erythrocytes. Research has shown multiple mechanisms are at play in this classical hypoxic vasodilatory response, with a potential role of red cell derived vasodilatory molecules, such as nitrite derived nitric oxide and red blood cell ATP, considered in the last 20 years. According to these hypotheses, red blood cells release vasodilatory molecules under low oxygen pressures. Candidate molecules released by erythrocytes and responsible for hypoxic vasodilation are nitric oxide, adenosine triphosphate and S-nitrosothiols. Our research group has characterized the biochemistry and physiological effects of the electron and proton transfer reactions from hemoglobin and other ferrous heme globins with nitrite to form NO. In addition to NO generation from nitrite during deoxygenation, hemoglobin has a high affinity for NO. Scavenging of NO by hemoglobin can cause vasoconstriction, which is greatly enhanced by cell free hemoglobin outside of the red cell. Therefore, compartmentalization of hemoglobin inside red blood cells and localization of red blood cells in the blood stream are important for healthy vascular function. Conditions where erythrocyte lysis leads to cell free hemoglobin or where erythrocytes adhere to the endothelium can result in hypertension and vaso constriction. These studies support a model where hemoglobin serves as an oxido-reductase, inhibiting NO and promoting higher vessel tone when oxygenated and reducing nitrite to form NO and vasodilate when deoxygenated.

**Keywords: erythrocytes, hemoglobin, hemolysis, hypoxic vasodilation, nitric oxide, nitrite**

OPEN ACCESS

***Edited by:***
*Dan E. Berkowitz,*
*Johns Hopkins University,*
*United States*

***Reviewed by:***
*Suowen Xu,*
*University of Rochester, United States*
*Jingyan Han,*
*Boston University, United States*

***Correspondence:**
*Christine C. Helms*
*chelms@richmond.edu*

***Specialty section:***
*This article was submitted to Vascular Physiology, a section of the journal Frontiers in Physiology*

***Received:*** *30 October 2017*
***Accepted:*** *07 February 2018*
***Published:*** *22 February 2018*

***Citation:***
*Helms CC, Gladwin MT and Kim-Shapiro DB (2018) Erythrocytes and Vascular Function: Oxygen and Nitric Oxide. Front. Physiol. 9:125. doi: 10.3389/fphys.2018.00125*

How erythrocytes modulate vascular tone has been widely studied over the last two decades. The vasodilation of the vasculature under hypoxic conditions has inspired much research ranging from the effect of oxygen partial pressure on smooth muscle cell contractility and endothelial nitric oxide synthase (eNOS) activity to nitrite reduction by hemoglobin (Hb) inside erythrocytes and subsequent production of nitric oxide (**Figure 1**). Here we review how red blood cells (RBCs) and hemoglobin regulate vascular function and blood flow.

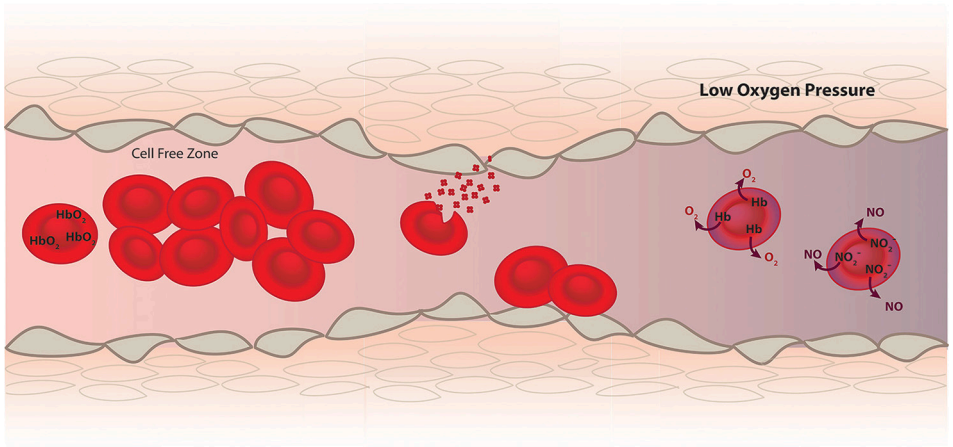


**FIGURE 1 |** RBCs function as a transporter of oxygen from the lungs to the tissue and help establish hemostasis and vascular function. Since Hb inside RBCs is a very effective scavenger of NO, a vasodilator produced by the endothelium (brown), mechanism such as a cell free zone created by fluid dynamics, RBC membrane and internal diffusion minimize NO scavenging. In diseases where hemolysis and RBC adhesion occur these mechanisms to minimize NO scavenging are compromised and vasoconstriction occurs. However, in addition to scavenging NO data supports a role of deoxygenated RBCs in the production of NO leading to vasodilation under hypoxic conditions.

## OXYGEN DELIVERY

Many biochemistry texts provide thorough descriptions of the basic mechanisms of oxygen delivery by hemoglobin. Therefore, we will limit our discussion to a brief introduction. The hemoglobin molecule is a heterotetramer of hemoglobin alpha-beta dimers. Under high oxygen tension, each monomer can bind an $O_2$ molecule. As hemoglobin binds oxygen, conformational changes occur to the protein and the binding affinity of the protein for molecular oxygen increases. Thus, binding is cooperative so that binding subsequent molecules of oxygen becomes easier after initial binding. Cooperative binding can be understood by a two-state model: The high affinity R-state and the low affinity T-state (Monod et al., 1965; Eaton et al., 1999). When hemoglobin has one or less oxygen molecules bound it is virtually always in the tense T-state. When it has 3–4 oxygen molecules bound it is virtually always in the R-state. Once 2 or more oxygen bind to a hemoglobin molecule that has no oxygen it will undergo a conformational change to the R-state where its oxygen affinity is now higher and it binds more oxygen. This homotropic regulation leads to a sigmoidal curve of hemoglobin fractional saturation vs. partial pressure of oxygen and allows hemoglobin to function as an efficient transporter of oxygen from the lungs to the tissues.

The complexity of oxygen delivery goes beyond the homotropic regulation. The pH of the blood also effects oxygen binding. The Bohr Effect, reported in the early 1900's, describes how increased acidity which occurs at low oxygen tension leads to protonation and stabilization of the T-state of hemoglobin promoting oxygen release. Additionally, carbon dioxide and 2,3-bisphosphate also act as heterotropic regulators, both decreasing the affinity of Hb for oxygen.

Therefore, RBCs contribute to vascular function through the delivery of oxygen by hemoglobin.

One mechanism through which oxygen tension and therefore RBCs effect vascular function is the contractile force of smooth muscle cells. Chang and Detar reported that a reduction in oxygen pressure led to a reduced contractile tension of helical strips cut from aorta, femoral arteries and small arteries from skeletal muscle (Chang and Detar, 1980). Additionally Taggart et al saw a decrease in smooth muscle force in hypoxia indicating smooth muscle response to oxygen may be independent of factors from the endothelium (Taggart and Wray, 1998). Potential mechanics of smooth muscle response to oxygen tension are increased ATP-sensitive $K^+$ efflux or decreased voltage-sensitive $Ca^{+2}$ influx (Franco-Obregón et al., 1995; Taggart and Wray, 1998). These effects have been recently reviewed (Jackson, 2016).

Alternatively, low oxygen tension effects the endothelial production of nitric oxide (NO) by eNOS, which requires oxygen as a substrate along with L-arginine (Palmer and Moncada, 1989; Kwon et al., 1990). Many researchers have shown diminished relaxation by endothelial cells under low oxygen tension (Furchgott and Zawadzki, 1980; De Mey and Vanhoutte, 1983; Lieberthal et al., 1989). Specifically, the apparent $K_m$ of eNOS for $O_2$ is 4 μM and NOS activity begins to slow down once oxygen tensions starts falling below 1% (7.6 torr or 10 μM) (Abu-Soud et al., 2000; van Faassen et al., 2009). In summary, through the management of oxygen delivery RBCs effect eNOS function and smooth muscle contractility.

## COMPARTMENTALIZATION AND LOCALIZATION OF HEMOGLOBIN

In addition to oxygen delivery, hemoglobin affects vascular function as a strong scavenger of NO. Furchgott and coworkers discovered that there is an agent produced in the endothelium

that relaxes blood vessels, the endothelium relaxation factor (EDRF) (Furchgott and Zawadzki, 1980). The EDRF was then identified as NO (Ignarro et al., 1987; Palmer et al., 1987) that acts via activation of soluble guanylyl cyclase (Arnold et al., 1977). Endothelial nitric oxide synthase located on endothelial cell membranes produces NO that binds to soluble guanylyl cyclase in smooth muscles cells triggering a cell-signaling cascade that results in vasodilation. Chu et al. demonstrated the physiological regulation of blood flow and vasomotion by endogenously produced NO in awake dogs (Chu et al., 1991) and Quyyumi et al. showed atherosclerosis risk factors altered the response of coronary arteries to diminished NO production (Quyyumi et al., 1995). Additionally, NO has the anti-thrombotic effect of diminishing platelet activation (Schafer et al., 1980) and the anti-inflammatory effect of inhibiting leukocyte adhesion to the endothelium (Kubes et al., 1991). NO also leads to indirect vasodilation by inhibiting sympathetic vasoconstriction (Zanzinger et al., 1994). This is only a very small selection of a strong body of work that displays the role of NO in vascular function, which has been recently reviewed (Lundberg et al., 2015).

Since hemoglobin is present in the blood at a concentration of 10 mM in heme and ferrous heme has a strong affinity for NO with a dissociation constant of $K_D$ $10^{-10}$ to $10^{-11}$ M (Cooper, 1999), and the association rate constant is $10^7$-$10^8$ $M^{-1}s^{-1}$ (Cassoly and Gibson, 1975), you might expect there to be no free NO at all.

$$\mathrm{HbFe(II)} + \mathrm{NO} \underset{slow}{\overset{fast}{\rightleftharpoons}} \mathrm{HbFe(II)NO}. \quad (1)$$

Moreover, oxygenated hemoglobin reacts with NO to form nitrate (dioxygenation of NO) extremely fast (6–8 $\times$ $10^8$ $M^{-1}s^{-1}$) (Doyle and Hoekstra, 1981; Eich et al., 1996; Herold et al., 2001) inactivating the NO, so that calculations predict that NO could not act as the EDRF (Lancaster, 1994; Vaughn et al., 1998).

$$\mathrm{HbFe(II)O_2} + \mathrm{NO} \rightarrow \mathrm{HbFe(III)} + \mathrm{NO_3^-}. \quad (2)$$

However, as demonstrated above in the work by Chu et al. endothelial NO does play a physiological role in vascular function (Chu et al., 1991).

One can explain this paradox of NO bioavailability and Hb concentration in the blood by considering Hb encapsulation by RBCs. Experiments where RBCs are mixed with NO in suspension or in a stopped flow apparatus show that RBCs scavenge NO 1,000 times slower than cell-free Hb (Liu et al., 1998; Vaughn et al., 2000). Researchers have attributed this change in the rate of scavenging to a few mechanisms. One mechanism is the diffusion of NO to the RBC, which contributes to an unstirred layer around the cell (Coin and Olson, 1979; Liu et al., 1998, 2002; Azarov et al., 2005). A second mechanism is the membrane of the RBC acting as a barrier to diffusion (Vaughn et al., 2000; Huang et al., 2001, 2007). Third is diffusion of NO inside the RBC (Vaughn et al., 2000; Sakai et al., 2008). Our work suggests that rate limitations due to diffusion to the RBC are predominant (Azarov et al., 2005, 2011).

In addition to these changes under static conditions, a cell free zone created by the fluid dynamics of blood flow further reduces NO scavenging. The velocity of blood near the vessel wall is slower than in the center of the vessel due to friction. This creates a pressure gradient that pushes RBCs toward the center of the vessel away from the NO producing endothelium. Bugliarello and Sevilla, Cokelet and Liao et al. experimentally showed the presence of a cell free zone and computational modeling by Butler et al. supported its ability to reduce NO scavenging (Bugliarello and Sevilla, 1970; Cokelet, 1972; Butler et al., 1998; Liao et al., 1999). Subsequently, Liao et al experimentally demonstrated its ability to reduce NO scavenging using arteriole myography (Liao et al., 1999). Therefore, the compartmentalization of Hb inside the RBC and the localization of RBCs to the center of vessels have a strong influence on vascular function by minimizing NO scavenging.

## RBC DISEASE—NO SCAVENGING

In disease, RBC membrane abnormalities promote thrombosis (Ataga, 2009). Setty et al. showed exposure of phosphatidylserine on RBC membranes correlates with plasma indicators of thrombosis (Setty et al., 2001). In addition, changes to the RBC membrane lead to RBC adhesion to the endothelium. Diseases such as malaria, beta-thalassemia, diabetes mellitus, and sickle cell disease show increased RBC adhesion to endothelial cells (Kaul et al., 1989; Hovav et al., 1999; Cooke et al., 2004). Adhesion disrupts the cell free zone, which brings RBCs and Hb closer to the endothelium. Hoover et al. showed increased adhesion of RBCs from sickle cell patients to endothelial cells (Hoover et al., 1979) and Hebbel et al further demonstrated sickle RBC adhesion and suggested the adhesion may be a pathogenic factor in microvascular occlusion (Hebbel et al., 1980b). Hebbel also demonstrated a correlation between erythrocyte adhesion and sickle cell disease severity (Hebbel et al., 1980a). Kaul et al. developed a two-stage model of RBC adhesion initiating vaso-occlusion (Kaul et al., 1989). Thus, a role of RBC adhesion in initiating vaso-occlusive crisis is a widely supported hypothesis (Manwani and Frenette, 2013).

In addition to adhesion, polymerization of hemoglobin in sickle cell disease leads to rigid, inflexible red blood cells, which effect blood rheology. Moreover, oxygenated sickle RBC also displays changes in cell mechanics and therefore blood rheology, attributed to altered hemoglobin concentration in the cell and changes to the cell membrane (Nash et al., 1984). Changes in blood rheology affect tissue perfusion and may affect NO production through changes in shear stress on vessel walls. In addition to sickle cell disease, many other diseases display altered RBC deformability. In hypertension RBC deformability decreases, blood viscosity increases and RBCs form more stable aggregates (Cicco and Pirrelli, 1999). These changes exacerbate hypertension and effect oxygen transport (Cicco and Pirrelli, 1999). Diabetes and hypercholesterolemia, both risk factors for cardiovascular disease, show abnormal RBC membrane architecture and impaired deformability, which alter blood rheology (Shin et al., 2005; Tomaiuolo, 2014). It is difficult

to determine if altered RBC deformability and therefore blood rheology are concurrent or contributing factors to the changes in vascular function in these diseases.

Work by Bor-Kucukatay et al. suggest vascular function, specifically nitric oxide production could play a role in RBC deformability and rheological alterations to RBCs during hypertension (Bor-Kucukatay et al., 2000, 2003). They suggest NO improves RBC deformability (Bor-Kucukatay et al., 2003). However, other labs have found that NO does not have a direct effect on RBC deformability (Barodka et al., 2014; Belanger et al., 2015). On the other hand, select NO donors, sodium nitroprusside and nitrite, protect against calcium-influx induced RBC dehydration and loss of deformability (Barodka et al., 2014; Belanger et al., 2015; Wajih et al., 2017). Use of sodium nitroprusside and nitrite to improve rheology in diseases affected by poor RBC deformability would thus be worth exploring.

As reviewed above, encapsulation of Hb inside RBCs greatly reduces its ability to scavenge NO produced by the endothelium. However, in multiple diseases RBC hemolysis occurs introducing cell-free Hb into the vasculature (Reiter et al., 2002; Sobolewski et al., 2005). The pathology associated with hemoglobin-based blood substitutes demonstrated the hypertensive effects of cell-free Hb (Doherty et al., 1998). Additionally, there is support for the implication of hemolysis in vaso-occlusive crisis (VOC) as hemolytic transfusion reactions can precipitate VOC (Jang et al., 2011; Manwani and Frenette, 2013).

Cell-free hemoglobin reactions in the vasculature and surrounding tissues through extravasation may add to disease conditions (Schaer et al., 2013). *In vitro* findings suggest cell-free hemoglobin has the potential to release hemin and take part in oxidative reactions resulting in oxidative stress and inflammation (Miller et al., 1997; Jia et al., 2007; Manwani and Frenette, 2013). Patients with elevated plasma Hb show a reduction in NO-dependent blood flow response, consistent with a decrease in vasodilatory response to NO donor sodium nitroprusside by patients with SCD (Rother et al., 2005).

In addition to releasing Hb, hemolysis also releases arginase, an enzyme that converts L-arginine to ornithine, into the blood stream. L-arginine is the substrate for nitric oxide synthesis by eNOS and therefore, the release of arginase further diminishes NO production and vascular function (Morris et al., 2003; Schnog et al., 2004). Hemolysis and changes to RBC membrane proteins in disease effect vascular function through promoting thrombosis, initiating vascular occlusion, scavenging NO, and oxidative stress.

Red blood cell breakdown not only decreases NO bioavailability through NO scavenging by cell-free Hb, but also by production of red blood cell microparticles (Donadee et al., 2011; Liu et al., 2013). Like cell-free Hb, red cell microparticles (on the order of 50-100 nm in diameter) scavenge NO hundreds of times faster than Hb encapsulated in the RBC, but not quite as fast as cell-free Hb (Donadee et al., 2011). In addition, these particles enter the cell-free zone (Liu et al., 2013). Red cell hemolysis and micropartcile formation have been proposed to contribute to poor outcomes associated with transfusion of older stored blood due to NO scavenging (Gladwin and Kim-Shapiro, 2009; Donadee et al., 2011). Substantial evidence suggests that extravasation plays a major role in NO dysregulation, so that proper compartmentalization of Hb is key (Kim-Shapiro and Patel, 2016; Schaer et al., 2016).

RBC hemolysis contributes to the vascular pathology of diseases and disorders such as thalassemia, hereditary spherocytosis, Glucose-6-phosphate dehydrogenase deficiency, paroxysmal nocturnal, hemoglobinuria, and autoimmune hemolytic anemia (Johnson et al., 1979; Rother et al., 2005). Additionally, these diseases and disorders also lead to the increased formation of RBC microparticles (Piccin et al., 2007; Westerman and Porter, 2016). Moreover, hemolysis is also associated with blood transfusion, hemodialysis and cardiac bypass surgery (Meyer et al., 2010).

## PRODUCTION OF NITRIC OXIDE

In contrast to the role played by RBCs in diminishing NO. Research shows deoxy-RBCs promote vasodilation in the presence of nitrite (Cosby et al., 2003; Jensen and Agnisola, 2005; Crawford et al., 2006). Other mechanisms of vasodilatory action by RBCs have been proposed. Researchers continue to debate the mechanism or mechanisms of hypoxic vasodilation which include: (1) ATP release by RBCs due to deoxygenation, (2) SNO-Hb formation and S-nitrosothiol release and delivery during oxy/deoxy hemoglobin cycling, and (3) nitrite reduction by hemoglobin to NO.

ATP activates purinoceptors on endothelial cells leading to the production of NO and alteration of vascular tone (Ralevic and Burnstock, 1991). In line with the mechanism of ATP release by RBC under hypoxia, Ellsworth et al. showed that RBCs release more ATP under low PO2 and low pH than RBCs under normoxia and normal pH (Ellsworth et al., 1995). Additionally, they demonstrated intraluminal ATP increased vessel diameter and flow rate (Ellsworth et al., 1995). Following this work, Dietrich et al. showed perfusion of RBCs at low $PO_2$ caused vessel dilation and an increased concentration of ATP in the effluent (Dietrich et al., 2000).

Addition of nitrite to deoxyRBCs showed an enhanced effect on vasodilation when infused (Cosby et al., 2003; Jensen and Agnisola, 2005; Crawford et al., 2006). In support of ATP release being responsible for this enhanced dilation in the presence of nitrite, Cao et al. measured an increased synthesis and hypoxic release of RBC ATP in the presence of nitrite (Cao et al., 2009). However, research showed a vasodilatory response in the presence of nitrite and RBCs when NOS inhibitors L-NAME and L-NMMA were used, suggesting a different mechanism of dilation is responsible for the enhancement by nitrite (Crawford et al., 2006; Liu et al., 2015).

The second proposed mechanism for the effect deoxyRBC and nitrite on vascular function is the formation of SNO-Hb in the presence of nitrite and subsequent release of NO from deoxygenated SNO-Hb. Research has demonstrated the hypoxic release of NO from SNO-Hb and the ability of the released NO to relax vessels (Stamler et al., 1997; McMahon et al., 2002). Diesen et al. showed a decrease in RBC SNO-Hb concentration correlated with abolished vessel hypoxic dilation (Diesen et al.,

2008). The proposed mechanism of release is a reduction in the stability of SNO-Hb when Hb transitions from the R-state to the T-state and work by Doctor et al. further supports the proposal coupling SNO-Hb concentration to oxygen saturation (Doctor et al., 2005). However, for this mechanism to be relevant *in vivo* SNO-Hb must form during the oxygenation/deoxygenation cycle of RBCs. This leads to the question of how SNO-Hb forms. Huang et al. and Xu et al. ruled out allosterically-controlled transfer of NO from HbNO to the beta-93 cysteine of Hb (Xu et al., 2003; Huang et al., 2006). In addition, the role of nitrite in the formation of a semi-stable metHb-NO intermediate capable of SNO-Hb formation was ruled out by Basu et al. (Angelo et al., 2006; Nagababu et al., 2006; Basu et al., 2007). Lastly, Isbell et al. demonstrated nitrite associated NO bioactivity in beta-93 knockout mice, demonstrating SNO-Hb is not responsible for nitrite associated hypoxic vasodilation (Isbell et al., 2007). While data supports the release of NO from SNO-Hb under deoxygenated conditions, research has yet to elucidate a physiological mechanism of SNO-Hb formation therefore bringing to question the physiological relevance of SNO-Hb in vascular function.

The last proposed mechanism of RBC vasodilation in the presence of nitrite is the reduction of nitrite to NO by Hb. Brooks first studied the nitrite Hb interaction in 1937 and this work was later extended by Doyle in 1981 (Brooks, 1937; Doyle et al., 1981). Nitrite reacts with deoxygenated Hb to form metHb and NO (Brooks, 1937; Doyle et al., 1981). NO then reacts rapidly with deoxygenated Hb, at a rate dependent on the conformation state of the Hb (Huang et al., 2005a,b), to form HbNO. *In vitro* studies have rejected a significant role in the reduction of nitrite by other RBC molecules such as xanthine oxidoreductase and carbonic anhydrase supporting the hypothesis that hemoglobin plays a dominant role (Liu et al., 2015). Due to the rapid scavenging of NO by Hb the question of how NO bioactivity escapes the RBC still remains. However, data continues to grow in support of NO bioactivity escaping the deoxy-RBC in the presence of nitrite. For example, platelets activation and aggregation by ADP is diminished in the presence of deoxyRBCs and nitrite (Srihirun et al., 2012; Park et al., 2014; Liu et al., 2015; Wajih et al., 2016). Platelets stimulated by ADP in the presence of nitrite alone do not show reduced activation (Srihirun et al., 2012). The addition of a NO scavenger to platelets stimulated by ADP in the presence of deoxy-RBCs and nitrite abrogates the diminished activation (Wajih et al., 2016). These data strongly support a role of RBCs in bioactivating nitrite.

However, once NO is formed inside a RBC, it must somehow escape rapid scavenging by the intraerythrocytic Hb. Proposed mechanisms of escape of NO bioactivity from the RBC have included S-nitrosothiol formation and the role of the RBC membrane. Research by Basu et al and Roche et al suggested S-nitrosothiol formation could occur through a metHb-nitrite mediated $N_2O_3$ formation (Basu et al., 2007; Roche et al., 2013). Pawloski proposed a mechanism where low molecular weight S-nitrosothiols could transnitrosylate AE1, an abundant RBC ion transporter, and eventually escape the RBC (Pawloski et al., 2001). Another proposed mechanism, is an increased affinity of metHb-NO or Hb-$NO^+$ for the RBC membrane, which in turn could also lead to NO escape through nitrosylation of AE1 (Salgado et al., 2015). Lastly, Wajih et al have published evidence supporting a role of RBC membrane nitrosation in the escape of NO bioactivity (Wajih et al., 2016). While this is a start in determining the mechanism of NO bioactivity, much work remains.

Other heme-globin nitrite reducers may play a role in modulating vascular function. Deoxymyoglobin reduces nitrite faster than Hb (Shiva et al., 2007). Nitrite reduction by vascular smooth muscle myoglobin has been shown to contribute significantly to vasodilation in a murine model (Ormerod et al., 2010). Neuroglobin and cytoglobin also have nitrite reducing activity that is modulated by cysteine oxidation state (Tiso et al., 2011; Li et al., 2012; Tejero et al., 2014; Amdahl et al., 2017). Globin X from fish red blood cells reduces nitrite about 200 times faster than Hb and may represent a primordial function of heme-globins in nitrite reduction (Corti et al., 2016).

## THERAPEUTICS FOR RBC ASSOCIATED VASCULOPATHY

The production of NO by deoxyRBCs in the presence of nitrite and other NO donors provide a potential therapeutic role for plasma nitrite in reducing vasoconstriction, RBC adhesion, and potentially improving RBC deformability (Space et al., 2000; Bor-Kucukatay et al., 2003; Lundberg et al., 2008; Horn et al., 2011). NO administration can neutralize the NO scavenging ability of cell-free Hb by preferentially reacting, converting oxygenated hemoglobin to non-scavenging methemoglobin (Reiter et al., 2002). Antioxidants aim to improve blood rheology and vascular function through reduction of oxidative stress, shown by researchers to exacerbate hemolysis and endothelial dysfunction (Fibach and Rachmilewitz, 2008; den Hartog et al., 2010). Hemin and hemoglobin scavenger proteins also provide a potential therapeutic against damage caused by cell free hemoglobin and hemin (Schaer et al., 2013). Lastly, adhesion molecule inhibitors may act as a therapeutic against RBC adhesion to the endothelium; for example, Hebbel et al. showed adhesion molecule inhibitor HDAC reduced endothelial activation (Hebbel et al., 2009; Vinchi and Tolosano, 2013). A recent trial of a compound that interferes with adhesion of neutrophils and other circulating blood cells to endothelial cells successfully decreased the frequency of painful crises in patients with sickle cell disease (Ataga et al., 2017).

## CONCLUSIONS

Red blood cells play an important role in vascular function. Through the compartmentalization of Hb, RBCs deliver oxygen, minimize NO scavenging, sense oxygen tension, and deliver NO bioactivity in hypoxia. In healthy conditions, RBCs promote hemostasis through the well-regulated delivery of oxygen and the balance of NO scavenging and production. As data has shown, the RBC, once only viewed as a sink for NO, has the ability to produce NO bioactivity under hypoxia. The important role of the RBC in vascular function becomes more evident in diseases that

alter or compromise the RBC membrane leading to conditions of oxidative stress, hypertension, thrombosis, and vaso-occlusion.

## AUTHOR CONTRIBUTIONS

CH, MG, and DK-S together conceptualized the article and its content. CH wrote the initial draft of the manuscript and further edited the manuscript. MG and DK-S heavily edited the manuscript.

## FUNDING

This work was supported by the National Institutes of Health grant number HL058091 and HL098032.

## REFERENCES

Abu-Soud, H. M., Ichimori, K., Presta, A., and Stuehr, D. J. (2000). Electron transfer, oxygen binding, and nitric oxide feedback inhibition in endothelial nitric-oxide synthase. *J. Biol. Chem.* 275, 17349–17357. doi: 10.1074/jbc.M000050200

Amdahl, M. B., Sparacino-Watkins, C., Corti, P., Gladwin, M. T., and Tejero, J. (2017). Efficient reduction of vertebrate cytoglobins by the cytochrome b5/cytochrome b5 reductase/NADH System. *Biochemistry* 56, 3993–4004. doi: 10.1021/acs.biochem.7b00224

Angelo, M., Singel, D. J., and Stamler, J. S. (2006). An S-nitrosothiol (SNO) synthase function of hemoglobin that utilizes nitrite as a substrate. *Proc. Natl. Acad. Sci.U.S.A.* 103, 8366–8371. doi: 10.1073/pnas.0600942103

Arnold, W. P., Mittal, C. K., Katsuki, S., and Murad, F. (1977). Nitric oxide activates guanylate cyclase and increases guanosine 3':5'-cyclic monophosphate levels in various tissue preparations. *Proc. Natl. Acad. Sci. U.S.A.* 74, 3203–3207. doi: 10.1073/pnas.74.8.3203

Ataga, K. (2009). Hypercoagulability and thrombotic complications in hemolytic anemias. *Haematologica* 94, 1481–1484. doi: 10.3324/haematol.2009.013672

Ataga, K. I., Kutlar, A., Kanter, J., Liles, D., Cancado, R., Friedrisch, J., et al. (2017). Crizanlizumab for the prevention of pain crises in sickle cell disease. *N. Engl. J. Med.* 376, 429–439. doi: 10.1056/NEJMoa1611770

Azarov, I., Huang, K., Basu, S., Gladwin, M., Hogg, N., and Kim-Shapiro, D. (2005). Nitric oxide scavenging by red blood cells as a function of hematocrit and oxygenation. *J. Biol. Chem.* 280:39024. doi: 10.1074/jbc.M509045200

Azarov, I., Liu, C., Reynolds, H., Tsekouras, Z., Lee, J., Gladwin, M., et al. (2011). Mechanisms of slower nitric oxide uptake by red blood cells and other hemoglobin-containing vesicles. *J. Biol. Chem.* 286:33567. doi: 10.1074/jbc.M111.228650

Barodka, V., Mohanty, J. G., Mustafa, A. K., Santhanam, L., Nyhan, A., Bhunia, A. K., et al. (2014). Nitroprusside inhibits calcium-induced impairment of red blood cell deformability. *Transfusion* 54, 434–444. doi: 10.1111/trf.12291

Basu, S., Grubina, R., Huang, J., Conradie, J., Huang, Z., Jeffers, A., et al. (2007). Catalytic generation of N2O3 by the concerted nitrite reductase and anhydrase activity of hemoglobin. *Nat. Chem. Biol.* 3, 785–794. doi: 10.1038/nchembio.2007.46

Belanger, A. M., Keggi, C., Kanias, T., Gladwin, M. T., and Kim-Shapiro, D. B. (2015). Effects of nitric oxide and its congeners on sickle red blood cell deformability. *Transfusion* 55, 2464–2472. doi: 10.1111/trf.13134

Bor-Kucukatay, M., Wenby, R. B., Meiselman, H. J., and Baskurt, O. K. (2003). Effects of nitric oxide on red blood cell deformability. *Am. J. Physiol. Heart Circul. Physiol.* 284, H1577–H1584. doi: 10.1152/ajpheart.00665.2002

Bor-Kucukatay, M., Yalcin, O., Gokalp, O., Kipmen-Korgun, D., Yesilkaya, A., Baykal, A., et al. (2000). Red blood cell rheological alterations in hypertension induced by chronic inhibition of nitric oxide synthasis in rats. *Clin. Hemorheol. Microcircul.* 22, 267–275.

Brooks, J. (1937). The action of nitrite on haemoglobin in the absence of oxygen. *Proc. R. Soc. London B. Biol. Sci.* 123, 368–382. doi: 10.1098/rspb.1937.0057

Bugliarello, G., and Sevilla, J. (1970). Velocity distribution and other characteristics of steady and pulsatile blood flow in fine glass tubes. *Biorheology* 7, 85–107. doi: 10.3233/BIR-1970-7202

Butler, A., Megson, I., and Wright, P. (1998). Diffusion of nitric oxide and scavenging by blood in the vasculature. *Biochim. Biophys. Acta* 1425:168. doi: 10.1016/S0304-4165(98)00065-8

Cao, Z., Bell, J. B., Mohanty, J. G., Nagababu, E., and Rifkind, J. M. (2009). Nitrite enhances RBC hypoxic ATP synthesis and the release of ATP into the vasculature: a new mechanism for nitrite-induced vasodilation. *Am. J. Physiol. Heart Circul. Physiol.* 297, H1494–H1503. doi: 10.1152/ajpheart.01233.2008

Cassoly, R., and Gibson, Q. H. (1975). Conformation, co-operativity and ligand binding in human hemoglobin. *J. Mol. Biol.* 91, 301–313. doi: 10.1016/0022-2836(75)90382-4

Chang, A. E., and Detar, R. (1980). Oxygen and vascular smooth muscle contraction revisited. *Am. J. Physiol. Heart Circ. Physiol.* 5:H716. doi: 10.1152/ajpheart.1980.238.5.H716

Chu, A., Chambers, D. E., Lin, C. C., Kuehl, W. D., Palmer, R. M., Moncada, S., et al. (1991). Effects of inhibition of nitric oxide formation on basal vasomotion and endothelium-dependent responses of the coronary arteries in awake dogs. *J. Clin. Invest.* 87, 1964–1968. doi: 10.1172/JCI115223

Cicco, G., and Pirrelli, A. (1999). Red blood cell (RBC) deformability, RBC aggregability and tissue oxygenation in hypertension. *Clin. Hemorheol. Microcircul.* 21, 169–177.

Coin, J. T., and Olson, J. S. (1979). The rate of oxygen uptake by human red blood cells. *J. Biol. Chem.* 254, 1178–1190.

Cokelet, G. R. (1972). "The Rheology of Human Blood" in *Biomechanics: Its Foundation and Objectives*, eds Y. C. Fung, N. Perrone, and M. Anliker (Englewood Cliffs, NJ: Prentice Hall), 63–103.

Cooke, B. M., Mohandas, N., and Coppel, R. L. (2004). Malaria and the red blood cell membrane. *Semin. Hematol.* 41, 173–188. doi: 10.1053/j.seminhematol.2004.01.004

Cooper, C. E. (1999). Nitric oxide and iron proteins. *Biochim. Biophys. Acta* 1411, 290–309.

Corti, P., Xue, J., Tejero, J., Wajih, N., Sun, M., Stolz, D. B., et al. (2016). Globin X is a six-coordinate globin that reduces nitrite to nitric oxide in fish red blood cells. *Proc. Natl. Acad. Sci.U.S.A.* 113, 8538–8543. doi: 10.1073/pnas.1522670113

Cosby, K., Partovi, K., Crawford, J., Patel, R., Reiter, C., Martyr, S., et al. (2003). Nitrite reduction to nitric oxide by deoxyhemoglobin vasodilates the human circulation. *Nat. Med.* 9:1498. doi: 10.1038/nm954

Crawford, J. H., Isbell, T. S., Huang, Z., Shiva, S., Chacko, B. K., Schechter, A. N., et al. (2006). Hypoxia, red blood cells, and nitrite regulate NO-dependent hypoxic vasodilation. *Blood* 107, 566–574. doi: 10.1182/blood-2005-07-2668

De Mey, J. G., and Vanhoutte, P. M. (1983). Anoxia and endothelium-dependent reactivity of the canine femoral artery. *J. Physiol.* 335, 65–74.

den Hartog, G. J. M., Boots, A. W., Adam-Perrot, A., Brouns, F., Verkooijen, I. W. C. M., Weseler, A. R., et al. (2010). Erythritol is a sweet antioxidant. *Nutrition* 26, 449–458. doi: 10.1016/j.nut.2009.05.004

Diesen, D. L., Hess, D. T., and Stamler, J. S. (2008). Hypoxic vasodilation by red blood cells: evidence for an S-nitrosothiol based signal. *Circ.Res.* 103, 545–553. doi: 10.1161/CIRCRESAHA.108.176867

Dietrich, H. H., Ellsworth, M. L., Sprague, R. S., and Dacey, R. G. (2000). Red blood cell regulation of microvascular tone through adenosine triphosphate. *Am. J. Physiol. Heart Circul. Physiol.* 278, H1294–H1298. doi: 10.1152/ajpheart.2000.278.4.H1294

Doctor, A., Platt, R., Sheram, M. L., Eischeid, A., McMahon, T., Maxey, T., et al. (2005). Hemoglobin conformation couples erythrocyte S-nitrosothiol content to O2 gradients. *Proc. Natl. Acad. Sci. U.S.A.* 102, 5709–5714. doi: 10.1073/pnas.0407490102

Doherty, D. H., Dolye, M. P., Curry, S. R., Vali, R. J., Fattor, T. J., Olson, J. S., et al. (1998). Rate of reaction with nitric oxide determines the hypertensive effect of cell-free hemoglobin. *Nat. Biotechnol.* 16, 672–676. doi: 10.1038/nbt0798-672

Donadee, C., Raat, N. J. H., Kanias, T., Tejero, J., Lee, J. S., Kelley, E. E., et al. (2011). Nitric oxide scavenging by red blood cell microparticles and cell-free

hemoglobin as a mechanism for the red cell storage lesion clinical perspective. *Circulation* 124, 465–476. doi: 10.1161/CIRCULATIONAHA.110.008698

Doyle, M. P., and Hoekstra, J. W. (1981). Oxidation of nitrogen oxides by bound dioxygen in hemoproteins. *J. Inorg. Biochem.* 14, 351–358. doi: 10.1016/S0162-0134(00)80291-3

Doyle, M. P., Pickering, R. A., DeWeert, T. M., Hoekstra, J. W., and Pater, D. (1981). Kinetics and mechanism of the oxidation of human deoxyhemoglobin by nitrites. *J. Biol. Chem.* 256, 12393–12398.

Eaton, W. A., Henry, E. R., Hofrichter, J., and Mozzarelli, A. (1999). Is cooperative oxygen binding by hemoglobin really understood? *Nat. Struct. Mol. Biol.* 6, 351–358. doi: 10.1038/7586

Eich, R. F., Li, T., Lemon, D. D., Doherty, D. H., Curry, S. R., Aitken, J. F., et al. (1996). Mechanism of NO-induced oxidation of myoglobin and hemoglobin. *Biochemistry* 35, 6976–6983.

Ellsworth, M. L., Forrester, T., Ellis, C. G., and Dietrich, H. H. (1995). The erythrocyte as a regulator of vascular tone. *Am. J. Physiol. Heart Circ. Physiol.* 269:H2155.

Fibach, E., and Rachmilewitz, E. (2008). The role of oxidative stress in hemolytic anemia. *Curr. Mol. Med.* 8, 609–619. doi: 10.2174/156652408786241384

Franco-Obregón, A., Ureña, J., and López-Barneo, J. (1995). Oxygen-sensitive calcium channels in vascular smooth muscle and their possible role in hypoxic arterial relaxation. *Proc. Natl. Acad. Sci. U.S.A.* 92, 4715–4719.

Furchgott, R. F., and Zawadzki, J. V. (1980). The obligatory role of endothelial cells in the relaxation of arterial smooth muscle by acetylcholine. *Nature* 288, 373–376. doi: 10.1038/288373a0

Gladwin, M. T., and Kim-Shapiro, D. B. (2009). Storage lesion in banked blood due to hemolysis-dependent disruption of nitric oxide homeostasis. *Curr. Opin. Hematol.* 16, 515–523. doi: 10.1097/MOH.0b013e32833157f4

Hebbel, R. P., Boogaerts, M. A. B., Eaton, J. W., and Steinberg, M. H. (1980a). Erythrocyte adherence to endothelium in sickle-cell anemia. *N. Engl. J. Med.* 302, 992–995. doi: 10.1056/NEJM198005013021803

Hebbel, R. P., Vercellotti, G. M., Pace, B. S., Solovey, A. N., Kollander, R., Abanonu, C. F., et al. (2009). The HDAC inhibitors trichostatin A and suberoylanilide hydroxamic acid exhibit multiple modalities of benefit for the vascular pathobiology of sickle transgenic mice. *Blood* 115, 2483–2490. doi: 10.1182/blood-2009-02-204990

Hebbel, R. P., Yamada, O., Moldow, C. F., Jacob, H. S., White, J. G., and Eaton, J. W. (1980b). Abnormal adherence of sickle erythrocytes to cultured vascular endothelium: possible mechanism for microvascular occlusion in sickle cell disease. *J. Clin. Invest.* 65, 154–160. doi: 10.1172/JCI109646

Herold, S., Exner, M., and Nauser, T. (2001). Kinetic and mechanistic studies of the NO center dot-mediated oxidation of oxymyoglobin and oxyhemoglobin. *Biochemistry* 40, 3385–3395. doi: 10.1021/bi002407m

Hoover, R., Rubin, R., Wise, G., and Warren, R. (1979). Adhesion of normal and sickle erythrocytes to endothelial monolayer cultures. *Blood* 54:872.

Horn, P., Cortese-Krott, M., Keymel, S., Kumara, I., Burghoff, S., Schrader, J., et al. (2011). Nitric oxide influences red blood cell velocity independently of changes in the vascular tone. *Free Radic. Res.* 45, 653–661. doi: 10.3109/10715762.2011.574288

Hovav, T., Goldfarb, A., Artmann, G., Yedgar, S., and Barshtein, G. (1999). Enhanced adherence of β-thalassaemic erythrocytes to endothelial cells. *Br. J. Haematol.* 106, 178–181. doi: 10.1046/j.1365-2141.1999.01489.x

Huang, K., Han, T. H., Hyduke, D. R., Vaughn, M. W., Van Herle, H., Hein, T. W., et al. (2001). Modulation of nitric oxide bioavailability by erythrocytes. *Proc. Natl. Acad. Sci. U.S.A.* 98, 11771–11776. doi: 10.1073/pnas.201276698

Huang, K. T., Azarov, I., Basu, S., Huang, J., and Kim-Shapiro, D. (2006). Lack of allosterically controlled intramolecular transfer of nitric oxide from the heme to cysteine in the β-93 subunit of hemoglobin. *Blood* 107, 2602–2604. doi: 10.1182/blood-2005-10-4104

Huang, K. T., Huang, Z., and Kim-Shapiro, D. B. (2007). Nitric oxide red blood cell membrane permeability at high and low oxygen tension. *Nitric Oxide* 16, 209–216. doi: 10.1016/j.niox.2006.11.002

Huang, K. T., Keszler, A., Patel, N., Patel, R. P., Gladwin, M. T., Kim-Shapiro, D. B., et al. (2005a). The reaction between nitrite and deoxyhemoglobin: reassessment of reaction kinetics and stoichiometry. *J. Biol. Chem.* 280, 31126–31131. doi: 10.1074/jbc.M501496200

Huang, Z., Shiva, S., Kim-Shapiro, D., Patel, R. P., Ringwood, L. A., Irby, C. E., et al. (2005b). Enzymatic function of hemoglobin as a nitrite reductase that produces NO under allosteric control. *J. Clin. Invest.* 115, 2099–2107. doi: 10.1172/JCI24650

Ignarro, L. J., Byrns, R. E., Buga, G. M., and Wood, K. S. (1987). Endothelium-derived relaxing factor from pulmonary-artery and vein possesses pharmacological and chemical-properties identical to those of nitric-oxide radical. *Circ. Res.* 61, 866–879. doi: 10.1161/01.RES.61.6.866

Isbell, T. S., Gladwin, M. T., and Patel, R. P. (2007). Hemoglobin oxygen fractional saturation regulates nitrite-dependent vasodilation of aortic ring bioassays. *Am. J. Physiol.* 293, H2565–H2572. doi: 10.1152/ajpheart.00759.2007

Jackson, W. F. (2016). Arteriolar oxygen reactivity: where is the sensor and what is the mechanism of action? *J. Physiol.* 594, 5055–5077. doi: 10.1113/JP270192

Jang, J., Hod, E. A., Spitalnik, S. L., and Frenette, P. S. (2011). CXCL1 and its receptor, CXCR2, mediate murine sickle cell vaso-occlusion during hemolytic transfusion reactions. *J. Clin. Invest.* 121, 1397–1401. doi: 10.1172/JCI45336

Jensen, F. B., and Agnisola, C. (2005). Perfusion of the isolated trout heart coronary circulation with red blood cells: effects of oxygen supply and nitrite on coronary flow and myocardial oxygen consumption. *J. Exp. Biol.* 208, 3665–3674. doi: 10.1242/jeb.01815

Jia, Y., Buehler, P. W., Boykins, R. A., Venable, R. M., and Alayash, A. I. (2007). Structural basis of peroxide-mediated changes in human hemoglobin: a novel oxidative pathway. *J. Biol. Chem.* 282, 4894–4907. doi: 10.1074/jbc.M609955200

Johnson, G. J., Allen, D. W., Cadman, S., Fairbanks, V. F., White, J. G., Lampkin, B. C., et al. (1979). Red-cell-membrane polypeptide aggregates in glucose-6-phosphate dehydrogenase mutants with chronic hemolytic disease. A clue to the mechanism of hemolysis. *N. Engl. J. Med.* 301, 522–527. doi: 10.1056/NEJM197909063011004

Kaul, D. K., Fabry, M. E., and Nagel, R. L. (1989). Microvascular sites and characteristics of sickle cell adhesion to vascular endothelium in shear flow conditions: pathophysiological implications. *Proc. Natl. Acad. Sci. U.S.A.* 86, 3356–3360. doi: 10.1073/pnas.86.9.3356

Kim-Shapiro, D., and Patel, R. P. (2016). Compartmentalization is key in limiting nitric oxide scavenging by cell-free hemoglobin. *Am. J. Respir. Crit. Care Med.* 193, 1072–1074. doi: 10.1164/rccm.201512-2481ED

Kubes, P., Suzuki, M., and Granger, D. N. (1991). Nitric oxide: an endogenous modulator of leukocyte adhesion. *Proc. Natl. Acad. Sci. U.S.A.* 88, 4651–4655. doi: 10.1073/pnas.88.11.4651

Kwon, N. S., Nathan, C. F., Gilker, C., Griffith, O. W., Matthews, D. E., and Stuehr, D. J. (1990). L-citrulline production from L-arginine by macrophage nitric oxide synthase. The ureido oxygen derives from dioxygen. *J. Biol. Chem.* 265, 13442–13445.

Lancaster, J. R. (1994). Simulation of the diffusion and reaction of endogenously produced nitric oxide. *Proc. Natl. Acad. Sci. U.S.A.* 91, 8137–8141. doi: 10.1073/pnas.91.17.8137

Li, H., Hemann, C., Abdelghany, T. M., El-Mahdy, M. A., and Zweier, J. L. (2012). Characterization of the mechanism and magnitude of cytoglobin-mediated nitrite reduction and nitric oxide generation under anaerobic conditions. *J. Biol. Chem.* 287, 36623–36633. doi: 10.1074/jbc.M112.342378

Liao, J. C., Hein, W. T., Vaughn, M. W., Huang, K., and Kuo, L. (1999). Intravascular flow decreases erythrocyte consumption of nitric oxide. *Proc. Natl. Acad. Sci. U.S.A.* 96, 8757–8761. doi: 10.1073/pnas.96.15.8757

Lieberthal, W., Wolf, E. F., Rennke, H. G., Valeri, C. R., and Levinsky, N. G. (1989). Renal ischemia and reperfusion impair endothelium-dependent vascular relaxation. *Am. J. Physiol. Renal Physiol.* 256:F894.

Liu, C., Wajih, N., Liu, X., Basu, S., Janes, J., Marvel, M., et al. (2015). Mechanisms of human erythrocytic bioactivation of nitrite. *J. Biol. Chem.* 290, 1281–1294. doi: 10.1074/jbc.M114.609222

Liu, C., Zhao, W., Christ, G. J., Gladwin, M. T., and Kim-Shapiro, D. B. (2013). Nitric oxide scavenging by red cell microparticles. *Free Radic. Biol. Med.* 65, 1164–1173. doi: 10.1016/j.freeradbiomed.2013.09.002

Liu, X., Miller, M. J. S., Joshi, M. S., Sadowska-Krowicka, H., Clark, D. A., and Lancaster, J. R. (1998). Diffusion-limited reaction of free nitric oxide with erythrocytes. *J. Biol. Chem.* 273, 18709–18713. doi: 10.1074/jbc.273.30.18709

Liu, X. P., Samouilov, A., Lancaster, J. R. Jr., and Zweier, J. L. (2002). Nitric oxide uptake by erythrocytes is primarily limited by extracellular diffusion not membrane resistance. *J. Biol. Chem.* 277, 26194–26199. doi: 10.1074/jbc.M201939200

Lundberg, J. O., Gladwin, M. T., and Weitzberg, E. (2015). Strategies to increase nitric oxide signalling in cardiovascular disease. *Nat. Rev. Drug Discov*. 14, 623–641. doi: 10.1038/nrd4623

Lundberg, J., Weitzberg, E., and Gladwin, M. (2008). The nitrate-nitrite-nitric oxide pathway in physiology and therapeutics. *Nat. Rev. Drug Disc.* 7:156. doi: 10.1038/nrd2466

Manwani, D., and Frenette, P. S. (2013). Vaso-occlusion in sickle cell disease: pathophysiology and novel targeted therapies. *Blood* 122, 3892–3898. doi: 10.1182/blood-2013-05-498311

McMahon, T. J., Moon, R. E., Luschinger, B. P., Carraway, M. S., Stone, A. E., Stolp, B. W., et al. (2002). Nitric oxide in the human respiratory cycle. *Nat. Med.* 8, 711–717. doi: 10.1038/nm718

Meyer, C., Heiss, C., Drexhage, C., Kehmeier, E. S., Balzer, J., Mühlfeld, A., et al. (2010). Hemodialysis-induced release of hemoglobin limits nitric oxide bioavailability and impairs vascular function. *J. Am. Coll. Cardiol.* 55, 454–459. doi: 10.1016/j.jacc.2009.07.068

Miller, Y. I., Altamentova, S. M., and Shaklai, N. (1997). Oxidation of low-density lipoprotein by hemoglobin stems from a heme-initiated globin radical: antioxidant role of haptoglobin. *Biochemistry* 36, 12189–12198. doi: 10.1021/bi970258a

Monod, J., Wyman, J., and Changeux, J. P. (1965). On the nature of allosteric transitions: a plausible model. *J. Mol. Biol.* 12, 88–118. doi: 10.1016/S0022-2836(65)80285-6

Morris, C. R., Morris, S. M. J., Hagar, W., van Warmerdam, J., Claster, S., Kepka-Lenhart, D., et al. (2003). Arginine therapy: a new treatment for pulmonary hypertension in sickle cell disease? *Am. J. Respir. Crit. Care* 168, 63–69. doi: 10.1164/rccm.200208-967OC

Nagababu, E., Ramasamy, S., and Rifkind, J. M. (2006). S-nitrosohemoglobin: a mechanism for its formation in conjunction with nitrite reduction by deoxyhemoglobin. *Nitric Oxide* 15, 20–29. doi: 10.1016/j.niox.2006.01.012

Nash, G. B., Johnson, C. S., and Meiselman, H. J. (1984). Mechanical properties of oxygenated red blood cells in sickle cell (HbSS) disease. *Blood* 63:73.

Ormerod, J. O. M., Ashrafian, H., Maher, A. R., Arif, S., Steeples, V., Born, G. V. R., et al. (2010). The role of vascular myoglobin in nitrite-mediated blood vessel relaxation. *Cardiovasc. Res.* 89, 560–565. doi: 10.1093/cvr/cvq299

Palmer, R. M. J., Ferrige, A. G., and Moncada, S. (1987). Nitric oxide release accounts for the biological activity of endothelium-derived relaxing factor. *Nature* 327, 524–526. doi: 10.1038/327524a0

Palmer, R. M. J., and Moncada, S. A. (1989).Novel citrulline-forming enzyme implicated in the formation of nitric oxide by vascular endothelial cells. *Biochem. Biophys. Res. Commun.* 158, 348–352. doi: 10.1016/S0006-291X(89)80219-0

Park, J. W., Piknova, B., Nghiem, K., Lozier, J. N., and Schechter, A. N. (2014). Inhibitory effect of nitrite on coagulation processes demonstrated by thrombelastography. *Nitric Oxide* 40, 45–51. doi: 10.1016/j.niox.2014.05.006

Pawloski, J. R., Hess, D. T., and Stamler, J. S. (2001). Export by red blood cells of nitric oxide bioactivity. *Nature* 409, 622–626. doi: 10.1038/35054560

Piccin, A., Murphy, W. G., and Smith, O. P. (2007). Circulating microparticles: pathophysiology and clinical implications. *Blood Rev.* 21, 157–171. doi: 10.1016/j.blre.2006.09.001

Quyyumi, A. A., Dakak, N., Andrews, N. P., Husain, S., Arora, S., Gilligan, D. M., et al. (1995). 3. Nitric oxide activity in the human coronary circulation. Impact of risk factors for coronary atherosclerosis. *J. Clin. Invest*. 95, 1747–1755. doi: 10.1172/JCI117852

Ralevic, V., and Burnstock, G. (1991). Roles of P2-purinoceptors in the cardiovascular system. *Circulation* 84:1.

Reiter, C. D., Wang, X., Tanus-Santos, J. E., Hogg, N., Cannon, R. O., Schechter, A. N., et al. (2002). Cell-free hemoglobin limits nitric oxide bioavailability in sickle-cell disease. *Nat. Med*. 8, 1383–1389. doi: 10.1038/nm1202-799

Roche, C. J., Cassera, M. B., Dantsker, D., Hirsch, R. E., and Friedman, J. M. (2013). Generating S-nitrosothiols from hemoglobin: mechanisms, conformational dependence, and physiological relevance. *J. Biol. Chem.* 288, 22408–22425. doi: 10.1074/jbc.M113.482679

Rother, R. P., Bell, L., Hillmen, P., and Gladwin, M. T. (2005). The clinical sequelae of intravascular hemolysis and extracellular plasma hemoglobin. *JAMA* 293, 1653–1662. doi: 10.1001/jama.293.13.1653

Sakai, H., Sato, A., Masuda, K., Takeoka, S., and Tsuchida, E. (2008). Encapsulation of concentrated hemoglobin solution in phospholipid vesicles retards the reaction with no, but not, C. O, by intracellular diffusion barrier. *J. Biol. Chem.* 283, 1508–1517. doi: 10.1074/jbc.M707660200

Salgado, M. T., Cao, Z., Nagababu, E., Mohanty, J. G., and Rifkind, J. M. (2015). Red blood cell membrane-facilitated release of nitrite-derived nitric oxide bioactivity. *Biochemistry* 54, 6712–6723. doi: 10.1021/acs.biochem.5b00643

Schaer, C. A., Deuel, J. W., Schildknecht, D., Mahmoudi, L., Garcia-Rubio, I., Owczarek, C., et al. (2016). Haptoglobin preserves vascular nitric oxide signaling during hemolysis. *Am. J. Respir. Crit. Care Med.* 193, 1111–1122. doi: 10.1164/rccm.201510-2058OC

Schaer, D. J., Buehler, P. W., Alayash, A. I., Belcher, J. D., and Vercellotti, G. M. (2013). Hemolysis and free hemoglobin revisited: exploring hemoglobin and hemin scavengers as a novel class of therapeutic proteins. *Blood* 121, 1276–1284. doi: 10.1182/blood-2012-11-451229

Schafer, A. I., Alexander, R. W., and Handin, R. I. (1980). Inhibition of platelet function by organic nitrate vasodilators. *Blood* 55:649.

Schnog, J. B., Jager, E. H., van der Dijs, F. P., Duits, A. J., Moshage, H., Muskiet, F. D., et al. (2004). Evidence for a metabolic shift of arginine metabolism in sickle cell disease. *Ann. Hematol.* 83, 371–375. doi: 10.1007/s00277-004-0856-9

Setty, B. N. Y., Rao, A. K., and Stuart, M. J. (2001). Thrombophilia in sickle cell disease: the red cell connection. *Blood* 98, 3228–3233. doi: 10.1182/blood.V98.12.3228

Shin, S., Ku, Y., Park, M., and Suh, J. (2005). Deformability of red blood cells: a determinant of blood viscosity. *J. Mech. Sci. Technol.* 19:216. doi: 10.1007/BF02916121

Shiva, S., Huang, Z., Grubina, R., Sun, J., Ringwood, L. A., MacArthur, P. H., et al. (2007). Deoxymyoglobin is a nitrite reductase that generates nitric oxide and regulates mitochondrial respiration. *Circ.Res.* 100:654. doi: 10.1161/01.RES.0000260171.52224.6b

Sobolewski, P., Gramaglia, I., Frangos, J., Intaglietta, M., and van der Heyde, H. C. (2005). Nitric oxide bioavailability in malaria. *Trends Parasitol.* 21, 415–422. doi: 10.1016/j.pt.2005.07.002

Space, S. L., Lane, P. A., Pickett, C. K., and Weil, J. V. (2000). Nitric oxide attenuates normal and sickle red blood cell adherence to pulmonary endothelium. *Am. J. Hemotol.* 63, 200–204. doi: 10.1002/(SICI)1096-8652(200004)63:4<200::AID-AJH7>3.0.CO;2-Q

Srihirun, S., Sriwantana, T., Unchern, S., Kittikool, D., Noulsri, E., Pattanapanyasat, K., et al. (2012). Platelet inhibition by nitrite is dependent on erythrocytes and deoxygenation. *PLoS ONE* 7:e30380. doi: 10.1371/journal.pone.0030380

Stamler, J. S., Jia, L., Eu, J. P., McMahon, T. J., Demchenko, I. T., Bonaventura, J., et al. (1997). Blood flow regulation by S-nitrosohemoglobin in the physiological oxygen gradient. *Science* 276, 2034–2037. doi: 10.1126/science.276.5321.2034

Taggart, M. J., and Wray, S. (1998). Hypoxia and smooth muscle function: key regulatory events during metabolic stress. *J. Physiol.* 509, 315–325. doi: 10.1111/j.1469-7793.1998.315bn.x

Tejero, J., Sparacino-Watkins, C., Ragireddy, V., Frizzell, S., and Gladwin, M. T. (2014). Exploring the mechanisms of the reductase activity of neuroglobin by site-directed mutagenesis of the heme distal pocket. *Biochemistry* 54, 722–733. doi: 10.1021/bi501196k

Tiso, M., Tejero, J., Basu, S., Azarov, I., Wang, X., Simplaceanu, V., et al. (2011). Human neuroglobin functions as a redox-regulated nitrite reductase. *J. Biol. Chem.* 286, 18277–18289. doi: 10.1074/jbc.M110.159541

Tomaiuolo, G. (2014). Biomechanical properties of red blood cells in health and disease towards microfluidics. *Biomicrofluidics* 8:051501. doi: 10.1063/1.4895755

van Faassen, E. E., Bahrami, S., Feelisch, M., Hogg, N., Kelm, M., Kim-Shapiro, D. B., et al. (2009). Nitrite as regulator of hypoxic signaling in mammalian physiology. *Med. Res. Rev.* 29, 683–741. doi: 10.1002/med.20151

Vaughn, M. W., Huang, K. T., Kuo, L., and Liao, J. C. (2000). Erythrocytes possess an intrinsic barrier to nitric oxide consumption. *J. Biol. Chem.* 275, 2342–2348. doi: 10.1074/jbc.275.4.2342

Vaughn, M. W., Kuo, L., and Liao, J. C. (1998). Effective diffusion distance of nitric oxide in the microcirculation. *Am. J. Physiol. Heart Circ. Physiol.* 274:H1705.

Vinchi, F., and Tolosano, E. (2013). Therapeutic approaches to limit hemolysis-driven endothelial dysfunction: scavenging free heme to preserve vasculature homeostasis. *Oxid. Med. Cell. Longev.* 2013:96527. doi: 10.1155/2013/396527

Wajih, N., Basu, S., Jailwala, A., Kim, H. W., Ostrowski, D., Perlegas, A., et al. (2017). Potential therapeutic action of nitrite in sickle cell disease. *Redox Biol.* 12, 1026–1039. doi: 10.1016/j.redox.2017.05.006

Wajih, N., Liu, X., Shetty, P., Basu, S., Wu, H., Hogg, N., et al. (2016). The role of red blood cell S-nitrosation in nitrite bioactivation and its modulation by leucine and glucose. *Redox Biol.* 8, 415–421. doi: 10.1016/j.redox.2016.04.004

Westerman, M., and Porter, J. B. (2016). Red blood cell-derived microparticles: an overview. *Blood Cells Molecules Dis.* 59, 134–139. doi: 10.1016/j.bcmd.2016.04.003

Xu, X., Cho, M., Spencer, N. Y., Patel, N., Huang, Z., Shields, H., et al. (2003). Measurements of nitric oxide on the heme iron and ß-93 thiol of human hemoglobin during cycles of oxygenation and deoxygenation. *Proc. Natl. Acad. Sci. U.S.A.* 100, 11303–11308. doi: 10.1073/pnas.2033883100

Zanzinger, J., Czachurski, J., and Seller, H. (1994). Inhibition of sympathetic vasoconstriction is a major principle of vasodilation by nitric oxide *in vivo*. *Circ.Res.* 75:1073.

**Conflict of Interest Statement:** The authors declare that the research was conducted in the absence of any commercial or financial relationships that could be construed as a potential conflict of interest.

*Copyright © 2018 Helms, Gladwin and Kim-Shapiro. This is an open-access article distributed under the terms of the Creative Commons Attribution License (CC BY). The use, distribution or reproduction in other forums is permitted, provided the original author(s) and the copyright owner are credited and that the original publication in this journal is cited, in accordance with accepted academic practice. No use, distribution or reproduction is permitted which does not comply with these terms.*

frontiers in Physiology

MINI REVIEW
published: 30 January 2018
doi: 10.3389/fphys.2018.00041

# Hemodynamic Functionality of Transfused Red Blood Cells in the Microcirculation of Blood Recipients

*Gregory Barshtein*[1], *Dan Arbell*[2] *and Saul Yedgar*[1]*

[1] Department of Biochemistry, Faculty of Medicine, Hebrew University, Jerusalem, Israel, [2] Department of Pediatric Surgery, Hadassah University Hospital, Jerusalem, Israel

The primary goal of red blood cell (RBC) transfusion is to supply oxygen to tissues and organs. However, due to a growing number of studies that have reported negative transfusion outcomes, including reduced blood perfusion, there is rising concern about the risks in blood transfusion. RBC are characterized by unique flow-affecting properties, specifically adherence to blood vessel wall endothelium, cell deformability, and self-aggregability, which define their hemodynamic functionality (HF), namely their potential to affect blood circulation. The role of the HF of RBC in blood circulation, particularly the microcirculation, has been documented in numerous studies with animal models. These studies indicate that the HF of transfused RBC (TRBC) plays an important role in the transfusion outcome. However, studies with animal models must be interpreted with reservations, as animal physiology may not reflect human physiology. To test this concept in humans, we have directly examined the effect of the HF of TRBC, as expressed by their deformability and adherence to vascular endothelium, on the transfusion-induced effect on the skin blood flow and hemoglobin increment in β-thalassemia major patients. The results demonstrated, for the first time in humans, that the TRBC HF is a potent effector of the transfusion outcome, expressed by the transfusion-induced increase in the recipients' hemoglobin level, and the change in the skin blood flow, indicating a link between the microcirculation and the survival of TRBC in the recipients' vascular system. The implication of these findings for blood transfusion practice and to vascular function in blood recipients is discussed.

**Keywords: microcirculation, red blood cells, blood transfusion, RBC deformability, RBC adhesion, RBC hemodynamic functionality**

OPEN ACCESS

***Edited by:***
*Joseph M. Rifkind,*
*Johns Hopkins University,*
*United States*

***Reviewed by:***
*Roland Pittman,*
*Virginia Commonwealth University,*
*United States*
*Dan Predescu,*
*Rush University, United States*

***Correspondence:**
*Saul Yedgar*
*yedgar@md.huji.ac.il*

***Specialty section:***
*This article was submitted to Vascular Physiology, a section of the journal Frontiers in Physiology*

***Received:*** *31 October 2017*
***Accepted:*** *11 January 2018*
***Published:*** *30 January 2018*

***Citation:***
*Barshtein G, Arbell D and Yedgar S (2018) Hemodynamic Functionality of Transfused Red Blood Cells in the Microcirculation of Blood Recipients. Front. Physiol. 9:41. doi: 10.3389/fphys.2018.00041*

## INTRODUCTION

Blood transfusion has long been considered a routine life-saving therapy that has revolutionized medicine (Diamond, 1980). Donated blood units, routinely stored as packed red blood cells (PRBC) are routinely stored for up to 35 or 42 days, depending on the preservation solution (Hess, 2006). However, in recent years, there has been a growing concern about the efficacy and safety of the transfusion of allogeneic stored blood (Glynn, 2008; Hillyer et al., 2008; Redlin et al., 2014), as many studies have shown that PRBC transfusion caused damage rather than benefit to recipients. This included prolonged mechanical ventilation, renal failure and sepsis, with increased hospitalization and mortality in transfusion recipients (Sherk et al., 2000; Ho et al., 2003; Gong et al., 2005; Aronson et al., 2008; Glynn, 2008; Hillyer et al., 2008; Koch et al., 2008; Leal-Noval et al., 2008; Marin et al., 2013; Almac et al., 2014; Zimring, 2015). In particular, studies with patients suffering from trauma

(Weinberg et al., 2012), sepsis (Sakr et al., 2007; Damiani et al., 2015), or thalassemia (Vasileiadis et al., 2013), as well as patients in the medical-surgical intensive care (Creteur et al., 2009), have reported that PRBC transfusion reduced blood perfusion (Sakr et al., 2007; Weinberg et al., 2012), oxygen saturation (Creteur et al., 2009; Vasileiadis et al., 2013), oxygen delivery, and induced tissue hypoxia (Hayes et al., 1994).

Some studies have attributed that to storage-induced lesion to PRBC, showing better outcome with fresher vs. long-stored PRBC (Tinmouth and Chin-Yee, 2001; Gonzalez et al., 2007; Kor et al., 2009; Hess, 2010; D'Alessandro and Zolla, 2013; Damiani et al., 2015; Kim et al., 2015; Obrador et al., 2015; Antonelou and Seghatchian, 2016; Parviz et al., 2016).

However, other studies have not found relation between storage duration and negative transfusion outcome, showing no clinical benefit to using fresher over long-stored RBC (Remy et al., 2016; Shah et al., 2016). The role of storage duration on transfusion outcome is thus still a matter of debate (Lelubre and Vincent, 2013; Brunskill et al., 2015).

Blood donations are routinely tested, on day of donation, for immune compatibility and infectious agents, and are supplied by the first-in-first-out (FIFO) criterion. However, the functionality of transfused RBC, namely their ability to affect the transfusion outcome is ignored. RBC transfusion is aimed at increasing the recipients' hemoglobin and tissue oxygenation. However, RBC have unique flow-affecting properties, which play a key role in blood circulation, and define their hemodynamic functionality, namely their capacity to affect the recipients' blood circulation. The present review focuses on the role of transfused RBC FP on the recipients' blood circulation.

## RBC FLOW-AFFECTING PROPERTIES (FP) IN BLOOD CIRCULATION

RBC FP refer mainly to the cells' deformability, potential adherence to blood vessel all endothelium, and self-aggregability (Shiga et al., 1990; Barshtein et al., 2007; Simmonds et al., 2013).

**RBC deformability** is the cells' ability to adapt their shape to enable their passage through microvessels, especially the capillaries, which are narrower than the RBC. Reduced deformability (**increased rigidity**) hinders blood perfusion and impairs oxygen delivery in peripheral tissues (Parthasarathi and Lipowsky, 1999; Sakr et al., 2007; Matot et al., 2013). Rigid RBC can attenuate perfusion in peripheral tissues and directly block microvessels, capillaries in particular (Mchedlishvili, 1998; Cabrales, 2007). It has been shown that exchange transfusion of rigid, aldehyde-fixated RBC reduced the flow rate in swine (Pantely et al., 1988), and the functional capillary density in hamsters (Cabrales, 2007). RBC deformability is also a major determinant of their passage through the splenic vasculature; reduced deformability hinders the cells passage and increases splenic RBC sequestration and destruction (Warkentin et al., 1990; Mohandas and Chasis, 1993; An and Mohandas, 2008; Huang et al., 2014).

**RBC adherence** to endothelial cells (EC) of the blood vessel walls ("adherence") is normally insignificant, but it is abnormally enhanced in many disease states. RBC/EC adhesion decreases blood flow and increases the residence time of RBC in the microcirculation (Yedgar et al., 2008). Enhanced RBC/EC adhesion contributes to microcirculatory disorders observed in diverse pathologies, particularly those associated with oxidative stress (OS). In particular, it has been suggested that micro-vessel occlusion observed in sickle cell disease and malaria, especially cerebral malaria, is due to the adherence of sickle/malaria-infected RBC to EC of the micro-vessel wall (Yedgar et al., 2008). RBC/EC adherence is thus considered a potent catalyst of micro-vessel occlusion (Hebbel et al., 1981; Kaul and Nagel, 1993; Kaul et al., 1998, 2008; Hebbel, 2000).

**RBC aggregability** refers to the cells' ability to form multi-cellular aggregates, normally in a rouleau shape, in the presence of plasma proteins, especially fibrinogen, or other macromolecules (Skalak et al., 1981; Barshtein et al., 2007). Under normal conditions, the flow-induced shear stress is sufficient to modulate the aggregation as physiologically required to enable adequate blood flow in the diverse blood vessels. However, in pathological states, mainly those with low-flow or RBC abnormalities, aggregates that are larger and stronger-than-normal are formed, and higher shear stress is required for their disaggregation (Chen et al., 1995; Ami et al., 2001). Elevated RBC aggregation has been shown to be associated with cardio-vascular diseases (Mohandas and Chasis, 1993; Barshtein et al., 2007), and found to be correlated well with inflammatory indices of patients with unstable angina, myocardial infarct and sepsis (Ami et al., 2001). Increased RBC aggregation elevates blood viscosity and is associated with the formation of an RBC-free layer at the wall of large blood vessels. Accordingly, some studies suggested that the increased viscosity elevates vascular resistance. However, other studies suggested that RBC aggregation facilitates blood flow due to the formation of a cell-free layer at the vessel wall. In addition the viscosity-elevated shear stress leads to the production of the vasodilator nitric oxide (Kim et al., 2006, 2009; Namgung et al., 2011; Cho et al., 2015; Katanov et al., 2015; Ng et al., 2016). These led to disparate views as to the role of RBC aggregation in circulatory functions and disorders.

It is well known that pathological conditions or experimental treatments of RBC usually affect multiple properties, whereas the studies of RBC FP have generally focused on one property at a time, thereby leaving the derivation of the specific, differential effect of individual FP unclear.

This question was specifically addressed in a study, in which the adherence of human RBC was differentially elevated by treatment with $H_20_2$ concentration that increased the adherence without affecting the deformability. The perfusion of these RBC into rat mesocecum, in a medium which did not induced aggregation (free of macromolecules) induced a considerable elevation of vascular resistance in rat mesocecum (Kaul et al., 2008). In another study (Matot et al., 2008), rat blood was stored for 7 days, during which its RBC deformability was markedly decreased, while their adherence and aggregation were insignificant, which is typical of rat RBC (Schlager et al., 2010). The perfusion of this blood to rats reduced the liver oxygenation, which led to liver necrosis. These studies (Kaul et al., 2008; Matot et al., 2008) thus provide direct evidence

for the independent contribution of RBC/EC adherence and deformability to circulatory disorders.

Notably, RBC aggregates, even with the high aggregability observed in pathological conditions, can be disaggregated by a relatively low shear stress, such as 3–4 dynes/cm$^2$, while a RBC with increased adherence or reduced deformability might remain adherent or rigid at a shear stress of 30–40 dynes/cm$^2$ (Yedgar et al., 2008). It thus seems that the potency of RBC aggregation to induce vascular occlusion is much less significant.

## TRANSFUSION OF PRBC AND RECIPIENTS' MICROCIRCULATION

The effect of PRBC transfusion on the recipients' blood circulation has been investigated in numerous studies, which together presented inconclusive, even opposing results.

Nielsen et al. (2017) reviewed 17 studies to examine whether or not PRBC transfusion improves tissue oxygenation and/or the microcirculation in critically ill patients. They concluded that the heterogeneity of study designs, methodologies and study populations did not enable an appropriate meta-analysis. Yet, in the majority of cases, RBC transfusion failed to result in significant improvement in either tissue oxygenation or microcirculatory flow in ICU patients.

A number of studies have made attempts to answer the question whether the microcirculatory response to the transfusion is sensitive to the storage duration of the transfused PRBC (Walsh et al., 2004; Bennett-Guerrero et al., 2009; Kiraly et al., 2009; Weinberg et al., 2013; Yürük et al., 2013; Stowell et al., 2017). While some studies reported that long-stored units impaired circulatory functions, such as gastric mucosal oxygenation status (Marik and Sibbald, 1993), and perfused capillary vascular density (Weinberg et al., 2013), others have not observed a significant correlation between the PRBC storage duration and the transfusion-induced change in the recipients' circulatory functions (Walsh et al., 2004; Stowell et al., 2017).

## ROLE OF RECIPIENTS' PRE-TRANSFUSION CONDITIONS IN TRANSFUSION-INDUCED CHANGE IN CIRCULATORY FUNCTIONS

On these grounds, of particular interest are the studies that pointed to the pre-transfusion conditions of the patients as an important factor in the transfusion-induced change in the recipients' circulation. These studies (Casutt et al., 1999; Sakr et al., 2007; Creteur et al., 2009; Sadaka et al., 2011; Weinberg et al., 2012) have suggested that patients who had lowered tissue oxygenation or microcirculatory flow indices prior to transfusion, have benefitted by the transfusion, showing a significant improvement in these indices. Conversely, patients who had normal values of these indices showed either no improvement or a decline after transfusion.

This is further supported by our recent study, showing that the transfusion-induced change in the recipients' skin blood flow (ΔSBF) was inversely related to the recipients' SBF before transfusion ($SBF_B$). ΔSBF decreased, and was even negative, with increasing $SBF_B$ (Barshtein et al., 2016). This implies that patients with the most severe tissue oxygenation or microcirculatory derangements (prior to transfusion) benefit the most from the transfusion.

This phenomenon also provides partial explanation for the discrepancy between the above studies showing opposing effects of PRBC transfusion on the recipients' blood circulation (Friedlander et al., 1998; Sakr et al., 2007).

RBC deformability had been shown to decrease in critically ill patients (Friedlander et al., 1998). As noted above, RBCs with decreased deformability are assumed to hinder the passage through the microvessels. However, Friedlander et al. found that the RBC deformability of transfused septic patients was elevated by the PRBC transfusion, and suggested that this improvement is due to the replacement of previously rigidified cells with newer, more functional RBCs (Friedlander et al., 1998). Hence, transfusion may be deleterious in patients with adequate RBC deformability, but may have positive outcome in patients with reduced RBC deformability.

The mechanism of this phenomenon is not fully understood, but we can speculate that for patients with relatively rigid RBC, such as those with critical illness, e.g., sepsis (Baskurt et al., 1998; Condon et al., 2003; Donadello et al., 2015), the transfusion of PRBCs may enter to the bloodstream RBC with relatively higher deformability, resulting in the improvement of microcirculatory perfusion (Friedlander et al., 1998). This points to the effect of PRBC FP on circulatory functions in transfusion recipients.

## ROLE OF TRANSFUSED RBC FLOW-AFFECTING PROPERTIES (FP) IN TRANSFUSION-INDUCED CHANGE IN RECIPIENTS' BLOOD CIRCULATION

As noted above, the experimental evidence in animal studies supports the hypothesis that FP of transfused RBC are important determinants of the transfusion outcome, especially the recipients' blood microcirculation. However, as already stated, "animal studies must be interpreted with a number of caveats, as animal biology may not reflect human biology" (Zimring, 2015).

To bridge this gap, we directly studied, for the first time in humans, the effect of the HF of TRBC, expressed by their deformability and adherence, on the immediate transfusion outcome. This was measured by the transfusion-induced change in the recipients' skin blood flow, ΔSBF, determined by the difference in SBF before ($SBF_B$) and after transfusion. In this study we employed β-thalassemia major (TM) patients, who are treated with long-life, frequent blood transfusions (every 2–4 weeks). It was clearly found that ΔSBF increased with increasing deformability of the TRBC (Barshtein et al., 2016). This was further supported by the data of the individual patients who received four consecutive transfusions over a period of 8–10 weeks. For each of the nine patients, ΔSBF increased with increasing TRBC deformability (Barshtein et al., 2016). In some cases, when the TRBC deformability was low and $SBF_B$

was relatively high, the transfusion reduced the recipients' SBF ($\Delta SBF < 0$) (Barshtein et al., 2016).

In another study (unpublished), we have found that $\Delta SBF$ depended on the difference in deformability and adherence between the TRBC and the recipients RBC; when the PRBC adherence/rigidity were lower than those of the recipients' RBC, the recipients' blood flow was increased ($\Delta SBF > 0$). Conversely, when the TRBC rigidity/adherence was higher, the recipients' blood flow was decreased ($\Delta SBF < 0$). This corresponds to the suggestion of Friedlander et al. (1998) that PRBC transfusion to critically ill patients improved their blood circulation, as their RBC deformability is especially low.

Taken together, these findings demonstrate, for the first time in humans, the important role of the hemodynamic functionality of transfused RBC, as expressed by their FP, in transfusion outcome.

## TRANSFUSED RBC HEMODYNAMIC FUNCTIONALITY AND VASCULAR FUNCTION

Transfused RBC (TRBC) can modulate vascular function in differing and opposing ways via their effect on the plasma NO level. On one hand, TRBC may induce vasodilation in two ways: the release of ATP, which activates NO production in the blood vessel wall endothelial cells (EC) (Cao et al., 2009; Cortese-Krott and Kelm, 2014; Sikora et al., 2014), and the direct release of NO from the *S*-nitrosylated hemoglobin (SNO-Hb) (Bennett-Guerrero et al., 2007; Reynolds et al., 2007). On the other hand, a significant part of the TRBC are hemolyzed in the vascular system shortly after transfusion, and release free Hb, which is a scavenger of NO, thereby exerting vasoconstriction (Rusak et al., 2014; Damiani et al., 2015). Notably, the lysis of TRBCs has been shown to correlate with the fraction of the rigid, undeformable RBC in the TRBCs (Orbach et al., 2017), and transfusion of rigid PRBC causes elevation of cell-free Hb level in the bloodstream (Damiani et al., 2015).

Taken together, the HF of TRBC seems to play a complex role in modulating vascular function, which seems to depend on the ratio between the cells with normal HF and those with impaired HF. Yet, further investigation is required to elucidate this complex mechanism.

## CONCLUSION

The findings and considerations summarized above demonstrate the important role played by the HF of TRBC in the response of the recipients' vascular function. However, this is a complex response consisting of various effects of the deformability and adherence of the transfused RBC. These include direct effects on blood flow, primarily in the microcirculation, and their differing and opposing effects on vaso-modulation.

The present review presents direct evidence, in animal models and in humans, that the HF of transfused PRBC, as expressed primarily by their deformability and adherence to EC, is a potent effector of transfusion outcome. This strongly supports the need for considering the hemodynamic quality of transfused RBC in blood banking. The assessment of PRBC HF would introduce a powerful tool for reducing transfusion-related risks and improving transfusion therapy.

## AUTHOR CONTRIBUTIONS

GB, DA, and SY have been involved in the analysis and discussion of studies relating to the subject and in the writing of the review.

## REFERENCES


Almac, E., Bezemer, R., Hilarius-Stokman, P. M., Goedhart, P., de Korte, D., Verhoeven, A. J., et al. (2014). Red blood cell storage increases hypoxia-induced nitric oxide bioavailability and methemoglobin formation *in vitro* and *in vivo*. *Transfusion* 54, 3178–3185. doi: 10.1111/trf.12738

Ami, R. B., Barshtein, G., Zeltser, D., Goldberg, Y., Shapira, I., Roth, A., et al. (2001). Parameters of red blood cell aggregation as correlates of the inflammatory state. *Am. J. Physiol. Heart Circ. Physiol.* 280, H1982–H1988. doi: 10.1152/ajpheart.2001.280.5.H1982

An, X., and Mohandas, N. (2008). Disorders of red cell membrane. *Br. J. Haematol.* 141, 367–375. doi: 10.1111/j.1365-2141.2008.07091.x

Antonelou, M. H., and Seghatchian, J. (2016). Insights into red blood cell storage lesion: toward a new appreciation. *Transfus. Apher. Sci.* 55, 292–301. doi: 10.1016/j.transci.2016.10.019

Aronson, D., Dann, E. J., Bonstein, L., Blich, M., Kapeliovich, M., Beyar, R., et al. (2008). Impact of red blood cell transfusion on clinical outcomes in patients with acute myocardial infarction. *Am. J. Cardiol.* 102, 115–119. doi: 10.1016/j.amjcard.2008.03.027

Barshtein, G., Ben-Ami, R., and Yedgar, S. (2007). Role of red blood cell flow behavior in hemodynamics and hemostasis. *Expert Rev. Cardiovasc. Ther.* 5, 743–752. doi: 10.1586/14779072.5.4.743

Barshtein, G., Pries, A. R., Goldschmidt, N., Zukerman, A., Orbach, A., Zelig, O., et al. (2016). Deformability of transfused red blood cells is a potent determinant of transfusion-induced change in recipient's blood flow. *Microcirculation* 23, 479–486. doi: 10.1111/micc.12296

Baskurt, O. K., Gelmont, D., and Meiselman, H. J. (1998). Red blood cell deformability in sepsis. *Am. J. Respir. Crit. Care Med.* 157, 421–427. doi: 10.1164/ajrccm.157.2.9611103

Bennett-Guerrero, E., Stafford-Smith, M., Waweru, P. M., Bredehoeft, S. J., Campbell, M. L., Haley, N. R., et al. (2009). A prospective, double-blind, randomized clinical feasibility trial of controlling the storage age of red blood cells for transfusion in cardiac surgical patients. *Transfusion* 49, 1375–1383. doi: 10.1111/j.1537-2995.2009.02152.x

Bennett-Guerrero, E., Veldman, T. H., Doctor, A., Telen, M. J., Ortel, T. L., Reid, T. S., et al. (2007). Evolution of adverse changes in stored RBCs. *Proc. Natl. Acad. Sci. U.S.A.* 104, 17063–17068. doi: 10.1073/pnas.0708160104

Brunskill, S. J., Wilkinson, K. L., Doree, C., Trivella, M., and Stanworth, S. (2015). Transfusion of fresher versus older red blood cells for all conditions. *Cochrane Database Syst. Rev.* 5:CD010801. doi: 10.1002/14651858.CD010801.pub2

Cabrales, P. (2007). Effects of erythrocyte flexibility on microvascular perfusion and oxygenation during acute anemia. *Am. J. Physiol. Heart Circ. Physiol.* 293, H1206–H1215. doi: 10.1152/ajpheart.00109.2007

Cao, Z., Bell, J. B., Mohanty, J. G., Nagababu, E., and Rifkind, J. M. (2009). Nitrite enhances RBC hypoxic ATP synthesis and the release of ATP into the vasculature: a new mechanism for nitrite-induced vasodilation. *Am. J. Physiol. Heart Circ. Physiol.* 297, H1494–H1503. doi: 10.1152/ajpheart.01233.2008

Casutt, M., Seifert, B., Pasch, T., Schmid, E. R., Turina, M. I., and Spahn, D. R. (1999). Factors influencing the individual effects of blood transfusions on

oxygen delivery and oxygen consumption. *Crit. Care Med.* 27, 2194–2200. doi: 10.1097/00003246-199910000-00021

Chen, S., Gavish, B., Zhang, S., Mahler, Y., and Yedgar, S. (1995). Monitoring of erythrocyte aggregate morphology under flow by computerized image analysis. *Biorheology* 32, 487–496. doi: 10.3233/BIR-1995-32406

Cho, S., Namgung, B., Kim, H. S., Leo, H. L., and Kim, S. (2015). Effect of erythrocyte aggregation at pathological levels on NO/O2 transport in small arterioles. *Clin. Hemorheol. Microcirc.* 59, 163–175. doi: 10.3233/CH-141837

Condon, M. R., Kim, J. E., Deitch, E. A., Machiedo, G. W., and Spolarics, Z. (2003). Appearance of an erythrocyte population with decreased deformability and hemoglobin content following sepsis. *Am. J. Physiol. Heart Circ. Physiol.* 284, H2177–H2184. doi: 10.1152/ajpheart.01069.2002

Cortese-Krott, M. M., and Kelm, M. (2014). Endothelial nitric oxide synthase in red blood cells: key to a new erythrocrine function? *Redox Biol.* 2, 251–258. doi: 10.1016/j.redox.2013.12.027

Creteur, J., Neves, A. P., and Vincent, J. L. (2009). Near-infrared spectroscopy technique to evaluate the effects of red blood cell transfusion on tissue oxygenation. *Crit. Care* 13 (Suppl. 5), S11. doi: 10.1186/cc8009

D'Alessandro, A., and Zolla, L. (2013). "Biochemistry of red cell aging *in vivo* and storage lesion," in *Haematology Education: the Education Programme for the Annual Congress of the European Hematology Association* (Stockholm: Haematologica), 388–396.

Damiani, E., Adrario, E., Luchetti, M. M., Scorcella, C., Carsetti, A., Mininno, N., et al. (2015). Plasma free hemoglobin and microcirculatory response to fresh or old blood transfusions in sepsis. *PLoS ONE* 10:e0122655. doi: 10.1371/journal.pone.0122655

Diamond, L. (1980). "A history of blood transfusion," in *Blood, Pure and Eloquent*, ed M. M. Wintrobe (New York, NY: McGraw-Hill Book Company), 659–690.

Donadello, K., Piagnerelli, M., Reggiori, G., Gottin, L., Scolletta, S., Occhipinti, G., et al. (2015). Reduced red blood cell deformability over time is associated with a poor outcome in septic patients. *Microvasc. Res.* 101, 8–14. doi: 10.1016/j.mvr.2015.05.001

Friedlander, M. H., Simon, R., and Machiedo, G. W. (1998). The relationship of packed cell transfusion to red blood cell deformability in systemic inflammatory response syndrome patients. *Shock* 9, 84–88. doi: 10.1097/00024382-199802000-00002

Glynn, S. A. (2008). Blood supply safety: an NHLBI perspective. *Transfusion* 48, 1541–1544. doi: 10.1111/j.1537-2995.2007.01754.x

Gong, M. N., Thompson, B. T., Williams, P., Pothier, L., Boyce, P. D., and Christiani, D. C. (2005). Clinical predictors of and mortality in acute respiratory distress syndrome: potential role of red cell transfusion. *Crit. Care Med.* 33, 1191–1198. doi: 10.1097/01.CCM.0000165566.82925.14

Gonzalez, A. M., Yazici, I., Kusza, K., and Siemionow, M. (2007). Effects of fresh versus banked blood transfusions on microcirculatory hemodynamics and tissue oxygenation in the rat cremaster model. *Surgery* 141, 630–639. doi: 10.1016/j.surg.2006.09.015

Hayes, M. A., Timmins, A. C., Yau, E. H., Palazzo, M., Hinds, C. J., and Watson, D. (1994). Elevation of systemic oxygen delivery in the treatment of critically ill patients. *N. Engl. J. Med.* 330, 1717–1722. doi: 10.1056/NEJM199406163302404

Hebbel, R. P. (2000). Blockade of adhesion of sickle cells to endothelium by monoclonal antibodies. *N. Engl. J. Med.* 342, 1910–1912. doi: 10.1056/NEJM200006223422512

Hebbel, R. P., Moldow, C. F., and Steinberg, M. H. (1981). Modulation of erythrocyte-endothelial interactions and the vasocclusive severity of sickling disorders. *Blood* 58, 947–952.

Hess, J. R. (2006). An update on solutions for red cell storage. *Vox Sang.* 91, 13–19. doi: 10.1111/j.1423-0410.2006.00778.x

Hess, J. R. (2010). Red cell storage. *J. Proteomics* 73, 368–373. doi: 10.1016/j.jprot.2009.11.005

Hillyer, C. D., Blumberg, N., Glynn, S. A., and Ness, P. M. (2008). Transfusion recipient epidemiology and outcomes research: possibilities for the future. *Transfusion* 48, 1530–1537. doi: 10.1111/j.1537-2995.2008.01807.x

Ho, J., Sibbald, W. J., and Chin-Yee, I. H. (2003). Effects of storage on efficacy of red cell transfusion: when is it not safe? *Crit. Care Med.* 31, S687–697. doi: 10.1097/01.CCM.0000099349.17094.A3

Huang, S., Amaladoss, A., Liu, M., Chen, H., Zhang, R., Preiser, P. R., et al. (2014). *In vivo* splenic clearance correlates with *in vitro* deformability of red blood cells from *Plasmodium yoelii*-infected mice. *Infect. Immun.* 82, 2532–2541. doi: 10.1128/IAI.01525-13

Katanov, D., Gompper, G., and Fedosov, D. A. (2015). Microvascular blood flow resistance: role of red blood cell migration and dispersion. *Microvasc. Res.* 99, 57–66. doi: 10.1016/j.mvr.2015.02.006

Kaul, D. K., Koshkaryev, A., Artmann, G., Barshtein, G., and Yedgar, S. (2008). Additive effect of red blood cell rigidity and adherence to endothelial cells in inducing vascular resistance. *Am. J. Physiol. Heart Circ. Physiol.* 295, H1788–H1793. doi: 10.1152/ajpheart.253.2008

Kaul, D. K., Liu, X. D., Nagel, R. L., and Shear, H. L. (1998). Microvascular hemodynamics and *in vivo* evidence for the role of intercellular adhesion molecule-1 in the sequestration of infected red blood cells in a mouse model of lethal malaria. *Am. J. Trop. Med. Hyg.* 58, 240–247. doi: 10.4269/ajtmh.1998.58.240

Kaul, D. K., and Nagel, R. L. (1993). Sickle cell vasoocclusion: many issues and some answers. *Experientia* 49, 5–15. doi: 10.1007/BF01928783

Kim, E., Kim, H. C., Park, S. Y., Lim, Y. J., Ro, S. H., Cho, W. S., et al. (2015). Effect of red blood cell transfusion on unfavorable neurologic outcome and symptomatic vasospasm in patients with cerebral aneurysmal rupture: old versus fresh blood. *World Neurosurg.* 84, 1877–1886. doi: 10.1016/j.wneu.2015.08.024

Kim, S., Ong, P. K., Yalcin, O., Intaglietta, M., and Johnson, P. C. (2009). The cell-free layer in microvascular blood flow. *Biorheology* 46, 181–189. doi: 10.3233/BIR-2009-0530.

Kim, S., Popel, A. S., Intaglietta, M., and Johnson, P. C. (2006). Effect of erythrocyte aggregation at normal human levels on functional capillary density in rat spinotrapezius muscle. *Am. J. Physiol. Heart Circ. Physiol.* 290, H941–H947. doi: 10.1152/ajpheart.00645.2005

Kiraly, L. N., Underwood, S., Differding, J. A., and Schreiber, M. A. (2009). Transfusion of aged packed red blood cells results in decreased tissue oxygenation in critically injured trauma patients. *J. Trauma* 67, 29–32. doi: 10.1097/TA.0b013e3181af6a8c

Koch, C. G., Li, L., Sessler, D. I., Figueroa, P., Hoeltge, G. A., Mihaljevic, T., et al. (2008). Duration of red-cell storage and complications after cardiac surgery. *N. Engl. J. Med.* 358, 1229–1239. doi: 10.1056/NEJMoa070403

Kor, D. J., Van Buskirk, C. M., and Gajic, O. (2009). Red blood cell storage lesion. *Bosn J. Basic Med. Sci.* (9 Suppl 1.), 21–27. doi: 10.17305/bjbms.2009.2750

Leal-Noval, S. R., Munoz-Gomez, M., Arellano-Orden, V., Marin-Caballos, A., Amaya-Villar, R., Marin, A., et al. (2008). Impact of age of transfused blood on cerebral oxygenation in male patients with severe traumatic brain injury. *Crit. Care Med.* 36, 1290–1296. doi: 10.1097/CCM.0b013e3181692dfc

Lelubre, C., and Vincent, J. L. (2013). Relationship between red cell storage duration and outcomes in adults receiving red cell transfusions: a systematic review. *Crit. Care* 17: R66. doi: 10.1186/cc12600

Marik, P. E., and Sibbald, W. J. (1993). Effect of stored-blood transfusion on oxygen delivery in patients with sepsis. *JAMA* 269, 3024–3029. doi: 10.1001/jama.1993.03500230106037

Marin, T., Moore, J., Kosmetatos, N., Roback, J. D., Weiss, P., Higgins, M., et al. (2013). Red blood cell transfusion-related necrotizing enterocolitis in very-low-birthweight infants: a near-infrared spectroscopy investigation. *Transfusion* 53, 2650–2658. doi: 10.1111/trf.12158

Matot, I., Cohen, K., Pappo, O., Barash, H., and Abramovitch, R. (2008). Liver response to hemorrhagic shock and subsequent resuscitation: MRI analysis. *Shock* 29, 16–24. doi: 10.1097/shk.0b013e3180556964

Matot, I., Katz, M., Pappo, O., Zelig, O., Corchia, N., Yedgar, S., et al. (2013). Resuscitation with aged blood exacerbates liver injury in a hemorrhagic rat model. *Crit. Care Med.* 41, 842–849. doi: 10.1097/CCM.0b013e3182711b38

Mchedlishvili, G. (1998). Disturbed blood flow structuring as critical factor of hemorheological disorders in microcirculation. *Clin. Hemorheol. Microcirc.* 19, 315–325.

Mohandas, N., and Chasis, J. A. (1993). Red blood cell deformability, membrane material properties and shape: regulation by transmembrane, skeletal and cytosolic proteins and lipids. *Semin. Hematol.* 30, 171–192.

Namgung, B., Ong, P. K., Johnson, P. C., and Kim, S. (2011). Effect of cell-free layer variation on arteriolar wall shear stress. *Ann. Biomed. Eng.* 39, 359–366. doi: 10.1007/s10439-010-0130-3

Ng, Y. C., Namgung, B., Leo, H. L., and Kim, S. (2016). Erythrocyte aggregation may promote uneven spatial distribution of NO/O2 in the

downstream vessel of arteriolar bifurcations. *J. Biomech.* 49, 2241–2248. doi: 10.1016/j.jbiomech.2015.11.051

Nielsen, N. D., Martin-Loeches, I., and Wentowski, C. (2017). The effects of red blood cell transfusion on tissue oxygenation and the microcirculation in the intensive care unit: a systematic review. *Transfus. Med. Rev.* 31, 205–222. doi: 10.1016/j.tmrv.2017.07.003

Obrador, R., Musulin, S., and Hansen, B. (2015). Red blood cell storage lesion. *J. Vet. Emerg. Crit. Care* 25, 187–199. doi: 10.1111/vec.12252

Orbach, A., Zelig, O., Yedgar, S., and Barshtein, G. (2017). Biophysical and biochemical markers of red blood cells fragility. *Transfus. Med. Hemother.* 44, 183–187 doi: 10.1159/000452106

Pantely, G. A., Swenson, L. J., Tamblyn, C. H., Seaman, G. V., Anselone, C. G., Johnson, W. B., et al. (1988). Increased vascular resistance due to a reduction in red cell deformability in the isolated hind limb of swine. *Microvasc. Res.* 35, 86–100. doi: 10.1016/0026-2862(88)90052-0

Parthasarathi, K., and Lipowsky, H. H. (1999). Capillary recruitment in response to tissue hypoxia and its dependence on red blood cell deformability. *Am. J. Physiol.* 277(6 Pt 2), H2145–H2157. doi: 10.1152/ajpheart.1999.277.6.H2145

Parviz, Y., Hsia, C., Alemayehu, M., Wall, S., Bagur, R., AbuRomeh, N., et al. (2016). The effect of fresh versus standard blood transfusion on microvascular endothelial function. *Am. Heart J.* 181, 156–161. doi: 10.1016/j.ahj.2016.05.021

Redlin, M., Habazettl, H., Schoenfeld, H., Kukucka, M., Boettcher, W., Kuppe, H., et al. (2014). Red blood cell storage duration is associated with various clinical outcomes in pediatric cardiac surgery. *Transfus. Med. Hemother.* 41, 146–151. doi: 10.1159/000357998

Remy, K. E., Sun, J., Wang, D., Welsh, J., Solomon, S. B., Klein, H. G., et al. (2016). Transfusion of recently donated (fresh) red blood cells (RBCs) does not improve survival in comparison with current practice, while safety of the oldest stored units is yet to be established: a meta-analysis. *Vox Sang.* 111, 43–54. doi: 10.1111/vox.12380

Reynolds, J. D., Ahearn, G. S., Angelo, M., Zhang, J., Cobb, F., and Stamler, J. S. (2007). S-nitrosohemoglobin deficiency: a mechanism for loss of physiological activity in banked blood. *Proc. Natl. Acad. Sci. U.S.A.* 104, 17058–17062. doi: 10.1073/pnas.0707958104

Rusak, T., Misztal, T., Piszcz, J., and Tomasiak, M. (2014). Nitric oxide scavenging by cell-free hemoglobin may be a primary factor determining hypertension in polycythemic patients. *Free Radic. Res.* 48, 230–238. doi: 10.3109/10715762.2013.860225

Sadaka, F., Aggu-Sher, R., Krause, K., O'Brien, J., Armbrecht, E. S., and Taylor, R. W. (2011). The effect of red blood cell transfusion on tissue oxygenation and microcirculation in severe septic patients. *Ann. Intensive Care* 1:46. doi: 10.1186/2110-5820-1-46

Sakr, Y., Chierego, M., Piagnerelli, M., Verdant, C., Dubois, M. J., Koch, M., et al. (2007). Microvascular response to red blood cell transfusion in patients with severe sepsis. *Crit. Care Med.* 35, 1639–1644. doi: 10.1097/01.CCM.0000269936.73788.32

Schlager, A., Zamir, G., Barshtein, G., Yedgar, S., and Arbell, D. (2010). Plasma factor in red blood cells adhesion to endothelial cells: humans and rats. *Cell Biochem. Biophys.* 58, 157–161. doi: 10.1007/s12013-010-9102-3

Shah, A., McKechnie, S., Brunskill, S. J., and Stanworth, S. J. (2016). Fresh versus old red cell transfusions: what have the recent clinical trials found? *Curr. Opin. Hematol.* 23, 550–556. doi: 10.1097/MOH.0000000000000283

Sherk, P. A., Granton, J. T., and Kapral, M. K. (2000). Red blood cell transfusion in the intensive care unit. *Intensive Care Med.* 26, 344–346. doi: 10.1007/s001340051160

Shiga, T., Maeda, N., and Kon, K. (1990). Erythrocyte rheology. *Crit. Rev. Oncol. Hematol.* 10, 9–48. doi: 10.1016/1040-8428(90)90020-S

Sikora, J., Orlov, S. N., Furuya, K., and Grygorczyk, R. (2014). Hemolysis is a primary ATP-release mechanism in human erythrocytes. *Blood* 124, 2150–2157. doi: 10.1182/blood-2014-05-572024

Simmonds, M. J., Meiselman, H. J., and Baskurt, O. K. (2013). Blood rheology and aging. *J. Geriatr. Cardiol.* 10, 291–301. doi: 10.3969/j.issn.1671-5411.2013.03.010.

Skalak, R., Zarda, P. R., Jan, K. M., and Chien, S. (1981). Mechanics of Rouleau formation. *Biophys. J.* 35, 771–781. doi: 10.1016/S0006-3495(81)84826-6

Stowell, C. P., Whitman, G., Granger, S., Gomez, H., Assmann, S. F., Massey, M. J., et al. (2017). The impact of red blood cell storage duration on tissue oxygenation in cardiac surgery. *J. Thorac. Cardiovasc. Surg* 153, 610–619. doi: 10.1016/j.jtcvs.2016.11.029

Tinmouth, A., and Chin-Yee, I. (2001). The clinical consequences of the red cell storage lesion. *Transfus. Med. Rev.* 15, 91–107. doi: 10.1053/tmrv.2001.22613

Vasileiadis, I., Basios, N., Gerovasili, N., Dimopoulos, S., Ladis, N., Kompoti, M., et al. (2013). Blood transfusion improves tissue oxygenation in beta-thalassemia major patients. *Health Sci. J.* 7, 448–453.

Walsh, T. S., McArdle, F., McLellan, S. A., Maciver, C., Maginnis, M., Prescott, R. J., et al. (2004). Does the storage time of transfused red blood cells influence regional or global indexes of tissue oxygenation in anemic critically ill patients? *Crit. Care Med.* 32, 364–371. doi: 10.1097/01.CCM.0000108878.23703.E0

Warkentin, T. E., Barr, R. D., Ali, M. A., and Mohandas, N. (1990). Recurrent acute splenic sequestration crisis due to interacting genetic defects: hemoglobin SC disease and hereditary spherocytosis. *Blood* 75, 266–270.

Weinberg, J. A., MacLennan, P. A., Vandromme-Cusick, M. J., Angotti, J. M., Magnotti, L. J., Kerby, J. D., et al. (2012). Microvascular response to red blood cell transfusion in trauma patients. *Shock* 37, 276–281. doi: 10.1097/SHK.0b013e318241b739

Weinberg, J. A., MacLennan, P. A., Vandromme-Cusick, M. J., Magnotti, L. J., Kerby, J. D., Rue, L. W. III., et al. (2013). The deleterious effect of red blood cell storage on microvascular response to transfusion. *J. Trauma Acute Care Surg.* 75, 807–812. doi: 10.1097/TA.0b013e3182a74a9b

Yedgar, S., Kaul, D. K., and Barshtein, G. (2008). RBC adhesion to vascular endothelial cells: more potent than RBC aggregation in inducing circulatory disorders. *Microcirculation* 15, 581–583. doi: 10.1080/10739680802105482

Yürük, K., Milstein, D. M., Bezemer, R., Bartels, S. A., Biemond, B. J., and Ince, C. (2013). Transfusion of banked red blood cells and the effects on hemorrheology and microvascular hemodynamics in anemic hematology outpatients. *Transfusion* 53, 1346–1352. doi: 10.1111/j.1537-2995.2012.03905.x

Zimring, J. C. (2015). Established and theoretical factors to consider in assessing the red cell storage lesion. *Blood* 125, 2185–2190. doi: 10.1182/blood-2014-11-567750

**Conflict of Interest Statement:** The authors declare that the research was conducted in the absence of any commercial or financial relationships that could be construed as a potential conflict of interest.

*Copyright © 2018 Barshtein, Arbell and Yedgar. This is an open-access article distributed under the terms of the Creative Commons Attribution License (CC BY). The use, distribution or reproduction in other forums is permitted, provided the original author(s) and the copyright owner are credited and that the original publication in this journal is cited, in accordance with accepted academic practice. No use, distribution or reproduction is permitted which does not comply with these terms.*

frontiers in Physiology

REVIEW
published: 12 January 2018
doi: 10.3389/fphys.2017.01120

# Physiologic Impact of Circulating RBC Microparticles upon Blood-Vascular Interactions

*Ahmed S. Said*[1], *Stephen C. Rogers*[1] *and Allan Doctor*[1,2]*

[1] Department of Pediatrics, Washington University in St. Louis, St. Louis, MO, United States, [2] Biochemistry and Molecular Biophysics, Washington University in St. Louis, St. Louis, MO, United States

Here, we review current data elucidating the role of red blood cell derived microparticles (RMPs) in normal vascular physiology and disease progression. Microparticles (MPs) are submicron-size, membrane-encapsulated vesicles derived from various parent cell types. MPs are produced in response to numerous stimuli that promote a sequence of cytoskeletal and membrane phospholipid changes and resulting MP genesis. MPs were originally considered as potential biomarkers for multiple disease processes and more recently are recognized to have pleiotropic biological effects, most notably in: promotion of coagulation, production and handling of reactive oxygen species, immune modulation, angiogenesis, and in initiating apoptosis. RMPs, specifically, form normally during RBC maturation in response to injury during circulation, and are copiously produced during processing and storage for transfusion. Notably, several factors during RBC storage are known to trigger RMP production, including: increased intracellular calcium, increased potassium leakage, and energy failure with ATP depletion. Of note, RMP composition differs markedly from that of intact RBCs and the nature/composition of RMP components are affected by the specific circumstances of RMP genesis. Described RMP bioactivities include: promotion of coagulation, immune modulation, and promotion of endothelial adhesion as well as influence upon vasoregulation via influence upon nitric oxide (NO) bioavailability. Of particular relevance, RMPs scavenge NO more avidly than do intact RBCs; this physiology has been proposed to contribute to the impaired oxygen delivery homeostasis that may be observed following transfusion. In summary, RMPs are submicron particles released from RBCs, with demonstrated vasoactive properties that appear to disturb oxygen delivery homeostasis. The clinical impact of RMPs in normal and patho-physiology and in transfusion recipients is an area of continued investigation.

**Keywords: erythrocytes, nitric oxide, endothelium, vasoregulation, blood flow, red blood cells, microparticle**

OPEN ACCESS

***Edited by:***
*Joseph M. Rifkind, Johns Hopkins University, United States*

***Reviewed by:***
*Bingmei Fu, City College of New York (CUNY), United States*
*Ana Denicola, University of the Republic, Uruguay*
*Adriana Georgescu, Institute of Cellular Biology and Pathology (ICBP), Romania*

***Correspondence:**
*Allan Doctor*
*doctor@wustl.edu*

***Specialty section:***
*This article was submitted to Vascular Physiology, a section of the journal Frontiers in Physiology*

***Received:*** *31 October 2017*
***Accepted:*** *18 December 2017*
***Published:*** *12 January 2018*

***Citation:***
*Said AS, Rogers SC and Doctor A (2018) Physiologic Impact of Circulating RBC Microparticles upon Blood-Vascular Interactions. Front. Physiol. 8:1120. doi: 10.3389/fphys.2017.01120*

## MICROPARTICLES (MP) OVERVIEW

Genesis of small membrane-encapsulated vesicles (termed microparticles, MPs) from activated and/or apoptotic cells was first reported ~40 years ago (Boulanger and Dignat-George, 2011). Formally defined, MPs are cell-derived vesicles that are 0.1–1.0 μm in size and are categorized by membrane proteins and cytosolic material that is specific to various parent cell

populations (Morel et al., 2011; **Figure 1**). MPs are distinguished from exosomes and apoptotic bodies by size, composition and mechanism of formation (Burger D. et al., 2013; **Figure 2**). Exosomes are generally smaller (40–100 nm) and form by a multistep process that involves intracellular generation and subsequent vesicle extrusion; apoptotic bodies are much larger (1–5 μm) and arise via shedding during apoptosis (Elmore, 2007).

## Cell-Cell Communication via MPs:

MPs serve as vehicles for inter-cellular exchange of biological material and information, for which two principle mechanisms have been proposed: (1) MPs act as circulating modules for complex signaling, activating receptors on target cells by presenting organized clusters of membrane-associated bioactive molecules (Del Conde et al., 2005), and/or (2) direct transfer of MP contents, including proteins, bioactive lipids or RNA to recipient cells—thereby, promoting phenotypic modification and reprogramming of cell functions (Whale et al., 2006). As such, MP based cell-cell communication enables a unique form of remote signaling from MP-parent to target cells, by presenting a complex array of ligands for membrane receptors, paired with a concentrated payload of bioactive molecules and substrate for intracellular delivery (Mause and Weber, 2010).

## MPs as Disease Biomarkers

MP formation is enhanced by stress and injury and consequently, MPs have been considered as potential biomarkers for disease onset and progression. As such, it is important to recognize that moment-specific abundance of circulating MPs is determined by the balance between MP formation and clearance (e.g., MP abundance and flux do not necessarily correlate and, high-flux low-abundance states may have physiologic significance that is belied by measured MP level, alone.). MP levels, in particular: for platelet-, leukocyte-, and endothelium-related MPs, are known to increase in the setting of vascular injury, pro-thrombotic and pro-inflammatory states that complicate a broad array of health conditions, such as diabetes (Feng et al., 2010), pulmonary hypertension (Forest et al., 2010), chronic kidney disease (Faure et al., 2006), preeclampsia (González-Quintero et al., 2003), atherosclerosis (Bernal-Mizrachi et al., 2003), and heart failure (Amabile et al., 2012) amongst others.

## MP Formation

MPs arise from diverse cell types, including vascular elements (endothelial and vascular smooth muscle cells) (Rautou et al., 2011), blood components [erythrocytes (Tissot et al., 2010), platelets and leukocytes], cardiomyocytes (Antoniak et al., 2009) and podocytes (Burger D. et al., 2013), as well as various cancers (Zahra et al., 2011) and progenitor cell populations (Chen et al., 2010). MPs form via outward blebbing and shedding of the plasma membrane (Dignat-George and Boulanger, 2011). This poorly understood process appears to involve two main steps: (1) an initial cytoskeletal re-organization (Cauwenberghs et al., 2006), involving actin filament rearrangement that appears initiated by activation of calpain (Nolan et al., 2008), rho kinase (Sapet et al., 2006), and transglutaminase (van den Akker et al., 2012; **Figure 3**) and (2) externalization of phosphatidylserine (PS), a negatively charged aminophospholipid found almost exclusively on the plasma membrane inner leaflet, in healthy cells (Bevers et al., 1999). In red blood cells, PS "sidedness" is controlled by an ATP/calcium dependent system involving three distinct enzymes: flippase, floppase, and scramblase (Kostova et al., 2015). Of note, defective PS externalization underlies Scott syndrome, a bleeding disorder associated with diminished platelet MP shedding (Leroyer et al., 2009).

Studies of cultured cells have identified several stimuli for MP formation, including: various hormones, fatty acids, reactive oxygen species (e.g., hydrogen peroxide) (Aoki et al., 2007) as well as increased intracellular calcium (Fox et al., 1991). Activation of several surface receptors has also been shown to drive MP production, such as by tumor necrosis factor (TNF)-α (Eyre et al., 2011) on monocytes, leukocytes, and neutrophils, as well as by pro-inflammatory [lipopolysaccharide (Ståhl et al., 2011), shiga toxin (Ståhl et al., 2011), and cytokines (Nomura et al., 2000)] and pro-coagulant ligands [thrombin (Terrisse et al., 2010), collagen (Takano et al., 2004), and norepinephrine (Tschuor et al., 2008)] on platelets and Toll-like receptor 4 on dendritic cells (Théry et al., 2009; **Figure 4**).

## MP Clearance

MP elimination via the mononuclear phagocyte system (MPS) appears to regulate circulating MP availability for target-cell fusion; however, less is known about this process than about MP formation (Burger D. et al., 2013). Macrophages ingest co-cultured MPs and externalized PS is thought to activate scavenger receptors, promoting MP endocytosis (Terrisse et al., 2010). MP surface IgM has also been shown to promote MP clearance by macrophages (Litvack et al., 2011).

## MP-Mediated Effects upon Vascular Physiology

Although MP shedding may be enhanced by stress, exocytosis is a constitutive process for the majority of blood and vascular cell types (Angelillo-Scherrer, 2012). Depending on the stimulus, however, protein content (of both "cytoplasm" and membrane) for MPs derived from the same cell lineage can vary (Jimenez et al., 2003). Moreover, the enzymes that govern MP shedding can be selective, depending on the activating agonist and/or parent cell microenvironment (Peterson et al., 2008; Bernimoulin et al., 2009). Such tight regulation of MP production suggests MPs may facilitate important cell-cell communication in a context-specific fashion. Of note, MPs are internalized by a variety of cells (macrophages and endothelial cells, amongst others) in a dose-dependent manner, enabling "MP cargo" transfer between cells in a fashion that influences target cell function and phenotype (Diehl et al., 2012).

The most well-characterized components of vascular physiology that are influenced by MPs include the following:

### Coagulation

This is perhaps the most clearly established example of MP-based influence. Platelet derived MPs have effects similar to activated platelets in initiation of thrombin generation and clot

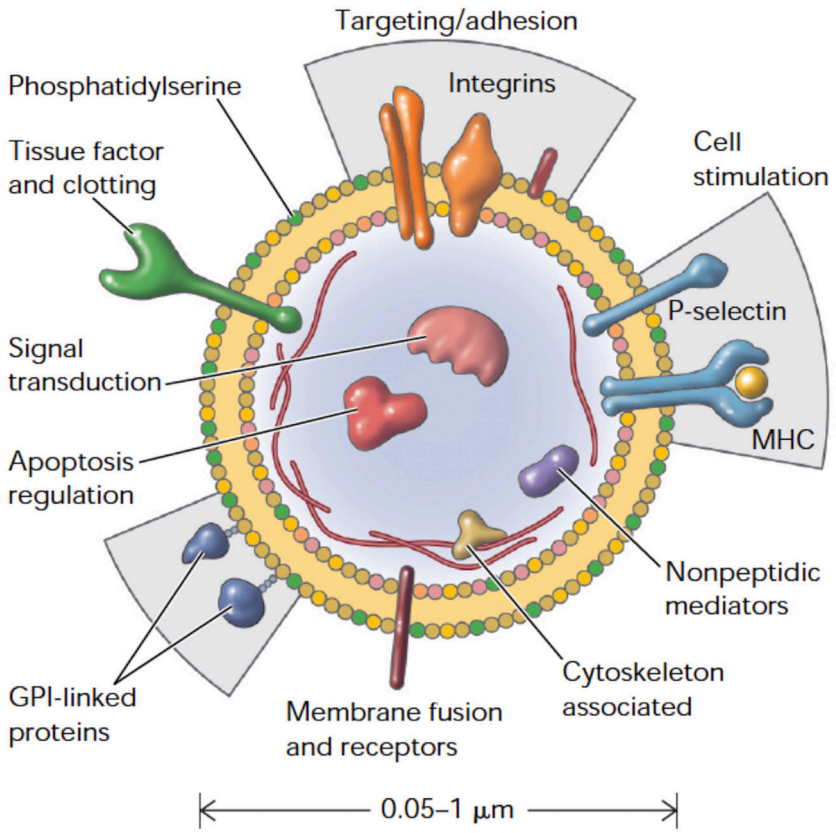


**FIGURE 1 |** Cellular microparticles: a mobile storage pool of bioactive effectors. Membrane microparticles are shed from the plasma membrane of stimulated cells, harboring cytoplasmic proteins as well as bioactive lipids implicated in a variety of fundamental processes. MHC, Major histocompatibility complex; GPI, glycosylphosphatidylinositol. Adapted with permission from Hugel et al. (2005).

propagation, despite having at least two-orders-of-magnitude difference in surface area (Sinauridze et al., 2007). Moreover, externalized phospholipids (mainly PS) create a negatively charged surface that anchors cationic domains of proteins involved in assembly of the multi-component (tenase) complex that leads to the thrombin burst (Owens and Mackman, 2011).

## Oxidative Stress

MPs of differing derivations, produced under various stimuli, have been shown to affect the enzymatic systems controlling reactive oxygen species generation. Both endothelial and monocyte derived MPs are known to increase superoxide (Mastronardi et al., 2011) and hydrogen peroxide production (Burger et al., 2012) as well as to uncouple nitric oxide synthase (NOS) (Essayagh et al., 2007). However, activated T-cell related MPs have been shown to dampen reactive oxygen species production and to increase nitric oxide (NO) production (Agouni et al., 2007).

## Inflammation

Pro-inflammatory signaling generally provokes MP shedding and, in an amplifying signaling loop, MPs may directly contribute to the inflammatory response (e.g., PMN derived MPs promote endothelial IL-6 and monocyte chemotactic protein release) (Mesri and Altieri, 1999). MPs are also thought to promote inter-cellular inflammatory cell interaction and adhesion; specifically, endothelial-derived MPs increase adhesion molecule expression and facilitate monocyte-endothelial cell interactions (Burger D. et al., 2011), in addition to binding to monocytes and promoting transendothelial migration (Jy et al., 2004).

## Angiogenesis

Platelet-derived MPs have been implicated in regulation of angiogenesis. In rats following myocardial ischemia, platelet MPs increase post-ischemic capillary density, and proliferation (Brill et al., 2005) and are reported to promote tube formation by human umbilical vein endothelial cells (Kim et al., 2004). This is not surprising, as platelets are known to contain at least 20 angiogenesis regulating factors. Moreover, certain stimulated T-cell related MPs have been shown to inhibit angiogenesis both *in vivo* and *in vitro* (Yang et al., 2012).

## Apoptosis

Endothelial- and monocyte-derived MPs are described to promote cellular senescence and apoptosis in circulating angiogenic and endothelial progenitor cells, respectively (Huang

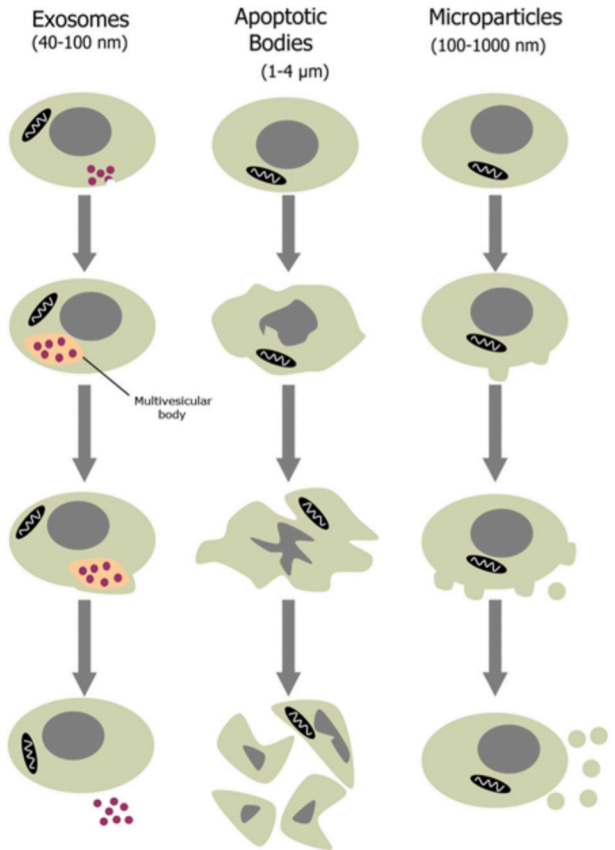


**FIGURE 2 |** Size classes of extracellular vesicles. Exosomes are formed through inward membrane budding, leading to formation of 40–100 nm intracellular vesicles which accumulate within multivesicular bodies that are subsequently released to the extracellular milieu. Apoptotic bodies may contain DNA and/or organelles and are formed during the late stages of apoptosis, after cell shrinkage. Microparticles are formed from the outward blebbing of membrane and released into the extracellular space. Adapted with permission from Burger D. et al. (2013).

et al., 2010; Distler et al., 2011). This process appears linked to phagocytosis of MPs that contain high amounts of membrane arachidonic acid, leading to caspase activation and initiation of apoptosis (Huber et al., 2007).

## RED BLOOD CELL (RBC) DERIVED MICROPARTICLES (RMPs)

RBC-derived MP formation occurs routinely during normal maturation *in vivo*; *ex vivo*, this process is accelerated by processing and storage, prior to transfusion (Greenwalt, 2006). RMPs are generally smaller than MPs of other origin, are more homogenous in size (∼0.15 μm in diameter), and are often accompanied by smaller vesicles, termed nanovesicles (Allan et al., 1980). During their 120-day lifespan, RBCs lose ∼20% of their volume through vesicle emission, increasing intra-erythrocytic Hb concentration by ∼14%; metrics for RMP production, circulating number and volume are presented in **Table 1** (Willekens et al., 2008). It was originally thought that vesiculation served to rid RBCs (which lack lysosomes) of damaged or harmful components that might otherwise accumulate over time, such as denatured Hb, C5b-9 complement attack complexes, or Band 3 neoantigens (Bosman et al., 2008b). It has also been suggested that RMP shedding promotes recognition and clearance of senescent and/or damaged RBCs by removing integral self-marker membrane proteins (e.g., CD47) (Stewart et al., 2005).

### RMP Production

RBCs spontaneously shed PS-positive MPs (Burger P. et al., 2013) and each individual RBC is estimated to generate ∼230 vesicles during it's lifespan (Bosch et al., 1994). As for other cell types, membrane phospholipid rearrangement is an integral step in RMP formation. The normal asymmetric distribution of the lipid bilayer is controlled by 3 different elements; flippase (ATP-dependent enzyme that promotes inward orientation of negatively charged lipids), floppase (responsible for maintaining outward orientation of phosphatidylcholine) and scramblase (facilitating bidirectional movement of all phospholipids) (Daleke, 2003). Consequent to RBC injury, metabolic stress, and/or senescence (and storage), ATP depletion and potassium leakage diminish flippase activity, while elevated intracellular calcium increases scramblase activity; consequently, normal membrane asymmetry is lost, PS is exposed on the RBC surface and vesicle shedding is promoted (Burger P. et al., 2013). There is lack of consensus with regard to the RBC sub-population most responsible for RMP production. Some suggest that senescent RBCs are responsible for the majority of RMP production *in vivo* (Willekens et al., 2003), while others have shown that during storage (or other periods of metabolic stress), younger RBC sub-populations produce the majority of RMPs (Greenwalt, 2006). Of note, during storage, RMP composition/content may vary with specific conditions and duration (Piccin et al., 2015). For example, RMPs generated *in vitro*, by stimulation with Ca ionophores, differ in size and cytoskeletal protein structure than RMPs generated during RBC storage (Allan et al., 1980; Salzer et al., 2002). Additionally, RMPs isolated during storage have less variation in size and shape than those isolated from circulation (Greenwalt, 2006). Moreover, hypotonic, alkaline storage solutions are associated with increased RMP production and with an RMPs that have diminished cholesterol, phospholipids, as well as band 3 and protein 4.1 (Greenwalt, 2006). Leukoreduction diminishes RMP production by up to 40–50%, particularly under anaerobic conditions (Jy et al., 2012). More generally, RBC storage (and other injury states) is characterized by progressive depletion of energy resources and antioxidant defenses, enabling accumulation of oxidative modification to proteins (and lipids), particularly involving the cytoskeleton and Band 3 (Kriebardis et al., 2008). Vesiculation may enable elimination of such markers as well as other dysfunctional elements that accumulate during storage, or consequent to *in vivo* injury (Delobel et al., 2012).

### Triggers for RMP Production

Little is known about the specific signaling that regulates RBC vesiculation, both during RBC aging *in vivo* and during *ex vivo*

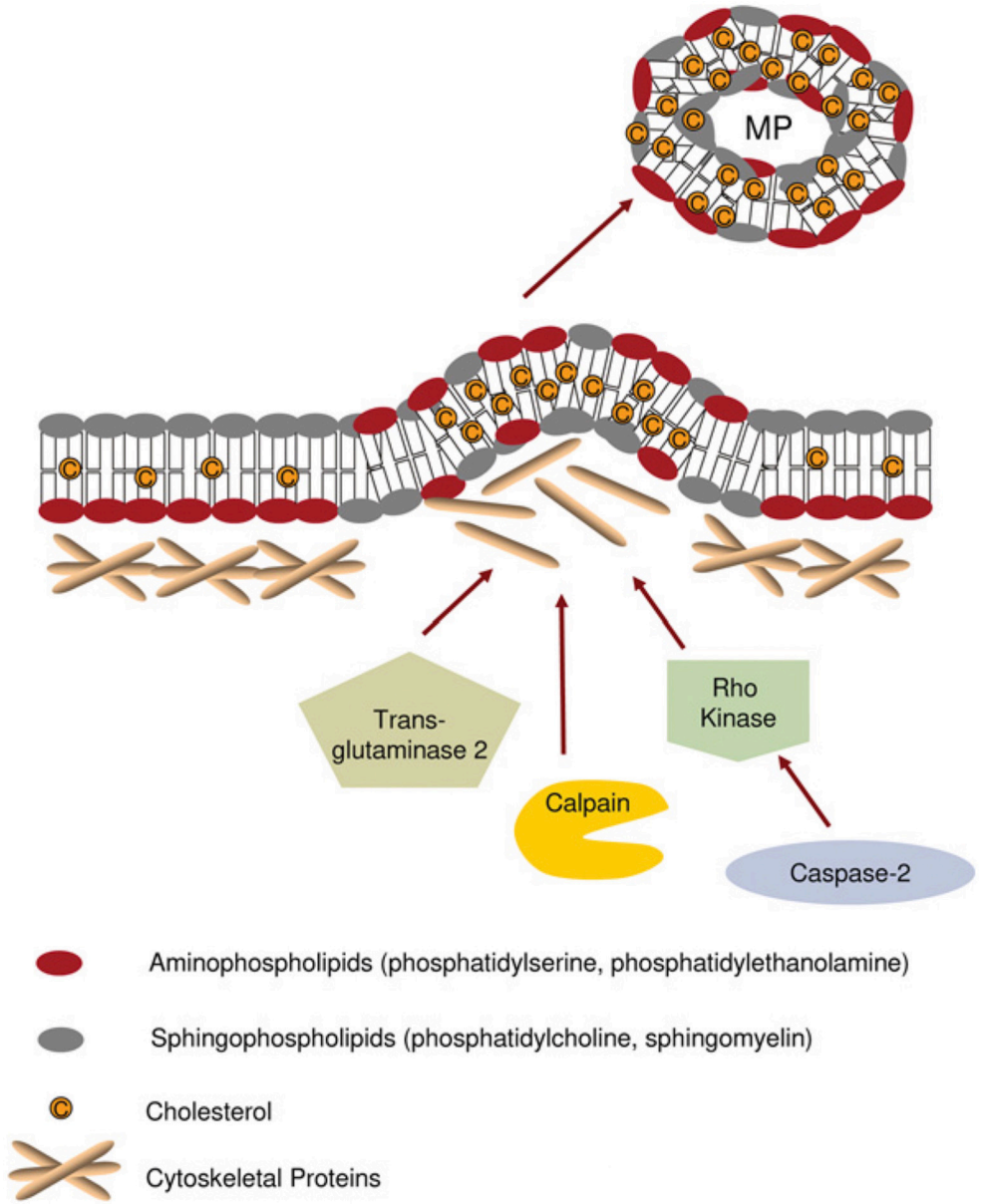


**FIGURE 3 |** Mechanisms proposed for cytoskeleton remodeling leading to microparticle (MP) formation. Under normal conditions, aminophospholipids (phosphatidylserine and phosphatidylethanolamine) are found exclusively on the inner leaflet of the plasma membrane. During MP formation, membrane asymmetry is lost as aminophospholipids redistribute to the outer leaflet of the plasma membrane. Cytoskeletal re-organization results in the outward blebbing of the plasma membrane and may be dependent upon actin polymerisation, caspase 2/Rho kinase, calpain, and/or transglutaminase 2. Such processes may vary between different cell types. MP formation appears to occur selectively in lipid-rich microdomains (lipid rafts/caveolae) within the plasma membrane. Adapted with permission from Burger D. et al. (2013).

storage. Further, it is also important to recognize that unique changes may occur to stored RBCs *in vivo*, following transfusion. Several RMP production triggers have been identified, mostly linked to (but not unique to) the changes RBCs undergo during storage. These include:

a. *Increased cytosolic calcium* ($Ca^{2+}$) is the most well-characterized trigger for activation of $Ca^{2+}$ dependent proteases, leading to cytoskeletal damage and activation of $Ca^{2+}$ dependent scramblase; both processes are result in PS exposure and MP shedding (Bevers et al., 1999).
b. *ATP depletion* impairs performance of the major ATP-dependent transporter proteins (flippase and floppase) responsible for maintaining cell membrane asymmetry; loss of asymmetry promotes MP budding and shedding (Burger P. et al., 2013).

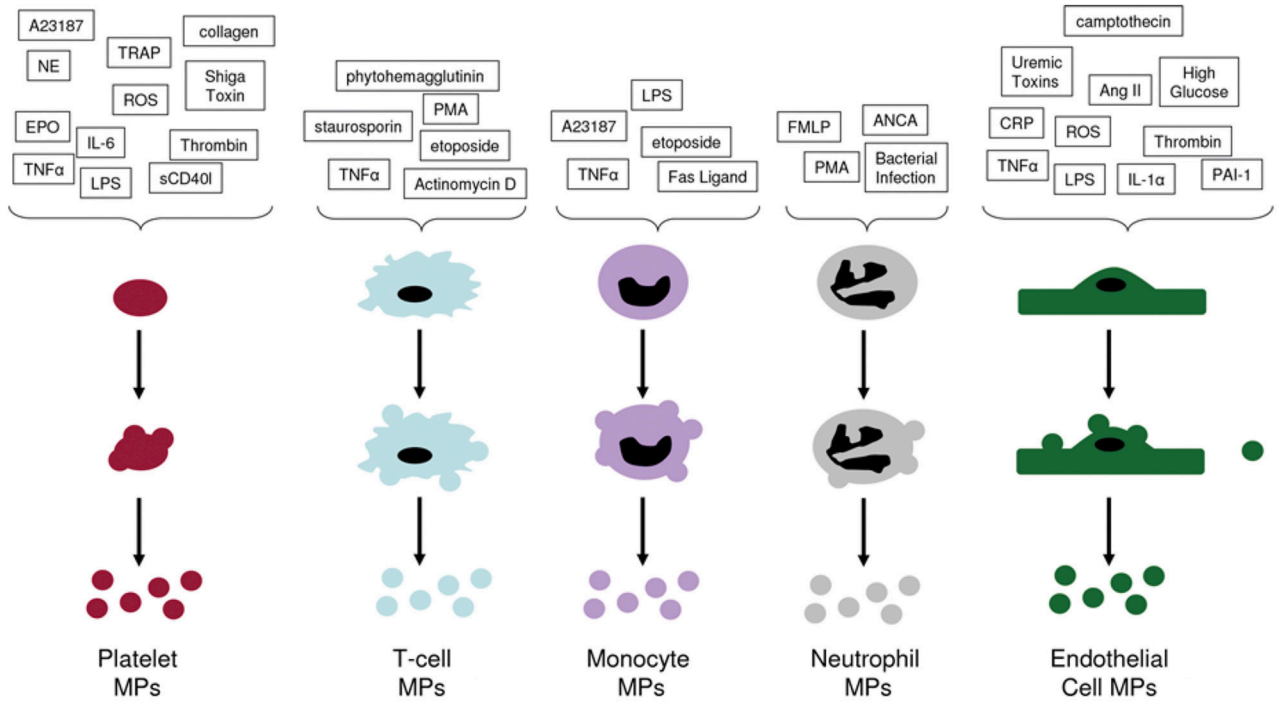


**FIGURE 4 |** Stimuli for microparticle (MP) formation from platelets, endothelial cells, and leukocytes. A summary of the stimuli which promote MP formation from platelets, endothelial cells and leukocytes. NE, Norepinephrine; EPO, erythropoietin; sCD40l, soluble CD40 ligand. With permission from Burger D. et al. (2013).

**TABLE 1 |** Estimated total circulating number, volume and rate of production of RMPs, intact RBCs and their respective ratios in a healthy adult male (Willekens et al., 2008).

| | Total circulating number | | Volume per RMP/RBC | | Rate of production | |
|---|---|---|---|---|---|---|
| | **RMP** | **RBC** | **RMP** | **RBC** | **RMP** | **RBC** |
| Absolute number | $8.5 \times 10^8$ | $2.5 \times 10^{13}$ | 0.065 $\mu m^3$ | 88 $\mu m^3$ | $5.8 \times 10^8$/s | $1.4 \times 10^6$/s |
| RMP: RBC ratio | $3.4 \times 10^{-5}$:1 | | $7.38 \times 10^{-4}$:1 | | 8,120:1 | |

c. *Increased potassium ($K^+$) leakage* has also been linked to disturbed erythrocytic membrane transporter activity, disturbing maintenance of membrane structure and leading to MP formation (Burger P. et al., 2013).

d. *Other cascades arising from energy failure* in RBCs have been shown to increase RBC vesiculation and MP formation. These include G protein-coupled receptor signaling, the phosphoinositide 3-kinase (PI3K-Akt protein kinase B) pathway, the Jak-STAT (Janus kinase-signal transducer and activator of transcription) pathway and the Raf-MEK (mitogen-activated protein kinase)-ERK (extracellular signal-regulated kinase) pathway (Kostova et al., 2015).

## RMP ~ RBC Differences

Proteomic analysis demonstrates that RMP protein content is diverse, including carbonic anhydrase, peroxiredoxins, and 14-3-3 proteins (regulators of a number of processes, such as protein kinase activity and signal transduction) (Rubin et al., 2008). RMPs, however, are structurally and functionally different from intact RBCs (i.e., RMPs are not "just small RBCs"). As discussed above, the RMP shedding process involves loss of normal membrane asymmetry, with increased density of negatively charged phospholipids (e.g., PS) on the outer RMP membrane (leading to differing surface potential). In comparison to parent RBCs, RMP membranes are also enriched with specific proteins (Band 3 dimers) (Bosman et al., 2008b). Moreover, in comparison to intact RBCs, storage-related RMPs appear enriched with stomatin, relatively depleted in actin and to have more stable glycophorin A (Rubin et al., 2008). Disruption of normal cytoskeletal protein structure (de Jong et al., 1996) is also integral to RMP shedding (Rubin et al., 2012) and distinguishes daughter from parent cells. These structural characteristics, in addition to size discrepancy, result in important differential "streaming" between RBCs and RMPs, with preferential RMP circulation in proximity to endothelial cells in the "cell free" zone of the micro-circulation (Liu et al., 2013) (N.B. This feature has significant physiologic implications, vide infra.). Finally, RMPs encapsulate a significant amount of Hb (Greenwalt et al., 1991), which confers physiologic characteristics closer to cell free Hb than to intact RBCs

[particularly with regard to interactions with nitric oxide (NO)].

## RMP Effects upon Vascular Physiology

There is increasing recognition of RMP biological effects, particularly in the context of transfusion. Proposed effects include the following:

### Promotion of Coagulation

It is well-established that negatively charged surfaces activate the zymogen components of the coagulation cascade, and it appears that RMPs promote coagulation in this fashion. In the presence of low exogenous tissue factor, RMPs increase thrombin generation and remarkably, are capable of initiating and propagating thrombin generation even in the absence of tissue factor (Rubin et al., 2013). There is some evidence that this pro-coagulant activity is dependent on Factor XII (Van Der Meijden et al., 2012). Some authors have suggested that tissue factor may be present on the RMP surface, contributing to their pro-coagulant effect (Biró et al., 2003). Of note, RMP abundance is known to increase in certain hypercoagulable states associated with hypercoagulability, such as sickle cell crises (van Beers et al., 2009). Conversely, RMPs also bind protein S, a cofactor for activated protein C, which enhances degradation of Factors VIIIa and Va, and inhibits tenase and prothrombinase and thus, promotes clot lysis (Koshiar et al., 2014). As such, depending on context, balance amongst these pleotropic effects determines RMP "coagulation phenotype (Koshiar et al., 2014)."

### Nitric Oxide (NO) Scavenging

Nitric oxide (NO) is a vasodilator effector component of physiologic reflexes that subserve dynamic matching between regional blood flow and tissue respiration (Doctor and Stamler, 2011). Of note, extra-erythrocytic hemoglobin (Hb) reacts with NO in a diffusion-limited oxidation reaction that quenches NO bioactivity, disrupting vasoregulation and oxygen delivery homeostasis; under normal conditions, this effect is limited by Hb compartmentalization within RBCs (Singel and Stamler, 2005). Specifically, constraints upon Hb∼NO interaction are substantially influenced by RBC size and membrane architecture (Huang et al., 2001); however, reaction between de-compartmentalized, cell-free Hb, and NO lacks such constraint (Lancaster, 1994). Notably, RMP:NO interaction more closely mirrors that of cell-free Hb than that of intact RBCs, and as such—RMPs act as potent NO scavengers [RMP reaction with NO is ∼1,000-fold faster than with RBC-encapsulated Hb (Donadee et al., 2011) and is only 2.5- to 3-fold slower than with cell-free Hb (Donadee et al., 2011)]. The potential impact of quenching NO bioactivity by RMPs (following transfusion) dramatically increases with the increase in RMP abundance that is observed during storage duration. Of note, the degree by which RMPs influence NO bioavailability *in vivo* is dependent on several factors, most importantly, the degree to which RMPs enter the cell-free zone in the microcirculation (e.g., stream in immediate proximity to endothelium) (Liu et al., 2013).

### Immune Modulation

Transfusion Related Immune Modulation (TRIM) is a recognized, but poorly characterized, complication of transfusion. Given the known increase in RMP generation with storage duration, a role for RMPs in TRIM pathobiology (which appears linked to RBC unit age) has been postulated (Muszynski et al., 2017). RMPs influence antigen presenting cells (APC) and boost mitogen driven T cell responses (Danesh et al., 2014); specifically, RMPs amplify APC-based induction of pro-inflammatory cytokines and chemokines from peripheral blood mononuclear cells (PBMC), promoting their survival (pro-inflammatory effect) (Danesh et al., 2014). Alternatively, RMPs may exert an immunosuppressive effect, by dampening release of various cytokines such as TNF-α, IL-8, or IL-10 (Sadallah et al., 2008). Of note, production of sickle cell derived RMP (SS RMPs) is enhanced during inflammation; moreover, when engulfed by myeloid cells, SS RMPs promote pro-inflammatory cytokine secretion and endothelial cell adhesion, suggesting that crosstalk between circulating inflammatory cells and SS RMPs contributes to sickle cell disease (SCD) pathogenesis (Awojoodu et al., 2014). Additionally, since RMPs have also been demonstrated to bear blood group antigens (Canellini et al., 2012); transfusion-related RMPs may therefore represent a significant immunogenic load (Willekens et al., 2008) and contribute to the severity of alloimmunization in chronically transfused patients (Canellini et al., 2012).

### Promotion of Endothelial Adhesion

As noted above, RMPs appear to play a significant role in the pathophysiology of SCD, during which RMP production is enhanced, promoting pro-inflammatory cytokine secretion (van Beers et al., 2009). SS RMPs have also been shown to enhance adhesion of intact RBCs to endothelial cells (Awojoodu et al., 2014). Of note, up to a third of the circulating extra-erythrocytic heme in patients with SCD may be carried by RMPs (Camus et al., 2015); moreover, externalized membrane PS on SS RMPs retains heme on the external RMP surface; such heme-laden SS RMPs transfer heme directly to vascular endothelium, generating oxidative stress and endothelial apoptosis (Camus et al., 2015). This linkage of hemolysis to endothelial injury has been proposed as a trigger for SCD vaso-occlusive crises.

## RMP Clearance

As for other MP populations, RMPs are likely to be cleared via the MPS, by hepatic Kupffer cells (Willekens et al., 2005). Such removal appears to occur very rapidly and is thought to be mediated by PS-binding scavenger receptors and senescent cell antigen specific autoantibodies (Willekens et al., 2005). Immunologic analysis of RMPs elaborated by senescent RBCs demonstrates Band 3 clustering; this RMP subpopulation may therefore be cleared in a fashion similar to that for intact senescent RBCs (Willekens et al., 2008).

## RMPs and RBC Processing and Storage for Transfusion

The RBC storage lesion is comprised by profoundly altered metabolism and biomechanics; in particular, energy failure

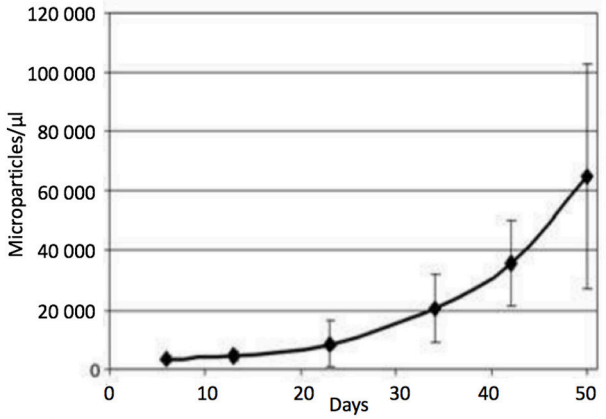


**FIGURE 5 |** Microparticle (MP) count in red blood cell units during storage (without centrifugation). Data are expressed as the mean *SD* ($n = 7$). At day 5: 3,371,188 MPs/µL were counted, whereas at day 50: MPs had increased in abundance by ∼20-fold. MPs were stained with anti-human CD47. With permission from Rubin et al. (2008).

(with impaired ATP and reducing equivalent production) is characteristic and is associated with a significant acidosis, decrease in 2,3-diphosphoglycerate and failure of the membrane $Na^+/K^+$ ATPase pump with continuous potassium leakage (Bennett-Guerrero et al., 2007; D'Alessandro et al., 2015) (e.g., conditions known to promote RMP genesis; Bosman et al., 2008a; Karon et al., 2009). Morphologically, stored RBCs slowly morph from smooth biconcave discs, to spiculated echinocytes, to dense sphero-echinocytes; these changes arise from membrane loss and RMP formation, and lead to loss of cell volume regulation and diminished deformability (Greenwalt, 2006), thus negaitvely impacting post-transfusion survival and rheology (Relevy et al., 2008). In fact, RMP genesis appears directly proportional to storage duration, with a 20-fold increase after 50 days (Rubin et al., 2008; **Figure 5**); the doubling time for RMP concentration during storage is estimated to be 9 days (95% CI: 7.7–10.7 days) (Donadee et al., 2011). The specific reasons for such significant RMP production remain unknown; it has been suggested that storage activates a physiologic process that serves (*in vivo*) as means to prevent premature RBC clearance, by shedding membrane proteins that would otherwise signal RBC senescence (Solheim et al., 2004; Willekens et al., 2008).

# PHYSIOLOGIC IMPACT OF STORAGE-GENERATED RMPS DURING RBC TRANSFUSION

## Oxygen ($O_2$) Delivery Homeostasis and Vasoregulation

Tissue $O_2$ delivery is a function of blood $O_2$ content and regional blood flow, with the latter being the principle determinant. As such, the volume and distribution of regional blood flow is actively regulated to maintain dynamic coupling between $O_2$ delivery and tissue respiration (Kulandavelu et al., 2015). It is now commonly appreciated that RBCs act as both sensors and transducers, comprising a signaling loop in this physiology, by linking bioavailability of vasoactive effectors in plasma to microcirculatory $O_2$ gradients (and thereby, modulating resistance vessel caliber to maintain perfusion sufficiency) (Doctor and Stamler, 2011). This key physiologic reflex is termed hypoxic vasodilation (HVD) and is primarily mediated by RBC-transported NO (Gonzalez-Alonso et al., 2001; McMahon et al., 2002; Doctor et al., 2005); as such, by serving as HVD effector elements, RBCs function as a key node in maintenance of $O_2$ delivery homeostasis (**Figure 6**). This paracrine RBC function is governed by $O_2$-linked transitions in Hb conformation which (because of differing reactions of deoxy- and oxy-Hb with NO) transduce regional $pO_2$ gradients into NO bioactivity, thereby effecting vasodilation to resolve perfusion insufficiency (e.g., HVD) (Singel and Stamler, 2005). Of note, this physiology is disrupted when RBCs release Hb into plasma. Specifically, although Hb packaging in RBCs blunts NO consumption ∼1,000-fold, once released, free Hb (and RMP contained Hb) readily inactivates NO, preventing facile NO-based traffic between RBCs and endothelium (Vaughn et al., 2000; Liu et al., 2013).

## Transfusion and Vasoregulation

Mounting evidence indicates that RBC transfusion impairs HVD efficacy, although the mechanism is not fully elucidated (Bennett-Guerrero et al., 2007; Bonaventura, 2007; Reynolds et al., 2011). In addition to the direct effects of cell-free Hb upon NO bioavailability in plasma, transfusion-associated hemolysis may also impair endothelial NO production via release of arginase (which, via substrate depletion, constrains eNOS activity) (Donadee et al., 2011; Alexander et al., 2013). Moreover, processed/stored RBCs are 2- to 4-fold more avid NO scavengers than fresh RBCs (Stapley et al., 2012) and exhibit more pronounced inhibition of NO mediated vasodilation. Further, mounting evidence implicates stored RBC-derived free-Hb and Hb-rich RMPs in dampening normal NO bioactivity in the microcirculation, leading to physiologically significant HVD impairment (Chen et al., 2008; Donadee et al., 2011; Kim-Shapiro et al., 2011; Roback, 2011). The latter observation is further supported by *in vivo* data demonstrating RMP contribution to the initiation of vasoocclusive crises in SCD (Camus et al., 2015).

## RMP Impact upon Vasoregulation

As discussed above, HVD is the principle physiologic reflex that maintains dynamic coupling between regional $O_2$ delivery and tissue respiration, particularly during physiologic stress. RMPs appear to impair RBC-based HVD support of $O_2$ delivery homeostasis, by: (1) preferential streaming in the cell free zone of the microcirculation and (2) acting as an NO sink. Specifically, animal studies demonstrate greater increase in mean arterial pressure (MAP) upon infusion of cell-free supernatants of longer stored RBC units (39 days) vs. fresher units (4 days) (Donadee et al., 2011; **Figure 7**); this increase correlates with the amount of extra-erythrocytic Hb (both free and in RMPs) in supernatants. Moreover, RMP half-life in this model was observed to be ∼15–20 min, which is consistent with the time course for blood pressure changes that occur with infusion of stored RBC supernatants (Donadee et al., 2011). This is particularly important since (unlike cell-free Hb), RMPs are not

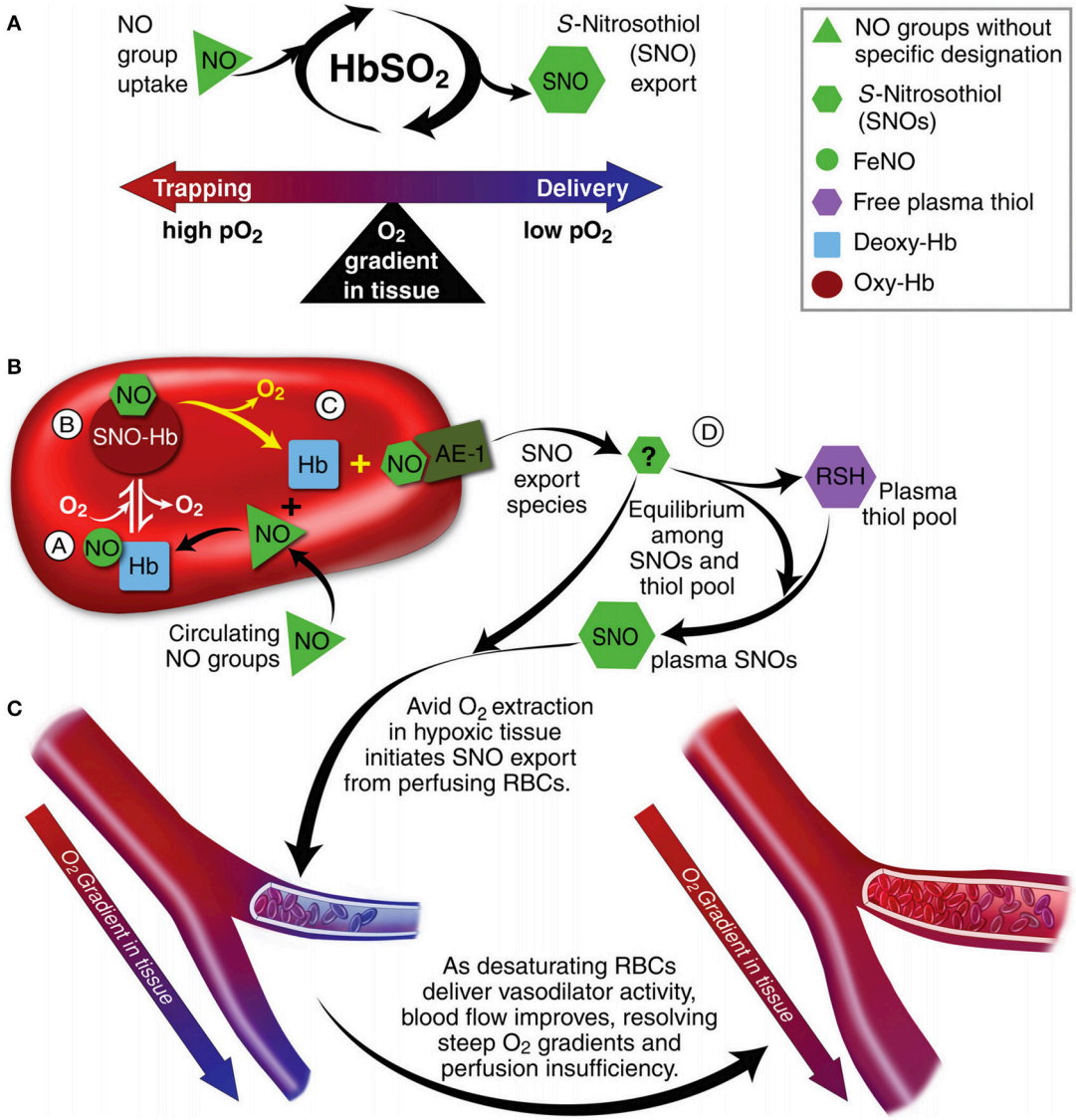


**FIGURE 6 |** Red blood cells (RBC) transduce regional $O_2$ gradients in tissue to control nitric oxide (NO) bioactivity in plasma by trapping or delivering NO groups as a function of hemoglobin (Hb) $O_2$ saturation (Hb $SO_2$). **(A)** Circulating NO groups are processed by Hb into the highly vasoactive (thiol-based) NO congener, S-nitrosothiol (SNO). By exporting SNOs as a function of Hb deoxygenation, RBCs precisely dispense vasodilator bioactivity in direct proportion to the lack of regional blood flow. **(B)** $O_2$ delivery homeostasis requires biochemical coupling of vessel tone to environmental cues that match perfusion sufficiency to metabolic demand. Because oxygenated Hb (oxy Hb) and deoxygenated Hb (deoxy Hb) process NO differently, allosteric transitions in Hb conformation afford context-responsive ($O_2$-coupled) control of NO bioavailability, thereby linking the sensor and effector arms of this system. Specifically, Hb conformation governs the equilibria among **(A)** deoxygenated Hb FeNO (NO sink), **(B)** oxygenated SNO-Hb (NO store), and **(C)** acceptor thiols including the membrane protein SNO-AE-1 (bioactive NO source). Direct SNO export from RBCs or S-transnitrosylation from RBCs to plasma thiols **(D)** yields vasoactive SNOs, which influence resistance vessel caliber and close this signaling loop. Thus, RBCs either trap **(A)** or export **(D)** NO groups to optimize blood flow. **(C)** NO processing in RBCs **(A,B)** couples vessel tone to tissue pO2; this system subserves hypoxic vasodilation in the arterial periphery and thereby calibrates blood flow to regional tissue hypoxia. Adapted with permission from Doctor and Stamler (2011).

bound by haptoglobin and may therefore contribute significantly to this phenomenon (Donadee et al., 2011).

## SUMMARY

MPs are submicron particles that originate from varied cell populations, that form in response to a multitude of stimuli through cell membrane re-organization, blebbing and shedding. MPs have pleotropic effects upon vascular physiology and may serve as vehicles for inter-cellular communication. RMPs form spontaneously during the RBC lifespan, with content and cytoskeletal structure distinct from intact RBCs. RMP production accelerates during RBC storage due to associated biochemical changes: increased cytosolic calcium, ATP depletion,

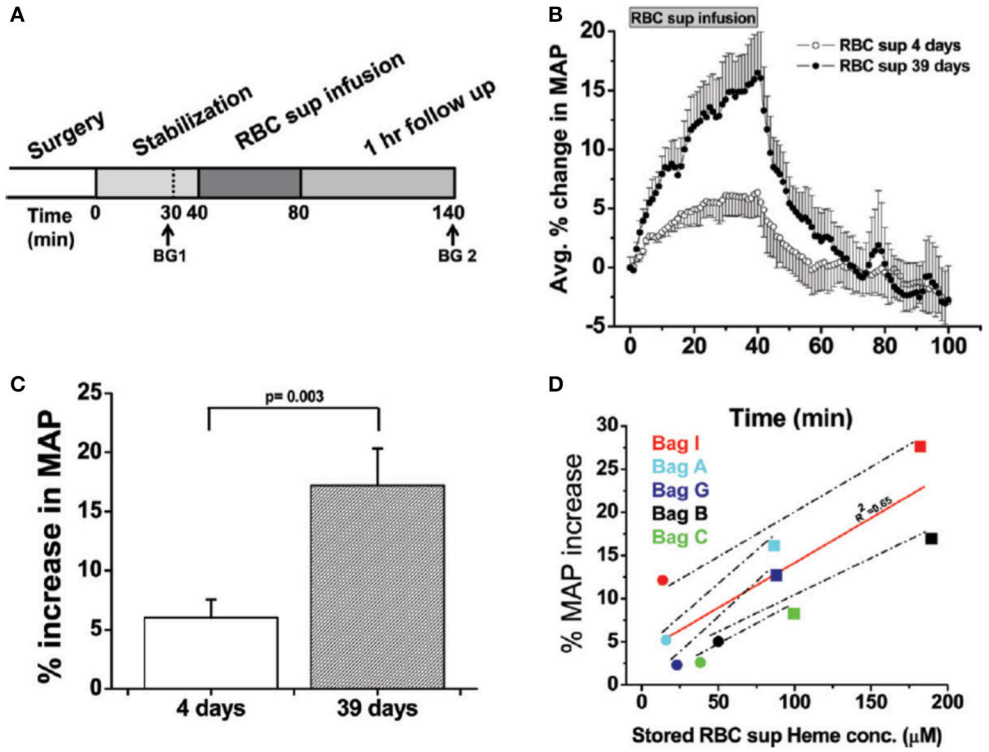


**FIGURE 7 |** Vasoactivity of infused packed red cell supernatant/plasma. **(A)** Experimental time line for packed red cell supernatant infusions. Rats were stabilized for 30 min after surgery, and blood gasses were drawn as indicated (BG 1 and BG 2). Supernatant (1.6 mL) of packed red blood cells stored for either 4 or 39 days was infused for 40 min, after which the rats were followed for 1 h ($n = 5$). **(B)** Change in mean arterial pressure (MAP) over time after packed red blood cell (RBC) supernatant infusion and 60-min follow up. **(C)** Average percentage peak increase in MAP after infusion of packed RBC supernatants (RBC sup) ($p = 0.003$). **(D)** Correlation (solid line) between packed red blood cell supernatant haeme concentration and percentage increase in MAP after 40-min infusion of packed red blood cell supernatant stored for either 4 days (black solid circle) or 39 days (black solid square; R20.65). Each data point was obtained from a separate rat infusion experiment, in a different rat (2 groups of $n = 5$). All values are displayed as mean standard error of mean (SEM). Student *t*-test was used to compare the 2 groups of rats. Avg, average; conc, concentration. Adapted with permission from Donadee et al. (2011).

and increased potassium leakage. Moreover, RMP composition is affected by the trigger for their formation and by different storage conditions.

Proposed RMP biological effects include promotion of coagulation, immune modulation, and enhanced endothelial adhesion. Of particular importance, RMPs demonstrate significant NO trapping/consumption, disrupting regional matching between blood flow and tissue respiration that is essential to oxygen delivery homeostasis physiology. These effects have been demonstrated in animal models evaluating storage related RMPs, which appear to provoke an increase in systemic vascular tone and blood pressure following infusion of cell-free RBC unit supernatants. This effect is progressive with storage duration.

## FUTURE DIRECTIONS

Our goals are to further elucidate the impact of RMPs on vasoregulation in critically ill subjects. We are currently examining the *in vivo* effects of RBC transfusions on hemodynamics, systemic vascular resistance and cardiac output, and tissue re-oxygenation during dynamic near infrared spectroscopy (NIRS), a novel non-invasive means to monitor hypoxic vasodilation (Creteur et al., 2009; Lipcsey et al., 2012). Concurrently, we are quantifying the peri-transfusion change in RMP burden and pharmacodynamics and the relationship to plasma vasoactivity which will be correlated with dynamic NIRS findings in humans.

## AUTHOR CONTRIBUTIONS

AS: performed experiments and analyzed data and drafted the manuscript. SR: performed experiments and analyzed data. AD: supervised experiments and edited the manuscript.

## FUNDING

AD is supported by R01GM113838.

## REFERENCES


Agouni, A., Mostefai, H. A., Porro, C., Carusio, N., Favre, J., Richard, V., et al. (2007). Sonic hedgehog carried by microparticles corrects endothelial injury through nitric oxide release. *FASEB J.* 21, 2735–2741. doi: 10.1096/fj.07-8079com

Alexander, J. T., El-Ali, A. M., Newman, J. L., Karatela, S., Predmore, B. L., Lefer, D. J., et al. (2013). Red blood cells stored for increasing periods produce progressive impairments in nitric oxide-mediated vasodilation. *Transfusion* 53, 2619–2628. doi: 10.1111/trf.12111

Allan, D., Thomas, P., and Limbrick, A. R. (1980). The isolation and characterization of 60 nm vesicles ('nanovesicles') produced during ionophore A23187-induced budding of human erythrocytes. *Biochem. J.* 188, 881–887. doi: 10.1042/bj1880881

Amabile, N., Guérin, A. P., Tedgui, A., Boulanger, C. M., and London, G. M. (2012). Predictive value of circulating endothelial microparticles for cardiovascular mortality in end-stage renal failure: a pilot study. *Nephrol. Dial. Transplant.* 27, 1873–1880. doi: 10.1093/ndt/gfr573

Angelillo-Scherrer, A. (2012). Leukocyte-derived microparticles in vascular homeostasis. *Circ. Res.* 110, 356–369. doi: 10.1161/CIRCRESAHA.110.233403

Antoniak, S., Boltzen, U., Eisenreich, A., Stellbaum, C., Poller, W., Schultheiss, H. P., et al. (2009). Regulation of cardiomyocyte full-length tissue factor expression and microparticle release under inflammatory conditions *in vitro*. *J. Thromb. Haemost.* 7, 871–878. doi: 10.1111/j.1538-7836.2009.03323.x

Aoki, N., Jin-no, S., Nakagawa, Y., Asai, N., Arakawa, E., Tamura, N., et al. (2007). Identification and characterization of microvesicles secreted by 3T3-L1 adipocytes: redox- and hormone-dependent induction of milk fat globule-epidermal growth factor 8-associated microvesicles. *Endocrinology* 148, 3850–3862. doi: 10.1210/en.2006-1479

Awojoodu, A. O., Keegan, P. M., Lane, A. R., Zhang, Y., Lynch, K. R., Platt, M. O., et al. (2014). Acid sphingomyelinase is activated in sickle cell erythrocytes and contributes to inflammatory microparticle generation in SCD. *Blood* 124, 1941–1950. doi: 10.1182/blood-2014-01-543652

Bennett-Guerrero, E., Veldman, T. H., Doctor, A., Telen, M. J., Ortel, T. L., Reid, T. S., et al. (2007). Evolution of adverse changes in stored RBCs. *Proc. Natl. Acad. Sci. U.S.A.* 104, 17063–17068. doi: 10.1073/pnas.0708160104

Bernal-Mizrachi, L., Jy, W., Jimenez, J. J., Pastor, J., Mauro, L. M., Horstman, L. L., et al. (2003). High levels of circulating endothelial microparticles in patients with acute coronary syndromes. *Am. Heart J.* 145, 962–970. doi: 10.1016/S0002-8703(03)00103-0

Bernimoulin, M., Waters, E. K., Foy, M., Steele, B. M., Sullivan, M., Falet, H., et al. (2009). Differential stimulation of monocytic cells results in distinct populations of microparticles. *J. Thromb. Haemost.* 7, 1019–1028. doi: 10.1111/j.1538-7836.2009.03434.x

Bevers, E. M., Comfurius, P., Dekkers, D. W., and Zwaal, R. F. (1999). Lipid translocation across the plasma membrane of mammalian cells. *Biochim. Biophys. Acta* 1439, 317–330. doi: 10.1016/S1388-1981(99)00110-9

Biró, E., Sturk-Maquelin, K. N., Vogel, G. M., Meuleman, D. G., Smit, M. J., Hack, C. E., et al. (2003). Human cell-derived microparticles promote thrombus formation *in vivo* in a tissue factor-dependent manner. *J. Thromb. Haemost.* 1, 2561–2568. doi: 10.1046/j.1538-7836.2003.00456.x

Bonaventura, J. (2007). Clinical implications of the loss of vasoactive nitric oxide during red blood cell storage. *Proc. Natl. Acad. Sci. U.S.A.* 104, 19165–19166. doi: 10.1073/pnas.0708871105

Bosch, F. H., Werre, J. M., Schipper, L., Roerdinkholder-Stoelwinder, B., Huls, T., Willekens, F. L., et al. (1994). Determinants of red blood cell deformability in relation to cell age. *Eur. J. Haematol.* 52, 35–41. doi: 10.1111/j.1600-0609.1994.tb01282.x

Bosman, G. J., Lasonder, E., Luten, M., Roerdinkholder-Stoelwinder, B., Novotný, V. M., Bos, H., et al. (2008a). The proteome of red cell membranes and vesicles during storage in blood bank conditions. *Transfusion* 48, 827–835. doi: 10.1111/j.1537-2995.2007.01630.x

Bosman, G. J., Werre, J. M., Willekens, F. L., and Novotný, V. M. (2008b). Erythrocyte ageing *in vivo* and *in vitro*: structural aspects and implications for transfusion. *Transfus. Med.* 18, 335–347. doi: 10.1111/j.1365-3148.2008.00892.x

Boulanger, C. M., and Dignat-George, F. (2011). Microparticles: an introduction. *Arterioscler. Thromb. Vasc. Biol.* 31, 2–3. doi: 10.1161/ATVBAHA.110.220095

Brill, A., Dashevsky, O., Rivo, J., Gozal, Y., and Varon, D. (2005). Platelet-derived microparticles induce angiogenesis and stimulate post-ischemic revascularization. *Cardiovasc. Res.* 67, 30–38. doi: 10.1016/j.cardiores.2005.04.007

Burger, D., Kwart, D. G., Montezano, A. C., Read, N. C., Kennedy, C. R., Thompson, C. S., et al. (2012). Microparticles induce cell cycle arrest through redox-sensitive processes in endothelial cells: implications in vascular senescence. *J. Am. Heart Assoc.* 1:e001842. doi: 10.1161/JAHA.112.001842

Burger, D., Montezano, A. C., Nishigaki, N., He, Y., Carter, A., and Touyz, R. M. (2011). Endothelial microparticle formation by angiotensin II is mediated via Ang II receptor type I/NADPH oxidase/ Rho kinase pathways targeted to lipid rafts. *Arterioscler. Thromb. Vasc. Biol.* 31, 1898–1907. doi: 10.1161/ATVBAHA.110.222703

Burger, D., Schock, S., Thompson, C. S., Montezano, A. C., Hakim, A. M., and Touyz, R. M. (2013). Microparticles: biomarkers and beyond. *Clin. Sci.* 124, 423–441. doi: 10.1042/CS20120309

Burger, P., Kostova, E., Bloem, E., Hilarius-Stokman, P., Meijer, A. B., van den Berg, T. K., et al. (2013). Potassium leakage primes stored erythrocytes for phosphatidylserine exposure and shedding of pro-coagulant vesicles. *Br. J. Haematol.* 160, 377–386. doi: 10.1111/bjh.12133

Camus, S. M., De Moraes, J. A., Bonnin, P., Abbyad, P., Le Jeune, S., Lionnet, F., et al. (2015). Circulating cell membrane microparticles transfer heme to endothelial cells and trigger vasoocclusions in sickle cell disease. *Blood* 125, 3805–3814. doi: 10.1182/blood-2014-07-589283

Canellini, G., Rubin, O., Delobel, J., Crettaz, D., Lion, N., and Tissot, J. D. (2012). Red blood cell microparticles and blood group antigens: an analysis by flow cytometry. *Blood Transfus.* 10(Suppl. 2), s39–s45. doi: 10.2450/2012.007S

Cauwenberghs, S., Feijge, M. A., Harper, A. G., Sage, S. O., Curvers, J., and Heemskerk, J. W. (2006). Shedding of procoagulant microparticles from unstimulated platelets by integrin-mediated destabilization of actin cytoskeleton. *FEBS Lett.* 580, 5313–5320. doi: 10.1016/j.febslet.2006.08.082

Chen, K., Pittman, R. N., and Popel, A. S. (2008). Nitric oxide in the vasculature: where does it come from and where does it go? A quantitative perspective. *Antioxid. Redox Signal.* 10, 1185–1198. doi: 10.1089/ars.2007.1959

Chen, T. S., Lai, R. C., Lee, M. M., Choo, A. B., Lee, C. N., and Lim, S. K. (2010). Mesenchymal stem cell secretes microparticles enriched in pre-microRNAs. *Nucleic Acids Res.* 38, 215–224. doi: 10.1093/nar/gkp857

Creteur, J., Neves, A. P., and Vincent, J. L. (2009). Near-infrared spectroscopy technique to evaluate the effects of red blood cell transfusion on tissue oxygenation. *Crit Care* 13(Suppl. 5):S11. doi: 10.1186/cc8009

Daleke, D. L. (2003). Regulation of transbilayer plasma membrane phospholipid asymmetry. *J. Lipid Res.* 44, 233–242. doi: 10.1194/jlr.R200019-JLR200

D'Alessandro, A., Kriebardis, A. G., Rinalducci, S., Antonelou, M. H., Hansen, K. C., Papassideri, I. S., et al. (2015). An update on red blood cell storage lesions, as gleaned through biochemistry and omics technologies. *Transfusion* 55, 205–219. doi: 10.1111/trf.12804

Danesh, A., Inglis, H. C., Jackman, R. P., Wu, S., Deng, X., Muench, M. O., et al. (2014). Exosomes from red blood cell units bind to monocytes and induce proinflammatory cytokines, boosting T-cell responses *in vitro*. *Blood* 123, 687–696. doi: 10.1182/blood-2013-10-530469

de Jong, K., Beleznay, Z., and Ott, P. (1996). Phospholipid asymmetry in red blood cells and spectrin-free vesicles during prolonged storage. *Biochim. Biophys. Acta* 1281, 101–110. doi: 10.1016/0005-2736(96)00026-0

Del Conde, I., Shrimpton, C. N., Thiagarajan, P., and López, J. A. (2005). Tissue-factor-bearing microvesicles arise from lipid rafts and fuse with activated platelets to initiate coagulation. *Blood* 106, 1604–1611. doi: 10.1182/blood-2004-03-1095

Delobel, J., Prudent, M., Rubin, O., Crettaz, D., Tissot, J. D., and Lion, N. (2012). Subcellular fractionation of stored red blood cells reveals a compartment-based protein carbonylation evolution. *J. Proteomics 76*, 181–193. doi: 10.1016/j.jprot.2012.05.004

Diehl, P., Fricke, A., Sander, L., Stamm, J., Bassler, N., Htun, N., et al. (2012). Microparticles: major transport vehicles for distinct microRNAs in circulation. *Cardiovasc. Res.* 93, 633–644. doi: 10.1093/cvr/cvs007

Dignat-George, F., and Boulanger, C. M. (2011). The many faces of endothelial microparticles. *Arterioscler. Thromb. Vasc. Biol.* 31, 27–33. doi: 10.1161/ATVBAHA.110.218123

Distler, J. H., Akhmetshina, A., Dees, C., Jüngel, A., Stürzl, M., Gay, S., et al. (2011). Induction of apoptosis in circulating angiogenic cells by microparticles. *Arthritis Rheum.* 63, 2067–2077. doi: 10.1002/art.30361

Doctor, A., and Stamler, J. S. (2011). Nitric oxide transport in blood: a third gas in the respiratory cycle. *Compr. Physiol.* 1, 541–568. doi: 10.1002/cphy.c090009

Doctor, A., Platt, R., Sheram, M. L., Eischeid, A., McMahon, T., Maxey, T., et al. (2005). Hemoglobin conformation couples erythrocyte S-nitrosothiol content to O2 gradients. *Proc. Natl. Acad. Sci. U.S.A.* 102, 5709–5714. doi: 10.1073/pnas.0407490102

Donadee, C., Raat, N. J., Kanias, T., Tejero, J., Lee, J. S., Kelley, E. E., et al. (2011). Nitric oxide scavenging by red blood cell microparticles and cell-free hemoglobin as a mechanism for the red cell storage lesion. *Circulation* 124, 465–476. doi: 10.1161/CIRCULATIONAHA.110.008698

Elmore, S. (2007). Apoptosis: a review of programmed cell death. *Toxicol. Pathol.* 35, 495–516. doi: 10.1080/01926230701320337

Essayagh, S., Xuereb, J. M., Terrisse, A. D., Tellier-Cirioni, L., Pipy, B., and Sié, P. (2007). Microparticles from apoptotic monocytes induce transient platelet recruitment and tissue factor expression by cultured human vascular endothelial cells via a redox-sensitive mechanism. *Thromb. Haemost.* 98, 831–837. doi: 10.1160/TH07-02-0082

Eyre, J., Burton, J. O., Saleem, M. A., Mathieson, P. W., Topham, P. S., and Brunskill, N. J. (2011). Monocyte- and endothelial-derived microparticles induce an inflammatory phenotype in human podocytes. *Nephron Exp. Nephrol.* 119, e58–e66. doi: 10.1159/000329575

Faure, V., Dou, L., Sabatier, F., Cerini, C., Sampol, J., Berland, Y., et al. (2006). Elevation of circulating endothelial microparticles in patients with chronic renal failure. *J. Thromb. Haemost.* 4, 566–573. doi: 10.1111/j.1538-7836.2005.01780.x

Feng, B., Chen, Y., Luo, Y., Chen, M., Li, X., and Ni, Y. (2010). Circulating level of microparticles and their correlation with arterial elasticity and endothelium-dependent dilation in patients with type 2 diabetes mellitus. *Atherosclerosis* 208, 264–269. doi: 10.1016/j.atherosclerosis.2009.06.037

Forest, A., Pautas, E., Ray, P., Bonnet, D., Verny, M., Amabile, N., et al. (2010). Circulating microparticles and procoagulant activity in elderly patients. *J. Gerontol. A Biol. Sci. Med. Sci.* 65, 414–420. doi: 10.1093/gerona/glp187

Fox, J. E., Austin, C. D., Reynolds, C. C., and Steffen, P. K. (1991). Evidence that agonist-induced activation of calpain causes the shedding of procoagulant-containing microvesicles from the membrane of aggregating platelets. *J. Biol. Chem.* 266, 13289–13295.

Gonzalez-Alonso, J., Richardson, R. S., and Saltin, B. (2001). Exercising skeletal muscle blood flow in humans responds to reduction in arterial oxyhaemoglobin, but not to altered free oxygen. *J. Physiol.* 530, 331–341. doi: 10.1111/j.1469-7793.2001.0331l.x

González-Quintero, V. H., Jiménez, J. J., Jy, W., Mauro, L. M., Hortman, L., O'Sullivan, M. J., et al. (2003). Elevated plasma endothelial microparticles in preeclampsia. *Am. J. Obstet. Gynecol.* 189, 589–593. doi: 10.1067/S0002-9378(03)00469-1

Greenwalt, T. J. (2006). The how and why of exocytic vesicles. *Transfusion* 46, 143–152. doi: 10.1111/j.1537-2995.2006.00692.x

Greenwalt, T. J., McGuinness, C. G., and Dumaswala, U. J. (1991). Studies in red blood cell preservation: 4. plasma vesicle hemoglobin exceeds free hemoglobin. *Vox Sang* 61, 14–17. doi: 10.1111/j.1423-0410.1991.tb00920.x

Huang, K. T., Han, T. H., Hyduke, D. R., Vaughn, M. W., Van Herle, H., Hein, T. W., et al. (2001). Modulation of nitric oxide bioavailability by erythrocytes. *Proc. Natl. Acad. Sci. U.S.A.* 98, 11771–11776. doi: 10.1073/pnas.201276698

Huang, P. H., Huang, S. S., Chen, Y. H., Lin, C. P., Chiang, K. H., Chen, J. S., et al. (2010). Increased circulating CD31+/annexin V+ apoptotic microparticles and decreased circulating endothelial progenitor cell levels in hypertensive patients with microalbuminuria. *J. Hypertens.* 28, 1655–1665. doi: 10.1097/HJH.0b013e32833a4d0a

Huber, L. C., Jüngel, A., Distler, J. H., Moritz, F., Gay, R. E., Michel, B. A., et al. (2007). The role of membrane lipids in the induction of macrophage apoptosis by microparticles. *Apoptosis* 12, 363–374. doi: 10.1007/s10495-006-0622-7

Hugel, B., Martínez, M. C., Kunzelmann, C., and Freyssinet, J. M. (2005). Membrane microparticles: two sides of the coin. *Physiology.* 20, 22–27. doi: 10.1152/physiol.00029.2004

Jimenez, J. J., Jy, W., Mauro, L. M., Soderland, C., Horstman, L. L., and Ahn, Y. S. (2003). Endothelial cells release phenotypically and quantitatively distinct microparticles in activation and apoptosis. *Thromb. Res.* 109, 175–180. doi: 10.1016/S0049-3848(03)00064-1

Jy, W., Bidot, C. Jr., Yoshida, T., Vassallo, R. Jr., Johansen, E. M., Horstman, L. L., et al. (2012). Release of microparticles during blood storage is influenced by residual platelets, leukocytes and oxygen levels. *Blood* 120:3435. Available online at: http://www.bloodjournal.org/content/120/21/3435/tab-article-info

Jy, W., Minagar, A., Jimenez, J. J., Sheremata, W. A., Mauro, L. M., Horstman, L. L., et al. (2004). Endothelial microparticles (EMP) bind and activate monocytes: elevated EMP-monocyte conjugates in multiple sclerosis. *Front. Biosci.* 9, 3137–3144. doi: 10.2741/1466

Karon, B. S., Hoyer, J. D., Stubbs, J. R., and Thomas, D. D. (2009). Changes in Band 3 oligomeric state precede cell membrane phospholipid loss during blood bank storage of red blood cells. *Transfusion* 49, 1435–1442. doi: 10.1111/j.1537-2995.2009.02133.x

Kim, H. K., Song, K. S., Chung, J. H., Lee, K. R., and Lee, S. N. (2004). Platelet microparticles induce angiogenesis *in vitro*. *Br. J. Haematol.* 124, 376–384. doi: 10.1046/j.1365-2141.2003.04773.x

Kim-Shapiro, D. B., Lee, J., and Gladwin, M. T. (2011). Storage lesion: role of red blood cell breakdown. *Transfusion* 51, 844–851. doi: 10.1111/j.1537-2995.2011.03100.x

Koshiar, R. L., Somajo, S., Norström, E., and Dahlbäck, B. (2014). Erythrocyte-derived microparticles supporting activated protein C-mediated regulation of blood coagulation. *PLoS ONE* 9:e104200. doi: 10.1371/journal.pone.0104200

Kostova, E. B., Beuger, B. M., Klei, T. R., Halonen, P., Lieftink, C., Beijersbergen, R., et al. (2015). Identification of signalling cascades involved in red blood cell shrinkage and vesiculation. *Biosci. Rep.* 35, 1–16. doi: 10.1042/BSR20150019

Kriebardis, A. G., Antonelou, M. H., Stamoulis, K. E., Economou-Petersen, E., Margaritis, L. H., and Papassideri, I. S. (2008). RBC-derived vesicles during storage: ultrastructure, protein composition, oxidation, and signaling components. *Transfusion* 48, 1943–1953. doi: 10.1111/j.1537-2995.2008.01794.x

Kulandavelu, S., Balkan, W., and Hare, J. M. (2015). Regulation of oxygen delivery to the body via hypoxic vasodilation. *Proc. Natl. Acad. Sci. U.S.A.* 112, 6254–6255. doi: 10.1073/pnas.1506523112

Lancaster, J. R. Jr. (1994). Simulation of the diffusion and reaction of endogenously produced nitric oxide. *Proc. Natl. Acad. Sci. U.S.A.* 91, 8137–8141. doi: 10.1073/pnas.91.17.8137

Leroyer, A. S., Ebrahimian, T. G., Cochain, C., Récalde, A., Blanc-Brude, O., Mees, B., et al. (2009). Microparticles from ischemic muscle promotes postnatal vasculogenesis. *Circulation* 119, 2808–2817. doi: 10.1161/CIRCULATIONAHA.108.816710

Lipcsey, M., Woinarski, N. C., and Bellomo, R. (2012). Near infrared spectroscopy (NIRS) of the thenar eminence in anesthesia and intensive care. *Ann. Intensive Care* 2:11. doi: 10.1186/2110-5820-2-11

Litvack, M. L., Post, M., and Palaniyar, N. (2011). IgM promotes the clearance of small particles and apoptotic microparticles by macrophages. *PLoS ONE* 6:e17223. doi: 10.1371/journal.pone.0017223

Liu, C., Zhao, W., Christ, G. J., Gladwin, M. T., and Kim-Shapiro, D. B. (2013). Nitric oxide scavenging by red cell microparticles. *Free Radic. Biol. Med.* 65, 1164–1173. doi: 10.1016/j.freeradbiomed.2013.09.002

Mastronardi, M. L., Mostefai, H. A., Soleti, R., Agouni, A., Martínez, M. C., and Andriantsitohaina, R. (2011). Microparticles from apoptotic monocytes enhance nitrosative stress in human endothelial cells. *Fundam. Clin. Pharmacol.* 25, 653–660. doi: 10.1111/j.1472-8206.2010.00898.x

Mause, S. F., and Weber, C. (2010). Microparticles: protagonists of a novel communication network for intercellular information exchange. *Circ. Res.* 107, 1047–1057. doi: 10.1161/CIRCRESAHA.110.226456

McMahon, T. J., Moon, R. E., Luschinger, B. P., Carraway, M. S., Stone, A. E., Stolp, B. W., et al. (2002). Nitric oxide in the human respiratory cycle. *Nat. Med.* 8, 711–717. doi: 10.1038/nm718

Mesri, M., and Altieri, D. C. (1999). Leukocyte microparticles stimulate endothelial cell cytokine release and tissue factor induction in a JNK1 signaling pathway. *J. Biol. Chem.* 274, 23111–23118. doi: 10.1074/jbc.274.33.23111

Morel, O., Jesel, L., Freyssinet, J. M., and Toti, F. (2011). Cellular mechanisms underlying the formation of circulating microparticles. *Arterioscler. Thromb. Vasc. Biol.* 31, 15–26. doi: 10.1161/ATVBAHA.109.200956

Muszynski, J. A., Spinella, P. C., Cholette, J. M., Acker, J. P., Hall, M. W., Juffermans, N. P., et al. (2017). Transfusion-related immunomodulation: review of the literature and implications for pediatric critical illness. *Transfusion* 57, 195–206. doi: 10.1111/trf.13855

Nolan, S., Dixon, R., Norman, K., Hellewell, P., and Ridger, V. (2008). Nitric oxide regulates neutrophil migration through microparticle formation. *Am. J. Pathol.* 172, 265–273. doi: 10.2353/ajpath.2008.070069

Nomura, S., Nakamura, T., Cone, J., Tandon, N. N., and Kambayashi, J. (2000). Cytometric analysis of high shear-induced platelet microparticles and effect of cytokines on microparticle generation. *Cytometry* 40, 173–181. doi: 10.1002/1097-0320(20000701)40:3<173::AID-CYTO1>3.0.CO;2-L

Owens, A. P., and Mackman, N. (2011). Microparticles in hemostasis and thrombosis. *Circ. Res.* 108, 1284–1297. doi: 10.1161/CIRCRESAHA.110.233056

Peterson, D. B., Sander, T., Kaul, S., Wakim, B. T., Halligan, B., Twigger, S., et al. (2008). Comparative proteomic analysis of PAI-1 and TNF-alpha-derived endothelial microparticles. *Proteomics* 8, 2430–2446. doi: 10.1002/pmic.200701029

Piccin, A., Van Schilfgaarde, M., and Smith, O. (2015). The importance of studying red blood cells microparticles. *Blood Transfus.* 13, 172–173. doi: 10.2450/2014.0276-14

Rautou, P. E., Vion, A. C., Amabile, N., Chironi, G., Simon, A., Tedgui, A., et al. (2011). Microparticles, vascular function, and atherothrombosis. *Circ. Res.* 109, 593–606. doi: 10.1161/CIRCRESAHA.110.233163

Relevy, H., Koshkaryev, A., Manny, N., Yedgar, S., and Barshtein, G. (2008). Blood banking-induced alteration of red blood cell flow properties. *Transfusion* 48, 136–146. doi: 10.1111/j.1537-2995.2007.01491.x

Reynolds, J. D., Hess, D. T., and Stamler, J. S. (2011). The transfusion problem: role of aberrant S-nitrosylation. *Transfusion* 51, 852–858. doi: 10.1111/j.1537-2995.2011.03097.x

Roback, J. D. (2011). Vascular effects of the red blood cell storage lesion. *Hematol. Am. Soc. Hematol. Educ. Program* 2011, 475–479. doi: 10.1182/asheducation-2011.1.475

Rubin, O., Canellini, G., Delobel, J., Lion, N., and Tissot, J. D. (2012). Red blood cell microparticles: clinical relevance. *Transfus. Med. Hemother.* 39, 342–347. doi: 10.1159/000342228

Rubin, O., Crettaz, D., Canellini, G., Tissot, J. D., and Lion, N. (2008). Microparticles in stored red blood cells: an approach using flow cytometry and proteomic tools. *Vox Sang.* 95, 288–297. doi: 10.1111/j.1423-0410.2008.01101.x

Rubin, O., Delobel, J., Prudent, M., Lion, N., Kohl, K., Tucker, E. I., et al. (2013). Red blood cell-derived microparticles isolated from blood units initiate and propagate thrombin generation. *Transfusion* 53, 1744–1754. doi: 10.1111/trf.12008

Sadallah, S., Eken, C., and Schifferli, J. A. (2008). Erythrocyte-derived ectosomes have immunosuppressive properties. *J. Leukoc. Biol.* 84, 1316–1325. doi: 10.1189/jlb.0108013

Salzer, U., Hinterdorfer, P., Hunger, U., Borken, C., and Prohaska, R. (2002). Ca(++)-dependent vesicle release from erythrocytes involves stomatin-specific lipid rafts, synexin (annexin VII), and sorcin. *Blood* 99, 2569–2577. doi: 10.1182/blood.V99.7.2569

Sapet, C., Simoncini, S., Loriod, B., Puthier, D., Sampol, J., Nguyen, C., et al. (2006). Thrombin-induced endothelial microparticle generation: identification of a novel pathway involving ROCK-II activation by caspase-2. *Blood* 108, 1868–1876. doi: 10.1182/blood-2006-04-014175

Sinauridze, E. I., Kireev, D. A., Popenko, N. Y., Pichugin, A. V., Panteleev, M. A., Krymskaya, O. V., et al. (2007). Platelet microparticle membranes have 50- to 100-fold higher specific procoagulant activity than activated platelets. *Thromb. Haemost.* 97, 425–434. doi: 10.1160/TH06-06-0313

Singel, D. J., and Stamler, J. S. (2005). Chemical physiology of blood flow regulation by red blood cells: the role of nitric oxide and S-nitrosohemoglobin. *Annu. Rev. Physiol.* 67, 99–145. doi: 10.1146/annurev.physiol.67.060603.090918

Solheim, B. G., Flesland, O., Seghatchian, J., and Brosstad, F. (2004). Clinical implications of red blood cell and platelet storage lesions: an overview. *Transfus. Apher. Sci.* 31, 185–189. doi: 10.1016/j.transci.2004.09.004

Ståhl, A. L., Sartz, L., and Karpman, D. (2011). Complement activation on platelet-leukocyte complexes and microparticles in enterohemorrhagic *Escherichia coli*-induced hemolytic uremic syndrome. *Blood* 117, 5503–5513. doi: 10.1182/blood-2010-09-309161

Stapley, R., Owusu, B. Y., Brandon, A., Cusick, M., Rodriguez, C., Marques, M. B., et al. (2012). Erythrocyte storage increases rates of NO and nitrite scavenging: implications for transfusion-related toxicity. *Biochem. J.* 446, 499–508. doi: 10.1042/BJ20120675

Stewart, A., Urbaniak, S., Turner, M., and Bessos, H. (2005). The application of a new quantitative assay for the monitoring of integrin-associated protein CD47 on red blood cells during storage and comparison with the expression of CD47 and phosphatidylserine with flow cytometry. *Transfusion* 45, 1496–1503. doi: 10.1111/j.1537-2995.2005.00564.x

Takano, K., Asazuma, N., Satoh, K., Yatomi, Y., and Ozaki, Y. (2004). Collagen-induced generation of platelet-derived microparticles in whole blood is dependent on ADP released from red blood cells and calcium ions. *Platelets* 15, 223–229. doi: 10.1080/09537100410001682797

Terrisse, A. D., Puech, N., Allart, S., Gourdy, P., Xuereb, J. M., Payrastre, B., et al. (2010). Internalization of microparticles by endothelial cells promotes platelet/endothelial cell interaction under flow. *J. Thromb. Haemost.* 8, 2810–2819. doi: 10.1111/j.1538-7836.2010.04088.x

Théry, C., Ostrowski, M., and Segura, E. (2009). Membrane vesicles as conveyors of immune responses. *Nat. Rev. Immunol.* 9, 581–593. doi: 10.1038/nri2567

Tissot, J. D., Rubin, O., and Canellini, G. (2010). Analysis and clinical relevance of microparticles from red blood cells. *Curr. Opin. Hematol.* 17, 571–577. doi: 10.1097/MOH.0b013e32833ec217

Tschuor, C., Asmis, L. M., Lenzlinger, P. M., Tanner, M., Härter, L., Keel, M., et al. (2008). *In vitro* norepinephrine significantly activates isolated platelets from healthy volunteers and critically ill patients following severe traumatic brain injury. *Crit. Care* 12:R80. doi: 10.1186/cc6931

van Beers, E. J., Schaap, M. C., Berckmans, R. J., Nieuwland, R., Sturk, A., van Doormaal, F. F., et al. (2009). Circulating erythrocyte-derived microparticles are associated with coagulation activation in sickle cell disease. *Haematologica* 94, 1513–1519. doi: 10.3324/haematol.2009.008938

van den Akker, J., van Weert, A., Afink, G., Bakker, E. N., van der Pol, E., Böing, A. N., et al. (2012). Transglutaminase 2 is secreted from smooth muscle cells by transamidation-dependent microparticle formation. *Amino Acids* 42, 961–973. doi: 10.1007/s00726-011-1010-3

Van Der Meijden, P. E., Van Schilfgaarde, M., Van Oerle, R., Renné, T., ten Cate, H., and Spronk, H. M. (2012). Platelet- and erythrocyte-derived microparticles trigger thrombin generation via factor XIIa. *J. Thromb. Haemost.* 10, 1355–1362. doi: 10.1111/j.1538-7836.2012.04758.x

Vaughn, M. W., Huang, K. T., Kuo, L., and Liao, J. C. (2000). Erythrocytes possess an intrinsic barrier to nitric oxide consumption. *J. Biol. Chem.* 275, 2342–2348. doi: 10.1074/jbc.275.4.2342

Whale, T. A., Wilson, H. L., Tikoo, S. K., Babiuk, L. A., and Griebel, P. J. (2006). Pivotal advance: passively acquired membrane proteins alter the functional capacity of bovine polymorphonuclear cells. *J. Leukoc. Biol.* 80, 481–491. doi: 10.1189/jlb.0206078

Willekens, F. L., Roerdinkholder-Stoelwinder, B., Groenen-Döpp, Y. A., Bos, H. J., Bosman, G. J., van den Bos, A. G., et al. (2003). Hemoglobin loss from erythrocytes *in vivo* results from spleen-facilitated vesiculation. *Blood* 101, 747–751. doi: 10.1182/blood-2002-02-0500

Willekens, F. L., Werre, J. M., Groenen-Döpp, Y. A., Roerdinkholder-Stoelwinder, B., de Pauw, B., and Bosman, G. J. (2008). Erythrocyte vesiculation: a self-protective mechanism? *Br. J. Haematol.* 141, 549–556. doi: 10.1111/j.1365-2141.2008.07055.x

Willekens, F. L., Werre, J. M., Kruijt, J. K., Roerdinkholder-Stoelwinder, B., Groenen-Döpp, Y. A., van den Bos, A. G., et al. (2005). Liver Kupffer

cells rapidly remove red blood cell-derived vesicles from the circulation by scavenger receptors. *Blood* 105, 2141–2145. doi: 10.1182/blood-2004-04-1578

Yang, C., Xiong, W., Qiu, Q., Shao, Z., Hamel, D., Tahiri, H., et al. (2012). Role of receptor-mediated endocytosis in the antiangiogenic effects of human T lymphoblastic cell-derived microparticles. *Am. J. Physiol. Regul. Integr. Comp. Physiol.* 302, R941–R949. doi: 10.1152/ajpregu.00527.2011

Zahra, S., Anderson, J. A., Stirling, D., and Ludlam, C. A. (2011). Microparticles, malignancy and thrombosis. *Br. J. Haematol.* 152, 688–700. doi: 10.1111/j.1365-2141.2010.08452.x

**Conflict of Interest Statement:** The authors declare that the research was conducted in the absence of any commercial or financial relationships that could be construed as a potential conflict of interest.

*Copyright © 2018 Said, Rogers and Doctor. This is an open-access article distributed under the terms of the Creative Commons Attribution License (CC BY). The use, distribution or reproduction in other forums is permitted, provided the original author(s) or licensor are credited and that the original publication in this journal is cited, in accordance with accepted academic practice. No use, distribution or reproduction is permitted which does not comply with these terms.*

frontiers in Physiology

ORIGINAL RESEARCH
published: 19 December 2017
doi: 10.3389/fphys.2017.01082

# Oxidized Mutant Human Hemoglobins S and E Induce Oxidative Stress and Bioenergetic Dysfunction in Human Pulmonary Endothelial Cells

*Sirsendu Jana[1], Fantao Meng[1], Rhoda E. Hirsch[2], Joel M. Friedman[3] and Abdu I. Alayash[1]**

*[1] Laboratory of Biochemistry and Vascular Biology, Center for Biologics Evaluation and Research, Food and Drug Administration, Silver Spring, MD, United States, [2] Hematology Division, Department of Medicine and Department of Anatomy and Structural Biology, Albert Einstein College of Medicine, Bronx, NY, United States, [3] Department of Physiology and Biophysics, Albert Einstein College of Medicine, Bronx, NY, United States*

Cell free hemoglobin (Hb), becomes oxidized in the circulation during hemolytic episodes in sickle cell disease (SCD) or thalassemia and may potentially cause major complications that are damaging to the vascular system. Hemolytic anemias are commonly associated with pulmonary hypertension (PH) and often result from dysfunction of lung endothelial cells. The aim of this study was to determine the effect of different Hbs on cultured human lung endothelial function. Toward this goal, endothelial permeability, oxidative stress response parameters, glycolytic and mitochondrial bioenergetic functions were monitored in cultured human pulmonary arterial endothelial cells (HPAEC) following incubation with human adult Hb (HbA), and Hb isolated from patients with sickle cell Hb (HbS, βV6E) and HbE (βE26K) that commonly co-exist with β-thalassemia. These mutant Hbs are known for their distinct oxidative profiles. HPAEC treated with the ferrous forms of HbE, HbS for 24 h showed higher loss of endothelial monolayer integrity with concomitant rise in reactive oxygen radical production, lipid hydroperoxide formation and higher expressions of oxidative stress response proteins including heme oxygenase-1 (HO-1) accompanied by a rise in uncoupled mitochondrial respiration. Loss of membrane permeability was diminished in part by haptoglobin (Hp, protein scavenger), hemopexin (Hpx, heme scavenger) or ascorbate (reducing agent). To understand the role of Hb oxidation, HPAEC were exposed to ferric or ferryl states of the mutant Hbs. Ferryl forms of all proteins caused a significant damage to the endothelial monolayer integrity at a higher degree than their respective ferric Hbs. Ferryl forms of HbS and HbE also caused a loss of respiratory chain complex activities in isolated endothelial mitochondria and basal oxygen consumption in HPAEC. However, longer incubation with ferryl Hbs produced bioenergetic reprogramming including higher degree of uncoupled respiration and glycolytic rate. The data in this report collectively indicate that higher oxidation forms of HbS and HbE cause endothelial dysfunction through distinct damaging mechanisms involving mitochondrial bioenergetic function.

**Keywords: mutant hemoglobins, hemoglobin S, hemoglobin E, ferryl hemoglobin, pulmonary endothelial cells**

OPEN ACCESS

***Edited by:***
*Joseph M. Rifkind, Johns Hopkins University, United States*

***Reviewed by:***
*Chunyu Niu, Hebei North University, China*
*Osama F. Harraz, University of Vermont, United States*

***Correspondence:**
*Abdu I. Alayash*
*abdu.alayash@fda.hhs.gov*

***Specialty section:***
*This article was submitted to Vascular Physiology, a section of the journal Frontiers in Physiology*

***Received:*** *27 September 2017*
***Accepted:*** *08 December 2017*
***Published:*** *19 December 2017*

***Citation:***
*Jana S, Meng F, Hirsch RE, Friedman JM and Alayash AI (2017) Oxidized Mutant Human Hemoglobins S and E Induce Oxidative Stress and Bioenergetic Dysfunction in Human Pulmonary Endothelial Cells. Front. Physiol. 8:1082. doi: 10.3389/fphys.2017.01082*

## INTRODUCTION

Hb constitutes almost 95% of all the proteins within red blood cells (RBC); it is a tetramer of two α and two β subunits (α2β2), with a heme ($Fe^{+2}$) moiety bound to each subunit. Hemolysis or rupture of RBCs occur in various disease conditions and most importantly in hemoglobinopathies including SCD and β-thalassemia leading to the release of free Hb molecules to the circulation (Buehler et al., 2011; Schaer et al., 2013). The Hb molecule is highly susceptible to heme/iron oxidation but the highly reducing environment within RBCs (due to the presence of antioxidant enzymes like catalase, superoxide dismutase (SOD) and methemoglobin reductase) prevents the oxidation of Hb and maintains it in the functional ferrous form ($HbFe^{2+}$). Cell free Hb in circulation undergoes oxidation to produce its primary oxidized derivative, ferric Hb ($HbFe^{3+}$) that dissociates into α-β dimers. At the tissue level ferric or ferrous Hb can also form highly reactive ferryl species ($HbFe^{4+}$) upon reacting with locally produced hydrogen peroxide ($H_2O_2$) or its own synthesized $H_2O_2$ in a pseudoperoxidase cycle (Alayash, 2014). The cycle consists of three distinct steps: (1) initial oxidation of $HbFe^{2+}$ to $HbFe^{4+}$, (2) autoreduction of the $HbFe^{4+}$ intermediate to $HbFe^{3+}$, and (3) reaction of ferric/metHb with an additional $H_2O_2$ molecule to regenerate the ferryl intermediate/ferryl protein radical ($\cdot HbFe^{4+} = O$) (Alayash, 2004, 2014). This radical may migrate to the oxidation "hotspot" to further damage the protein, including the irreversible oxidation of βCys93 and subsequent dimerization of the protein (Alayash, 2004). Because this surface amino acid is an important endpoint for free radical induced oxidation (Jia et al., 2007; Pimenova et al., 2010) our group has developed βCys93 as a quantitative reporter for $H_2O_2$ induced oxidation (Kassa et al., 2017; Strader and Alayash, 2017). Both ferric and ferryl species are known to release highly toxic heme moieties in the circulation from the parent Hb molecule (Kassa et al., 2016). These oxidized species of Hb and heme may cause vascular complications involving inflammation, vasoconstriction and endothelial dysfunction. Dysfunction of lung endothelial cells leading to pulmonary arterial hypertension (PAH) has increasingly been recognized in severe β-thalassemic or SCD patients and in other hemolytic conditions (Gladwin et al., 2010; Morris and Vichinsky, 2010).

Heme resulting from Hb oxidation has been shown to act as a damage-associated molecular pattern (DAMP) molecule that can activate Toll-like receptor-4 (TLR4) of the innate immune system leading to oxidant production, inflammation and vascular injury (Gladwin et al., 2010; Belcher et al., 2014). Several other mechanisms, e.g., nitric oxide (NO) sequestration by Hb, chronic inflammatory reactions triggered by activation of NF-κB transcription factor and the hypoxia inducible factor (HIF-1α), have all been also proposed to contribute to the endothelial dysfunction mediated by cell free Hb proteins (Manalo et al., 2008). Although endothelial cells are relatively more dependent on glycolysis for their ATP source, growing numbers of experiments have highlighted the importance of mitochondrial bioenergetics and signal-modulatory roles played by mitochondria in the maintenance of endothelial health that ultimately contributes to normal vascular function (Davidson and Duchen, 2007). Because mitochondria are one of the most critical regulators in cell survival, recently various functional mitochondrial bioenergetic parameters have been utilized for the assessment of human bioenergetic health index (BHI) (Chacko et al., 2014). In this context, the effects of cell free Hb on cellular functions, mitochondrial bioenergetics have not been fully explored. We and others have recently shown the potential of Hb molecules particularly in their oxidized forms promoting various degrees of bioenergetic impairment in cultured cells and in platelets (Higdon et al., 2012; Cardenes et al., 2014; Kassa et al., 2015; Chintagari et al., 2016). Using mouse lung epithelial cells (E10), we specifically showed differential toxicity of the oxidized ferric and ferryl species of HbA and HbS affecting some key signaling pathways and bioenergetic functions through oxidative insults to those cells (Kassa et al., 2015; Chintagari et al., 2016).

It is known that plasma levels of Hb in thalassemic patients, due to hemolysis, can increase significantly, and in sickle cell disease it can reach as high as 25 μM in patients experiencing typical sickle cell crises (Schaer et al., 2013). Moreover, as we have recently shown, both HbE and HbS exhibit defective pseudoperoxidase activities resulting in accumulation of higher levels of ferryl Hb in solutions (Kassa et al., 2015; Strader et al., 2016).

Since, several toxicity studies emphasizing the effect of Hb on endothelial function have indicated the possible involvement of oxidative reactions triggering the activation of inflammatory and death pathways we thought it would be interesting to explore the toxicity of different naturally occurring Hb variants with distinct oxidative profiles on pulmonary endothelial cells in the context of PAH. In this investigation, we focused our efforts on the impact of Hb oxidative pathways on endothelial functions and modulation of metabolic responses using different naturally occurring Hb variants with distinct oxidative profiles in the context of PAH. Toward this goal we used human pulmonary artery endothelial cells (HPAEC) and monitored endothelial permeability, oxidative stress response parameters following exposure to either HbA or HbS (βV6E) or HbE (βE26K). Simultaneously, for the first time to the best of our knowledge, we also compared the changes in mitochondrial bioenergetics and glycolytic rate in HPAECs exposed to these different Hbs by measuring the oxygen consumption rate (OCR) and extracellular acidification rates (ECAR), respectively using an extracellular flux analyzer. Further, we showed that the exposure of HPAEC to the ferryl forms of these mutant Hbs resulted in impairments of electron transport chain complex function, specifically complex IV activity in isolated endothelial mitochondria. Therefore, this work establishes a link between the loss of endothelial permeability and bioenergetic impairment conferred by oxidized forms of naturally occurring and mutant cell free Hbs.

## MATERIALS AND METHODS

### Preparation of Various Hemoglobins (HbA, HbE, and HbS)

Blood was obtained from normal and SCD patients attending the National Institutes of Health, Bethesda, Maryland with

informed consent. Hemoglobin E was purified from red blood cells obtained from transgenic mice expressing solely human HbE as described earlier (Chen et al., 2012). Hb (HbS/HbE/HbA) was purified from erythrocyte lysates from all sources by anion DEAE and cation CM chromatography respectively (Manjula and Acharya, 2003). Red blood cells were washed three times with PBS and centrifuged at 500 g for 20 min using a Legend X1R centrifuge (Thermo Scientific). RBCs were lysed with 3-fold volumes of water and mixed gently with a glass rod at room temperature for 30 min. Final salt concentration was adjusted to about 0.9% with NaCl. The lysate was then centrifuged at 12,000 g for 40 mins. The supernatant was filtered with 0.2 μM membranes, and then dialyzed against 50 mM Tris-acetate buffer, pH 8.3, at 4°C.

The lysate was loaded onto a DEAE Sepharose Fast Flow column, which was equilibrated with 6 column volumes of 50 mM Tris-acetate at pH 8.3 (buffer A) using an AKTA FPLC System. Hb was eluted at 4°C with a linear gradient of 25–100% buffer B, 50 mM Tris-acetate at pH 7.0 in 12 column volumes. The column was eluted at a flow rate of 2 ml/min and the effluent was monitored at 540 and 630 nm. Hb was collected, concentrated, and then dialyzed against extensive 10 mM phosphate buffer (buffer C), pH 6.5, at 4°C. The Hb solution was then applied to a CM Sepharose Fast Flow column, which was equilibrated with 6 column volumes of buffer C using an AKTA FPLC system. Hb was eluted (at 4°C) with a linear gradient of 0-100% buffer D, 15 mM phosphate buffer (at pH 8.5) in 12 column volume (2 mL/min) and the effluent was monitored at 540 and 630 nm. Hb was collected, concentrated, dialyzed against PBS, and was stored at −80°C for future use. Purified Hb in PBS solutions was then dialyzed against water for 12 h at 4°C for 3 times. The complete removal of antioxidative enzymes, namely SOD and catalase in the purified Hb solutions was verified as previously reported (Aebi, 1984). The criteria of purity of three proteins were verified by isoelectric focusing and HPLC. Molar concentrations for all Hb solutions in this paper are calculated and based on heme (Meng and Alayash, 2017).

## Preparation of Ferric and Ferryl Hemoglobins

The ferric (met) Hb was generated as previously reported (Meng and Alayash, 2017) by incubating 2 mM ferrous (oxy) Hb with 3 mM potassium ferricyanide in PBS at room temperature for 15 min. Excess ferro- and ferricyanide were removed by passing the reaction solution through a Sephadex G-25 column equilibrated with PBS at 4°C. Ferryl Hb solutions were prepared as previously reported by mixing metHb (1 mM) with $H_2O_2$ (20 mM) in PBS buffer at room temperature for 1 min, and then the excess $H_2O_2$ was rapidly removed by passing the reaction solution through two G25 desalting columns (HitrapTM, 5 mL, GE Healthcare) connected in series (Kassa et al., 2015).

## Endothelial Cell Culture

Cryopreserved human pulmonary artery endothelial cells (HPAEC) were purchased from Life Technologies Corporation (Thermo Fisher Scientific, Waltham, MA) and were cultured in Medium 200 supplemented with Low Serum Growth Supplement (LSGS) containing FBS (Thermo Fisher Scientific, Waltham, MA). Some HPAEC were also cryopreserved per the manufacturer's protocol within passage 4. The cells were used between passages 6–10 after thawing. The media was changed every 48 h. Cells were subcultured after attaining 80% confluency.

## Exposure of HPAEC to Hemoglobins

For all experiments HPAEC were grown to 80–90% confluency in complete media. Before any treatment, cells were serum starved for 6 h in a medium composed of Medium 200 supplemented with all the components of LSGS Kit except FBS (Thermo Fisher Scientific, Waltham, MA). The cells were then exposed to ferrous ($HbFe^{2+}$), ferric ($HbFe^{3+}$) or ferryl ($HbFe^{4+}$) for varying periods of time up to 12 h. Antioxidants, scavengers or other protective agents were added to the media prior to the addition of Hb. In most of the experiments HPAEC were washed three times with either pre-warmed phosphate buffered saline (PBS) or with complete media to remove Hb proteins and other additions otherwise mentioned. Following exposure to specified time periods, cell lysates were prepared for further studies.

## Endothelial Permeability Study

For permeability determinations, HPAEC were grown to confluence on collagen coated PTFE-Transwell membrane inserts (Corning Inc. Corning, NY) placed on a 24-well culture plate forming a two-compartment system. Approximately, $2 \times 10^5$ cells in 0.1 ml of complete medium were seeded onto the membrane insert with pore size of 0.4 μm following a previously published method (Nooteboom et al., 2000). The lower compartment was then supplemented with 0.6 ml of complete media to equilibrate the hydrostatic fluid pressures across the membranes per the manufacturer's protocol. Cells were grown up to 5–6 days until they form a tight confluent monolayer.

To determine the macromolecular passage across the membranes, 0.1 ml of FITC-labeled dextran, 40 KD (200 μg/ml) solution prepared in complete media with or without Hbs and other additives was added onto the membrane insert following complete removal of culture medium. Simultaneously each well in the lower chamber was replenished with 0.6 ml of fresh culture medium. Diffusion of dextran was monitored after varying periods of incubation by measuring the FITC-green fluorescence in the medium in the lower chamber using a Synergy HTX Multi-Mode Reader (Biotek Instruments, Inc., Winooski, VT).

## Immunoblotting and Microscopy

HPAEC were rinsed in phosphate-buffered saline following incubation and lysed in RIPA buffer containing protease inhibitor to prepare whole cell lysate. Cell lysate proteins were separated by electrophoresis using precast 4–20% NuPAGE bis-tris gels (Thermo Fisher Scientific, Waltham, MA) and then transferred to nitrocellulose membranes (BioRad, Hercules, CA). Membranes were blocked in 5% milk-PBS and then processed for Western analysis using specific primary antibodies as described in the figure legends. Mouse monoclonal anti-hemoxygenase-1,

rabbit polyclonal anti-H-ferritin antibodies were purchased from Abcam (Cambridge, MA). Rabbit polyclonal phospho-NF-κB p65, rabbit polyclonal NF-κB p65 were purchased from Cell Signaling Technology (Danvers, MA).

To detect DMPO-nitrone adduct formation in Hb treated HPAEC; cells grown on coverslips were treated with various Hb species for 2 h. Cells were thoroughly washed in PBS and then treated with 1 mM DMPO for 30 min in the culture media. Cells were then fixed in 4% paraformaldehyde after three consecutive wash with PBS. Immunocytochemistry was done as described earlier (Kassa et al., 2015) following incubation with polyclonal primary antibody against DMPO-nitrone adduct, (Cayman Chemical) at 4°C overnight. Alexa Fluor-594 conjugated goat anti-rabbit secondary antibody was used to visualize the cells under EVOS epifluorescence microscope (Thermo Fisher Scientific, Waltham, MA).

## Cellular Oxidative Stress Parameters

Following treatment with various Hb species, endothelial lipid hydroperoxide levels were measured in HPAEC using a commercially available kit (Cayman Chemical Co., Ann Arbor, MI). Mitochondrial superoxide generation in HPAEC was monitored by a Synergy HTX multimode plate reader (Biotek Instruments, Inc., Winooski, VT) at 580 nm by labeling the cells with MitoSOX red dye (5 μM) (Thermo Fisher Scientific, Waltham, MA) for 30 min following incubation with a specific Hb species.

## Mitochondrial Bioenergetic and Glycolytic Flux Measurements

Mitochondrial bioenergetic function and glycolytic flux were simultaneously monitored in HPAEC using the XF24 extracellular flux analyzer (Seahorse Bioscience, Billerica, MA) as described before (Kassa et al., 2016). Briefly, HPAEC were seeded (100,000 cells/well) and cultured for 24 h in 24-well XF-cell culture plate (V7) obtained from Seahorse Bioscience and pre-coated with collagen I (Thermo Fisher Scientific, Waltham, MA). Prior to exposure, media was changed with serum-free media for 6 h. Cells were exposed to various Hb proteins for up to 24 h. Mitochondrial OCR was assessed after washing the Hb containing media with XF-assay media (Seahorse Bioscience, Billerica, MA) supplemented with 10 mM glucose, 5 mM pyruvate, and 2 mM glutamate as per the manufacturer's instructions. The XF-assay media used for measuring the extracellular acidification rate (ECAR) was free of glucose. For some experiments, Hb solutions were directly injected onto cells through the automated injection ports; and OCR/ECAR and were monitored up to 2 h prior to other additions. To obtain OCR profile, a sequential injection of oligomycin (1 μM), carbonyl cyanide-p-trifluoro-methoxyphenylhydrazone (FCCP, 1 μM) and a combination of rotenone and antimycin A (1 μM each) were made following manufacturer recommended protocol (Seahorse Bioscience, Billerica, MA). Similarly, to obtain ECAR profile glucose (10 mM), oligomycin (1 μM) and glycolytic inhibitor 2-deoxyglucose (2-DG, 100 mM) were sequentially added to the wells through automated injections. The values from individual wells were recorded and plotted using XF24 software, version 1.8. Blank wells with Hb variants were also run to eliminate any background OCR. However, Hb species showed no noticeable interference on either OCR or ECAR. Various cellular bioenergetic parameters e.g., basal and maximal respiration were calculated as described earlier (Kassa et al., 2015). Glycolytic parameters e.g., basal glycolysis, glycolytic capacities were calculated following a previously published method (TeSlaa and Teitell, 2014).

## Isolation of Mitochondria

Mitochondrial fractions were isolated from HPAEC cells following the manufacturer's protocol, using the mitochondria isolation kit designed for cultured cells (Pierce Biotechnology, Rockford, IL, USA). The final mitochondrial pellet was resuspended in an isotonic buffer containing 145 mM KCl, 50 mM sucrose, 5 mM NaCl, 1 mM EGTA, 1 mM magnesium chloride, 10 mM phosphate buffer, pH 7.4 and stored at −80°C for further use.

## Mitochondrial Respiratory Chain Complex Activity

Frozen and thawed samples of mitochondria were incubated for 2 h at 37°C in the presence or absence of the Hb proteins in a total volume of 200 μl. Following incubation, mitochondria were thoroughly washed by centrifugation at 4°C with an excess of ice-cold 50 mM phosphate, pH7.4 to ensure complete removal of the residual Hb proteins. Interference of any residual Hb bound to mitochondria was monitored by using appropriate blanks and blank values were subsequently subtracted. An aliquot of the mitochondrial suspension (20 μg of protein) was utilized to measure complex I or complex IV activities. Complex I activity was assayed by using ferricyanide as the electron acceptor (Hatefi, 1978; Khan et al., 2005). The assay was carried out at 30°C in a reaction system containing 0.17 mM NADH, 0.6 mM potassium ferricyanide, 0.1% (v/v) Triton-X 100 in 50 mM phosphate buffer, pH 7.4. The rate of oxidation of NADH was monitored by the decrease in absorbance at 340 nm after the addition of mitochondrial suspension to the sample cuvette (Khan et al., 2005).

Succinate supported reduction of ferricytochrome c to ferrocytochrome c at 550 nm was monitored to measure the activity of mitochondrial complex II–III (succinate–cytochrome c reductase) following the method by Jana et al. (2011). The reaction was initiated by adding the mitochondrial suspension (20 μg) to the sample cuvette. The absorbance change at 550 nm was monitored for a period of 3 min. The assay was repeated with antimycin A (10 μM) and the enzyme activity was calculated by subtracting the antimycin A sensitive rate from overall rate and expressed as μmoles oxidized cytochrome c reduced/min/mg protein (Jana et al., 2011).

The activity of complex IV was assayed following the oxidation of reduced cytochrome c (ferrocytochrome c) at 550 nm in 10 mM phosphate buffer, pH 7.4 at room temperature (Khan et al., 2005). K-ferricyanide (1 mM) was added to oxidize ferrocytochrome c in the blank cuvette and the reaction was initiated in the sample cuvette by the addition of mitochondrial suspension. The activity of the enzyme was calculated from

the first order rate constant and the concentration of reduced cytochrome c in the sample cuvette as published earlier (Khan et al., 2005).

## Statistical Analysis

All values are expressed as mean ± SEM. Values from two treatment groups were compared using non-parametric Mann-Whitney *U*-test (Altman, 1991). Data obtained from bioenergetic experiments using extracellular flux analyzer were compared using paired Student's *t*-test following previously published work (Kassa et al., 2015). A $p$-value of $<0.05$ was considered as statistically significant.

# RESULTS

## Autooxidation Kinetics of Hemoglobin Variants and Heme Release

To illustrate the differences in oxidative profiles of the Hbs included in this study, **Table 1** summarizes previously published autoxidation kinetics of the ferrous as well as heme loss from the ferric forms of HbE and HbS. These autoxidation rates are compared with those derived for human HbA. Also, included in this table are the oxygen affinity parameters of Hbs in solutions under normal experimental conditions. $P_{50}$ values for HbA and HbE are reported in **Table 1** and show little difference as reported earlier (Bunn et al., 1972; Gacon et al., 1974). The initial rate of autoxidation ($k_{auto}$) for HbE is close to that of Human HbA, but as can be seen HbS undergoes a slightly higher rate of oxidation than HbA and HbE respectively. Heme loss from the ferric forms from both mutant Hbs run at much higher rates than that of normal HbA. Both HbE and HbS were shown to have unique pseudoperoxidative pathways that set them apart from normal HbA (Kassa et al., 2015; Strader et al., 2016).

## Hemoglobin Variants Cause Endothelial Oxidative Stress

To explore cellular stress signaling in pulmonary endothelial cells, we first incubated Hb variants at equimolar concentration (100 μM/heme) with cultured HPAECs for up to 12 h and monitored the expression of HO-1 and H-ferritin protein levels in in these cells. HO-1 and H-ferritin both are strong indicators of oxidative stress as a result of heme release and subsequent iron load within the cellular compartment. Exposure to HbA and mutants HbE (βE26K) and HbS (βV6E) caused a robust increase in both HO-1 and H-ferritin expression (**Figure 1A**). In fact, at equimolar concentrations both HbE and HbS treated HPAECs showed significantly higher HO-1 and H-ferritin than the corresponding HbA. To monitor any upstream signaling event, we also probed the immunoblotted proteins from Hb-treated cell lysates for phosphorylated NF-κB p65 subunit. Both HbE and HbS treatment caused higher levels of phosphorylation in NF-κB p65 subunit as seen in **Figure 1A**.

To assess the extent of oxidative toxicity in various Hb exposed HPAEC, we measured lipid hydroperoxide formation following 12 h of incubation. Consistent with our results on HO-1 and H-ferritin expressions, all the Hb proteins caused a significant accumulation of lipid-hydroperoxides in HPAEC membrane lipid extracts. However, compared to HbA, levels of lipid hydroperoxides were substantially higher in both HbE and HbS treated cells (**Figure 1B**).

Our previous studies on the effects of normal human Hb on lung epithelial cells and other cell lines have shown a link between HO-1 expression and mitochondrial functional alteration (Converso et al., 2006; Bindu et al., 2015; Kassa et al., 2015; Chintagari et al., 2016). Since, (1) mitochondria are the most potent intra-cellular source of reactive oxygen species (ROS), and (2) to correlate our results with HO-1 expression, we first monitored mitochondrial superoxide generation as an indicator of electron flow impairment through the mitochondrial respiratory complexes by using the fluorescent MitoSOX-probe. As expected, both HbE and HbS caused significant increase in MitoSOX fluorescence in HPAEC (**Figure 1C**).

Next we used the extracellular flux analyzer (XF Assay) to assess the energy utilization in HPAEC exposed to Hbs by monitoring mitochondrial bioenergetics and glycolytic proton flux in real time. oxygen consumption rate (OCR) and extra-cellular acidification rate (ECAR) in HPAEC were obtained from the XF assays as indicators of mitochondrial respiration and cellular glycolytic activity respectively. Exposure to HbA did not cause any significant changes in either basal OCR or maximal OCR obtained after FCCP injection in the HPAEC (**Figures 2A,B**). However, both HbE and HbS treated cells showed a higher rate of oxygen consumption following FCCP addition, indicating a mild uncoupling effect by those two Hb variants. Although, HbE and HbS treated HPAECs had no difference in the basal OCR (**Figures 2A,B**). We also measured glycolytic rates in HPAEC under the influence of Hb variants under similar experimental conditions. Basal glycolysis and

**TABLE 1 |** Oxygen equilibrium parameters, autooxidation and heme loss kinetics of mutant hemoglobins (HbE and HbS) contrasted with values for normal human hemoglobin.

| Sample | $P_{50}$ | $n_{50}$ | $k_{auto}$ | $K_{auto}$ + Cat | Heme loss | |
|---|---|---|---|---|---|---|
| | mm Hg | | $h^{-1}$ | $h^{-1}$ | $k_1$ ($h^{-1}$) | $k_2$ ($h^{-1}$) |
| HbA | 14.0[a] | 2.6[b] | 0.054 ± 0.002[b] | 0.007 ± 0.003[b] | 11.75[b] | 0.86[b] |
| HbE | 12.4[c] | 2.8[c] | 0.051 ± 0.054[b] | 0.089 ± 0.002[b] | 19.07[b] | 2.12[b] |
| HbS | 35.5[e] | 1.75[e] | 0.177 ± 0.042[d] | 0.073 ± 0.016[d] | 15.5[d] | 1.68[d] |

[a]*Strader et al. (2016),* [b]*Strader et al. (2017),* [c]*May and Huehns (1975),* [d]*Kassa et al. (2015),* [e]*Kassa et al. (2017).*

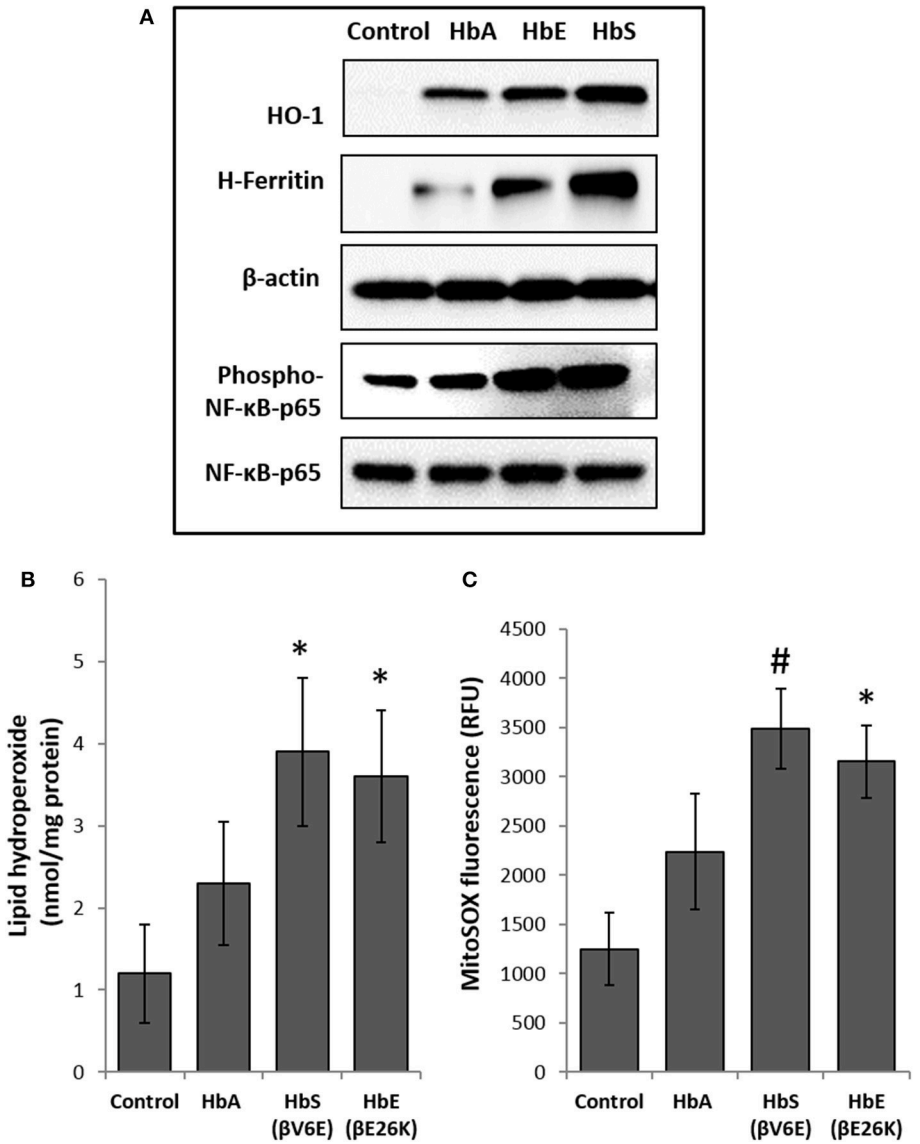


**FIGURE 1 |** Effect of normal and mutant human hemoglobins on human pulmonary arterial endothelial cells (HPAEC). **(A)** HPAEC were exposed to ferrous forms of either HbA, HbS, or HbE at equimolar concentration (100 μM) for 12 h. Cell lysates were immunoblotted with primary antibodies against HO-1, H-ferritin, phospho-NF-κB-p65 and NF-κB-p65 proteins. Equal loading was confirmed by re-probing the blots against β-actin. Blots are representative of three independent experiments. **(B)** Levels of lipid hydroperoxides and **(C)** mitochondrial superoxide radical generation was measured in HPAEC following exposure to different Hb proteins as described in the methods section ($N = 3$). Values from different treatment groups were compared using Mann-Whitney *U*-test. $^{*}P < 0.05$ vs. untreated control, $^{\#}P < 0.001$ vs. untreated control.

glycolytic capacity were mostly unaffected by Hb variants as shown in **Figure 2C**.

## Effect of Hemoglobin Variants on Pulmonary Endothelial Permeability

To explore the effects of Hb oxidation intermediates and toxicity on pulmonary endothelial cells, we first incubated different naturally occurring Hb variants at equimolar concentration (100 μM/heme) with cultured HPAECs grown on a tight monolayer on specially designed Transwell inserts for up to 12 h, and then observed endothelial permeability by measuring the passage of FITC conjugated-dextran (40 KD) through the monolayers (Nooteboom et al., 2000). The ferrous form of normal Hb (HbA) did not cause any significant changes in permeability within the first 6 h, however, we found higher but significant dextran passage after 12 h (**Figure 3A**). In contrast, both ferrous Hbs i.e., HbE (βE26K) and HbS (βV6E) caused significant changes in dextran permeability of HPAEC monolayers within 6 h (**Figure 3A**). The impairment of barrier function by both HbE and HbS was more pronounced after 12 h. However, hemin caused a robust change in dextran-permeability in those cells when used at a low concentration (5 μM) compared to the Hb proteins, which

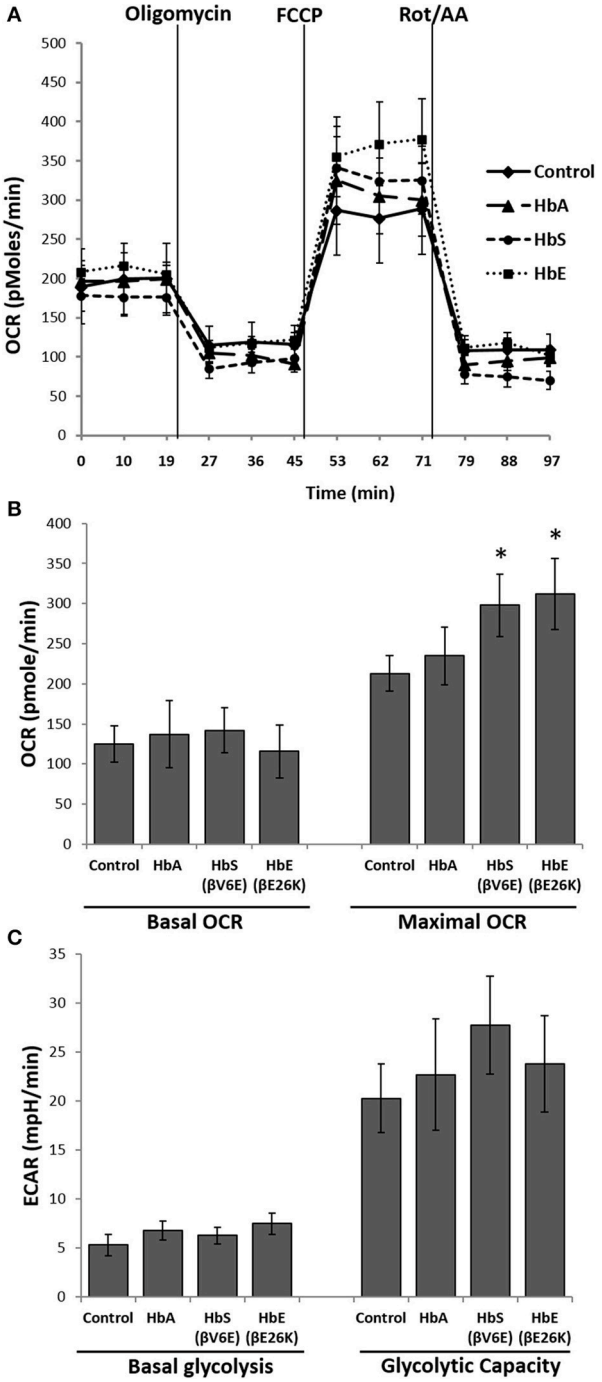


**FIGURE 2 |** Effect of mutant hemoglobins on pulmonary endothelial bioenergetics. HPAEC were exposed to ferrous forms of HbA, HbS, or HbE at equimolar concentration (100 μM) for 12 h. Mitochondrial oxygen consumption rates (OCR) and extracellular acidification rates (ECAR) were measured in real time using XF24 extracellular flux analyzer. **(A)** A representative OCR plot showing the components of mitochondrial bioenergetic parameters. Average OCR values from individual set of experiments repeated four times were plotted to make bioenergetic profile of each Hb treated HPAEC. **(B)** Basal and maximal OCR obtained from HPAEC following exposure to Hb ($N = 4$). **(C)** Basal glycolysis rate and glycolytic capacity were calculated from HPAEC following exposure to Hb ($N = 3$). Differences between two different groups were compared using a paired Student's *t*-test. *$P < 0.05$ vs. control.

suggests that heme released from Hb as result of oxidation of the protein may play a key role in genesis of oxidative stress.

To understand the oxidative mechanism behind the impairment of permeability function by both HbE and HbS, we introduced several scavengers and antioxidants, e.g., haptoglobin (Hp), hemopexin (Hpx), antioxidant ascorbate (Asc), and thiol antioxidant N-acetyl cysteine (NAC) to the medium. Hp, a scavenger of Hb almost completely prevented the loss of barrier functions by either HbE or HbS when added at equimolar concentration (100 μM) (**Figure 3B**). On the other hand, only a partial protection (∼40–50%) was achieved by co-incubation with 100 μM of the heme scavenger Hpx. Further, Asc (100 μM) provided partial but significant protection against HbE or HbS mediated permeability changes in the cultured HPAECs indicative of an underlying oxidative mechanism driving these processes (**Figure 3B**). However, NAC failed to confer any protection against HbS or HbE (**Figure 3B**).

## Effect of Oxidized Hemoglobin Variants on Pulmonary Endothelial Permeability

To explore further the oxidative toxicity on pulmonary endothelial cells we utilized oxidized forms of individual Hb variants, e.g., ferric and ferryl, for the endothelial permeability experiments. Unlike the ferrous forms all the ferric forms of Hb variants could disrupt the endothelial barrier function to a much greater degree (**Figure 4A**). Similarly, when the ferryl forms were used, we noticed greater leakage of dextran molecules through the HPAEC monolayer compared to respective ferric Hb treatments within a short period of incubation (6 h).

To assess the extent of oxidative changes within endothelial cells following treatment with higher oxidation Hb, we first loaded cells with DMPO and then used a polyclonal antibody-based immunofluorescence approach directed against multiple epitopes bearing DMPO-nitrone protein adducts. For this purpose, we selected HbS due to its higher oxidative potential as already observed in our earlier published results (Kassa et al., 2015). HPAEC were exposed to either reduced or oxidized (ferric or ferryl) of HbS for 2 h followed by labeling with DMPO. **Figure 4B** shows a gradual appearance of DMPO-bound protein adducts (labeled as red) with higher oxidation states of Hb reaching maximum with the ferryl state.

## Ferryl Hemoglobin Causes Bioenergetic Impairment in HPAEC

Rapid impairment of endothelial permeability by oxidized species of Hb prompted us to investigate metabolic changes in HPAEC following exposure to ferryl species of the different Hb variants. We carried out bioenergetic measurements in the presence of different ferryl Hb species to assess their impact on endothelial respiration. To achieve this, first we added freshly prepared ferryl Hb variants directly on the loading cartridge of XF-analyzer. Upon injection of ferryl HbA directly into the cell culture media, an insignificant decrease in basal respiration was observed over control cells treated with vehicle. However, a gradual but consistent decrease in basal respiration occurred in HPAECs following addition of equimolar ferryl HbS

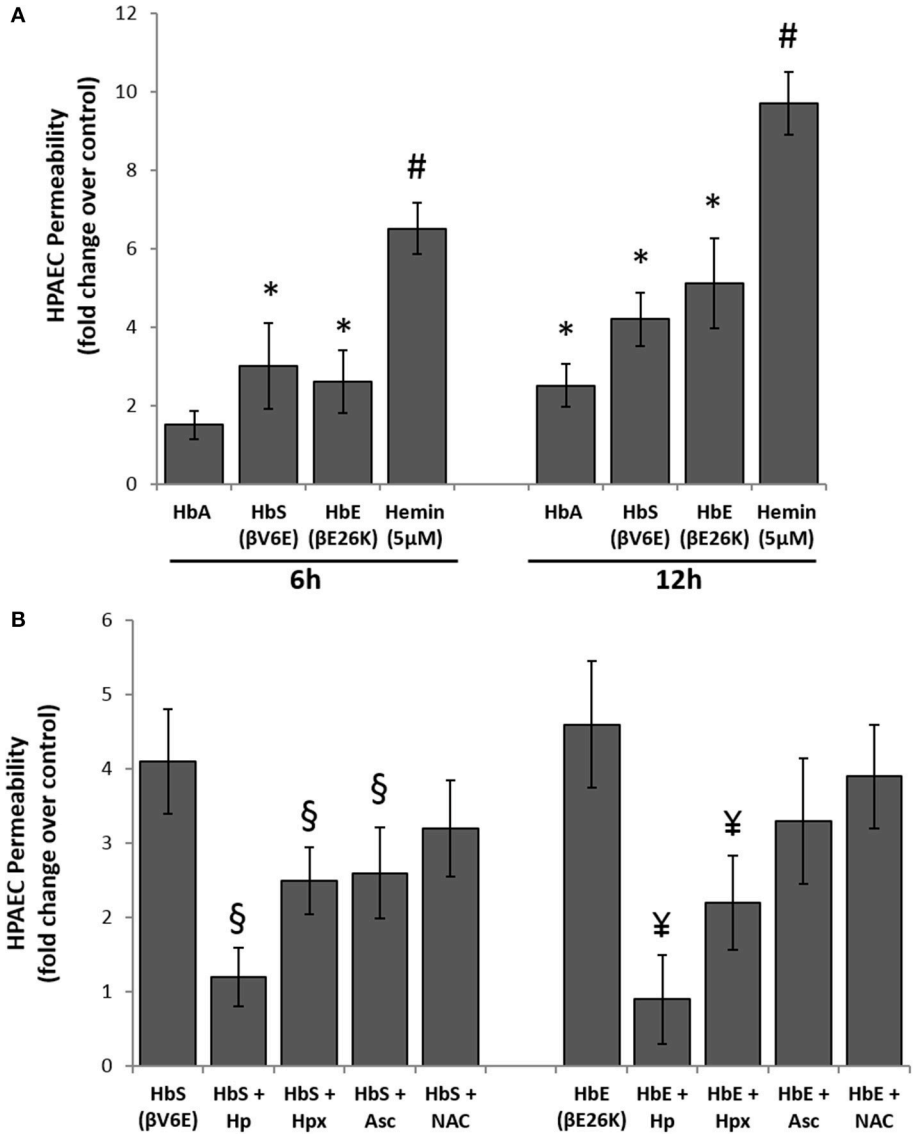


**FIGURE 3 |** Cell free hemoglobin variants causes disruption of pulmonary endothelial monolayer. **(A)** HPAEC monolayer were grown on Transwell inserts and then exposed to ferrous forms of HbA or HbS or HbE at equimolar concentration (100 μM) either for 6 or 12 h in the presence of FITC conjugated dextran, 40 KD. Endothelial monolayer integrity was assessed by measuring the passage of FITC-dextran molecule through monolayer. FITC-green fluorescence was monitored by fluorescence plate reader as described in the methods section. Values are presented as average fold difference over control ($N = 3$). **(B)** In a similar set of experiments HPAEC were exposed to either HbS (100 μM) or HbE (100 μM) with or without equimolar of either Hp, Hpx or Asc or NAC for 12 h in the presence of FITC conjugated dextran. Endothelial monolayer integrity was assessed as mentioned before by measuring FITC-dextran fluorescence in the bottom chamber ($N = 3$). Values obtained from different treatment groups were compared using Mann-Whitney *U*-test. $^{*}P < 0.05$ vs. untreated control, $^{\#}P < 0.001$ vs. untreated control, $^{\S}P < 0.05$ vs. HbS, $^{¥}P < 0.05$ vs. HbE.

into the media (**Figures 5A,B**). A similar bioenergetic pattern was also obtained following a direct addition of ferryl HbE (**Figures 5A,B**). However, ferryl Hbs did not cause any noticeable changes in respiration in the uncoupled state following FCCP treatment (**Figure 5A**). We also studied changes in glycolytic rate by monitoring ECAR in HPAEC within short incubation time of 2 h. Ferryl Hbs in a similar experimental set up did not cause any changes in glycolysis within 2 h incubation as evidenced by unaltered ECAR in HPAEC (data not shown).

To understand the role of ferryl Hb in causing endothelial bioenergetic impairment various scavengers and antioxidants were added to the medium with either ferryl HbS or HbE. Haptoglobin (Hp) almost completely abolished ferryl Hb mediated loss of basal respiration whereas heme scavenger Hpx showed only partial protection (**Figure 5C**). Ascorbate was also able to partially prevent ferryl HbS or ferryl HbE mediated fall of basal OCR. However, ferryl HbA induced loss of basal OCR was not prevented by NAC (**Figure 5C**). Unlike the general-purpose

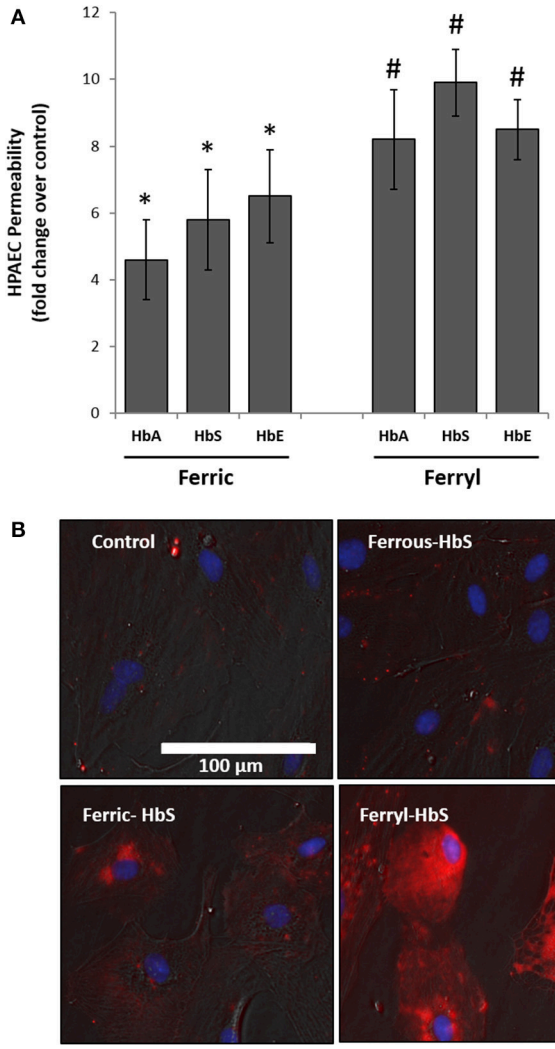


**FIGURE 4 |** Oxidized hemoglobin variants cause rapid disruption of pulmonary endothelial monolayer and generate oxidative stress. **(A)** HPAEC monolayer were grown on Transwell inserts and then exposed to either ferric or ferryl forms of HbA, HbS, or HbE at equimolar concentration (100 μM) for 6 h in the presence of FITC conjugated dextran, 40 KD. Endothelial monolayer integrity was assessed by measuring the passage of FITC-dextran as mentioned in the methods section. Values are presented as average fold difference over control ($N = 3$). Differences between groups were compared using Mann-Whitney $U$-test. $^{*}P < 0.05$ and $^{\#}P < 0.001$ vs. respective controls. **(B)** HPAEC were exposed to ferryl Hb proteins at equimolar concentration (100 μM) for 6 h. Following incubation cells were washed thoroughly and probed with spin trapping agent DMPO. DMPO-nitrone adducts formed with oxidatively modified proteins within HPAEC were visualized by immunofluorescence method using anti-DMPO-nitrone antibody. Images shown are from one representative set of experiments repeated three times.

antioxidant NAC, Asc is known to specifically reduce both ferric and ferryl forms of Hb to their lower redox state (Dunne et al., 2006).

In the presence of substrates electrons shuttle through mitochondrial respiratory complexes by oxidative phosphorylation and represent the basal OCR. Complex V is a point of proton reentry from the mitochondrial intermembrane space to the matrix, and inhibition of this activity could decrease basal OCR and alter membrane potential ($\Delta\psi$) and ROS generation (Cardenes et al., 2014). To test whether ferryl Hb induces any impairment in the mitochondrial respiratory chain components we first isolated mitochondrial fraction from cultured HPAEC and then exposed mitochondrial fractions to highly reactive ferryl Hb variants for 2 h at 37°C. Following incubation with Hb, individual electron transport chain complexes were assayed using specific substrates and inhibitors as described earlier in the methods. **Figure 5D** shows that oxidation of reduced NADH by mitochondrial complex I was marginally compromised by ferryl HbS and ferryl HbE but not by ferryl HbA. In contrast, antimycin A sensitive reduction of cytochrome c by complex II–III (succinate–cytochrome c reductase) was not affected by any of the ferryl Hb variants (**Figure 5E**). However, cyanide sensitive oxidation of ferro-cytochrome c by complex IV (cytochrome c oxidase) was markedly impacted by all the ferryl Hb variants following an incubation of 2 h (**Figure 5F**).

## Ferryl Hemoglobin Induces Metabolic Reprogramming

Next we examined the bioenergetic profile of pulmonary endothelium following a prolonged incubation (12 h) with various ferryl species of Hb. Surprisingly, all the ferryl Hb proteins caused a significant increase in FCCP-induced uncoupled respiration (maximal respiration) in HPAEC over untreated control (**Figure 6A**). In a similar experimental setup, ferryl species of both mutant Hb proteins i.e., ferryl HbS and ferryl HbE significantly impacted glycolytic rates (ECAR) within HPAECs following addition of glucose (**Figures 6B,C**). **Figure 6B** highlights the fall in glycolytic reserve in HPAECs induced by ferryl HbS and ferryl HbE.

# DISCUSSION

The primary aim of this study was to evaluate the unique oxidative pathways of HbS and HbE and their impact on human pulmonary arterial endothelial cells (HPAEC) and to compare that to normal HbA. Cell free plasma Hb, and its prosthetic heme, are known to disrupt endothelial function, drive oxidative and inflammatory stress. Heme, the byproduct of Hb oxidation is also recognized as a damage-associated molecular pattern (DAMP) molecule (Gladwin et al., 2010). Studies in a sickle cell mice model showed unequivocally that heme released from plasma oxidized Hb binds to the toll-like receptor-4 (TLR-4) on macrophages that can activate the innate immune system (Belcher et al., 2014). Persistent intravascular hemolysis in SCD leads, over decades, to chronic vasculopathy, with some ∼10% of patients developing pulmonary hypertension (Potoka and Gladwin, 2015). Adult and children with HbE-β thalassemia are also reported to present vascular complications as a result of the oxidative stress experienced by these patients (Kukongviriyapan et al., 2008). In both diseases, RBC-derived microparticles were shown to promote vascular complications as they carry both highly oxidized Hb and considerable quantities of free heme to

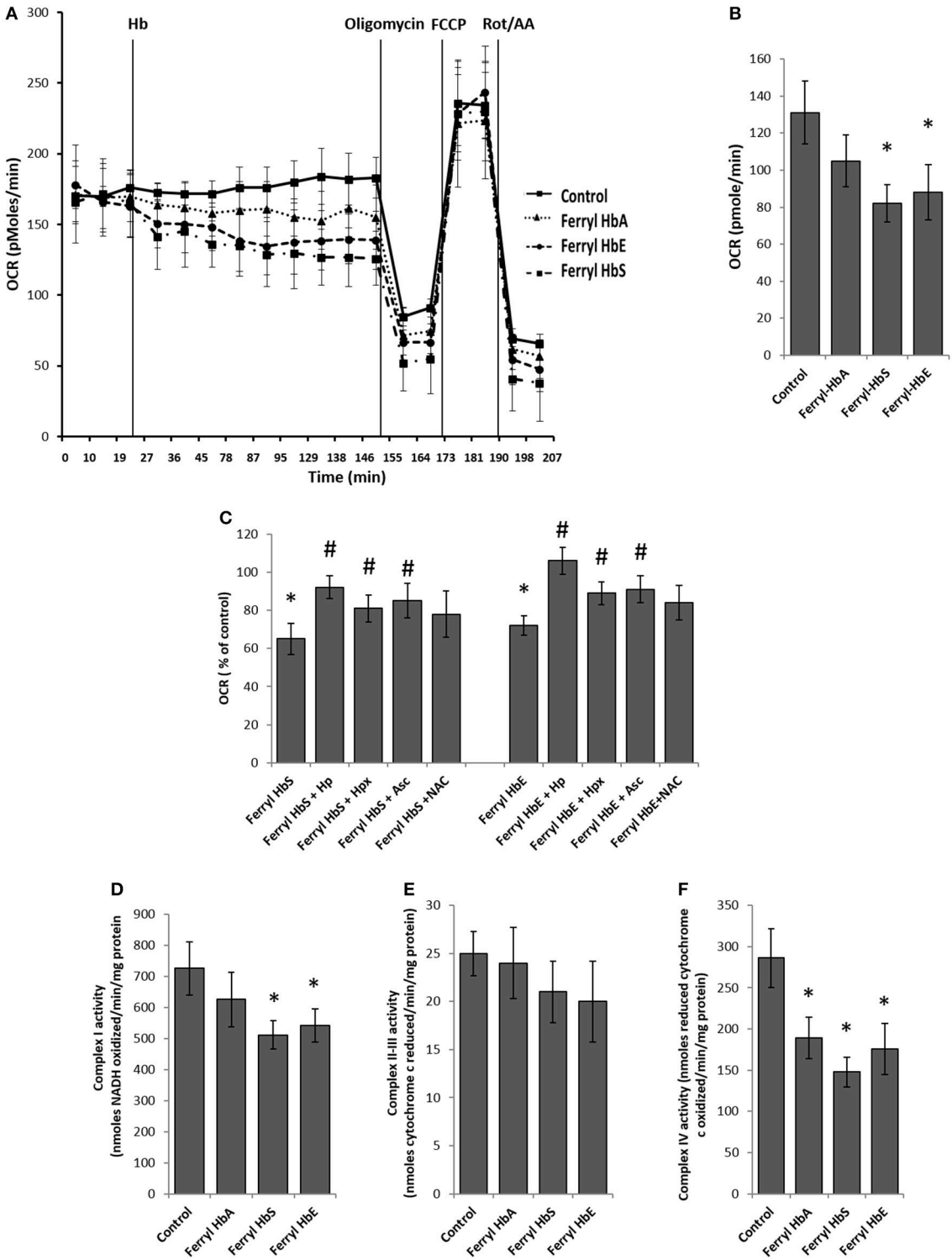


**FIGURE 5 |** Oxidized ferryl hemoglobins disrupt pulmonary endothelial bioenergetics. **(A)** HPAEC were grown on 24 well XF-plates. Mitochondrial oxygen consumption rates (OCR) were measured for 2 h using XF24 extracellular flux analyzer with direct infusion of ferryl forms of HbA, HbS, or HbE at equimolar concentration (100 μM) ($N = 3$). **(B)** Basal OCR following 2 h incubation with ferryl Hbs ($N = 3$). **(C)** Average basal OCR values from a similar set of experiments in which HPAEC were exposed to either ferryl HbS (100 μM) or ferryl HbE (100 μM) for 2 h co-incubated with or without equimolar Hp or Hpx or Asc or NAC ($N = 3$). Statistical significance between means was calculated by paired Student's *t*-test. $^{*}P < 0.05$ vs. untreated control, $^{\#}P < 0.05$ vs. respective ferryl Hb. **(D)** Complex I activity **(E)** complex II-III and **(F)** complex IV activities were measured in isolated mitochondrial fractions incubated with different ferryl Hb proteins for 2 h at 37°C ($N = 4$). Differences between individual treated groups and respective untreated controls were compared using Mann-Whitney *U*-test. $^{*}P < 0.05$ vs. controls.

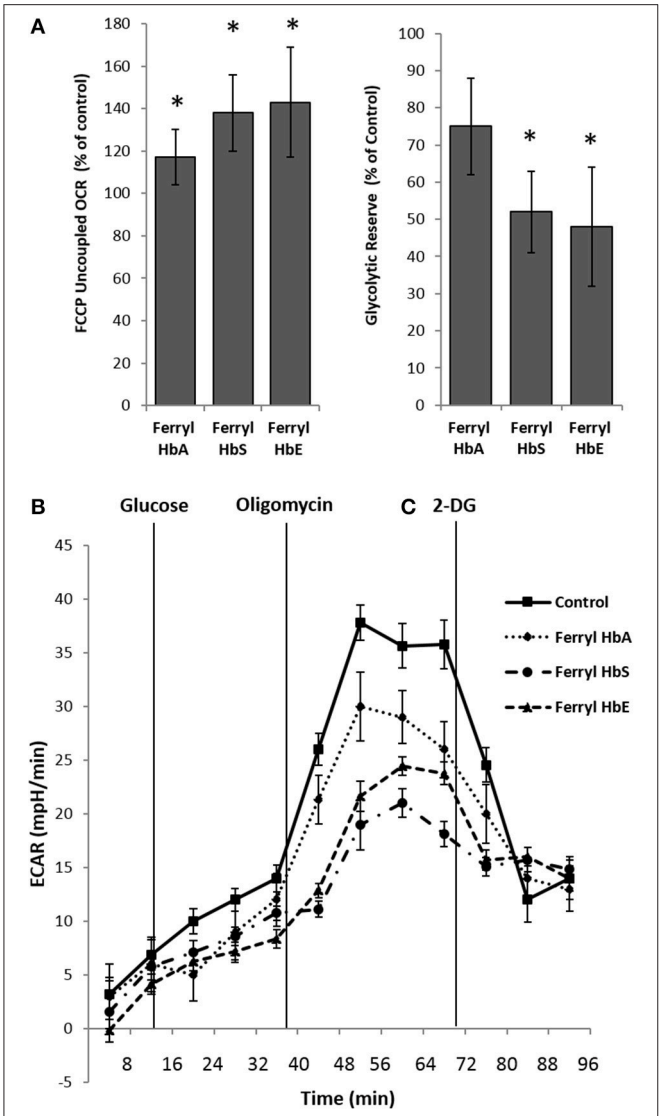


**FIGURE 6 |** Oxidized hemoglobins cause bioenergetic reprogramming in pulmonary endothelial cells. HPAEC were exposed to ferryl forms of HbA or HbS or HbE at equimolar concentration (100 μM) for 12 h. Mitochondrial oxygen consumption rates (OCR) and extracellular acidification rates (ECAR) were measured in real time using XF24 extracellular flux analyzer. **(A)** Average maximal OCR values expressed as % of control in HPAEC obtained after uncoupling of mitochondria following FCCP treatment ($N = 3$). **(B)** Average glycolytic reserve capacity expressed as (%) of control in HPAEC ($N = 4$) **(C)** representative ECAR plots of ferryl Hb treated HPAEC from an individual set of experiment repeated three times. Statistical significance between means was calculated by paired Student's *t*-test. *$P < 0.05$ vs. untreated control.

the vascular system (Chaichompoo et al., 2012; Camus et al., 2015)

Naturally occurring human Hb variants (resulting mostly from single point mutations) alter Hb structure and biochemical properties with physiological effects ranging from insignificant to severe (Thom et al., 2013). These Hb mutants, which are subjected to evolutionary pressures, can provide unique model systems to address the question as to why some Hb variants are more oxidatively stable while others succumb to oxidative stress and develop into a full circulatory disorder (Thom et al., 2013). An example of an oxidatively stable Hb mutant we reported recently is Hb Providence, in which two mutations exist in these patient RBCs: βLys82-Asp (βK82D) and at βLys82-Asn (βK82N) positions; both of these fractions resist $H_2O_2$ induced oxidation by internalizing radicals through the ferric/ferryl pseudoperoxidase cycle (Abraham et al., 2011). Conversely, single amino acid variant Hbs linked to severe pathology, including sickle cell Hb (HbS) (β6 Glu-Val) and HbE (β26 Glu-Lys), are less oxidatively stable than HbA. We have recently found that both ferryl forms and associated radicals of HbS and HbE persist longer *in vitro* than their HbA counterpart by targeting and specifically oxidizing βCys93 which subsequently leads to heme loss from the proteins (Kassa et al., 2015; Strader et al., 2016).

To assess the role of HbS and HbE in promoting endothelial functional impairment, we monitored endothelial permeability, intracellular oxidative stress response parameters and some key metabolic changes involving mitochondrial bioenergetics and changes in glycolytic flux. Vascular endothelium very selectively allows passage of blood or plasma components into the adjacent tissues by acting as a dynamic barrier. However, vascular endothelial integrity is highly susceptible to damage by various stress conditions including production of inflammatory mediators (Nooteboom et al., 2000). The passage of FITC-conjugated 10KD dextran molecules through HPAEC monolayers grown on Transwell inserts used in our investigation clearly demonstrated the impairment of membrane integrity by HbS and HbE, but not by HbA, during a prolonged incubation with a concomitant rise in intracellular oxidative stress response in HPAEC. This phenomenon may be attributed to the previously documented higher rates of autoxidation, oxidative instability and heme release from the two mutant Hb proteins compared to common HbA (**Table 1**). Higher rates of autoxidation of mutant Hbs coupled with the formation of more persistent and damaging ferryl species under oxidative stress conditions can target other biological molecules (Kassa et al., 2015). We have recently shown that ferric Hb loses heme at rates substantially higher than that of ferryl Hb (Kassa et al., 2016). This was also supported by a higher expression of heme oxygenase-1 (HO-1) when ferric Hb was added to cultured lung alveolar epithelial cells (E10). The mitochondrial dysfunction reported here may therefore be attributed to a combination of accelerated heme loss from the ferric form and protein radical formation associated with the ferryl Hb. This is consistent with a recent study in which it was shown that ferric (metHb) causes oxidative damage to myelin basic protein (MBP) and myelin lipids, partly by transferring its heme moiety to protein and lipid, but mostly as an intact protein possibly via formation of a ferryl radical (Bamm et al., 2017). Our finding of high levels of DMPO-bound protein radicals within ferryl Hb treated HPAECs supports this possibility. Interestingly, we also noticed a high degree of HPAEC membrane leakage mediated by the oxidized Hb molecules; this finding is consistent with a recent observation where a greater loss of endothelial monolayer integrity was evident under ferryl Hb exposure (Lisk et al., 2013). The resulting endothelial damage was largely

attributed to the MyD88 mediated mechanism involving NF-κB and HIF-1α activation. Our results further show that mutant Hb proteins, e.g., HbS and HbE, due to their distinct oxidative profile can elicit a more profound oxidative stress response than common HbA in human endothelial cells through upregulation of HO-1, ferritin and activation of NF-κB. Findings from another previous work showing differential reactivity of these mutant Hbs causing lipid peroxidation also strongly supports our results (Chiu et al., 1996). These events can be attributed to their heme releasing capability in addition to their high redox potential (Bonaventura et al., 2002; Roche et al., 2011).

Studies on endothelial energy metabolism have shown the dominance of glycolysis over mitochondrial ATP production, although endothelial mitochondria are considered critical for the maintenance of functional integrity of these special vascular cells (Davidson and Duchen, 2007; Groschner et al., 2012). Endothelial mitochondria can integrate several cell death and survival pathways through transition pore opening, intracellular calcium signaling and redox signaling (Davidson and Duchen, 2007). Growing evidence supports the notion that endothelial mitochondria may actually act as a sensor for oxygen and for the vasodilatory response of endothelial nitric oxide and thus can play a "reconnaissance" role through relaying information to adjacent cardiac myocytes or smooth muscle cells (Davidson and Duchen, 2007). Our present study is undoubtedly the first to observe bioenergetic changes in human endothelial cells mediated by the Hb variants. Since, endothelial cells are more dependent on glycolytic ATP production, we also for the first time monitored changes in glycolytic rates under the influence of Hb exposure. Despite some early signs of leakage in endothelial monolayers, neither of the Hb variants in reduced states showed any imbalance in basal respiration or glycolysis in HPAECs. However, an augmentation of uncoupled respiration by both HbS and HbE associated with more mitochondrial oxygen radical production and lipid peroxidation supports a mechanism linked to higher rates of oxidation and greater heme release by the two proteins. Carbon monoxide is one of the major byproduct of heme catabolism by HO-1 and is known to cause inhibition of glycolysis and uncoupling of mitochondrial respiration by opening mitochondria specific ion-channels in endothelium (Kaczara et al., 2015, 2016).

Our results clearly show that direct interactions of oxidized Hbs with vascular endothelium can cause severe impairment of selective electron transport chain complexes especially cytochrome c oxidase. This explains the ferryl Hb mediated loss of mitochondrial function in intact endothelial cells during a short co-incubation. In contrast, all the ferryl Hbs also augmented uncoupled respiration quite significantly after a longer incubation. We have previously shown that HO-1 is strongly expressed by both ferric and ferryl Hbs (Chintagari et al., 2016; Kassa et al., 2016). Therefore, a boost in maximal respiration following uncoupling by FCCP can be easily correlated with our finding that Hb proteins promote high expression of stress response proteins in varying degree depending on their oxidative profile and possibly be considered as an outcome of HO-1 mediated CO production. A concomitant loss of glycolytic reserve in HPAEC by ferryl Hbs after a long incubation also indicates a metabolic reprogramming in the endothelium probably due to an exhaustive loss of glycolytic capacity in HPAEC. Similar observations have been seen in some cancer cells where a prolonged uncoupled state of mitochondrial respiration resulted in metabolic exhaustion and loss of glycolysis (Wegiel et al., 2013).

In summary, we show for the first time a comparative toxicity of different mutant Hbs on a pulmonary endothelial model based on their distinct oxidative profile; and also propose a mechanism that explains Hb-induced metabolic and functional alteration. Our results elucidating the mechanism of extracellular Hb-induced oxidative damage to the mitochondrial respiratory chain will contribute to better understanding of some of the underlying pathophysiology of pulmonary arterial hypertension caused by cell free Hbs; and, in addition, lend new insight into potential antioxidative therapeutic interventions in hemolytic diseases.

## AUTHOR CONTRIBUTIONS

Conception and design: SJ and AA. Experiments: SJ and FM. Data Analysis: SJ and FM. Drafting manuscript: SJ, RH, JF, and AA.

## ACKNOWLEDGMENTS

This work was supported by National Institutes of Health NHLBI Grant P01-HL110900 (AA and JF) and, in part, by The Albert Einstein College of Medicine Global Health Center Microgrant (RH and JF).

## REFERENCES

Abraham, B., Hicks, W., Jia, Y., Baek, J. H., Miller, J. L., and Alayash, A. I. (2011). Isolated Hb Providence beta82Asn and beta82Asp fractions are more stable than native HbA(0) under oxidative stress conditions. *Biochemistry* 50, 9752–9766. doi: 10.1021/bi200876e

Aebi, H. (1984). Catalase *in vitro*. *Meth. Enzymol.* 105, 121–126. doi: 10.1016/S0076-6879(84)05016-3

Alayash, A. I. (2004). Oxygen therapeutics: can we tame haemoglobin? *Nat. Rev. Drug Discov.* 3, 152–159. doi: 10.1038/nrd1307

Alayash, A. I. (2014). Blood substitutes: why haven't we been more successful? *Trends Biotechnol.* 32, 177–185. doi: 10.1016/j.tibtech.2014.02.006

Altman, D. (1991). *Practical Statistics for Medical Research*. London: Chapman and Hall.

Bamm, V. V., Henein, M. E. L., Sproul, S. L. J., Lanthier, D. K., and Harauz, G. (2017). Potential role of ferric hemoglobin in MS pathogenesis: effects of oxidative stress and extracellular methemoglobin or its degradation products on myelin components. *Free Radic. Biol. Med.* 112, 494–503. doi: 10.1016/j.freeradbiomed.2017.08.022

Belcher, J. D., Chen, C., Nguyen, J., Milbauer, L., Abdulla, F., Alayash, A. I., et al. (2014). Heme triggers TLR4 signaling leading to endothelial cell activation and vaso-occlusion in murine sickle cell disease. *Blood* 123, 377–390. doi: 10.1182/blood-2013-04-495887

Bindu, S., Pal, C., Dey, S., Goyal, M., Alam, A., Iqbal, M. S., et al. (2015). Translocation of heme oxygenase-1 to mitochondria is a novel

cytoprotective mechanism against non-steroidal anti-inflammatory drug-induced mitochondrial oxidative stress, apoptosis, and gastric mucosal injury. *J. Biol. Chem.* 290, 13667–13668. doi: 10.1074/jbc.A111.279893

Bonaventura, C., Taboy, C. H., Low, P. S., Stevens, R. D., Lafon, C., and Crumbliss, A. L. (2002). Heme redox properties of S-nitrosated hemoglobin A0 and hemoglobin S: implications for interactions of nitric oxide with normal and sickle red blood cells. *J. Biol. Chem.* 277, 14557–14563. doi: 10.1074/jbc.M107658200

Buehler, P. W., Karnaukhova, E., Gelderman, M. P., and Alayash, A. I. (2011). Blood aging, safety, and transfusion: capturing the radical menace. *Antioxid. Redox Signal.* 14, 1713–1728. doi: 10.1089/ars.2010.3447

Bunn, H. F., Meriwether, W. D., Balcerzak, S. P., and Rucknagel, D. L. (1972). Oxygen equilibrium of hemoglobin E. *J. Clin. Invest.* 51, 2984–2987. doi: 10.1172/JCI107125

Camus, S. M., De Moraes, J. A., Bonnin, P., Abbyad, P., Le Jeune, S., Lionnet, F., et al. (2015). Circulating cell membrane microparticles transfer heme to endothelial cells and trigger vasoocclusions in sickle cell disease. *Blood* 125, 3805–3814. doi: 10.1182/blood-2014-07-589283

Cardenes, N., Corey, C., Geary, L., Jain, S., Zharikov, S., Barge, S., et al. (2014). Platelet bioenergetic screen in sickle cell patients reveals mitochondrial complex V inhibition, which contributes to platelet activation. *Blood* 123, 2864–2872. doi: 10.1182/blood-2013-09-529420

Chacko, B. K., Kramer, P. A., Ravi, S., Benavides, G. A., Mitchell, T., Dranka, B. P., et al. (2014). The Bioenergetic Health Index: a new concept in mitochondrial translational research. *Clin. Sci.* 127, 367–373. doi: 10.1042/CS20140101

Chaichompoo, P., Kumya, P., Khowawisetsut, L., Chiangjong, W., Chaiyarit, S., Pongsakul, N., et al. (2012). Characterizations and proteome analysis of platelet-free plasma-derived microparticles in beta-thalassemia/hemoglobin E patients. *J. Proteom.* 76, 239–250. doi: 10.1016/j.jprot.2012.06.004

Chen, Q., Fabry, M. E., Rybicki, A. C., Suzuka, S. M., Balazs, T. C., Etzion, Z., et al. (2012). A transgenic mouse model expressing exclusively human hemoglobin E: indications of a mild oxidative stress. *Blood Cells Mol. Dis.* 48, 91–101. doi: 10.1016/j.bcmd.2011.12.002

Chintagari, N. R., Jana, S., and Alayash, A. I. (2016). Oxidized ferric and ferryl forms of hemoglobin trigger mitochondrial dysfunction and injury in Alveolar Type I Cells. *Am. J. Respir. Cell Mol. Biol.* 55, 288–298. doi: 10.1165/rcmb.2015-0197OC

Chiu, D. T., van den Berg, J., Kuypers, F. A., Hung, I.-J., Wei, J.-S., and Liu, T.-Z. (1996). Correlation of membrane lipid peroxidation with oxidation of hemoglobin variants: possibly related to the rates of hemin release. *Free Radic. Biol. Med.* 21, 89–95. doi: 10.1016/0891-5849(96)00035-4

Converso, D. P., Taillé, C., Carreras, M. C., Jaitovich, A., Poderoso, J. J., and Boczkowski, J. (2006). HO-1 is located in liver mitochondria and modulates mitochondrial heme content and metabolism. *FASEB J.* 20, 1236–1238. doi: 10.1096/fj.05-4204fje

Davidson, S. M., and Duchen, M. R. (2007). Endothelial mitochondria: contributing to vascular function and disease. *Circ. Res.* 100, 1128–1141. doi: 10.1161/01.RES.0000261970.18328.1d

Dunne, J., Caron, A., Menu, P., Alayash, A. I., Buehler, P. W., Wilson, M. T., et al. (2006). Ascorbate removes key precursors to oxidative damage by cell-free haemoglobin *in vitro* and *in vivo*. *Biochem. J.* 399, 513–524. doi: 10.1042/BJ20060341

Gacon, G., Wajcman, H., Labie, D., and Najman, A. (1974). Hemoglobin E: its oxygen affinity in relation with the ionic environment. *FEBS Lett.* 41, 147–150. doi: 10.1016/0014-5793(74)80975-0

Gladwin, M. T., Barst, R. J., Castro, O. L., Gordeuk, V. R., Hillery, C. A., Kato, G. J., et al. (2010). Pulmonary hypertension and NO in sickle cell. *Blood* 116, 852–854. doi: 10.1182/blood-2010-04-282095

Groschner, L. N., Waldeck-Weiermair, M., Malli, R., and Graier, W. F. (2012). Endothelial mitochondria–less respiration, more integration. *Pflug. Arch.* 464, 63–76. doi: 10.1007/s00424-012-1085-z

Hatefi, Y. (1978). Preparation and properties of NADH: ubiquinone oxidoreductase (complexI), EC 1.6.5.3. *Meth. Enzymol.* 53, 11–14. doi: 10.1016/S0076-6879(78)53006-1

Higdon, A. N., Benavides, G. A., Chacko, B. K., Ouyang, X., Johnson, M. S., Landar, A., et al. (2012). Hemin causes mitochondrial dysfunction in endothelial cells through promoting lipid peroxidation: the protective role of autophagy. *Am. J. Physiol. Heart Circ. Physiol.* 302, H1394–H1409. doi: 10.1152/ajpheart.00584.2011

Jana, S., Sinha, M., Chanda, D., Roy, T., Banerjee, K., Munshi, S., et al. (2011). Mitochondrial dysfunction mediated by quinone oxidation products of dopamine: implications in dopamine cytotoxicity and pathogenesis of Parkinson's disease. *Biochim. Biophys. Acta* 1812, 663–673. doi: 10.1016/j.bbadis.2011.02.013

Jia, Y., Buehler, P. W., Boykins, R. A., Venable, R. M., and Alayash, A. I. (2007). Structural basis of peroxide-mediated changes in human hemoglobin: a novel oxidative pathway. *J. Biol. Chem.* 282, 4894–4907. doi: 10.1074/jbc.M609955200

Kaczara, P., Motterlini, R., Kus, K., Zakrzewska, A., Abramov, A. Y., and Chlopicki, S. (2016). Carbon monoxide shifts energetic metabolism from glycolysis to oxidative phosphorylation in endothelial cells. *FEBS Lett.* 590, 3469–3480. doi: 10.1002/1873-3468.12434

Kaczara, P., Motterlini, R., Rosen, G. M., Augustynek, B., Bednarczyk, P., Szewczyk, A., et al. (2015). Carbon monoxide released by CORM-401 uncouples mitochondrial respiration and inhibits glycolysis in endothelial cells: a role for mitoBKCa channels. *Biochim. Biophys. Acta* 1847, 1297–1309. doi: 10.1016/j.bbabio.2015.07.004

Kassa, T., Strader M. B., Nakagawa, A., Zapol, W. M., and Alayash, A. I. (2017). Targeting betaCys93 in hemoglobin S with an antisickling agent possessing dual allosteric and antioxidant effects. *Metallomics* 9, 1260–1270. doi: 10.1039/C7MT00104E

Kassa, T., Jana, S., Meng, F., and Alayash, A. I. (2016). Differential heme release from various hemoglobin redox states and the upregulation of cellular heme oxygenase-1. *FEBS Open Bio* 6, 876–884. doi: 10.1002/2211-5463.12103

Kassa, T., Jana, S., Strader, M. B., Meng, F., Jia, Y., Wilson, M. T., et al. (2015). Sickle Cell Hemoglobin in the Ferryl State Promotes betaCys-93 Oxidation and Mitochondrial Dysfunction in Epithelial Lung Cells (E10). *J. Biol. Chem.* 290, 27939–27958. doi: 10.1074/jbc.M115.651257

Khan, F. H., Sen, T., Maiti, A. K., Jana, S., Chatterjee, U., and Chakrabarti, S. (2005). Inhibition of rat brain mitochondrial electron transport chain activity by dopamine oxidation products during extended *in vitro* incubation: implications for Parkinson's disease. *Biochim. Biophys. Acta* 1741, 65–74. doi: 10.1016/j.bbadis.2005.03.013

Kukongviriyapan, V., Somparn, N., Senggunprai, L., Prawan, A., Kukongviriyapan, U., and Jetsrisuparb, A. (2008). Endothelial dysfunction and oxidant status in pediatric patients with hemoglobin E-beta thalassemia. *Pediatr. Cardiol.* 29, 130–135. doi: 10.1007/s00246-007-9107-x

Lisk, C., Kominsky, D., Ehrentraut, S., Bonaventura, J., Nuss, R., Hassell, K., et al. (2013). Hemoglobin-induced endothelial cell permeability is controlled, in part, via a myeloid differentiation primary response gene-88-dependent signaling mechanism. *Am. J. Respir. Cell Mol. Biol.* 49, 619–626. doi: 10.1165/rcmb.2012-0440OC

Manalo, D. J., Buehler, P. W., Baek, J. H., Butt, O., D'Agnillo, F., and Alayash, A. I. (2008). Acellular haemoglobin attenuates hypoxia-inducible factor-1alpha (HIF-1alpha) and its target genes in haemodiluted rats. *Biochem. J.* 414, 461–469. doi: 10.1042/BJ20080313

Manjula, B. N., and Acharya, S. A. (2003). Purification and molecular analysis of hemoglobin by high-performance liquid chromatography. *Methods Mol. Med.* 82, 31–47. doi: 10.1385/1-59259-373-9:031

May, A., and Huehns, E. R. (1975). The oxygen affinity of haemoglobin E. *Br. J. Haematol.* 30, 177–184. doi: 10.1111/j.1365-2141.1975.tb00532.x

Meng, F., and Alayash, A. I. (2017). Determination of extinction coefficients of human hemoglobin in various redox states. *Anal. Biochem.* 521, 11–19. doi: 10.1016/j.ab.2017.01.002

Morris, C. R., and Vichinsky, E. P. (2010). Pulmonary hypertension in thalassemia. *Ann. N.Y. Acad. Sci.* 1202, 205–213. doi: 10.1111/j.1749-6632.2010.05580.x

Nooteboom, A., Hendriks, T., Ottehöller, I., and van der Linden, C. J. (2000). Permeability characteristics of human endothelial monolayers seeded on different extracellular matrix proteins. *Mediat. Inflamm.* 9, 235–241. doi: 10.1080/09629350020025755

Pimenova, T., Pereira, C. P., Gehrig, P., Buehler, P. W., Schaer, D. J., and Zenobi, R. (2010). Quantitative mass spectrometry defines an oxidative hotspot in hemoglobin that is specifically protected by haptoglobin. *J. Proteome Res.* 9, 4061–4070. doi: 10.1021/pr100252e

Potoka, K. P., and Gladwin, M. T. (2015). Vasculopathy and pulmonary hypertension in sickle cell disease. *Am. J. Physiol. Lung Cell. Mol. Physiol.* 308, L314–324. doi: 10.1152/ajplung.00252.2014

Roche, C. J., Malashkevich, V., Balazs, T. C., Dantsker, D., Chen, Q., Moreira, J., et al. (2011). Structural and functional studies indicating altered redox properties of hemoglobin E: implications for production of bioactive nitric oxide. *J. Biol. Chem.* 286, 23452–23466. doi: 10.1074/jbc.M110.183186

Schaer, D. J., Buehler, P. W., Alayash, A. I., Belcher, J. D., and Vercellotti, G. M. (2013). Hemolysis and free hemoglobin revisited: exploring hemoglobin and hemin scavengers as a novel class of therapeutic proteins. *Blood* 121, 1276–1284. doi: 10.1182/blood-2012-11-451229

Strader, M. B., and Alayash, A. I. (2017). Exploring oxidative reactions in hemoglobin variants using mass spectrometry: lessons for engineering oxidatively stable oxygen therapeutics. *Antioxid. Redox Signal.* 26, 777–793. doi: 10.1089/ars.2016.6805

Strader, M. B., Bangle, R., Parker Siburt, C. J., Varnado, C. L., Soman, J., Benitez Cardenas, A. S., et al. (2017). Engineering oxidative stability in human hemoglobin based on the Hb providence (betaK82D) mutation and genetic crosslinking. *Biochem. J.* 474, 4171–4192. doi: 10.1042/BCJ20170491

Strader, M. B., Kassa, T., Meng, F., Wood, F. B., Hirsch, R. E., Friedman, J. M., et al. (2016). Oxidative instability of hemoglobin E (β26 Glu–>Lys) is increased in the presence of free α subunits and reversed by α-hemoglobin stabilizing protein (AHSP): relevance to HbE/β-thalassemia. *Redox Biol.* 8, 363–374. doi: 10.1016/j.redox.2016.03.004

TeSlaa, T., and Teitell, M. A. (2014). Techniques to monitor glycolysis. *Meth. Enzymol.* 542, 91–114. doi: 10.1016/B978-0-12-416618-9.00005-4

Thom, C. S., Dickson, C. F., Gell, D. A., and Weiss, M. J. (2013). Hemoglobin variants: biochemical properties and clinical correlates. *Cold Spring Harb. Perspect. Med.* 3:a011858. doi: 10.1101/cshperspect.a011858

Wegiel, B., Gallo, D., Csizmadia, E., Harris, C., Belcher, J., Vercellotti, G. M., et al. (2013). Carbon monoxide expedites metabolic exhaustion to inhibit tumor growth. *Cancer Res.* 73, 7009–7021. doi: 10.1158/0008-5472.CAN-13-1075

**Conflict of Interest Statement:** The authors declare that the research was conducted in the absence of any commercial or financial relationships that could be construed as a potential conflict of interest.

*Copyright © 2017 Jana, Meng, Hirsch, Friedman and Alayash. This is an open-access article distributed under the terms of the Creative Commons Attribution License (CC BY). The use, distribution or reproduction in other forums is permitted, provided the original author(s) or licensor are credited and that the original publication in this journal is cited, in accordance with accepted academic practice. No use, distribution or reproduction is permitted which does not comply with these terms.*

frontiers in Physiology

ORIGINAL RESEARCH
published: 13 December 2017
doi: 10.3389/fphys.2017.01053

# Nitrite-Mediated Hypoxic Vasodilation Predicted from Mathematical Modeling and Quantified from *in Vivo* Studies in Rat Mesentery

*Donald G. Buerk*, Yien Liu, Kelly A. Zaccheo, Kenneth A. Barbee and Dov Jaron*

*School of Biomedical Engineering, Science and Health Systems, Drexel University, Philadelphia, PA, United States*

Nitric oxide (NO) generated from nitrite through nitrite reductase activity in red blood cells has been proposed to play a major role in hypoxic vasodilation. However, we have previously predicted from mathematical modeling that much more NO can be derived from tissue nitrite reductase activity than from red blood cell nitrite reductase activity. Evidence in the literature suggests that tissue nitrite reductase activity is associated with xanthine oxidoreductase (XOR) and/or aldehyde oxidoreductase (AOR). We investigated the role of XOR and AOR in nitrite-mediated vasodilation from computer simulations and from *in vivo* exteriorized rat mesentery experiments. Vasodilation responses to nitrite in the superfusion medium bathing the mesentery equilibrated with 5% $O_2$ (normoxia) or zero $O_2$ (hypoxia) at either normal or acidic pH were quantified. Experiments were also conducted following intraperitoneal (IP) injection of nitrite before and after inhibiting XOR with allopurinol or inhibiting AOR with raloxifene. Computer simulations for NO and $O_2$ transport using reaction parameters reported in the literature were also conducted to predict nitrite-dependent NO production from XOR and AOR activity as a function of nitrite concentration, $PO_2$ and pH. Experimentally, the largest arteriolar responses were found with nitrite >10 mM in the superfusate, but no statistically significant differences were found with hypoxic and acidic conditions in the superfusate. Nitrite-mediated vasodilation with IP nitrite injections was reduced or abolished after inhibiting XOR with allopurinol ($p < 0.001$). Responses to IP nitrite before and after inhibiting AOR with raloxifene were not as consistent. Our mathematical model predicts that under certain conditions, XOR and AOR nitrite reductase activity in tissue can significantly elevate smooth muscle cell NO and can serve as a compensatory pathway when endothelial NO production is limited by hypoxic conditions. Our theoretical and experimental results provide further evidence for a role of tissue nitrite reductases to contribute additional NO to compensate for reduced NO production by endothelial nitric oxide synthase during hypoxia. Our mathematical model demonstrates that under extreme hypoxic conditions with acidic pH, endogenous nitrite levels alone can be sufficient for a functionally significant increase in NO bioavailability. However, these conditions are difficult to achieve experimentally.

**Keywords: aldehyde oxidoreductase, allopurinol, hypoxic vasodilation, nitrite reductases, nitric oxide, raloxifene, xanthine oxidoreductase**

OPEN ACCESS

***Edited by:***
*Joseph M. Rifkind, Johns Hopkins University, United States*

***Reviewed by:***
*Charles Dionisio Eggleton, University of Maryland, Baltimore County, United States*
*Rolando Juan Jose Ramirez, University of Akron, United States*

****Correspondence:***
*Donald G. Buerk*
*donald.gene.buerk@drexel.edu*

***Specialty section:***
*This article was submitted to Vascular Physiology, a section of the journal Frontiers in Physiology*

***Received:*** *27 September 2017*
***Accepted:*** *01 December 2017*
***Published:*** *13 December 2017*

***Citation:***
*Buerk DG, Liu Y, Zaccheo KA, Barbee KA and Jaron D (2017) Nitrite-Mediated Hypoxic Vasodilation Predicted from Mathematical Modeling and Quantified from in Vivo Studies in Rat Mesentery. Front. Physiol. 8:1053. doi: 10.3389/fphys.2017.01053*

## INTRODUCTION

The primary source of the nitrite anion ($NO_2^-$) in mammalian systems is from the oxidation of nitric oxide (NO) produced by the L-arginine/NO enzymatic pathway in vascular endothelium by the $O_2$-dependent endothelial isoform of NO synthase (eNOS). Although physiological effects of nitrite on the cardiovascular system have been known since 1880 (Reichert and Mitchell, 1880), the consensus view had been that nitrite is an inert byproduct of NO production. This viewpoint has changed radically in the past few decades with the emergence of abundant evidence that nitrite serves as a reversible storage reservoir for NO, which can restore NO bioavailability under certain physiological conditions. However, the mechanisms for recovering NO from nitrite are incompletely understood since the biochemical formation of NO metabolic byproducts and regulation of NO bioavailability is complex (Kim-Shapiro and Gladwin, 2014; Blood, 2017; Helms et al., 2017). Furthermore, the accurate measurement of nitrite and related nitrogen species in blood and tissue is technically difficult (MacArthur et al., 2007).

Infusion of sodium nitrite ($NaNO_2$) into the bloodstream has been shown to cause vasodilation in humans, presumably due to conversion of nitrite to NO (Cosby et al., 2003; Dejam et al., 2007; Pluta et al., 2011). Evidence that inorganic nitrite anion therapy may have therapeutic effects for numerous pathological conditions, especially for treating cardiovascular disease, has been reviewed (Kevil et al., 2011; Omar et al., 2016; Blood, 2017), along with substantial experimental evidence for a protective effect from ischemia-reperfusion injury (e.g., see Table 1 in Blood, 2017). Pluta et al. (2011) report that 48 h of continuous IV infusion of $NaNO_2$ is well tolerated in humans, with a maximal tolerable dose of 267 μg/kg/hr. Three of the 12 subjects in this clinical study showed some toxicity at doses of 445.7 μg/kg/hr with a significant decrease in mean arterial blood pressure by more than 15 mmHg in two subjects, and in one subject the methemoglobin level exceeded 5%. Earlier studies using much higher doses of nitrite reported incidences of severe hypotension and lethal methemoglobinemia (Weiss et al., 1937; Wilkins et al., 1937), which curtailed further interest in therapeutic applications for decades. Despite these observed negative effects, nitrite is an approved therapeutic antidote for cyanide and hydrogen sulfide poisoning (Lloyd, 1957; Smith and Gosselin, 1979). More recently, interest in using nitrite for therapeutic purposes has been resurrected. A search of clinicaltrials.gov using nitrite as a keyword presently lists 48 clinical trials that include nitrite as the study drug. Many more dietary studies evaluating the effect of oral nitrate supplements are also listed.

NO generated from nitrite through the deoxyhemoglobin nitrite reductase pathway in red blood cells (RBCs) is proposed to play a major role in hypoxic vasodilation (Gladwin, 2008; Gladwin et al., 2009). However, our previous mathematical model (Buerk et al., 2011a) for coupled NO and $O_2$ transport around an arteriole predicted that only negligible amounts of NO could reach smooth muscle cells (SMC) in the vascular wall due to very strong scavenging of NO by hemoglobin (Hb) in RBCs. Azizi et al. (2005) used the analogy that the RBC is a "black hole" for NO—it can get in but can't get out. Our previous mathematical model predicted that substantially more NO could be derived from nitrite reductase activity in tissue compared with the deoxyhemoglobin nitrite reductase pathway (Buerk et al., 2011a). Our model prediction for the minor contribution of NO from the deoxyhemoglobin nitrite reductase pathway is consistent with a mathematical model by another group (Chen et al., 2008), which predicted that only picomolar levels of NO could be delivered to vascular SMC. Buerk et al. (2011b) has reviewed other mathematical modeling predictions and relevant experimental data in the literature with respect to several signaling pathways in the microcirculation that involve NO. In general, we found that mathematical predictions for NO values are often lower than reported from experimental measurements, and that very few models developed by other investigators include both the $O_2$-dependance of NO production from eNOS and the inhibitory effect of NO on $O_2$ consumption in tissue (coupled NO and $O_2$ transport), which we always include in our models.

More recently, we developed an alternative deoxyhemoglobin nitrite reductase model to investigate whether dinitrogen trioxide ($N_2O_3$) can act as a stable intermediate to preserve NO (Liu Y. et al., 2016). The model is based on the assumption that $N_2O_3$ does not react in the bloodstream (Basu et al., 2007; Hopmann et al., 2011) and will only release NO after it homolyzes in tissue (Butler and Ridd, 2004). Our alterative model predicts that NO is rapidly released from RBC-generated $N_2O_3$ after it leaves the bloodstream, primarily in the endothelium, with a resulting increase in SMC NO in the vascular wall (Liu Y. et al., 2016). Furthermore, this reaction is enhanced at low blood $PO_2$ and increases with acidic pH.

We did not include generation of NO by tissue nitrite reductase activity in our recent model (Liu Y. et al., 2016), since we were examining a theoretical mechanism that could spare NO generated in RBCs from strong scavenging by Hb. However, tissue nitrite reductase activity is hypothesized to be a significant source of NO, especially during hypoxia. Both *in vitro* and *in vivo* studies demonstrate that NO generation from nitrite in tissue is associated with the molybdoenzymes xanthine oxidoreductase (XOR) and aldehyde oxidoreductase (AOR) (Li et al., 2008; Webb et al., 2008; Golwala et al., 2009). For the present report, we conducted experiments to test the hypothesis that tissue nitrite reductases increase NO bioavailability and modulate vascular tone of arterioles (20–80 μm diameter range) in the rat mesentery microvasculature under varying $PO_2$ and pH conditions. We also modified our previous mathematical models (Buerk et al., 2011a; Liu Y. et al., 2016) using available reaction kinetic parameters in the literature for the tissue nitrite reductases XOR and AOR (Maia and Moura, 2011; Maia et al., 2015) to predict NO changes in arteriolar SMC as a function of nitrite concentration, $PO_2$ and pH.

## METHODS

### Animals and Animal Care

All animals received humane care according to the criteria outlined in the Guide for the Care and Use of Laboratory Animals prepared by the National Academy of Sciences and published by the National Institutes of Health. All animal protocols were

approved by the Institutional Animal Care and Use Committee at Drexel University. Every effort was made to minimize animal pain and suffering. Male Sprague-Dawley rats (250–300 g, aged 8 weeks) were kept one or two per cage in a temperature-controlled room at 28°C (thermoneutrality for rats) under a 12-h light/12-h dark cycle. All male subjects were used to avoid confounding effects of estrogen on eNOS.

## *In Vivo* Microcirculation Studies

Exteriorized rat mesentery experiments were conducted under isoflurane anesthesia to measure perivascular NO with recessed microelectrodes, arteriolar diameter (D) from video imaging (Neild, 1989) (DiamTrak software purchased from Dr. T.O. Neild, Flinders Univ., Adelaide, Australia), tissue perfusion (relative volumetric RBC flow in capillaries; Bonner et al., 1981) by laser Doppler (LDF, Transonic model BLF22, Ithaca, NY), and small artery (∼270 micron diameter) blood flow with an ultrasonic probe (Transonic model 420, Ithaca, NY). All physiological signals were sampled at 10 Hz with 12-bit accuracy using a computer-controlled data acquisition system. The DiamTrak output was filtered to remove occasional out of range artifacts using Excel, and smoothed with a running average filter. Arteriolar vasodilation was quantified in response to $NaNO_2$ in the superfusion medium (Krebs-ringer bicarbonate buffer) bathing the mesentery equilibrated with either 5% or 10% $O_2$ and 5% $CO_2$ (normoxic solution) or zero $O_2$ (95% $N_2$) and 5% $CO_2$ (hypoxic solution) at normal (pH = 7.4) or acidic pH (range 6.5–6.7) and maintained at 37°C. Typically, paired measurements were made for each arteriole, alternating $NaNO_2$ exposures between normoxic or hypoxic solutions. The concentration of $NaNO_2$ in the superfusate was varied up to 25 mM, exposing the preparation to $NaNO_2$ for only short periods of time (typically 3 min duration).

In addition, some superfusion experiments were conducted to quantify arteriolar responses before and after inhibiting XOR with the pyrazolopyrimidine-based inhibitor allopurinol (3.4–6 mg/kg IP). Allopurinol dissolved in normal saline was delivered by a single intraperitoneal (IP) injection through a tube inserted into the abdominal cavity. In addition to $NaNO_2$ exposures in the superfusion solution, *in vivo* experiments were also conducted with measurements taken after an acute IP injection of 3–6 mg/kg mg of $NaNO_2$ while the mesentery was superfused with hypoxic solution at pH = 7.4. After recording control measurements for 3–4 arterioles, XOR oxidase was inhibited with allopurinol and measurements were repeated for the same arterioles. We also conducted studies using either superfusion or an acute IP injection of $NaNO_2$ before and after inhibiting AOR with the estrogen receptor antagonist raloxifene (2.9–10 mg/kg IP).

## Mathematical Model

NO and $O_2$ transport were simulated in a microcirculatory arteriole and surrounding tissue model and solved for steady state conditions using finite element method numerical methods (COMSOL v5.3, Burlington, MA). Coupled non-linear partial differential equations for mass transport were written in cylindrical coordinates including the sum of reactions ($R_i$) for all chemical species ($C_i = O_2$, NO, $NO_2^-$)

$$\nabla \cdot (D_i \nabla C_i) - v \nabla C_i \pm \sum R_i = 0 \tag{1}$$

as detailed in our previous modeling efforts (Buerk et al., 2003, 2011a; Lamkin-Kennard et al., 2004a,b; Chen et al., 2006; Chen X. et al., 2007; Liu et al., 2017), where $D_i$ is the diffusion coefficient for each species, and $v$ is the fluid velocity profile in the lumen (assumed to be parabolic).

The model has five concentric cylindrical layers: (i) RBC core, radius = 13 μm, (ii) RBC-free plasma layer, 13 < r < 14 μm, width = 1 μm, (iii) endothelium, 14 < r < 15 μm, width = 1 μm, (iv) vascular wall smooth muscle cell (SMC) layer, 15 < r < 25 μm, width = 10 μm, and (v) perivascular tissue, 25 < r < 130 μm, width = 105 μm. Each layer was assumed to have homogenous properties with uniformly distributed reactions. Both convective and diffusive mass transports are included in the vessel lumen, with only diffusive transport in tissue. NO is produced in the endothelium by eNOS, and generated from nitrite in tissue by either XOR or AOR, or in blood from conversion of nitrite to $N_2O_3$ (Basu et al., 2007) by Hb in RBCs, with subsequent homolysis to release NO. The model includes $O_2$-dependent NO production by eNOS, and inhibition of $O_2$ consumption by NO, using parameters as described for one of our previous models (Chen et al., 2006). The present model now includes reactions for nitrite in blood or tissue, which are compared to a baseline simulation without XOR or AOR.

We modeled the reaction of nitrite with Hb in the bloodstream as

$$\frac{d[NO]}{dt} = k_N \left[Hb\right] [NO_2^-] \tag{2}$$

where the bimolecular rate constant $k_N$ was characterized as a function of blood $PO_2$ using a modified Monod-Wyman-Changeux (MWC) model of allostery for the oxyhemoglobin equilibrium curve, as described by Rong et al. (2013a,b). We further modified this model (Liu Y. et al., 2016), adding the production of $N_2O_3$ from NO and nitrite-methemoglobin, catalyzed by the nitrous anhydrase activity of deoxyHb. The $O_2$-dependent function for $k_N$ in Equation (2) and the complete model parameters used in our simulation are summarized in Liu Y. et al. (2016).

In tissue, the reaction rate for nitrite reduction by XOR was characterized using a Michaelis-Menten equation with competitive inhibition by $O_2$:

$$v_{Nitrite\ Reduction} = \frac{k_{cat}\left[NO_2^-\right][XOR]}{K_m NO_2^- \left(1 + \frac{[O_2]}{K_m O_2}\right) + [NO_2^-]} \tag{3}$$

where the reaction parameters $k_{cat}$, $K_m NO_2^-$, and $K_m O_2$ vary depending on tissue pH values (Li et al., 2008; Maia and Moura, 2011; Maia et al., 2015; see **Table 1**). XOR was assumed to be uniformly distributed in the endothelium, SMC layer, and perivascular tissue (Ray and Shah, 2005). Blood $PO_2$ was varied between normoxic conditions (90 Torr) down to hypoxic

**TABLE 1 |** Physical parameters and rate constants used in the simulation.

| Parameter | Value(s) | References |
|---|---|---|
| Tissue nitrite | 0–300 μM | |
| Nitrite diffusion coefficient | 410 $\mu m^2/s$ | Pinotti et al., 2002; Li et al., 2008; Kim-Shapiro and Gladwin, 2014 |
| XOR concentration | | |
| Heart | 0.03 μM | |
| Liver | 0.3 μM | |
| Reaction parameters at pH = 7.4 | | Maia and Moura, 2011; Maia et al., 2015 |
| $k_{cat}$ | 0.545 $s^{-1}$ | |
| $K_m NO_2^-$ | 1918 μM | |
| $K_m O_2$ | 24.3 μM | |
| at pH = 6.3 | | |
| $k_{cat}$ | 0.581 $s^{-1}$ | |
| $K_m NO_2^-$ | 251 μM | |
| $K_m O_2$ | 24.3 μM | |

levels (10 Torr). Simulations were performed with tissue XOR concentrations ranging between 0.03 and 0.3 μM as found in heart and liver, respectively, where tissue nitrite reduction has been shown to produce a functionally significant elevation in NO (Kim-Shapiro and Gladwin, 2014). The nitrite anion was assumed to be uniformly distributed in all perivascular tissue regions. Simulations were performed with nitrite varying between physiological (<2 μM; Li et al., 2008; van Faassen et al., 2010) to elevated (300 μM) concentrations. Simulations were solved at steady state with a relative tolerance for convergence of 0.001 and an absolute tolerance of 0.0001. The initial mesh for the computational domain consisted of 19,976 domain elements and 1,678 boundary elements. Meshing was calibrated such that further refinement did not change predicted NO concentration more than 0.01 nM.

## RESULTS

The presence of $NaNO_2$ in the superfusion medium usually elicited vasodilatory responses for the arterioles observed in this study, consistent with an increase in NO bioavailability. In a few cases, no change or minor vasoconstriction was observed. However, we were not able to accurately measure perivascular tissue NO due to electrochemical interference with nitrite at the high concentrations used in our superfusion experiments. Quantitative results using superfusion protocols are summarized in **Figure 1** for several individual experiments using short exposures to $NaNO_2$ (typically 3 min duration, indicated by striped bars). There were approximately 30 s transport delays from the time when the superfusion pump was switched between reservoirs at $t = 0$ to the time that changes in concentration reached the tissue. The transport delay was determined by observing the time for a bubble introduced at the inlet to emerge at the outlet of the tubing. Representative changes in arteriolar diameter (ΔD) are shown in **Figure 1A** with average responses for 6–7 arterioles from 1 rat experiment, demonstrating enhanced vasodilation with hypoxic conditions in the superfusate. Initial diameters ± SE are indicated. Greater vasodilation responses to $NaNO_2$ were often, but not always, observed using hypoxic solutions with acidic pH compared with hypoxic solutions at normal pH = 7.4. An example from 1 rat experiment with averaged measurements from 6 arteriole pairs is shown in **Figure 1B**. Note that the time rate of diameter change (ΔD/Δt, dashed lines) during the period of $NaNO_2$ superfusion was 38% faster in the acidic solution (0.759 μm/min) compared with the rate of increase at pH = 7.4 (0.55 μm/min) that occurred following a transient decrease in ΔD for this experiment. This transient may reflect a decrease in NO during the period of hypoxic superfusion preceding the exposure to $NaNO_2$. We also recorded the laser Doppler signal (LDF), which is proportional to capillary blood flow and reported with arbitrary tissue perfusion units (tpu). For the example shown in **Figure 1C**, the average change (ΔLDF) during $NaNO_2$ superfusion was negligible when the superfusate pH = 7.4 (open circles). There were increases in capillary blood flow during $NaNO_2$ superfusion with acidic pH (**Figure 1C**, solid circles), although the difference compared with normal pH was not statistically significant. Overall results for the average ΔD ± SE for 44 paired arterioles from $n = 9$ rats are shown in **Figure 1D** for $NaNO_2$ concentrations ranging between 4 and 24 mM in hypoxic superfusion solution. The average ± SE initial diameter was $D_{initial} = 43.4 \pm 1.6$ μm for these measurements. Note that there were many experiments (4/9) where the average increase in ΔD with $NaNO_2$ in acidic superfusion solution was smaller compared to superfusion solutions at normal pH. In three experiments, the average D was slightly negative (no increase in D for two experiments with pH = 7.4 and one experiment for acidic pH). Consequently, there was no statistically significant difference in ΔD determined during $NaNO_2$ superfusion with normal or acidic pH (Mann–Whitney Rank Sum test).

Evidence for the role of XOR was found by comparing vascular responses before and after treating animals with allopurinol (3.4–6 mg/kg IP). Results for the average ΔD with hypoxia and $NaNO_2$ in the 10–12 mM range for three rat experiments is shown in **Figure 2A**, demonstrating a significant reduction in the vasodilatory response after allopurinol (solid circles) compared to control measurements (open circles). The small artery blood flow (BF) to the segment of mesentery under study in a representative experiment (**Figure 2B**) was also affected by $NaNO_2$ and hypoxic superfusion, presumably due to downstream vasodilation. There was a prolonged increase in BF that persisted for several minutes after 3 min exposure to $NaNO_2$, which was abolished after allopurinol treatment. Capillary perfusion as determined by LDF for this same experiment showed a similar increase with $NaNO_2$ and hypoxia that was attenuated after allopurinol (**Figure 2C**).

We also investigated the role of AOR using raloxifene (2.9–10 mg/kg IP) to inhibit its activity. An example using superfusion with 10 mM $NaNO_2$ in hypoxic and acidic solution is shown in **Figure 3A**, showing vasodilation before treatment (open circles), and complete blocking of the response after raloxifene treatment (solid circles). However, in another experiment shown in **Figure 3B**, treatment with raloxifene did not abolish the vasodilatory response to $NaNO_2$ in hypoxic and acidic solution.

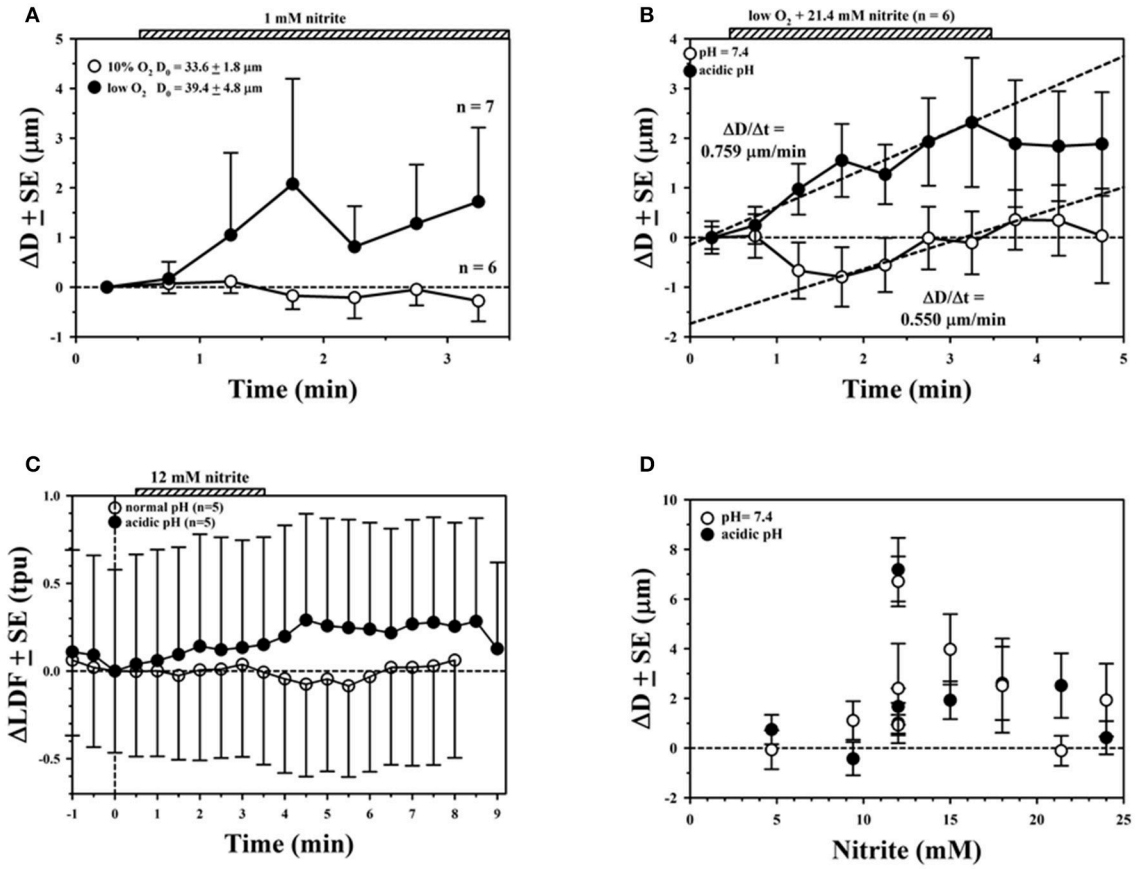


**FIGURE 1 |** Average ± SE changes in arteriolar diameter (ΔD) measured in rat mesentery during superfusion experiments. **(A)** No effect was seen with 1 mM sodium nitrite ($NaNO_2$) in 10% oxygenated solution (open circles), whereas increases in D were observed with hypoxic solution (solid circles). **(B)** Much larger and more rapid changes in D with $NaNO_2$ were often observed with acidic solution (solid circles) than solution with normal pH (open circles). **(C)** Changes in laser Doppler signal (LDF) showing larger response with acidic superfusion solution. **(D)** Overall ΔD ± SE during superfusion with normal (open circles) or acidic pH (solid circles) over a wide range of $NaNO_2$ concentrations.

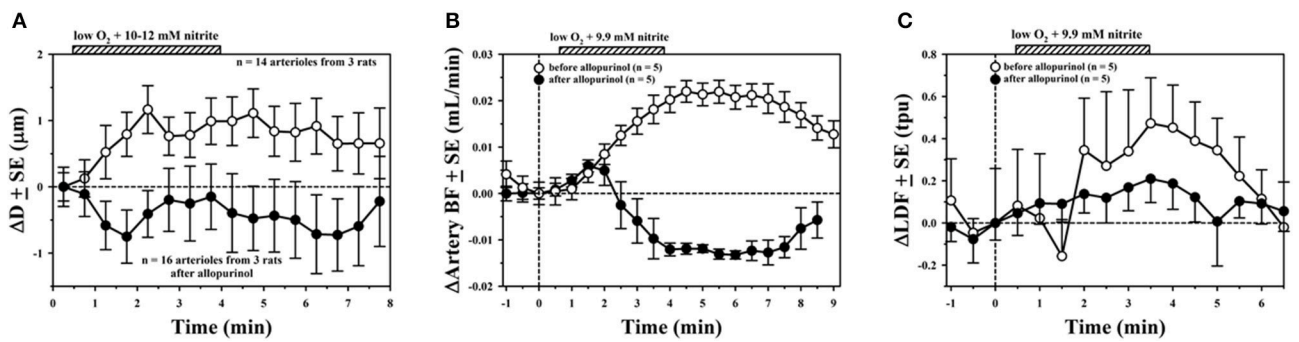


**FIGURE 2 |** Average ± SE changes before (open circles) and after inhibiting XOR with allopurinol (solid circles) in **(A)** arteriolar diameter, **(B)** small artery blood flow, and **(C)** laser Doppler signal.

In addition to superfusion experiments, we also quantified the effect of $NaNO_2$ delivered to the animal by IP injection. NO microelectrodes were used in these experiments to measure perivascular NO for the arterioles since there was no nitrite in the superfusion solution to interfere with the electrochemical measurement. A representative NO microelectrode measurement is shown in the lower panel of **Figure 4A**. At $t = 0$, the NO microelectrode tip was in

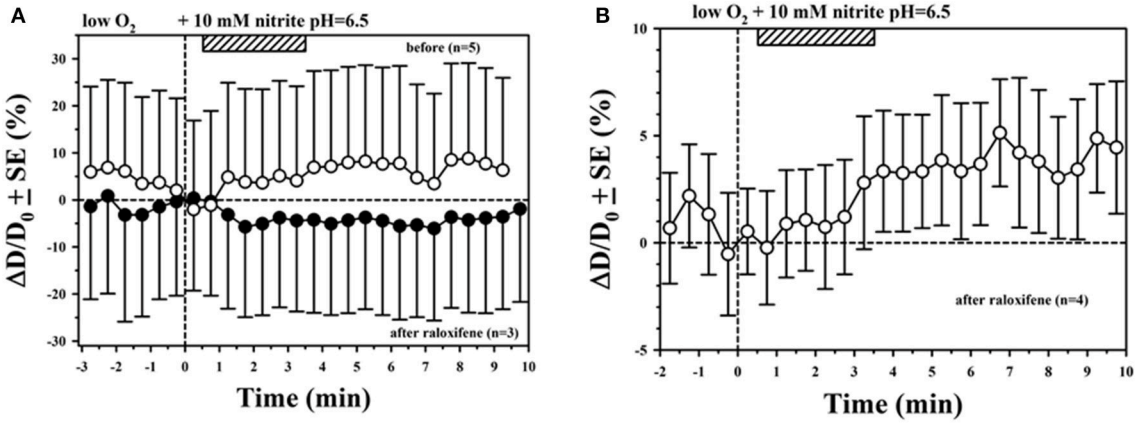


**FIGURE 3 |** Mixed results for inhibition of AOR with raloxifene. **(A)** Inhibition of vasodilation with superfused $NaNO_2$ was observed in this experiment. **(B)** Vasodilation with superfused $NaNO_2$ was still observed after treating with raloxifene in this experiment.

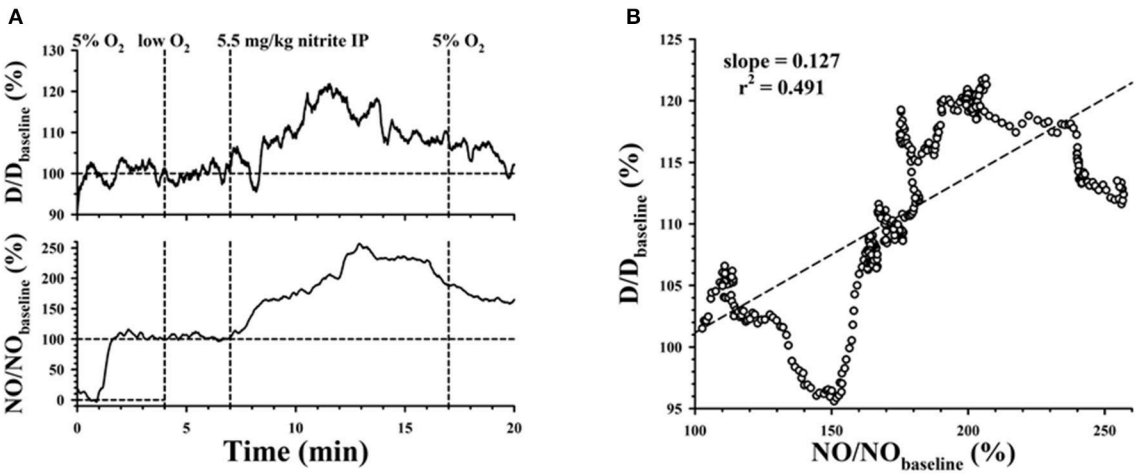


**FIGURE 4 | (A)** Simultaneous measurements of arteriolar diameter and perivascular NO, normalized by baseline diameter and electrode current. Superfusion was changed from 5% $O_2$ to low $O_2$ at $t = 4$ min, then back to 5% $O_2$ at $t = 17$ min, following an IP injection of $NaNO_2$ at $t = 7$ min. **(B)** Correlation between the normalized perivascular NO and normalized diameter.

the superfusate flowing above the preparation, where there is negligible NO concentration with resulting minimum electrochemical current. The tip was then moved close to the outer surface of the arteriole to measure the baseline perivascular NO, which was used to normalize the measurement. At $t =$ 4 min, the superfusate was changed from a solution with 5% $O_2$ and 5% $CO_2$ to a hypoxic solution equilibrated with 0% $O_2$ and 5% $CO_2$. At approximately $t = 7$ min, 5.5 mg/kg of $NaNO_2$ was injected IP. Relative changes in diameter, normalized to the baseline diameter, are shown in the upper panel of **Figure 4A**. The peak change in NO occurs about 6 min afterwards, with the peak change in D around 5 min after IP injection. Nevertheless, time courses for the relative changes in NO and D were similar. The correlation between the relative increase in D with NO for normalized data between 7 and 13 min is shown in **Figure 4B**, with positive slope = 0.127%/%. At $t = 17$ min, the superfusion was changed back to oxygenated solution (5% $O_2$, 5% $CO_2$) and the arteriolar diameter returned close to baseline, although NO remained elevated for this example. At the end of each measurement, the microelectrode tip was drawn back up into the superfusate to obtain another zero NO current measurement. Any change in the zero NO current from the beginning to the end of the measurement was used to correct for drift, assuming a linear time course.

Further evidence for the role of XOR was found from experiments where nitrite in the bloodstream was increased following IP delivery. Microelectrode measurements confirmed that there was an increase in perivascular NO after IP delivery of $NaNO_2$, which was attenuated after allopurinol. Examples for the time course of relative average changes in diameter (**Figure 5A**) and perivascular NO (**Figure 5B**) for 7 arterioles from 1 rat experiment are shown following IP delivery of 3.4 mg/kg $NaNO_2$

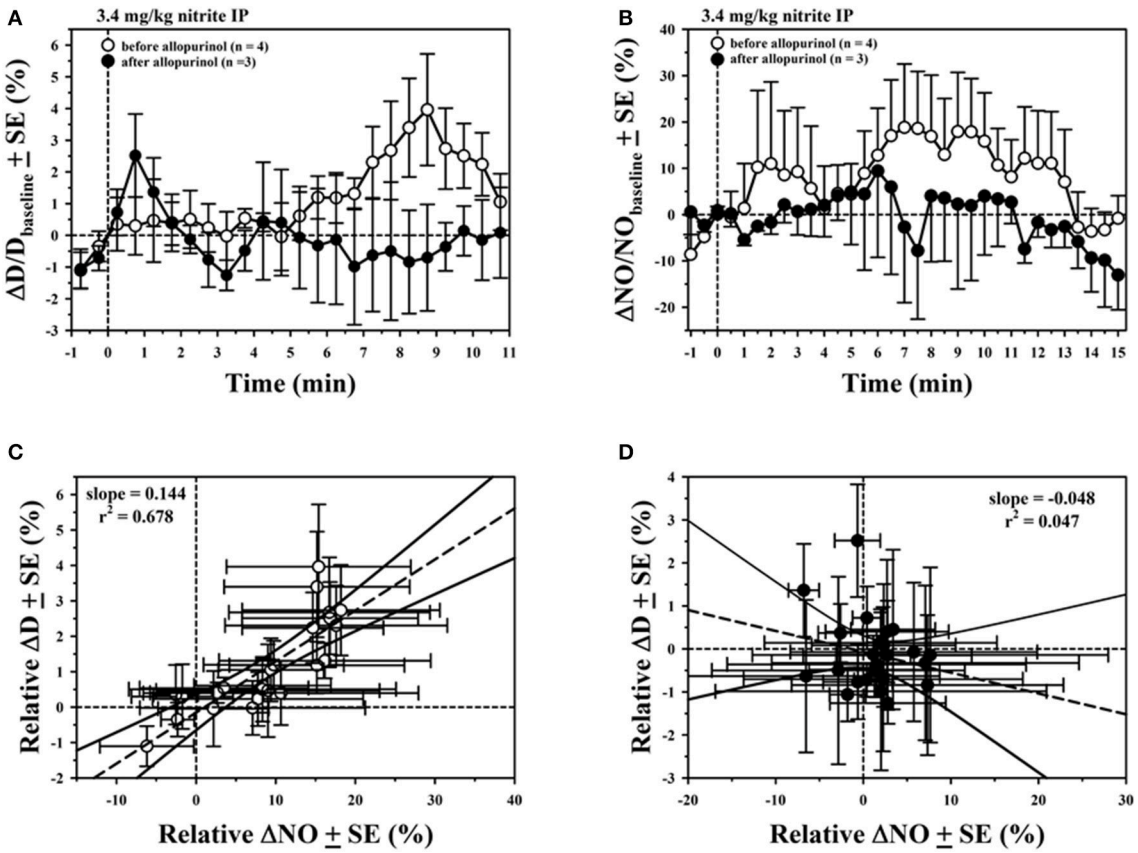


**FIGURE 5 |** Average ± SE changes in **(A)** normalized arteriolar diameter, **(B)** normalized perivascular NO, following IP injection of $NaNO_2$ at $t = 0$ before (open circles) and after inhibiting XOR with allopurinol (solid circles). Correlations between normalized perivascular NO and normalized diameter are shown **(C)** before and **(D)** after allopurinol.

before and after allopurinol. The ΔD are normalized with respect to the initial diameter ($D_{initial} = 37.0 \pm 1.9\,\mu m$) and ΔNO with respect to the baseline NO level before each nitrite injection. Before allopurinol, the peak change in D after IP injection of $NaNO_2$ occurred around 8.5 min in **Figure 5A**, and around 5 min in **Figure 5B**. There is a significant positive correlation (slope = 0.144%/%) between the normalized average ΔD and ΔNO (**Figure 5C**) with $NaNO_2$ before inhibiting XOR. After a single dose of allopurinol (5 mg/kg IP), there is no longer any correlation (slight negative slope = −0.048%/%, **Figure 5D**). A total of $n = 3$ rat experiments using IP $NaNO_2$ delivery were conducted with allopurinol, and in all three cases, a positive correlation between ΔD and ΔNO was observed before allopurinol ($n = 11$ arterioles) and a negative correlation between ΔD and ΔNO was observed after allopurinol ($n = 9$ arterioles).

## Model Predictions

Reducing values for blood $PO_2$ in the simulation from normoxic (90 Torr) to severely hypoxic levels (10 Torr), predicts a decrease in NO across the computational domain for a baseline case without any generation of NO from nitrite either in blood or tissue (**Figure 6A**). The average NO in the SMC layer decreases monotonically with increasing hypoxia (inset, **Figure 6A**), predicting a 17.1 nM decrease in NO (−29.3%) as blood $PO_2$ drops from 90 to 10 torr. As reviewed by Gladwin et al. (2009), changes in conformation as hemoglobin becomes deoxygenated results in changes in the rate of nitrite reduction, with a maximum rate in the hypoxic $PO_2$ range. Our previous simulations (Liu Y. et al., 2016) demonstrate that SMC NO can be significantly elevated through the deoxyhemoglobin nitrite reductase pathway, and further increased in magnitude with increasing nitrite concentration and greater hypoxia. For the case where blood $PO_2$ drops from 90 to 10 torr, the decrease in SMC NO can be compensated through the deoxyhemoglobin nitrite reductase pathway by increasing the blood nitrite concentration to 284.9 μM (**Figure 6B**).

The effect of tissue XOR nitrite reduction on SMC NO with tissue nitrite = 100 μM was compared against the baseline case (zero nitrite reduction in **Figure 6A**) as a function of blood $PO_2$ for low (0.03 μM) and high (0.3 μM) concentrations of XOR (**Figures 6C,D**). The contribution to SMC NO from the deoxyhemoglobin nitrite reductase pathway is also shown. NO elevation by XOR has the greatest effect with the highest XOR concentrations at the acidic pH and lowest blood $PO_2$. For this concentration of nitrite (100 μM), the additional NO is predicted to be +2.4 nM from deoxyhemoglobin nitrite reductase

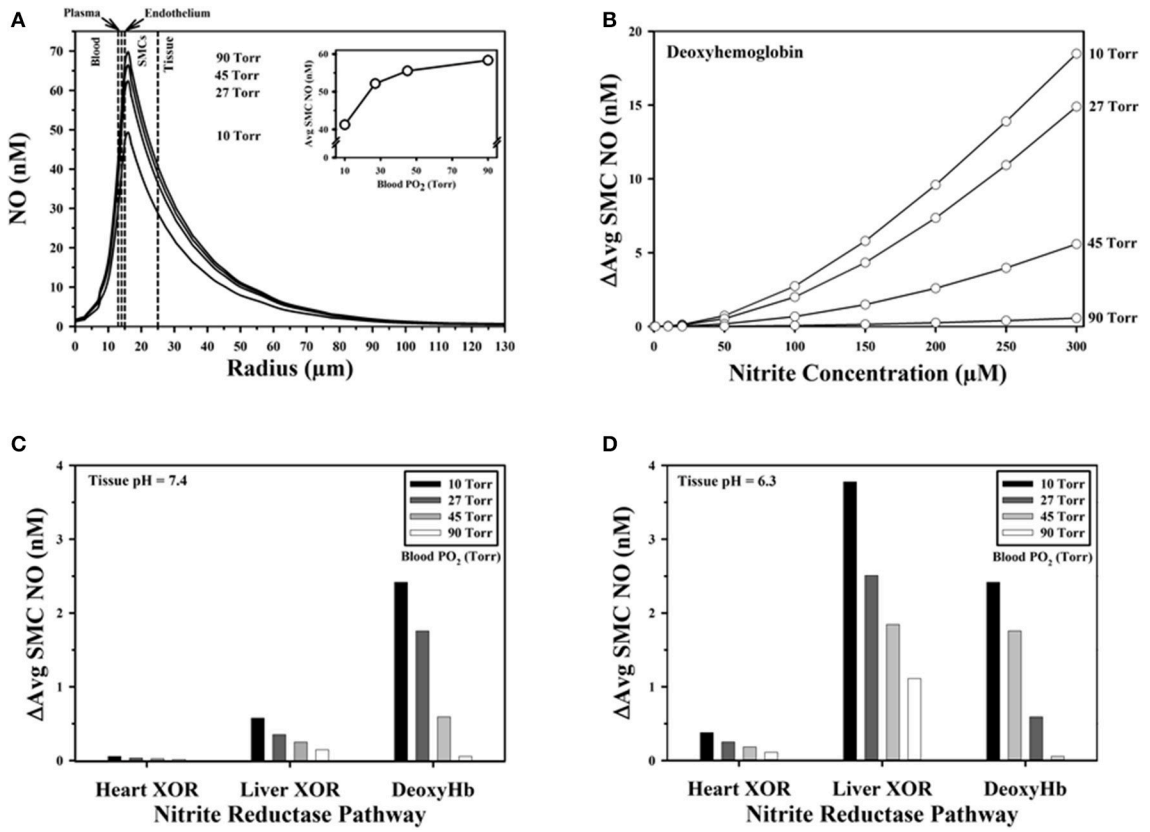


**FIGURE 6 |** Model predictions. **(A)** Baseline NO concentration profiles across the computational domain predicted for different blood $PO_2$ values without additional NO released from nitrite. Vertical dashed lines mark boundaries between the five radial model layers. (Inset) Average NO concentration in the smooth muscle cell (SMC) region with decreasing blood $PO_2$. **(B)** Increase in average SMC NO above baseline predicted with formation of $N_2O_3$ from deoxyhemoglobin nitrite reductase activity and subsequent release of NO shown as a function of blood $PO_2$ and nitrite concentration in blood. Effect of low (e.g., in heart) and high (e.g., in liver) tissue nitrite reductase XOR concentrations on elevation of average SMC NO above baseline for **(C)** pH = 7.4 and **(D)** pH = 6.3.

and +3.8 nM from XOR, for a total compensation of +6.2 nM, representing a recovery of 36% from the drop in NO due to the decrease in blood $PO_2$. The total compensation in NO at pH = 7.4 with the 0.3 μM XOR concentration would be only +3 nM (17.5% recovery), and only +2.47 nM (14.4% recovery) with the lower 0.03 μM XOR concentration. Simulations were also run for the AOR nitrite reductase pathway. AOR has slightly lower reaction rate constants compared with XOR (Maia et al., 2015), and AOR concentrations are generally lower than XOR in the heart and liver (Li et al., 2008). Simulations with AOR predicted ∼10–20% less elevation in SMC NO for pH = 7.4 and 6.3 (not shown).

A sensitivity analysis (**Figure 7**) was conducted for the model parameters listed in **Table 1** to examine the effect of small variations (±5%) in the parameter values on the predicted average SMC NO. Other parameters were held constant for simulations with tissue nitrite = 100 μM, blood $PO_2$ = 10 Torr, and baseline flow in liver tissue (**Figure 7**). Variations in the concentration of XOR or AOR had the largest effect on the predicted NO, with an intermediate sensitivity to the nitrite diffusion coefficient. The sensitivity was relatively low (<0.1% at +5% variation) for $K_mO_2$, and the reaction parameters $k_{cat}$ at pH = 7.4. There was a larger effect for variations in the reaction parameter $k_{cat}$ at pH = 6.3 (+0.508% at +5% variation). A 5% increase in the values for $K_mNO_2^-$ at pH = 7.4 and $K_mNO_2^-$ at pH = 6.3 results in small decreases in the SMC NO by −0.079 and −0.385%, respectively.

## DISCUSSION

Our *in vivo* results from the rat mesentery microcirculation provide further evidence that nitrite reductases in tissue play a role in increasing NO bioavailability during nitrite-mediated hypoxic vasodilation. We confirmed this by using allopurinol to inhibit XOR (3.4–6 mg/kg IP). Due to time constraints for the *in vivo* experimental procedure, we did not investigate whether a second, higher dose of allopurinol would further inhibit the vasodilatory response. Golwala et al. (2009) used a higher dose of allopurinol (25 mg/kg IV) for their *in vivo* rat studies, and demonstrated that a second 25 mg/kg dose had little further inhibitory effect. They also inhibited AOR using cyanamide (25 mg/kg IV), and alternated the order of inhibitor delivery to discriminate between the contribution of each nitrite

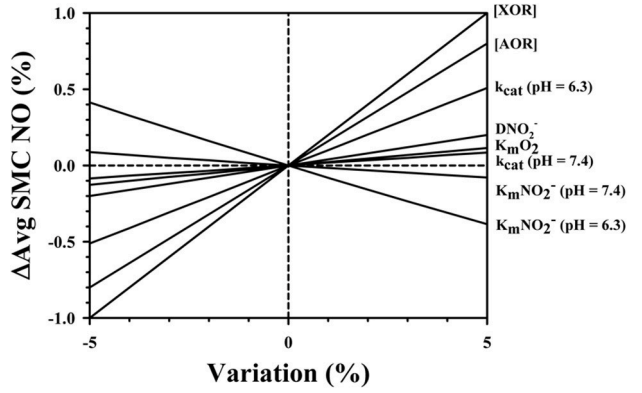


**FIGURE 7 |** Sensitivity analysis showing the effect of ±5% variations in the model parameters listed in **Table 1** (identified at right of figure) on relative differences in average NO in the SMC region.

reductase on nitrite responses. Nitrite doses of 0.01, 0.03, or 0.1 mM/kg were delivered IV and the changes in systemic blood pressure were measured. Both inhibitors attenuated the decrease in systemic blood pressure with IV delivery of $NaNO_2$. The authors concluded that both XOR and AOR pathways act in parallel in the vasculature.

In our study, we found that it was necessary to use high $NaNO_2$ concentrations (>1 mM in the superfusion solution) to elicit vasodilation (**Figure 1D**). A possible explanation for this finding is that the hypoxic superfusion solution did not significantly lower the blood $PO_2$ of the arterioles under study, even though we did see a difference (greater vasodilation) with $NaNO_2$ in hypoxic solution compared with $NaNO_2$ in oxygenated solution (**Figure 1A**). The high $NaNO_2$ concentration used in our superfusion experiments is much greater than used for intra-arterial infusions in humans, which demonstrate greater vasodilation under hypoxia than normoxia (Maher et al., 2008). The necessity to use high concentrations of nitrite to generate NO under anoxic conditions *in vitro* was pointed out in the review by Kelley (2015). Consequently, we were not able to directly measure perivascular NO due to electrochemical interference with high nitrite concentrations during superfusion, but we were able to confirm that there was an increase in perivascular NO from the measurements using IP delivery of nitrite. A direct correlation between the increase in NO and vascular diameter was found from these IP injection experiments, which was essentially abolished after inhibiting XOR. The review by Kelley (2015) identifies key factors which allow significant recovery of NO through XOR, including acidic pH and low $O_2$, as well as other biochemical factors. For example, a recent *in vitro* study using aortic ring preparations and isolated mesenteric arterial bed perfusion found that the nitrate anion ($NO_3^-$) attenuates XOR-mediated NO generation from nitrite (Damacena-Angelis et al., 2017). To validate the inhibitory effects of nitrate, this study also included experiments with purified XOR using a different inhibitor (febuxostat), which is more potent than allopurinol (Okamoto et al., 2003).

Bryan et al. (2005) studied the time course for uptake and metabolism of nitrite in different organ systems of Wistar rats following IP injection of $NaNO_2$ (range 0.1–10 mg/kg), reporting that tissue nitrite levels were essentially in equilibrium by ∼5 min, when presumably the uptake rate from the abdominal cavity matches the decay rate in blood. Our measurements for the maximum ΔD and ΔNO for the examples shown (**Figures 4A**, **5**) ranged between 5 and 8.5 min. Bryan et al. (2005) reported that nitrate levels as well as the total nitroso/nitrosyl products (RSNO + RNNO + NO-heme) also increased following IP injection of nitrite. We cannot rule out the possibility that some inhibition of the vascular responses by nitrate might occur after repeated IP injections of nitrite in our study as suggested from the results reported by Damacena-Angelis et al. (2017). Bryan et al. (2005) also conducted *in vitro* experiments, and presented evidence that NO formation from nitrite is not required for nitrosation (RSNO) or nitrosylation (RNNO) of thiols, and conclude that these reactions can occur at nitrite concentrations far below that required for vasodilation. A randomized, placebo controlled dose-response study of $NaNO_2$ infusion in humans by Rosenbaek et al. (2017) investigating effects on kidney function and blood pressure found a dose-dependent decrease in urine output with reduced blood pressure. Since they observed no increase in GMP, they concluded that their results supported a direct effect of nitrite or nitrate on the renal tubules and vascular bed with little or no systemic conversion of nitrite to NO.

Many previous studies that have examined the conversion of nitrite to bioactive NO have focused on the role of RBCs through the reductase activity of deoxyhemoglobin (e.g., see Kim-Shapiro and Gladwin, 2014). However, we cannot discriminate whether our experimental results can be specifically attributed to nitrite reductases in blood or tissue (or both). There is strong evidence for greater involvement of tissue nitrite reductases (Feelisch et al., 2008; Li et al., 2008; Arif et al., 2015; Piknova et al., 2015). *In vitro* studies with isolated rabbit aortic rings demonstrate that 10 μM nitrite in the absence of hemoglobin can increase maximal dilation under hypoxic conditions, which can occur with or without the endothelium (Pinder et al., 2009). The authors concluded that AOR, but not XOR, was primarily responsible for nitrite-mediated hypoxic vasorelaxation measured in their study, with some contribution from the cyclooxygenase (COX) pathway. Another *in vitro* study with isolated rat thoracic aorta rings demonstrated attenuation of hypoxic vasorelaxation with nitrite (concentration range from 1 nM to 100 μM) after inhibiting AOR with cyanamide (Arif et al., 2015). We did not get consistent results inhibiting vascular responses to nitrite with raloxifene. We found nitrite-mediated vasodilation was unaffected after raloxifene in one study (**Figure 3B**). Since there is evidence that high concentrations of raloxifene can also inhibit XOR (Weidert et al., 2014), we cannot rule out the possibility that our results showing inhibition of vascular responses with raloxifene (**Figure 3A**) might be due to inhibition of XOR instead of AOR. There might also be vasoactive effects of raloxifene that are independent of NO. We estimated that the raloxifene dose chosen for our studies was not high enough to inhibit XOR. However, it is difficult to discriminate between NO contributions

between XOR and AOR pathways since blocking either pathway depends on inhibitor specificity and dose (Weidert et al., 2014).

It should be recognized that there are other possible mechanisms for the RBC to contribute to hypoxic vasodilation besides the deoxyhemoglobin nitrite reductase-mediated release of NO from nitrite. It has been proposed that the RBC contains a form of eNOS (Kleinbongard et al., 2006), which can produce NO, although it would be subject to immediate scavenging due to the high Hb concentration in the RBC. It has been proposed that formation of Hb(III)NO as an intermediate can account for the majority of NO produced from RBCs (Nagababu et al., 2003). Salgado et al. (2015) propose that this intermediate preferentially locates to the RBC membrane with a greater affinity than Hb. They suggest that a significant amount of NO might be transferred to the vasculature from this pool, avoiding quenching by Hb. Alternately, there is evidence that the RBC releases ATP during hypoxia, which can in turn stimulate NO production by eNOS (Sprague et al., 2007; Cao et al., 2009). We have modeled this effect to predict how ATP can increase shear-stress mediated NO production (Kirby et al., 2016), based on *in vitro* NO measurements with cultured ECs (Andrews et al., 2014). Another proposed mechanism is the formation of S-nitrosohemoglobin (SNO-Hb), as reviewed by Singel and Stamler (2005). However, there is contradictory evidence for this mechanism (Isbell et al., 2008). Furthermore, a mathematical model by Chen K. et al. (2007) did not predict a significant NO contribution from this pathway.

There are also other mechanisms in tissue beside nitrite reductases that can contribute NO during hypoxia, as reviewed by Buerk (2007) and Kim-Shapiro and Gladwin (2014). There is evidence that cytochrome c in the mitochondria can be a source of NO by reducing nitrite (Kozlov et al., 1999). It has also been proposed that there is a mitochondrial form of NOS (mtNOS) that can produce NO, although the existence of mtNOS is questioned (Lacza et al., 2006). NO or related reactive species can modify tissue proteins, forming *S*-nitrosothiols, *S*-nitrosoalbumin, and other *S*-nitrosoprotein species under normal physiological conditions which might serve as a storage pool in tissue for NO or other vasoactive species (Jourd'heuil et al., 2000; Liu T. et al., 2016). On the other hand, these reactions may modify vascular tone signaling pathways independently from any NO recovered from nitrite. While normally myoglobin is a strong scavenger of NO, it is recognized that myoglobin can also cause nitrite bioactivation by reducing nitrite (Shiva et al., 2007; Totzeck et al., 2012, 2014; Piknova et al., 2015). We have developed a mathematical model for a cardiac arteriole and surrounding myocardium (Liu et al., 2017), showing how myoglobin functions as a nitrite reductase to elevate SMC NO during hypoxia in an $O_2$- and pH-dependent manner.

## Limitations of Mathematical Model

Our simulations assume that published reaction parameters (Maia and Moura, 2011; Maia et al., 2015) were constant with abundant substrate, and were only affected by changing $O_2$ or pH levels. The model assumes that all $N_2O_3$ homolyzes to NO, ignoring other nitrosation reactions that are known to occur (Basu et al., 2007; Kim-Shapiro and Gladwin, 2014), thus we may be overestimating the increase in SMC NO. It is also possible, as suggested by Koppenol (2012) and Tu et al. (2009), that it is not energetically possible for the reactions to generate $N_2O_3$ to occur. As with any computer simulation, the accuracy of model parameters determines whether the predictions are physiologically relevant. The measurement of reaction rates is hindered by experimental difficulties and complex interactions among XOR, AOR, nitrite, nitrate, and NO (Jourd'heuil et al., 2000; Maia and Moura, 2011; Cantu-Medellin and Kelley, 2013; Damacena-Angelis et al., 2017). The concentration of nitrite reductase enzymes in tissue is not well-characterized and may not be uniformly distributed. We are not aware of any estimates for the enzyme concentrations and reaction parameters in mesentery. Future simulations would be necessary if more precise information about reaction rates, localized spatial distributions, and concentrations become available. The predicted changes in SMC NO with physiologically relevant nitrite concentrations in the 0.2–2 $\mu$M range are quite small ($<$1 nM) even for hypoxic conditions. Even with much higher nitrite levels (up to 300 $\mu$M), the increase in SMC NO predicted for the deoxyhemoglobin nitrite reductase pathway is $<$20 nM during severe hypoxia with blood $PO_2 = 10$ torr (**Figure 6B**).

In conclusion, our *in vivo* experimental results are consistent with other studies that suggest that the reduction of nitrite through the activity of tissue nitrite reductases can contribute NO to vascular smooth muscle to enhance hypoxic vasodilation. However, it is difficult to assess whether hypoxic vasodilation can be specifically attributed to nitrite reductase activity in blood or tissue, or both. It is also very difficult to experimentally create the severe *in vivo* physiological conditions for maximal effects. Our theoretical model demonstrates that is possible to compensate for the loss of NO production by eNOS during hypoxia by all three pathways: deoxyhemoglobin nitrite reductase in RBCs, and the tissue nitrite reductases XOR and AOR. This modeling approach can be further developed to explore other biochemical pathways that can contribute NO or other nitrogen species that enhance hypoxic vasodilation.

## AUTHOR CONTRIBUTIONS

DB was responsible for the experimental design, conducting animal research, data analysis, model development, writing and editing the paper. YL was responsible for computer simulations and contributed written content. KZ assisted with animal surgery and editing the paper. KB and DJ were responsible for model development and editing the paper.

## FUNDING

Supported by HL 116256 from NIH.

## REFERENCES


Andrews, A. M., Jaron, D., Buerk, D. G., and Barbee, K. A. (2014). Shear stress-induced NO production is dependent on ATP autocrine signaling and capacitative calcium entry. *Cell Mol. Bioeng.* 7, 510–520. doi: 10.1007/s12195-014-0351-x

Arif, S., Borgognone, A., Lin, E. L., O'Sullivan, A. G., Sharma, V., Drury, N. E., et al. (2015). Role of aldehyde dehydrogenase in hypoxic vasodilator effects of nitrite in rats and humans. *Br. J. Pharmacol.* 172, 3341–3352. doi: 10.1111/bph.13122

Azizi, F., Kielbasa, J. E., Adeyiga, A. M., Maree, R. D., Frazier, M., Yakubu, M., et al. (2005). Rates of nitric oxide dissociation from hemoglobin. *Free Radic. Biol. Med.* 39, 145–151. doi: 10.1016/j.freeradbiomed.2005.03.001

Basu, S., Grubina, R., Huang, J., Conradie, J., Huang, Z., Jeffers, A., et al. (2007). Catalytic generation of $N_2O_3$ by the concerted nitrite reductase and anhydrase activity of hemoglobin. *Nat. Chem. Biol.* 3, 785–794. doi: 10.1038/nchembio.2007.46

Blood, A. B. (2017). The medicinal chemistry of nitrite as a source of nitric oxide signaling. *Curr. Top Med. Chem.* 17, 1758–1768. doi: 10.2174/1568026617666161116145046

Bonner, R. F., Clem, T. R., Bowen, P. D., and Bowman, R. L. (1981). "Laser-doppler continuous real-time monitor of pulsatile and mean blood flow," in *Tissue Microcirculation. Scattering Techniques Applied to Supra-Molecular and Nonequilibrium Systems*, eds S. H. Chen, B. Chu, and R. Nossal (New York, NY: Plenum), 685–702.

Bryan, N. S., Fernandez, B. O., Bauer, S. M., Garcia-Saura, M. F., Milsom, A. B., Rassaf, T., et al. (2005). Nitrite is a signaling molecule and regulator of gene expression in mammalian tissues. *Nat. Chem. Biol.* 1, 290–297. doi: 10.1038/nchembio734

Buerk, D. G. (2007). Nitric oxide regulation of microvascular oxygen. *Antioxid. Redox Signal.* 9, 829–843. doi: 10.1089/ars.2007.1551

Buerk, D. G., Barbee, K. A., and Jaron, D. (2011a). Modeling $O_2$-dependent effects of nitrite reductase activity in blood and tissue on coupled NO and $O_2$ transport around arterioles. *Adv. Exp. Med. Biol.* 701, 271–276. doi: 10.1007/978-1-4419-7756-4_36

Buerk, D. G., Barbee, K. A., and Jaron, D. (2011b). Nitric oxide signaling in the microcirculation. *Crit. Rev. Biomed. Eng.* 39, 397–433. doi: 10.1615/CritRevBiomedEng.v39.i5.40

Buerk, D. G., Lamkin-Kennard, K., and Jaron, D. (2003). Modeling the influence of superoxide dismutase on superoxide and nitric oxide interactions, including reversible inhibition of oxygen consumption. *Free Radic. Biol. Med.* 34, 1488–1503. doi: 10.1016/S0891-5849(03)00178-3

Butler, A. R., and Ridd, J. H. (2004). Formation of nitric oxide from nitrous acid in ischemic tissue and skin. *Nitric Oxide* 10, 20–24. doi: 10.1016/j.niox.2004.01.004

Cantu-Medellin, N., and Kelley, E. E. (2013). Xanthine oxidoreductase-catalyzed reduction of nitrite to nitric oxide: insights regarding where, when and how. *Nitric Oxide* 34, 19–26. doi: 10.1016/j.niox.2013.02.081

Cao, Z., Bell, J. B., Mohanty, J. G., Nagababu, E., and Rifkind, J. M. (2009). Nitrite enhances RBC hypoxic ATP synthesis and the release of ATP into the vasculature: a new mechanism for nitrite-induced vasodilation. *Am. J. Physiol. Heart Circ. Physiol.* 297, H1494–H1503. doi: 10.1152/ajpheart.01233.2008

Chen, K., Piknova, B., Pittman, R. N., Schechter, A. N., and Popel, A. S. (2008). Nitric oxide from nitrite reduction by hemoglobin in the plasma and erythrocytes. *Nitric Oxide* 18, 47–60. doi: 10.1016/j.niox.2007.09.088

Chen, K., Pittman, R. N., and Popel, A. S. (2007). Vascular smooth muscle NO exposure from intraerythrocytic SNOHb: a mathematical model. *Antioxid. Redox Signal.* 9, 1097–1110. doi: 10.1089/ars.2007.1594

Chen, X., Buerk, D. G., Barbee, K. A., and Jaron, D. (2007). A model of NO/$O_2$ transport in capillary-perfused tissue containing an arteriole and venule pair. *Ann. Biomed. Eng.* 35, 517–529. doi: 10.1007/s10439-006-9236-z

Chen, X., Jaron, D., Barbee, K. A., and Buerk, D. G. (2006). The influence of radial RBC distribution, blood velocity profiles, and glycocalyx on coupled NO/$O_2$ transport. *J. Appl. Physiol.* 100, 482–492. doi: 10.1152/japplphysiol.00633.2005

Cosby, K., Partovi, K. S., Crawford, J. H., Patel, R. P., Reiter, C. D., Martyr, S., et al. (2003). Nitrite reduction to nitric oxide by deoxyhemoglobin vasodilates the human circulation. *Nat. Med.* 9, 1498–1505. doi: 10.1038/nm954

Damacena-Angelis, C., Oliveira-Paula, G. H., Pinheiro, L. C., Crevelin, E. J., Portella, R. L., Moraes, L. A. B., et al. (2017). Nitrate decreases xanthine oxidoreductase-mediated nitrite reductase activity and attenuates vascular and blood pressure responses to nitrite. *Redox. Biol.* 12, 291–299. doi: 10.1016/j.redox.2017.03.003

Dejam, A., Hunter, C. J., Tremonti, C., Pluta, R. M., Hon, Y. Y., Grimes, G., et al. (2007). Nitrite infusion in humans and nonhuman primates: endocrine effects, pharmacokinetics, and tolerance formation. *Circulation* 116, 1821–1831. doi: 10.1161/CIRCULATIONAHA.107.712133

Feelisch, M., Fernandez, B. O., Bryan, N. S., Garcia-Saura, M. F., Bauer, S., Whitlock, D. R., et al. (2008). Tissue processing of nitrite in hypoxia: an intricate interplay of nitric oxide-generating and -scavenging systems. *J. Biol. Chem.* 283, 33927–33934. doi: 10.1074/jbc.M806654200

Gladwin, M. T. (2008). Evidence mounts that nitrite contributes to hypoxic vasodilation in the human circulation. *Circulation* 117, 594–597. doi: 10.1161/CIRCULATIONAHA.107.753897

Gladwin, M. T., Grubina, R., and Doyle, M. P. (2009). The new chemical biology of nitrite reactions with hemoglobin: R-state catalysis, oxidative denitrosylation, and nitrite reductase/anhydrase. *Acc. Chem. Res.* 42, 157–167. doi: 10.1021/ar800089j

Golwala, N. H., Hodenette, C., Murthy, S. N., Nossaman, B. D., and Kadowitz, P. J. (2009). Vascular responses to nitrite are mediated by xanthine oxidoreductase and mitochondrial aldehyde dehydrogenase in the rat. *Can. J. Physiol. Pharmacol.* 87, 1095–1101. doi: 10.1139/Y09-101

Helms, C. C., Liu, X., and Kim-Shapiro, D. B. (2017). Recent insights into nitrite signaling processes in blood. *Biol. Chem.* 398, 319–329. doi: 10.1515/hsz-2016-0263

Hopmann, K. H., Cardey, B., Gladwin, M. T., Kim-Shapiro, D. B., and Ghosh, A. (2011). Hemoglobin as a nitrite anhydrase: modeling methemoglobin-mediated N2O3 formation. *Chemistry* 17, 6348–6358. doi: 10.1002/chem.201003578

Isbell, T. S., Sun, C. W., Wu, L. C., Teng, X., Vitturi, D. A., Branch, B. G., et al. (2008). SNO-hemoglobin is not essential for red blood cell-dependent hypoxic vasodilation. *Nat. Med.* 14, 773–777. doi: 10.1038/nm1771

Jourd'heuil, D., Hallen, K., Feelisch, M., and Grisham, M. B. (2000). Dynamic state of S-nitrosothiols in human plasma and whole blood. *Free Radic. Biol. Med.* 28, 409–417. doi: 10.1016/S0891-5849(99)00257-9

Kelley, E. E. (2015). A new paradigm for XOR-catalyzed reactive species generation in the endothelium. *Pharmacol. Rep.* 67, 669–674. doi: 10.1016/j.pharep.2015.05.004

Kevil, C. G., Kolluru, G. K., Pattillo, C. B., and Giordano, T. (2011). Inorganic nitrite therapy: historical perspective and future directions. *Free Radic. Biol. Med.* 51, 576–593. doi: 10.1016/j.freeradbiomed.2011.04.042

Kim-Shapiro, D. B., and Gladwin, M. T. (2014). Mechanisms of nitrite bioactivation. *Nitric Oxide* 38, 58–68. doi: 10.1016/j.niox.2013.11.002

Kirby, P. L., Buerk, D. G., Parikh, J., Barbee, K. A., and Jaron, D. (2016). Mathematical model for shear stress dependent NO and adenine nucleotide production from endothelial cells. *Nitric Oxide* 52, 1–15. doi: 10.1016/j.niox.2015.10.004

Kleinbongard, P., Schulz, R., Rassaf, T., Lauer, T., Dejam, A., Jax, T., et al. (2006). Red blood cells express a functional endothelial nitric oxide synthase. *Blood* 107, 2943–2951. doi: 10.1182/blood-2005-10-3992

Koppenol, W. H. (2012). Nitrosation, thiols, and hemoglobin: energetics and kinetics. *Inorg. Chem.* 51, 5637–5641. doi: 10.1021/ic202561f

Kozlov, A. V., Staniek, K., and Nohl, H. (1999). Nitrite reductase activity is a novel function of mammalian mitochondria. *FEBS Lett.* 454, 127–130. doi: 10.1016/S0014-5793(99)00788-7

Lacza, Z., Pankotai, E., Csordas, A., Gero, D., Kiss, L., Horvath, E. M., et al. (2006). Mitochondrial, N. O., and reactive nitrogen species production: does mtNOS exist? *Nitric Oxide* 14, 162–168. doi: 10.1016/j.niox.2005.05.011

Lamkin-Kennard, K. A., Buerk, D. G., and Jaron, D. (2004a). Interactions between NO and $O_2$ in the microcirculation: a mathematical analysis. *Microvasc. Res.* 68, 38–50. doi: 10.1016/j.mvr.2004.03.001

Lamkin-Kennard, K. A., Jaron, D., and Buerk, D. G. (2004b). Impact of the fahraeus effect on NO and $O_2$ biotransport: a computer model. *Microcirculation* 11, 337–349. doi: 10.1080/10739680490437496

Li, H., Cui, H., Kundu, T. K., Alzawahra, W., and Zweier, J. L. (2008). Nitric oxide production from nitrite occurs primarily in tissues not in the blood: critical role of xanthine oxidase and aldehyde oxidase. *J. Biol. Chem.* 283, 17855–17863. doi: 10.1074/jbc.M801785200

Liu, T., Schroeder, H. J., Wilson, S. M., Terry, M. H., Romero, M., Longo, L. D., et al. (2016). Local and systemic vasodilatory effects of low molecular weight S-nitrosothiols. *Free Radic. Biol. Med.* 91, 215–223. doi: 10.1016/j.freeradbiomed.2015.12.009

Liu, Y., Buerk, D. G., Barbee, K. A., and Jaron, D. (2016). A mathematical model for the role of $N_2O_3$ in enhancing nitric oxide bioavailability following nitrite infusion. *Nitric Oxide* 60, 1–9. doi: 10.1016/j.niox.2016.08.003

Liu, Y., Buerk, D. G., Barbee, K. A., and Jaron, D. (2017). Nitric oxide release by deoxymyoglobin nitrite reduction during cardiac ischemia: a mathematical model. *Microvasc. Res.* 112, 79–86. doi: 10.1016/j.mvr.2017.03.009

Lloyd, N. L. (1957). A new kit for sodium nitrite-thiosulphate therapy in the treatment of acute cyanide poisoning. *Br. J. Ind. Med.* 14:137. doi: 10.1136/oem.14.2.137

MacArthur, P. H., Shiva, S., and Gladwin, M. T. (2007). Measurement of circulating nitrite and S-nitrosothiols by reductive chemiluminescence. *J. Chromatogr. B Analyt. Technol. Biomed. Life Sci.* 851, 93–105. doi: 10.1016/j.jchromb.2006.12.012

Maher, A. R., Milsom, A. B., Gunaruwan, P., Abozguia, K., Ahmed, I., Weaver, R. A., et al. (2008). Hypoxic modulation of exogenous nitrite-induced vasodilation in humans. *Circulation* 117, 670–677. doi: 10.1161/CIRCULATIONAHA.107.719591

Maia, L. B., and Moura, J. J. (2011). Nitrite reduction by xanthine oxidase family enzymes: a new class of nitrite reductases. *J. Biol. Inorg. Chem.* 16, 443–460. doi: 10.1007/s00775-010-0741-z

Maia, L. B., Pereira, V., Mira, L., and Moura, J. J. (2015). Nitrite reductase activity of rat and human xanthine oxidase, xanthine dehydrogenase, and aldehyde oxidase: evaluation of their contribution to NO formation *in vivo*. *Biochemistry* 54, 685–710. doi: 10.1021/bi500987w

Nagababu, E., Ramasamy, S., Abernethy, D. R., and Rifkind, J. M. (2003). Active nitric oxide produced in the red cell under hypoxic conditions by deoxyhemoglobin-mediated nitrite reduction. *J. Biol. Chem.* 278, 46349–46356. doi: 10.1074/jbc.M307572200

Neild, T. O. (1989). Measurement of arteriole diameter changes by analysis of television images. *Blood Vessels* 26, 48–52.

Okamoto, K., Eger, B. T., Nishino, T., Kondo, S., Pai, E. F., and Nishino, T. (2003). An extremely potent inhibitor of xanthine oxidoreductase. crystal structure of the enzyme-inhibitor complex and mechanism of inhibition. *J. Biol. Chem.* 278, 1848–1855. doi: 10.1074/jbc.M208307200

Omar, S. A., Webb, A. J., Lundberg, J. O., and Weitzberg, E. (2016). Therapeutic effects of inorganic nitrate and nitrite in cardiovascular and metabolic diseases. *J. Intern. Med.* 279, 315–336. doi: 10.1111/joim.12441

Piknova, B., Park, J. W., Swanson, K. M., Dey, S., Noguchi, C. T., and Schechter, A. N. (2015). Skeletal muscle as an endogenous nitrate reservoir. *Nitric Oxide* 47, 10–16. doi: 10.1016/j.niox.2015.02.145

Pinder, A. G., Pittaway, E., Morris, K., and James, P. E. (2009). Nitrite directly vasodilates hypoxic vasculature via nitric oxide-dependent and -independent pathways. *Br. J. Pharmacol.* 157, 1523–1530. doi: 10.1111/j.1476-5381.2009.00340.x

Pinotti, A., Graiver, N., Califano, A., and Zaritzky, N. (2002). Diffusion of nitrite and nitrate salts in pork tissue in the presence of sodium chloride. *J. Food Sci.* 67, 2165–2171. doi: 10.1111/j.1365-2621.2002.tb09521.x

Pluta, R. M., Oldfield, E. H., Bakhtian, K. D., Fathi, A. R., Smith, R. K., Devroom, H. L., et al. (2011). Safety and feasibility of long-term intravenous sodium nitrite infusion in healthy volunteers. *PLoS ONE* 6:e14504. doi: 10.1371/journal.pone.0014504

Ray, R., and Shah, A. M. (2005). NADPH oxidase and endothelial cell function. *Clin. Sci.* 109, 217–226. doi: 10.1042/CS20050067

Reichert, E. T., and Mitchell, S. W. (1880). On the physiological action of potassium nitrite. *Am. J. Med. Sci.* 156, 158–180. doi: 10.1097/00000441-188007000-00011

Rong, Z., Alayash, A. I., Wilson, M. T., and Cooper, C. E. (2013a). Modulating hemoglobin nitrite reductase activity through allostery: a mathematical model. *Nitric Oxide* 35, 193–198. doi: 10.1016/j.niox.2013.10.007

Rong, Z., Wilson, M. T., and Cooper, C. E. (2013b). A model for the nitric oxide producing nitrite reductase activity of hemoglobin as a function of oxygen saturation. *Nitric Oxide* 33, 74–80. doi: 10.1016/j.niox.2013.06.008

Rosenbaek, J. B., Al Therwani, S., Jensen, J. M., Mose, F. H., Wandall-Frostholm, C., Pedersen, E. B., et al. (2017). Effect of sodium nitrite on renal function and sodium and water excretion and brachial and central blood pressure in healthy subjects: a dose-response study. *Am. J. Physiol. Renal. Physiol.* 313, F378–F387. doi: 10.1152/ajprenal.00400.2016

Salgado, M. T., Cao, Z., Nagababu, E., Mohanty, J. G., and Rifkind, J. M. (2015). Red blood cell membrane-facilitated release of nitrite-derived nitric oxide bioactivity. *Biochemistry* 54, 6712–6723. doi: 10.1021/acs.biochem.5b00643

Shiva, S., Huang, Z., Grubina, R., Sun, J., Ringwood, L. A., MacArthur, P. H., et al. (2007). Deoxymyoglobin is a nitrite reductase that generates nitric oxide and regulates mitochondrial respiration. *Circ. Res.* 100, 654–661. doi: 10.1161/01.RES.0000260171.52224.6b

Singel, D. J., and Stamler, J. S. (2005). Chemical physiology of blood flow regulation by red blood cells: the role of nitric oxide and S-nitrosohemoglobin. *Annu. Rev. Physiol.* 67, 99–145. doi: 10.1146/annurev.physiol.67.060603.090918

Smith, R. P., and Gosselin, R. E. (1979). Hydrogen sulfide poisoning. *J. Occup. Med.* 21, 93–97. doi: 10.1097/00043764-197902000-00008

Sprague, R. S., Stephenson, A. H., and Ellsworth, M. L. (2007). Red not dead: signaling in and from erythrocytes. *Trends Endocrinol. Metab.* 18, 350–355. doi: 10.1016/j.tem.2007.08.008

Totzeck, M., Hendgen-Cotta, U. B., Kelm, M., and Rassaf, T. (2014). Crosstalk between nitrite, myoglobin and reactive oxygen species to regulate vasodilation under hypoxia. *PLoS ONE* 9:e105951. doi: 10.1371/journal.pone.0105951

Totzeck, M., Hendgen-Cotta, U. B., Luedike, P., Berenbrink, M., Klare, J. P., Steinhoff, H. J., et al. (2012). Nitrite regulates hypoxic vasodilation via myoglobin-dependent nitric oxide generation. *Circulation* 126, 325–334. doi: 10.1161/CIRCULATIONAHA.111.087155

Tu, C., Mikulski, R., Swenson, E. R., and Silverman, D. N. (2009). Reactions of nitrite with hemoglobin measured by membrane inlet mass spectrometry. *Free Radic. Biol. Med.* 46, 14–19. doi: 10.1016/j.freeradbiomed.2008.09.016

van Faassen, E. E., Bahrami, S., Feelisch, M., Hogg, N., Kelm, M., Kim-Shapiro, D. B., et al. (2010). Nitrite as regulator of hypoxic signaling in mammalian physiology. *Med. Res. Rev.* 29, 683–741. doi: 10.1002/med.20151

Webb, A. J., Milsom, A. B., Rathod, K. S., Chu, W. L., Qureshi, S., Lovell, M. J., et al. (2008). Mechanisms underlying erythrocyte and endothelial nitrite reduction to nitric oxide in hypoxia: role for xanthine oxidoreductase and endothelial nitric oxide synthase. *Circ. Res.* 103, 957–964. doi: 10.1161/CIRCRESAHA.108.175810

Weidert, E. R., Schoenborn, S. O., Cantu-Medellin, N., Choughule, K. V., Jones, J. P., and Kelley, E. E. (2014). Inhibition of xanthine oxidase by the aldehyde oxidase inhibitor raloxifene: implications for identifying molybdopterin nitrite reductases. *Nitric Oxide* 37, 41–45. doi: 10.1016/j.niox.2013.12.010

Weiss, S., Wilkins, R. W., and Haynes, F. W. (1937). The nature of circulatory collapse induced by sodium nitrite. *J. Clin. Invest.* 16, 73–84. doi: 10.1172/JCI100840

Wilkins, R. W., Haynes, F. W., and Weiss, S. (1937). The role of the venous system in circulatory collapse induced by sodium nitrite. *J. Clin. Invest.* 16, 85–91. doi: 10.1172/JCI100841

**Conflict of Interest Statement:** The authors declare that the research was conducted in the absence of any commercial or financial relationships that could be construed as a potential conflict of interest.

*Copyright © 2017 Buerk, Liu, Zaccheo, Barbee and Jaron. This is an open-access article distributed under the terms of the Creative Commons Attribution License (CC BY). The use, distribution or reproduction in other forums is permitted, provided the original author(s) or licensor are credited and that the original publication in this journal is cited, in accordance with accepted academic practice. No use, distribution or reproduction is permitted which does not comply with these terms.*

frontiers in Physiology

ORIGINAL RESEARCH
published: 29 November 2017
doi: 10.3389/fphys.2017.00963

# Near-Wall Migration Dynamics of Erythrocytes *in Vivo*: Effects of Cell Deformability and Arteriolar Bifurcation

*Bumseok Namgung*[1,2], *Yan Cheng Ng*[1,3], *Hwa Liang Leo*[1], *Joseph M. Rifkind*[4] *and Sangho Kim*[1,2,3]*

[1] *Department of Biomedical Engineering, National University of Singapore, Singapore, Singapore,* [2] *Biomedical Institute for Global Health Research and Technology, National University of Singapore, Singapore, Singapore,* [3] *NUS Graduate School for Integrative Sciences and Engineering, National University of Singapore, Singapore, Singapore,* [4] *Department of Anesthesiology and Critical Care Medicine, Johns Hopkins Medicine, Baltimore, MD, United States*

Red blood cell (RBC) deformability has a significant impact on microcirculation by affecting cell dynamics. Despite previous studies that have demonstrated the margination of rigid cells and particles *in vitro*, little information is available on the *in vivo* margination of deformability-impaired RBCs under physiological flow and hematocrit conditions. Thus, in this study, we examined how the deformability-dependent, RBC migration alters the cell distribution under physiological conditions, particularly in arteriolar network flows. The hardened RBCs (*h*RBCs) were found to preferentially flow near the vessel walls of small arterioles (diameter = 47.1–93.3 μm). The majority of the *h*RBCs (63%) were marginated within the range of 0.7*R*-0.9*R* (*R*: radial position normalized by vessel radius), indicating that the *h*RBCs preferentially accumulated near the vessel walls. The laterally marginated *h*RBCs maintained their lateral positions near the walls while traversing downstream with attenuated radial dispersion. In addition, the immediate displacement of RBCs while traversing a bifurcation also contributes to the near-wall accumulation of *h*RBCs. The notable difference in the inward migration between the marginated *n*RBCs and *h*RBCs after bifurcations further supports the potential role of bifurcations in the accumulation of *h*RBCs near the walls.

**Keywords: hemodynamics, microcirculation, bifurcation flow, RBC deformability, RBC margination**

OPEN ACCESS

***Edited by:***
*John D. Imig,*
*Medical College of Wisconsin,*
*United States*

***Reviewed by:***
*Daniel Goldman,*
*University of Western Ontario, Canada*
*Timothy W. Secomb,*
*University of Arizona, United States*

***Correspondence:**
*Sangho Kim*
*bieks@nus.edu.sg*

***Specialty section:***
*This article was submitted to Vascular Physiology, a section of the journal Frontiers in Physiology*

***Received:*** *30 August 2017*
***Accepted:*** *13 November 2017*
***Published:*** *29 November 2017*

***Citation:***
*Namgung B, Ng YC, Leo HL, Rifkind JM and Kim S (2017) Near-Wall Migration Dynamics of Erythrocytes in Vivo: Effects of Cell Deformability and Arteriolar Bifurcation. Front. Physiol. 8:963. doi: 10.3389/fphys.2017.00963*

## INTRODUCTION

At physiological levels of hematocrit (35–45%), red blood cells (RBCs) are continuously subjected to inter-cellular collisions in the microvascular network. Accordingly, alterations in RBC aggregation and deformability are expected to lead to a substantial modification in the distribution of RBCs over the microvascular network. In previous studies, a pathological elevation of RBC aggregation has been shown to result in the formation of a thicker cell-free layer (CFL) near the vessel wall (Ong et al., 2011), which can promote a plasma-skimming effect (Fung, 1973) resulting in a reduction in microvascular perfusion (Namgung et al., 2015).

In addition, RBC deformability is a key physical determinant in the distribution of RBCs in the microcirculation. Normal RBCs are highly deformable and thus able to travel through capillaries even narrower than their diameter. A pathological decrease in RBC deformability, however, leads

to an elevation in the peripheral vascular resistance and consequently a decrease in the tissue perfusion (Simchon et al., 1987). Moreover, RBC deformability is an important factor determining the sequestration of the aged RBCs in the spleen (MacDonald et al., 1987; Mebius and Kraal, 2005) as well as affecting the shear-dependent behavior of blood viscosity (Chien, 1987). The clinical significance of RBC deformability has long been highlighted (Weed, 1970; Chien, 1987; Mokken et al., 1992) in many diseases such as sepsis (Condon et al., 2003), malaria infected blood (Dondorp et al., 2000, 2002), and in prolonged storage of blood (Haradin et al., 1969; Stuart and Nash, 1990).

Despite the clinical significance of RBC deformability, there exists limited information of its potential effects on cell migration in the microcirculation. A previous *in vitro* study, Hou et al. (2010) reported the outward lateral migration (margination) of less deformable malaria-infected RBCs toward the channel walls. It was further highlighted that an elevation in hematocrit promoted the cell–cell interaction between the normal and less-deformable RBCs, which leads to an enhanced displacement of the malaria-infected cells toward the walls (Hou et al., 2010). In addition, a recent *in vivo* study, Lee et al. (2013) showed that ∼70% of rigid particles (diameter = 1 μm) infused into mice preferentially accumulated near the vessel walls ($0.8R-1.0R$, $R$: normalized radial position by vessel radius) in small vessels (diameter = 15–30 μm). It was also demonstrated that less deformable (stiff) particles were increasingly localized near the walls, whereas deformable (floppy) particles had enhanced hydrodynamic migration away from the walls resulting in their accumulation near the center of the vessel (Kumar and Graham, 2012a,b).

Such redistribution of RBCs would lead to local hematocrit changes. This could consequently influence the plasma-skimming effect and hematocrit partitioning in bifurcations (Schmid-Schonbein et al., 1980; Pries et al., 1989; Enden and Popel, 1994; Barber et al., 2008; Li et al., 2012). In a previous *in vitro* study (Shevkoplyas et al., 2006), RBC perfusion in a microchannel network was found to be highly sensitive to RBC deformability. It was demonstrated that the attenuated plasma skimming effect in *h*RBCs eventually led to blockages of capillary channels (ID = 5 μm) and also a more heterogeneous distribution of RBCs in the microchannel network. Importantly, this could in turn alter the microvascular oxygen and metabolite distributions as well as the effective viscosity of blood in the microvessels (Pries et al., 1996).

Consecutive multiple branching of the microvasculature is an essential morphological feature, which allows extensive perfusion to all peripheral tissue regions. This *in vivo* bifurcation have a major impact on flow patterns through the microcirculation. The impact of the arteriolar network is indicated by the finding that the travel distance required for less deformable RBCs to show a distinct margination in a straight vessel (Hou et al., 2010) has been reported to be one (or two) order of magnitude greater than an inter-bifurcation distance in the arteriolar network (Pries et al., 1989; Kiani et al., 1993; Ong et al., 2012). In this study, we examined how the diverging structure of the arteriolar networks contribute to the disparity in the migration rates of deformable and rigid RBCs toward the flow center. The radial distribution of chemically-hardened RBCs (*h*RBCs) was quantified *in vivo* after their infusion into the rat circulatory system. The contribution of bifurcations was examined using *in vitro* microchannel studies to further examine the suspension characteristics of the *h*RBCs in the presence of bifurcations.

# METHODS

## Animal Preparation

All animal handling procedures were in accordance with *National University of Singapore Institutional Animal Care and Use Committee Guidelines and Ethics on Animal Experimentation* (approved protocol no. R15-0225). A total of six male rats (Sprague-Dawley) weighing 183 ± 27 g were used for the *in vivo* study. The animals were initially anesthetized with the ketamine (37.5 mg/mL) and xylazine (5 mg/mL) cocktail (2 mL/kg) through intraperitoneal injection. The surgery was performed on a heating pad while maintaining the body temperature at 37°C. The animal was tracheotomized to assist breathing. The jugular vein was catheterized for the administration of additional anesthetic and dextran solutions. The femoral artery was catheterized for the withdrawal of blood sample and real-time pressure monitoring (Biopac TSD 104A, Goleta, USA). All catheters were heparinized with saline (30 IU/mL) solution to prevent blood clotting. The rat cremaster muscle was exteriorized to visualize arteriolar network flows. After the surgical exposure of the muscle, warm Plasma-Lyte A (35°C, pH 7.4; Baxter, USA) was continuously applied to the muscle to keep it moist. Nerves and blood supply were ensured to be remained intact. The muscle was then stretched and secured on a Plexiglas platform for the clear visualization of the desired blood vessels. The platform was fitted with two heating elements to maintain the muscle temperature at 35°C during the experiment. The muscle was then irrigated with the Plasma-Lyte A before covering it with a polyvinyl film (Saran, S. C. Johnson & Son, Singapore). At the end of the experiment, the animal was euthanized with an overdose of pentobarbital sodium.

## Microscopic Systems and Image Acquisition

After the surgical preparation, the rat was placed on the microscopic stage and left to stabilize over a period of ∼10 min. The arterial cannulation was connected to a physiological data-acquisition system (MP 100 System, BIOPAC Systems, USA) for continuous arterial pressure monitoring during the experiment. A straight arteriole [Inner diameter (ID) < 100 μm] located at least two vessel diameters away from the upstream bifurcation was selected for tracking labeled cells. All video recordings were taken with the criteria of a stable flow, clear image focus and good image contrast. An intravital microscope (BX51, Olympus, Japan) was used with a 40X water-immersion objective (LUMPlanFL 40xW, Olympus, Japan). Fluorescent images were acquired for 60 s, with a sCMOS fluorescent camera (Pco.edge, PCO AG, Kelheim, Germany) that provides the resolution of 512 by 512 (pixel by pixel) at 200 frame/s. All image analysis was performed with a custom-built MATLAB script (Mathworks, Natick, MA, USA).

## RBC Labeling and Hardening

Whole blood from a donor rat was withdrawn and transferred into a heparinized tube. The blood was then centrifuged at 2,500 g for 10 min (Sigma 2-6, Goettingen, Germany). The buffy coat and plasma were gently removed after the first centrifugation, and the remaining RBCs were washed three times more with 1X Phosphate Buffer Saline (PBS, pH 7.4, Life Technologies, CA, USA). Subsequently, the normal RBCs (*n*RBCs) were labeled with PKH-67 (PKH67 Green Fluorescent Cell Linker, Sigma-Aldrich, USA) at a final concentration of 2 μM. The labeling of RBCs with PKH-67 has been widely used in previous studies for reliable cell viability (Deplaine et al., 2011; Progatzky et al., 2013). The labeled RBCs were washed three times and hardened RBCs (*h*RBCs) were prepared by additionally incubating the cells in glutaraldehyde (GA) solution (Grade I, 25% in $H_2O$, Sigma-Aldrich, USA) at 1.0 mM for 30 min at room temperature. After the incubation, the cell mixture was washed three times with PBS and resuspended in saline (NaCl 0.9%, B. Braun, Melsungen, Germany) at the same hematocrit as that found in the recipient rat to maintain the total blood volume and the systemic hematocrit in the circulatory system after the exchange-transfusion. The GA-treated *h*RBCs were stored at 4°C before the RBC exchange. The deformability difference between the *n*RBCs and *h*RBCs was verified using a commercially available ektacytometer (RheoScan-D, RheoMeditech, Korea) that provides the elongation index (EI) defined by the ellipsoid diffraction pattern.

## Adjustment of RBC Aggregation and Exchange of *h*RBCs

To ascertain the hemorheological relevance to humans, the degree of rat blood aggregation was adjusted to levels seen in normal human blood. This was achieved by infusing a total of 200 mg/kg of Dextran 500 (Avg. MW = 450–550 kDa, Pharmacosmos A/S, Denmark) dissolved in saline into rats over the course of 1–2 min to obtain plasma-dextran concentrations of ∼0.63% in the rat blood (Ong et al., 2011). The level of RBC aggregation (M-index) was determined with an optical aggregometer (Myrenne Aggregometer MA-1, Myrenne GmbH, Roetgen, Germany) at the stasis mode (M0). The dextran concentration used in this study induced aggregating conditions to that found in normal human blood ($M = 12$–$16$) (Ong et al., 2011; Namgung and Kim, 2014).

Whole blood in the recipient rat was exchange-transfused with the *h*RBCs. The target volume of *h*RBCs for the exchange was ∼10% of the total RBC population by assuming that the total blood volume of the rat is 5.5% of its body weight (Bishop et al., 2001). The target volume of whole blood was first withdrawn from the femoral artery before the infusion of the *h*RBCs. Immediately after the withdrawal, the *h*RBCs were infused at ∼100 μL/min via the jugular vein (Cabrales et al., 2005).

A blood sample (<0.1 mL) was withdrawn from the femoral artery for hematocrit and aggregation measurements. Hematocrit was determined with a microhematocrit centrifuge (Sigma 1–14 Microcentrifuge, Sigma, Germany). All the blood sample measurements were repeated before and 15-min after the dextran infusion and *h*RBC exchange.

## Determination of *h*RBCs Radial Position

To determine the radial position of the *h*RBCs in the equatorial plane of the vessel, a previously reported approach (Bishop et al., 2001) was adopted in this study (**Figure 1A**). Random scattered noise in the image was minimized with a median filter for better detection of the fluorescent-labeled *h*RBCs. The labeled cells in an 8-μm section (cells in focus) showed a clear and sharp transition of intensity profile from dark to white. Based on this criterion, we differentiated between cells in and out of focus. The radial position of the cells ($R$) was defined at the center of the cell width normalized by the vessel radius (**Figure 1B**), where $R$ ranges from 0 (flow center) to 1 (vessel wall). Since the radial position of the cells was determined at the center of cells (**Figure 1B**), it is noted that the radial position of cells adjacent to the wall cannot be $1.0R$ in our results.

## *In Vitro* Microchannel Study

*In vitro* microchannels were fabricated with polydimethylsiloxane (PDMS, Dow Corning, MI) by the standard soft lithography and replica molding techniques. The detailed design of the microchannel is depicted in Supplementary Figure S1. The labeled target RBCs (*n*RBC or *h*RBC) were suspended in the PBS-dextran solution (∼0.63%) to simulate the *in vivo* aggregating condition, and then flowed in the microchannel at 1% hematocrit. To initialize the lateral position of the target RBCs at the outer wall of the main branch, a sheath RBC fluid (*n*RBCs at 40% hematocrit in the PBS-dextran solution) was introduced from another inlet. The lateral positions ($L$) of the target RBCs were analyzed at every $5D$ before (from $-50D_m$ to $0D_m$) and after the bifurcation [from $0D_d$ to $25D_d$) ($D$: travel distance along microchannel normalized by the channel width of the main (m) or daughter (d) channel]. The baselines of each branch segment ($0D_m$ or $0D_d$) were determined at the end of the filleted corners (see Supplementary Figure S1). The inlet flow rates for the target RBCs and the sheath fluid were controlled using a syringe pump (KDS210, KD Scientific, Holliston, MA) at 1 and 2.6 μL/min, respectively.

## Statistical Analysis and Data Presentation

A statistical software package (Prism 6.0, GraphPad) was used for all statistical analyses. Two-tailed unpaired $t$-tests were performed to determine the statistical difference between two groups. All physiological and rheological values were represented as means ± SD. The analysis of covariance (ANCOVA) was performed to determine the difference between two slopes is significant. $p < 0.05$ was considered statistically significant.

# RESULTS

## Systemic Parameters and RBC Deformability

No statistical difference was found in the systemic parameters (MAP, ID, PSR, Hct and M-value) before and after the exchange of *h*RBCs as presented in **Table 1**. The *h*RBCs were consistently less deformable than *n*RBCs over a wide range of shear stresses ($\tau$

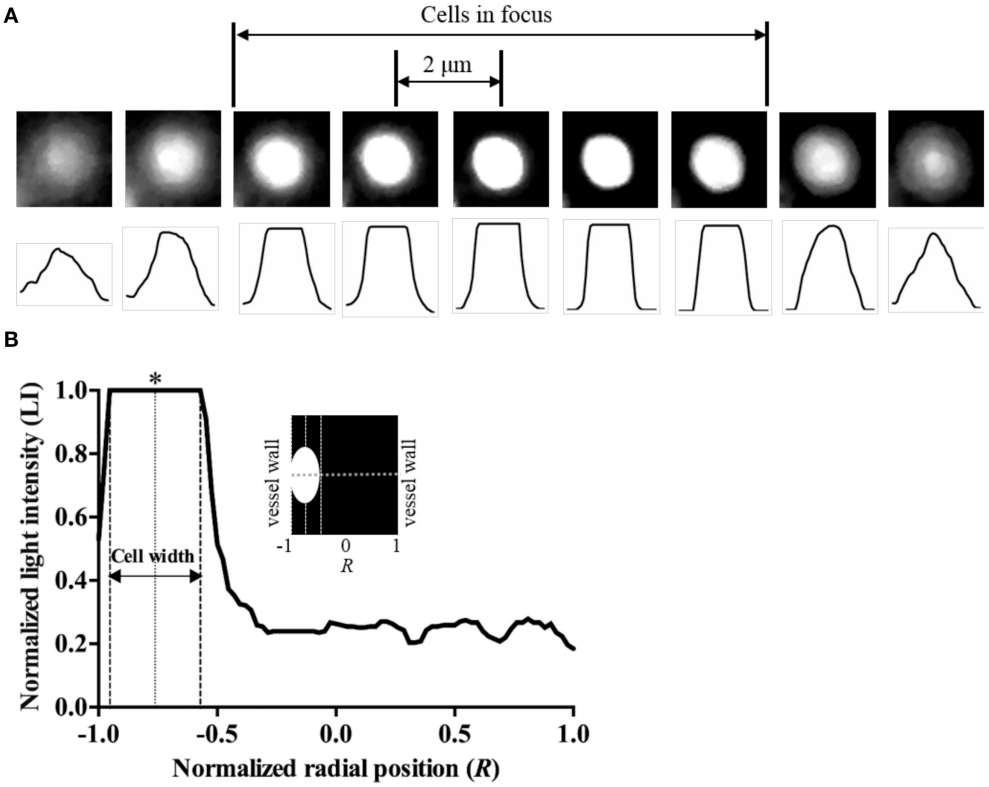


**FIGURE 1 |** Determination of radial position of cells. **(A)** Microscopic images of a labeled *h*RBC in stasis condition and corresponding line intensity profiles with 2-μm vertical shifts of the microscope stage. **(B)** Typical light intensity profile across the vessel with a RBC flowing near the vessel wall. Radial position of the cell was determined at the center of the cell width (marked as *).

**TABLE 1 |** Systemic parameters.

| *h*RBCs exchange | MAP (mmHg) | ID (μm) | PSR ($s^{-1}$) | Hct (%) | *M*-value |
|---|---|---|---|---|---|
| Before | 94 ± 17 | 76 ± 16 | 63 ± 17 | 42 ± 1.0 | 13.8 ± 2.5 |
| After | 93 ± 19 | 75 ± 17 | 52 ± 9 | 41 ± 1.0 | 13.2 ± 1.8 |

*Values are in mean ± SD. MAP, mean arterial pressure; ID, inner diameter of vessel; PSR, pseudoshear rate (mean velocity / ID); Hct, hematocrit; M-value, aggregation index.*

= 0.5–20 Pa) as shown in **Figure 2**. Thus, the GA treatment used in this study resulted in a noticeable reduction in EI by 35% at $\tau$ = 0.5 Pa and 5.6% at $\tau$ = 20 Pa.

## Radial Distribution and Migration of *h*RBCs *in Vivo*

**Figure 3A** shows a typical example of *h*RBC flow in an arteriole. The two *h*RBCs maintained their radial positions near the opposite walls of the vessel during the flow. We analyzed a total of 112 *h*RBCs for their radial locations (**Figure 3B**). The non-linear regression curve clearly shows that ∼28% (at the maximum peak) of the *h*RBCs were flowing at the radial position of 0.8*R*. Furthermore, the majority of the *h*RBCs (63%)

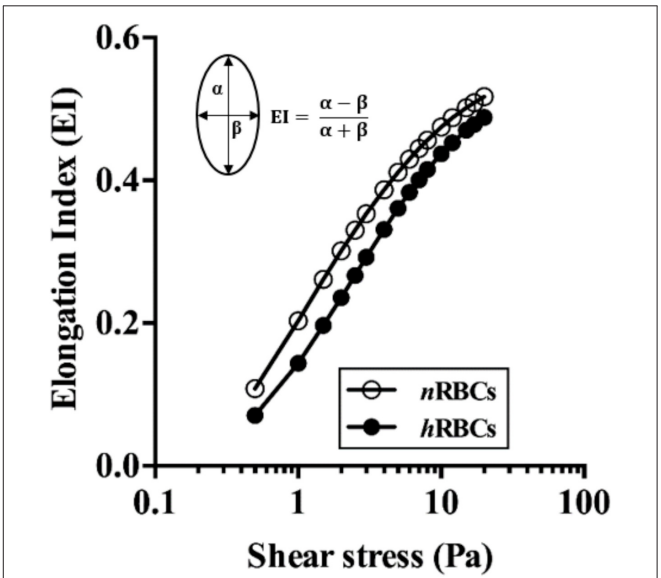


**FIGURE 2 |** Deformability of *n*RBCs and *h*RBCs. EI is defined by major ($\alpha$) and minor ($\beta$) axes of ellipsoid diffraction pattern from the ekatacytometer. Standard deviation was too small to be noticed ($n$ = 4).

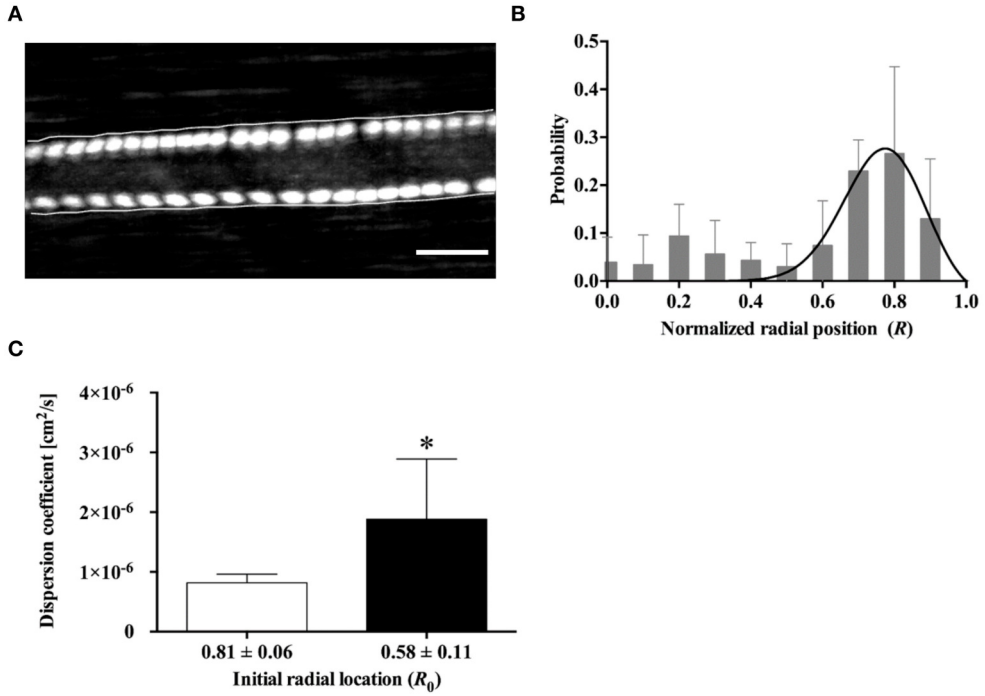


**FIGURE 3 |** Radial distribution of *h*RBCs *in vivo*. **(A)** Fluorescent image of two labeled *h*RBCs flowing near the vessel walls in an arteriole (ID = 55.1 ± 2.9 μm, averaged along longitudinal direction). The overlaid cell trajectory image was obtained by continuously taking the maximum intensity of the consecutive images of cell flow (cumulative maximum intensity image). Scale bar = 50 μm. **(B)** Probability distribution for the radial position of *h*RBCs (A total of 112 cells were analyzed from six different vessels). A solid line represent a hyperbolic regression fit for experimental data ($y = a{\cdot}\tanh(1-x){\cdot}\text{sech}^b\,(x-c)$ where $a = 1.443$, $b = 62.23$, $c = 0.8431$; $R^2 = 0.4$). **(C)** Dispersion coefficient of *h*RBCs at $R_0 = 0.81$ and $R_0 = 0.58$ ($n = 7$); $^*p < 0.05$.

were marginated within the range of $0.7R{-}0.9R$, indicating that the *h*RBCs preferentially accumulated near the vessel walls.

In addition, the radial dispersion of the *h*RBCs was examined based on the initial locations ($R_0$) of the cells by tracking their trajectories along the vessel. To provide a quantitative description on the dispersion of the cells, a dispersion coefficient ($D_{\text{RBC}}$) of the *h*RBCs was determined: $D_{\text{RBC}} = \Delta R^2 \,/\, 2\Delta t$, where $\Delta R$ represents a radial displacement during a given time interval ($\Delta t$) (Bishop et al., 2002). It was observed that *h*RBCs initially located near the vessel wall ($R_0 = 0.81$) showed a significantly ($p < 0.05$) lower $D_{\text{RBC}}$ than those located away from the wall ($R_0 = 0.58$) (**Figure 3C**).

## Immediate Margination of *h*RBCs at a Bifurcation *in Vivo*

The trajectory of the *h*RBCs was additionally examined along the upstream section of an arteriolar bifurcation, particularly at the inner vessel wall near the bifurcating point. We found that the *h*RBCs exhibited an abrupt shift in their radial positions immediately after the bifurcation (**Figure 4A**). Specifically, the *h*RBC, initially located near the center ($0R$) of the parent vessel and aligned with the bifurcating point, seemed to be relocated at the wall ($0.75R$) of the downstream daughter vessel (**Figure 4B**). This is expected since the cells near the center streamline of the parent vessel eventually coincide with the apex of the bifurcation, thus leading to their repositioning near the vessel wall.

## Disparity in Inward Migration of *n*RBCs and *h*RBCs at a Bifurcation

For comparison of migration tendencies between *n*RBCs and *h*RBC, an *in vitro* microchannel study was performed to overcome the technical limitations of our *in vivo* study including the limited field of view for tracking target cells and the limited tracking time due to photo bleaching. Particularly, to further elucidate the flow dynamics of the marginated RBCs (*n*RBCs and *h*RBCs) at a bifurcation, a Y-bifurcation microchannel was used to examine the difference in the inward migration of the laterally displaced RBCs (Supplementary Figure S1). No discernible difference was observed between the migration of *n*RBCs and *h*RBCs from $-50D_{\text{m}}$ to $0\ D_{\text{m}}$ in the main channel (**Figure 5A**). Moreover, both the laterally displaced *n*RBCs and *h*RBCs did not exhibit any statistically significant inward migration despite the long travel distance in the straight region of the microchannel.

Interestingly, as the target RBCs traverse through the bifurcation from $0D_{\text{m}}$ to $0D_{\text{d}}$ (**Figure 5B**), they exhibited a slight, but significant ($p < 0.0001$) inward migration toward the flow center regardless of the cell rigidity (*n*RBC: $0.86L \rightarrow 0.82L$, *h*RBCs: $0.87L \rightarrow 0.83L$). However, the difference in the lateral position between *n*RBCs and *h*RBCs at $0D_{\text{d}}$ progressively

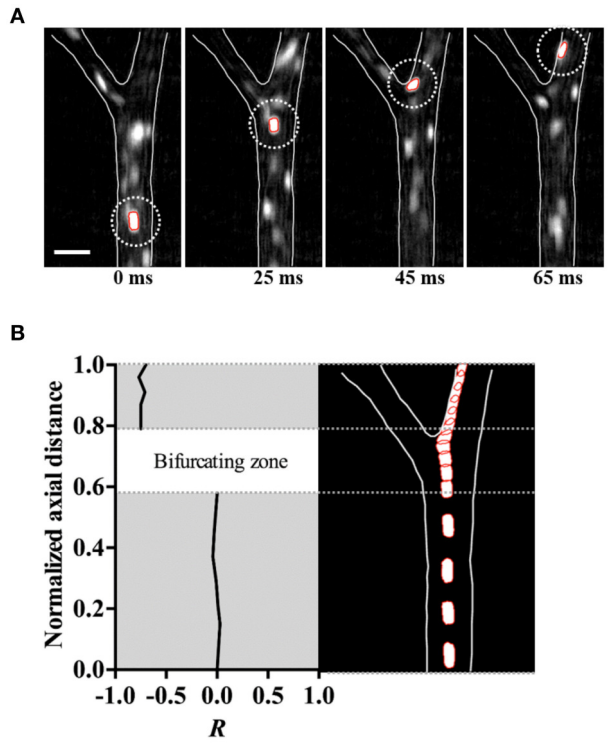


**FIGURE 4 |** Immediate margination of *h*RBC. **(A)** Consecutive *in vivo* images of *h*RBC (white dotted circle) flowing over 65 ms in an arteriole (ID = 50.2 ± 1.5 μm). Scale bar = 50 μm. **(B)** Normalized radial position (*R*) (left) and trajectory (right) of *h*RBC in **(A)**.

increased along the daughter branch (**Figure 5C**). In particular, the lateral position of the *n*RBCs (0.82*L*) was ∼20% farther away from the outer wall than the *h*RBCs (0.66*L*) at $25D_d$. Accordingly, the inward migration tendency of *n*RBCs was significantly greater than that of the *h*RBCs ($p < 0.0001$) after the bifurcation. Similar to our *in vivo* observations in this study (**Figure 3B**), the *h*RBCs persistently retained their lateral positions near the wall. It is also noteworthy that the lateral position of the *h*RBCs (0.82*L*) at $25D_d$ falls within the range of the radial positions of the *h*RBCs observed *in vivo* (0.8*R*).

## DISCUSSION

In this study, rat RBCs were chemically hardened with glutaraldehyde (GA) solution (1.0 mM). GA is a non-specific protein cross-linker that induces cross-linking in all the components of the cell (cytosol, cytoskeleton, transmembrane) (Forsyth et al., 2010; Sosa et al., 2013), thus resulting in an overall increase in the RBC rigidity similar to a single-component solid particle. In the present study, the deformability of GA-treated RBCs (*h*RBCs) was consistently lower than that of the *n*RBCs based on the EI measured over the range of shear stresses (0.5-20 Pa). Previously, it was reported that the averaged wall shear stress in an arteriole (ID = 29.5–67.1 μm) of the rat cremaster muscle ranged from ∼0.3 (MAP = 47 ± 5.5 mmHg) to 7.5 Pa (108 ± 4.7 mmHg) (Namgung et al., 2011). Another study reported that the arteriolar wall shear stress (ID = 160–220 μm) ranged from 1.0 to 4.5 Pa under physiological flow conditions (Bakker et al., 2003). Thus, under such physiological ranges of shear stresses, the difference in RBC deformability found between the *h*RBCs and *n*RBCs (5.6–35% at $\tau$ = 25–0.5 Pa in **Figure 2**) could lead to alterations in the suspension characteristics, which in turn result in the preferential near-wall accumulation of *h*RBCs. However, it is of note that the EI-based measurement of the RBC deformability only indicates the ability of the cell to elongate. RBCs are in general subjected to various types of deformations (folding, bending, and elongating) while traversing the microvasculature. Therefore, the GA-induced decrease in the RBC deformability possibly results in a different suspension behavior as compared to that of the pathologically hardened RBCs in different diseases.

It has been known that in arteriolar flows, the formation of CFL near the vessel wall is due to the shear-induced inward migration of *n*RBCs toward the flow center and their accumulation in the core region. Previous computational studies (Pranay et al., 2012; Hariprasad and Secomb, 2014) demonstrated that the inward migration of cells (or elastic capsules) arises from fluid mechanical interactions between the cells and the vessel walls. Particularly for RBCs, their inward migration is enhanced by the tank-treading motion of their flexible membrane. In contrast, the outward migration is elicited mainly from shear-induced dispersions due to interactions between the cells (Pranay et al., 2012; Hariprasad and Secomb, 2014). In this study, the near-wall margination (outward migration) of *h*RBCs shown in **Figure 3B** could be attributed in part to the inward migration of *n*RBCs, which is similar to that reported for the margination of leukocytes (Freund, 2007; Munn and Dupin, 2008). The preferential margination of leukocytes to the vessel walls at a physiological level of hematocrit is mainly due to the continuous hydrodynamic collisions with neighboring flexible *n*RBCs (Schmid-Schönbein et al., 1980; Goldsmith and Spain, 1984). In addition, the relatively faster inward migration of the *n*RBCs also partly contributed to such a margination phenomenon (Goldsmith and Spain, 1984). The rotation of the deformable *n*RBC membrane around its center of mass (tank-treading motion) promotes the axial migration, which subsequently displaces it away from the vessel walls (Dupire et al., 2012). In contrast, *h*RBCs displayed an enhanced tumbling motion (Forsyth et al., 2010) resulting in a diminished tank–treading motion. This attenuation in the tank-treading motion of the *h*RBCs is expected to limit their inward migration toward the flow center.

The marginated *h*RBCs ($R_0 \rightarrow 1$) tended to maintain their radial positions with reduced radial dispersions (**Figures 3B,C**). In contrast, the significantly higher dispersion of *h*RBCs near the RBC core region ($R_0 \rightarrow 0.5$) implied that the cell–cell interaction was dominant in the region where the cells were more concentrated. Similarly, a previous *in vivo* study Lee et al. (2013) reported that the dispersion of rigid 1-μm particles in the blood stream was greatly reduced near the walls relative to the RBC core region. Although the marginated

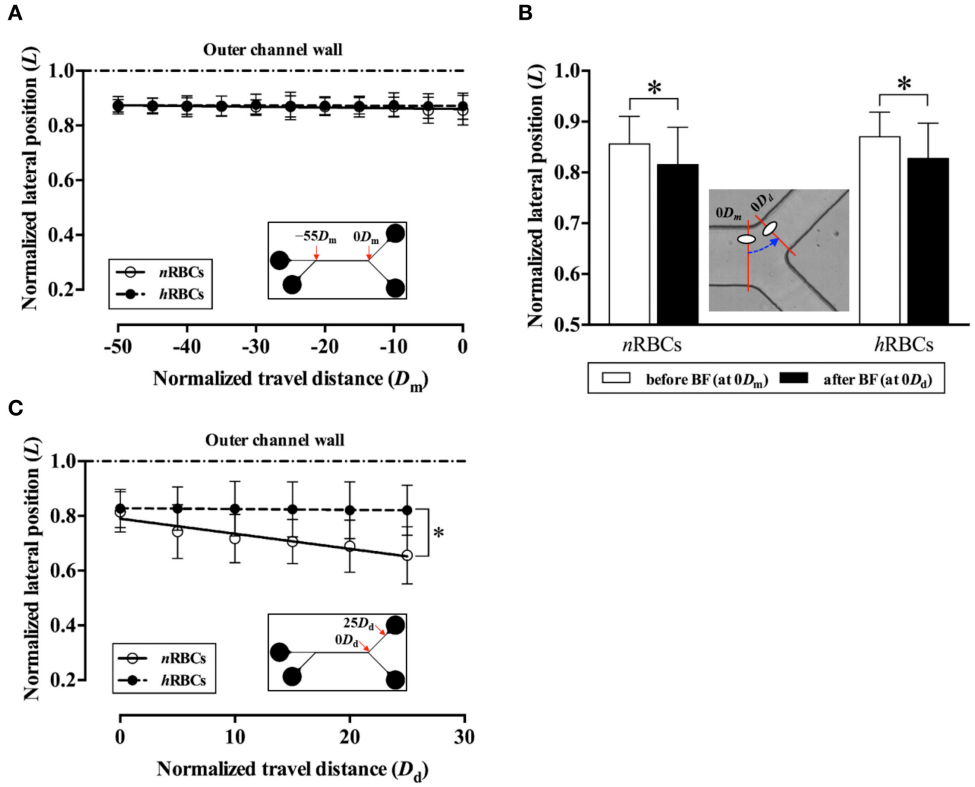


**FIGURE 5 |** Difference in migration dynamics between *n*RBCs and *h*RBCs across the bifurcation (BF) in the *in vitro* system. **(A)** Normalized lateral position ($L$) of the target RBCs in the main channel before the bifurcation. The lateral position ($L$) and travel distance ($D_m$) of the target RBCs were normalized by the half width ($w/2$) and the full width ($w$) of the channel, respectively. Each line (solid and dashed) represents a linear regression fit of the data. ($y = -2.8 \times 10^{-4}x + 0.86$; $R^2 = 0.61$ for *n*RBCs, $y = -0.44 \times 10^{-4}x + 0.87$; $R^2 = 0.17$ for *h*RBCs). **(B)** Normalized lateral position ($L$) of the target RBCs at $0D_m$ and $0D_d$ across the bifurcation. The dashed line with an arrow indicates the transit of RBC (*$p < 0.0001$). **(C)** Normalized lateral position ($L$) of the target RBCs in the daughter channel after the bifurcation. Each line (solid and dashed) represents a linear regression fit of the data. ($y = -5.51 \times 10^{-3}x + 0.79$; $R^2 = 0.90$ for *n*RBCs, $y = -0.30 \times 10^{-3}x + 0.83$; $R^2 = 0.91$ for *h*RBCs; *$p < 0.0001$; significant difference between two slopes). A total of 300 cells (150 *n*RBCs and 150 *h*RBCs) were analyzed for each data point.

*h*RBCs remained in contact with the boundary of the RBC core while flowing near the walls, they were unable to penetrate into the boundary. This suggests that the *h*RBCs were in an equilibrium position (Munn and Dupin, 2008). In addition, the attenuated deformability-dependent wall lift force experienced by the *h*RBCs potentially further contribute to the decreased radial dispersion near the wall. Accordingly, it was previously reported that deformable RBCs were affected by the lift force ranging from 31 to 155 pN at wall shear stresses between 0.2 to 1 Pa, whereas undeformed spherical leukocytes experienced zero lift force (Abkarian and Viallat, 2008).

It is important to note that the outward migration of *h*RBCs in a straight vessel requires a long travel distance to complete their near-wall margination induced by the hydrodynamic interaction with neighboring cells. A previous study Jain and Munn (2009) showed that the number of marginated leukocytes increased almost linearly with the length (up to 5 mm) of a rectangular microchannel with widths of 50 and 75 μm. A separate *in vitro* study, Hou et al. (2010) demonstrated the separation of malaria-infected RBCs (more rigid than *n*RBCs) based on their near-wall margination, which was achieved with an extreme channel ratio of 1: 2,000 (width: length). However, such extremely long and straight vessels are not observable in the microvasculature. The mean inter-bifurcation distance was reported to be approximately 5 to 33 vessel-diameter in arterioles (ID = 4–104 μm) of the rat cremaster muscle (Ong et al., 2012), rat mesenteric muscle (Pries et al., 1989) and hamster cremaster muscle (Kiani et al., 1993). Therefore, based on the previously proposed mechanism for the cell margination, the complete near-wall margination of *h*RBCs is not observed within the short inter-bifurcation distance in arteriolar network flows. A previous computational study, Müller et al. (2016) highlighted that rigid particles generally exhibit greater margination than soft particles. This could be explained by the increased lift force with correspondingly larger deformations that drives deformable particles away from the wall. Therefore, the elevation in rigidity of RBCs under pathological conditions would further increase their margination rate.

The immediate displacement of the RBCs at the inner vessel wall along the bifurcating point (**Figure 4**) seemed to

contribute to the near-wall margination of *h*RBCs observed *in vivo* (**Figure 3B**). This phenomenon is likely amplified by the multiple bifurcations present in the arteriolar networks, thus resulting in the enhanced accumulation of *h*RBCs near the vessel walls. Due to the limited field of view of our microscopic system, it was unfeasible to perform a quantitative analysis on the radial position of *h*RBCs in a series of bifurcations *in vivo*. However, it is expected that the marginated *h*RBCs maintain their radial positions near the walls due to the reduced dispersion after the bifurcation (**Figure 3C**). This is in good agreement with a previous numerical study, Takeishi et al. (2014) which showed that the margination of leukocytes was sustained by the continuous passing motion of the RBCs in the RBC core (Takeishi et al., 2014).

The RBCs flowing at the outer channel wall exhibited a sudden inward shift by ∼5% in their lateral locations (*n*RBC: $0.86L \rightarrow 0.82L$, *h*RBCs: $0.87L \rightarrow 0.83L$) immediately after the bifurcation (**Figure 5B**). This is likely due to a sudden local reduction in hematocrit adjacent to the outer wall which is induced by the asymmetric velocity profile developed at the bifurcation (Sherwood et al., 2014), resulting in thicker CFL formation near walls. The enhanced CFL formation at the outer wall (Ong and Kim, 2013) allows cells to migrate inward with minimal collisions with the neighboring cells. This was subsequently verified in our supplementary *in vitro* experiments using diluted RBC suspensions (Hct = 0.2%). The target RBCs in the diluted suspension showed a larger extent of sudden displacement away from the outer wall after the bifurcation (Supplementary Figure S2) as compared to the target RBCs in the concentrated suspension (**Figure 5B**). This strongly supports that the local reduction in hematocrit and the CFL formation near the outer wall at the bifurcation provide the marginal space for cells to exhibit an accelerated inward migration. Consequently, the *n*RBCs were able to cross the streamlines toward the flow center more effectively with a larger extent of deformation and tank-treading motions than the *h*RBCs. This becomes more apparent at physiological levels of hematocrit since the cell–cell interactions effectively attenuate the inward migration of *h*RBCs but not the *n*RBCs (**Figure 5C**).

The cumulative contribution of bifurcations to the accumulation of *h*RBCs near the vessel walls *in vivo* is depicted in **Figure 6**. In the blood flow, *h*RBCs located near the flow center are relocated to the inner wall ($H \rightarrow H'$) after a bifurcating point ($BF_1$). Due to their diminished inward migration, *h*RBCs maintain their lateral positions near the inner wall farther downstream until the next bifurcating point ($BF_2$), where the inner wall in the upstream vessel becomes the outer wall in the downstream vessel ($IW_1 \rightarrow OW_2$). As the *h*RBCs traverse through $BF_2$ ($H' \rightarrow H''$), they continue to remain their marginated positions along the walls. In contrast, laterally displaced *n*RBCs are able to migrate progressively toward the flow center ($N \rightarrow N' \rightarrow N''$) in the downstream vessels after a series of bifurcations. This is due to the enhanced inward migration of *n*RBCs as well as the sudden inward shift toward the flow center at the bifurcations as observed in the present study. The disparity in the migration between *n*RBC and *h*RBC across the bifurcations consequentially leads to the selective accumulation of *h*RBCs near the vessel walls.

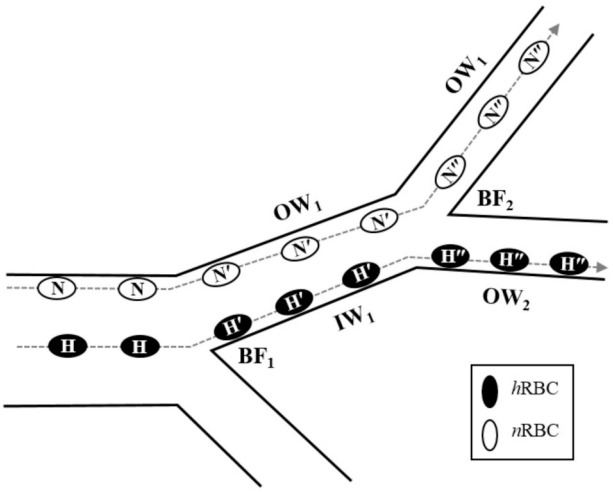


**FIGURE 6 |** Potential role of bifurcation in radial migration of *n*RBCs (N) and *h*RBCs (H). The dashed lines with arrows indicated the trajectories of each RBC. N′ and H′ represent the *n*RBCs and *h*RBCs after the 1st bifurcating point ($BF_1$) while N″ and H″ represent the *n*RBCs and *h*RBCs after the 2nd bifurcating point ($BF_2$), respectively. OW and IW stand for the outer and inner walls, respectively.

The near-wall accumulation of *h*RBCs could contribute to the decrease in the mean CFL width (Zhang et al., 2009). Under moderate RBC aggregation and a discharged hematocrit of ∼38%, the mean normalized CFL width was predicted to decrease from 0.269 to 0.152 due to the 20-time increase in RBC rigidity. Accordingly, the increase in membrane rigidity prevented large deformation and reduced the cell–cell contact area, thus resulting in the formation of a less dense RBC core and thinner CFL. Although a direct comparison between the previous study and our findings is limited due to the stark differences in the magnitude of cell rigidity and volume concentration of *h*RBCs used, the decreasing trend in the CFL width due to the hardening of RBCs would still be expected. Importantly, the reduction in the CFL width could lead to a myriad of physiological influences including flow resistance (Maeda et al., 1996; Zhang et al., 2009), oxygen delivery and nutrients exchange (Tateishi et al., 2001), as well as wall shear stress-dependent nitric oxide (NO) bioavailability (Vaughn et al., 1998; Ng et al., 2015).

## CONCLUSION

This study shows that a change in the overall RBC deformability significantly alters the distribution of the RBCs in arterioles. The laterally marginated *h*RBCs tend to maintain their lateral positions near the walls while traversing downstream with attenuated radial dispersion. Moreover, the immediate displacement of RBCs while traversing a bifurcation also contributes to the *in vivo* near-wall accumulation of *h*RBCs. The notable difference in the inward migration between the marginated *n*RBCs and *h*RBCs after the bifurcation further

supports the contribution of bifurcations to the accumulation of *h*RBCs near the walls.

## AUTHOR CONTRIBUTIONS

BN: Involved in study design, conducted *in vivo* experiments, analyzed the data and prepared the manuscript; YN: Conducted *in vitro* experiments, analyzed the data and revised the manuscript; HL: Verified results and revised the manuscript; JR: Verified results and revised the manuscript; SK: Designed and coordinated research, verified results and revised the manuscript.

## ACKNOWLEDGMENTS

This work was supported by National Medical Research Council (NMRC)/Cooperative Basic Research Grant (CBRG) No./0078/2014. The authors wish to thank Ms. Veena Salim for her expert technical assistance.

## SUPPLEMENTARY MATERIAL

The Supplementary Material for this article can be found online at: https://www.frontiersin.org/articles/10.3389/fphys.2017.00963/full#supplementary-material

## REFERENCES

Abkarian, M., and Viallat, A. (2008). Vesicles and red blood cells in shear flow. *Soft Matter*. 4, 653–657. doi: 10.1039/b716612e

Bakker, E. N. T. P., Versluis, J. P., Sipkema, P., VanTeeffelen, J. W. G. E., Rolf, T. M., Spaan, J. A. E., et al. (2003). Differential structural adaptation to haemodynamics along single rat cremaster arterioles. *J. Physiol.* 548(Pt 2), 549–555. doi: 10.1113/jphysiol.2002.035907

Barber, J. O., Alberding, J. P., Restrepo, J. M., and Secomb, T. W. (2008). Simulated two-dimensional red blood cell motion, deformation, and partitioning in microvessel bifurcations. *Ann. Biomed. Eng.* 36, 1690–1698. doi: 10.1007/s10439-008-9546-4

Bishop, J. J., Nance, P. R., Popel, A. S., Intaglietta, M., and Johnson, P. C. (2001). Effect of erythrocyte aggregation on velocity profiles in venules. *Am. J. Physiol. Heart Circ. Physiol.* 280, H222–H236. Available online at: http://ajpheart.physiology.org/content/280/1/H222

Bishop, J. J., Popel, A. S., Intaglietta, M., and Johnson, P. C. (2002). Effect of aggregation and shear rate on the dispersion of red blood cells flowing in venules. *Am. J. Physiol. Heart Circ. Physiol.* 283, H1985–H1996. doi: 10.1152/ajpheart.00888.2001

Cabrales, P., Tsai, A. G., Winslow, R. M., and Intaglietta, M. (2005). Effects of extreme hemodilution with hemoglobin-based $O_2$ carriers on microvascular pressure. *Am. J. Physiol. Heart Circ. Physiol.* 288, H2146–H2153. doi: 10.1152/ajpheart.00749.2004

Chien, S. (1987). Red cell deformability and its relevance to blood flow. *Annu. Rev. Physiol.* 49, 177–192. doi: 10.1146/annurev.ph.49.030187.001141

Condon, M. R., Kim, J. E., Deitch, E. A., Machiedo, G. W., and Spolarics, Z. (2003). Appearance of an erythrocyte population with decreased deformability and hemoglobin content following sepsis. *Am. J. Physiol. Heart Circ. Physiol.* 284, H2177–H2184. doi: 10.1152/ajpheart.01069.2002

Deplaine, G., Safeukui, I., Jeddi, F., Lacoste, F., Brousse, V., Perrot, S., et al. (2011). The sensing of poorly deformable red blood cells by the human spleen can be mimicked *in vitro*. *Blood* 117, e88–e95. doi: 10.1182/blood-2010-10-312801

Dondorp, A. M., Kager, P. A., Vreeken, J., and White, N. J. (2000). Abnormal blood flow and red blood cell deformability in severe malaria. *Parasitol. Today* 16, 228–232. doi: 10.1016/S0169-4758(00)01666-5

Dondorp, A. M., Nyanoti, M., Kager, P. A., Mithwani, S., Vreeken, J., and Marsh, K. (2002). The role of reduced red cell deformability in the pathogenesis of severe falciparum malaria and its restoration by blood transfusion. *Trans. R. Soc. Trop. Med. Hyg.* 96, 282–286. doi: 10.1016/S0035-9203(02)90100-8

Dupire, J., Socol, M., and Viallat, A. (2012). Full dynamics of a red blood cell in shear flow. *Proc. Natl. Acad. Sci. U.S.A.* 109, 20808–20813. doi: 10.1073/pnas.1210236109

Enden, G., and Popel, A. S. (1994). A numerical study of plasma skimming in small vascular bifurcations. *J. Biomech. Eng.* 116, 79–88. doi: 10.1115/1.2895708

Forsyth, A. M., Wan, J., Ristenpart, W. D., and Stone, H. A. (2010). The dynamic behavior of chemically "stiffened" red blood cells in microchannel flows. *Microvasc. Res.* 80, 37–43. doi: 10.1016/j.mvr.2010.03.008

Freund, J. B. (2007). Leukocyte margination in a model microvessel. *Phys. Fluids* 19:023301. doi: 10.1063/1.2472479

Fung, Y. (1973). Stochastic flow in capillary blood-vessels. *Microvasc. Res.* 5, 34–48. doi: 10.1016/S0026-2862(73)80005-6

Goldsmith, H. L., and Spain, S. (1984). Margination of leukocytes in blood flow through small tubes. *Microvasc. Res.* 27, 204–222. doi: 10.1016/0026-2862(84)90054-2

Haradin, A. R., Weed, R. I., and Reed, C. F. (1969). Changes in physical properties of stored erythrocytes relationship to survival *in vivo*. *Transfusion* 9, 229–237. doi: 10.1111/j.1537-2995.1969.tb04929.x

Hariprasad, D. S., and Secomb, T. W. (2014). Two-dimensional simulation of red blood cell motion near a wall under a lateral force. *Phys. Rev. E* 90:053014. doi: 10.1103/PhysRevE.90.053014

Hou, H. W., Bhagat, A. A., Chong, A. G., Mao, P., Tan, K. S., Han, J., et al. (2010). Deformability based cell margination–a simple microfluidic design for malaria-infected erythrocyte separation. *Lab Chip*. 10, 2605–2613. doi: 10.1039/c003873c

Jain, A., and Munn, L. L. (2009). Determinants of leukocyte margination in rectangular microchannels. *PLoS ONE* 4:e7104. doi: 10.1371/journal.pone.0007104

Kiani, M. F., Cokelet, G. R., and Sarelius, I. H. (1993). *Effect of* diameter variability along a microvessel segment on pressure drop. *Microvasc. Res.* 45, 219–232. doi: 10.1006/mvre.1993.1020

Kumar, A., and Graham, M. D. (2012a). Margination and segregation in confined flows of blood and other multicomponent suspensions. *Soft Matter*. 8, 10536–10548. doi: 10.1039/C2SM25943E

Kumar, A., and Graham, M. D. (2012b). Mechanism of margination in confined flows of blood and other multicomponent suspensions. *Phys. Rev. Lett.* 109:108102. doi: 10.1103/PhysRevLett.109.108102

Lee, T. R., Choi, M., Kopacz, A. M., Yun, S. H., Liu, W. K., and Decuzzib, P. (2013). On the near-wall accumulation of injectable particles in the microcirculation: smaller is not better. *Sci. Rep.* 3:2079. doi: 10.1038/srep02079

Li, X., Popel, A. S., and Karniadakis, G. E. (2012). Blood-plasma separation in Y-shaped bifurcating microfluidic channels: a dissipative particle dynamics simulation study. *Phys. Biol.* 9:026010. doi: 10.1088/1478-3975/9/2/026010

MacDonald, I. C., Ragan, D. M., Schmidt, E. E., and Groom, A. C. (1987). Kinetics of red blood cell passage through interendothelial slits into venous sinuses in rat spleen, analyzed by *in vivo* microscopy. *Microvasc. Res.* 33, 118–134. doi: 10.1016/0026-2862(87)90011-2

Maeda, N., Suzuki, Y., Tanaka, J., and Tateishi, N. (1996). Erythrocyte flow and elasticity of microvessels evaluated by marginal cell-free layer and flow resistance. *Am. J. Physiol.* 271, H2454–H2461.

Mebius, R. E., and Kraal, G. (2005). Structure and function of the spleen. *Nat. Rev. Immunol.* 5, 606–616. doi: 10.1038/nri1669

Mokken, F. C., Kedaria, M., Henny, C. P., Hardeman, M. R., and Gelb, A. W. (1992). The clinical importance of erythrocyte deformability, a hemorrheological parameter. *Ann. Hematol.* 64, 113–122. doi: 10.1007/BF01697397

Müller, K., Fedosov, D. A., and Gompper, G. (2016). Understanding particle margination in blood flow–A step toward optimized drug delivery systems. *Med. Eng. Phys.* 38, 2–10. doi: 10.1016/j.medengphy.2015.08.009

Munn, L. L., and Dupin, M. M. (2008). Blood cell interactions and segregation in flow. *Ann. Biomed. Eng.* 36, 534–544. doi: 10.1007/s10439-007-9429-0

Namgung, B., and Kim, S. (2014). Effect of uneven red cell influx on formation of cell-free layer in small venules. *Microvasc. Res.* 92, 19–24. doi: 10.1016/j.mvr.2014.01.007

Namgung, B., Ng, Y. C., Nam, J., Leo, H. L., and Kim, S. (2015). Alteration of blood flow in a venular network by infusion of dextran 500: evaluation with a laser speckle contrast imaging system. *PLoS ONE* 10:e0140038. doi: 10.1371/journal.pone.0140038

Namgung, B., Ong, P. K., Johnson, P. C., and Kim, S. (2011). Effect of cell-free layer variation on arteriolar wall shear stress. *Ann. Biomed. Eng.* 39, 359–366. doi: 10.1007/s10439-010-0130-3

Ng, Y. C., Namgung, B., and Kim, S. (2015). Two-dimensional transient model for prediction of arteriolar NO/O2 modulation by spatiotemporal variations in cell-free layer width. *Microvasc. Res.* 97, 88–97. doi: 10.1016/j.mvr.2014.08.010

Ong, P. K., and Kim, S. (2013). Effect of erythrocyte aggregation on spatiotemporal variations in cell-free layer formation near on arteriolar bifurcation. *Microcirculation* 20, 440–453. doi: 10.1111/micc.12045

Ong, P. K., Jain, S., and Kim, S. (2012). Spatio-temporal variations in cell-free layer formation near bifurcations of small arterioles. *Microvasc. Res.* 83, 118–125. doi: 10.1016/j.mvr.2011.11.003

Ong, P. K., Jain, S., Namgung, B., Woo, I. Y., and Kim, S. (2011). Cell-free layer formation in small arterioles at pathological levels of erythrocyte aggregation. *Microcirculation* 18, 541–551. doi: 10.1111/j.1549-8719.2011.00114.x

Pranay, P., Henríquez-Rivera, R. G., and Graham, M. D. (2012). Depletion layer formation in suspensions of elastic capsules in Newtonian and viscoelastic fluids. *Phys. Fluids* 24:061902. doi: 10.1063/1.4726058

Pries, A. R., Ley, K., Claassen, M., and Gaehtgens, P. (1989). Red cell distribution at microvascular bifurcations. *Microvasc. Res.* 38, 81–101. doi: 10.1016/0026-2862(89)90018-6

Pries, A. R., Secomb, T. W., and Gaehtgens, P. (1996). Biophysical aspects of blood flow in the microvasculature. *Cardiovasc. Res.* 32, 654–667. doi: 10.1016/S0008-6363(96)00065-X

Progatzky, F., Dallman, M. J., and Lo Celso, C. (2013). From seeing to believing: labelling strategies for *in vivo* cell-tracking experiments. *Interface Focus* 3:20130001. doi: 10.1098/rsfs.2013.0001

Schmid-Schonbein, G. W., Skalak, R., Usami, S., and Chien, S. (1980). Cell distribution in capillary networks. *Microvasc. Res.* 19, 18–44. doi: 10.1016/0026-2862(80)90082-5

Schmid-Schönbein, G. W., Usami, S., Skalak, R., and Chien, S. (1980). The interaction of leukocytes and erythrocytes in capillary and postcapillary vessels. *Microvasc. Res.* 19, 45–70. doi: 10.1016/0026-2862(80)90083-7

Sherwood, J. M., Holmes, D., Kaliviotis, E., and Balabani, S. (2014). Spatial distributions of red blood cells significantly alter local haemodynamics. *PLoS ONE* 9:e100473. doi: 10.1371/journal.pone.0100473

Shevkoplyas, S. S., Yoshida, T., Gifford, S. C., and Bitensky, M. W. (2006). Direct measurement of the impact of impaired erythrocyte deformability on microvascular network perfusion in a microfluidic device. *Lab Chip*. 6, 914–920. doi: 10.1039/b601554a

Simchon, S., Jan, K. M., and Chien, S. (1987). Influence of reduced red cell deformability on regional blood flow. *Am. J. Physiol. Heart Circul. Physiol.* 253, H898–H903.

Sosa, J. M., Nielsen, N. D., Vignes, S. M., Chen, T. G., and Shevkoplyas, S. S (2013). The relationship between red blood cell deformability metrics and perfusion of an artificial microvascular network. *Clin. Hemorheol. Microcirc.* 57, 275–289. doi: 10.3233/CH-131719

Stuart, J., and Nash, G. B. (1990). Red cell deformability and haematological disorders. *Blood Rev.* 4, 141–147. doi: 10.1016/0268-960X(90)90041-P

Takeishi, N., Imai, Y., Nakaaki, K., Yamaguchi, T., and Ishikawa, M, T. (2014). Leukocyte margination at arteriole shear rate. *Physiol. Rep*. 2:e12037. doi: 10.14814/phy2.12037

Tateishi, N., Suzuki, Y., Cicha, I., and Maeda, N. (2001). O(2) release from erythrocytes flowing in a narrow O(2)-permeable tube: effects of erythrocyte aggregation. *Am. J. Physiol. Heart Circ. Physiol.* 281, H448–H456. Available online at: http://ajpheart.physiology.org/content/281/1/H448

Vaughn, M. W., Kuo, L., and Liao, J. C. (1998). Effective diffusion distance of nitric oxide in the microcirculation. *Am. J. Physiol.* 274, H1705–H1714.

Weed, R. I. (1970). The importance of erythrocyte deformability. *Am. J. Med*. 49, 147–150. doi: 10.1016/S0002-9343(70)80069-9

Zhang, J., Johnson, P. C., and Popel, A. S. (2009). Effects of erythrocyte deformability and aggregation on the cell free layer and apparent viscosity of microscopic blood flows. *Microvasc. Res.* 77, 265–272. doi: 10.1016/j.mvr.2009.01.010

**Conflict of Interest Statement:** The authors declare that the research was conducted in the absence of any commercial or financial relationships that could be construed as a potential conflict of interest.

*Copyright © 2017 Namgung, Ng, Leo, Rifkind and Kim. This is an open-access article distributed under the terms of the Creative Commons Attribution License (CC BY). The use, distribution or reproduction in other forums is permitted, provided the original author(s) or licensor are credited and that the original publication in this journal is cited, in accordance with accepted academic practice. No use, distribution or reproduction is permitted which does not comply with these terms.*

frontiers in Physiology

METHODS
published: 02 November 2017
doi: 10.3389/fphys.2017.00855

# A Pulse Wave Velocity Based Method to Assess the Mean Arterial Blood Pressure Limits of Autoregulation in Peripheral Arteries

*Ananya Tripathi[1†], Yurie Obata[1†], Pavel Ruzankin[2,3], Narwan Askaryar[1], Dan E. Berkowitz[1], Jochen Steppan[1] and Viachaslau Barodka[1*]*

[1] Department of Anesthesiology and Critical Care Medicine, Johns Hopkins University School of Medicine, Baltimore, MD, United States, [2] Sobolev Institute of Mathematics, Novosibirsk, Russia, [3] Department of Mathematics and Mechanics, Novosibirsk State University, Novosibirsk, Russia

**Background:** Constant blood flow despite changes in blood pressure, a phenomenon called autoregulation, has been demonstrated for various organ systems. We hypothesized that by changing hydrostatic pressures in peripheral arteries, we can establish these limits of autoregulation in peripheral arteries based on local pulse wave velocity (PWV).

**Methods:** Electrocardiogram and plethysmograph waveforms were recorded at the left and right index fingers in 18 healthy volunteers. Each subject changed their left arm position, keeping the right arm stationary. Pulse arrival times (PAT) at both fingers were measured and used to calculate PWV. We calculated ΔPAT (ΔPWV), the differences between the left and right PATs (PWVs), and compared them to the respective calculated blood pressure at the left index fingertip to derive the limits of autoregulation.

**Results**: ΔPAT decreased and ΔPWV increased exponentially at low blood pressures in the fingertip up to a blood pressure of 70 mmHg, after which changes in ΔPAT and ΔPWV were minimal. The empirically chosen 20 mmHg window (75–95 mmHg) was confirmed to be within the autoregulatory limit (slope = 0.097, $p = 0.56$). ΔPAT and ΔPWV within a 20 mmHg moving window were not significantly different from the respective data points within the control 75–95 mmHg window when the pressure at the fingertip was between 56 and 110 mmHg for ΔPAT and between 57 and 112 mmHg for ΔPWV.

**Conclusions**: Changes in hydrostatic pressure due to changes in arm position significantly affect peripheral arterial stiffness as assessed by ΔPAT and ΔPWV, allowing us to estimate peripheral autoregulation limits based on PWV.

**Keywords: limits of autoregulation, pulse wave velocity, pulse arrival time, hydrostatic pressure, peripheral artery**

OPEN ACCESS

***Edited by:***
*Agustín Guerrero-Hernández, Center for Research and Advanced Studies of the National Polytechnic Institute (CINVESTAV), Mexico*

***Reviewed by:***
*Roland Pittman, Virginia Commonwealth University, United States*
*Erik Josef Behringer, Loma Linda University, United States*

***Correspondence:**
*Viachaslau Barodka*
*vbarodk1@jhmi.edu*

*[†] These authors have contributed equally to this work.*

***Specialty section:***
*This article was submitted to Vascular Physiology, a section of the journal Frontiers in Physiology*

***Received:*** *04 August 2017*
***Accepted:*** *13 October 2017*
***Published:*** *02 November 2017*

***Citation:***
*Tripathi A, Obata Y, Ruzankin P, Askaryar N, Berkowitz DE, Steppan J and Barodka V (2017) A Pulse Wave Velocity Based Method to Assess the Mean Arterial Blood Pressure Limits of Autoregulation in Peripheral Arteries. Front. Physiol. 8:855. doi: 10.3389/fphys.2017.00855*

## INTRODUCTION

Various organs are equipped with an autoregulation mechanism in order to maintain constant blood flow as local blood pressure changes (Peterson et al., 2011). These autoregulation mechanisms rely on robust arterial reactivity: as blood pressure decreases, muscular arterioles dilate, and as blood pressure increases, muscular arterioles constrict (Meng and Gelb, 2015). The lower limit of autoregulation represents the pressure at which arteries are maximally dilated and organ perfusion

becomes pressure dependent. If blood pressure falls below the lower limit of autoregulation, then blood flow decreases. The upper limit of autoregulation represents the pressure at which the arteries are maximally constricted (Meng and Gelb, 2015). If blood pressure goes above the upper limit of autoregulation, then blood flow increases. This physiological mechanism has been demonstrated for the brain, kidney, bone, intestinal tracts, and even the peripheral arteries in the lower extremities (Lassen, 1959; Johnson, 1967; Cupples and Braam, 2007; Vogt et al., 2013).

Limits of autoregulation have been assessed by measuring arterial blood flow velocity during changes of mean arterial blood pressure (Czosnyka et al., 2009). However, it remains challenging to measure the lower limit of autoregulation in humans, especially in vital organs, as this requires inducing potentially dangerously low mean arterial blood pressures, which of course is not ethically acceptable. However, peripheral arteries are routinely exposed to periods of low blood pressures. Raising the arm with respect to the level of the heart is a non-invasive way to decrease local blood pressure by introducing a hydrostatic pressure gradient. Decreasing local blood pressure then leads to a physiologic decrease in wall tension of the corresponding peripheral arteriole. The resultant changes in wall tension elicited by hydrostatic pressure gradients can be quantified precisely since blood density is known and arm length can be measured easily (Butlin et al., 2015).

Measuring arterial blood flow velocity to detect the limits of autoregulation can be done in real time and non-invasively using Doppler ultrasound, a technique which is operator-dependent and time consuming. It has been reported previously that pulse wave velocity (PWV) and the velocity of flow velocity wave transmission are nearly identical (Pai and Shah, 1999). Hence as blood pressure decreases, PWV should have a similar relationship to flow and exhibit a noticeable lower limit of autoregulation.

PWV is a measure of arterial stiffness and depends on the elasticity of the arterial wall (Bramwell and Hill, 1922). The elasticity of the arterial wall in turn depends on both the intrinsic arterial wall composition and wall tension. We have shown previously that PWV increases as MAP increases (Steppan et al., 2014). However, the relationship between PWV and MAP is not linear as PWV increases exponentially at high blood pressures, whereas the changes in PWV are relatively minor when blood pressure is in the normal range. This phenomenon is based on the composition and structure of the arterial wall and its load-bearing components (mainly elastin and collagen) (Steppan et al., 2014). Similar to active blood flow autoregulation, the elastin fibers dampen the changes in blood pressure, thereby maintaining a relatively constant PWV.

We hypothesize that by inducing hydrostatic pressure changes in peripheral arteries by changing arm position, we can evaluate the limits of autoregulation in those arteries via assessing changes in local PWV.

# METHODS AND MATERIALS

## Subjects

This study was approved by the Johns Hopkins Medicine Institutional Review Board (IRB00074229). 18 healthy volunteers were recruited to participate through email or word of mouth following Institutional Review Board approval. Informed oral consent was obtained from all subjects. Inclusion criteria were: healthy adults, aged 18–50 years, and both genders. Exclusion criteria were: subject refusal to participate, known cardiovascular disease of any kind, and pregnancy. After confirming that each subject could participate in the study, each subject self-reported her/his weight, height, age, handedness, and gender.

## Study Protocol

A standard 3 lead electrocardiogram (ECG; Bio Amp FE132, ADInstruments, Australia) was placed on the volunteer to allow for continuous measurement of electrical cardiac activity. We utilized clinically used standard lead locations as suggested by the American Heart Association (AHA) Scientific Statement on Practice Standards for Electrocardiographic Monitoring in Hospital Settings (Drew et al., 2004). A PowerLab analog to digital converter (PowerLab 4/26, ADInstruments, Australia) along with LabChart 8.0 software (LabChart8, Ad Instruments Ltd, Australia) were both used to convert and digitally record the data. Capillary plethysmograph sensors (MLT1020PPG IR Plethysmograph, ADInstruments, Australia) were then placed on the left and right index fingers. The ECG and plethysmograph simultaneously recorded data for each position for 60 s per position. The subject was seated on a chair with both arm rests at equal heights at the level of the heart. The first position (position A0) was used for a baseline measurement in which the subject had her/his arms resting on the armrests in a horizontal position, at the same height as the subject's heart. The next position (position A1) was identical to position A0 with the difference being that the volunteers left forearm was raised upward, such that subject's forearm was perpendicular to the subject's upper-arm, which was resting on the armrest. The subject was then instructed to switch to the up position (position A2), in which the subject raised her/his left arm vertically up above their head while keeping her/his right arm in the same position as it was resting before. The subject then went back to the horizontal position (position B0), with both arms were resting along the same plane as the heart as in position A0. The subject then took her/his left forearm vertically downward, in a half-down position, while keeping her/his upper-arm flat on the armrest (position B1), such as in position A1, just in the opposite direction. The subject did this while holding the right arm in the same position as before. The subject then switched to the final down position (position B2) in which he/she extended her/his left arm all the way down while keeping her/his right arm in the same position as it was resting before (opposite to position A2). After position B2 was completed, the sensors were removed and the subject's blood pressure was recorded using the oscillometric method over the brachial artery. Several lengths were then measured: wingspan (distance from left index finger to right index finger with both arms in 90° lateral extension), half wingspan on the left side (distance from sternal notch to left index finger with left arm in 90° lateral extension), the distance between the sternal notch and the axilla on the left arm, the distance between the axilla and the elbow on the left arm, the distance between the elbow and the

wrist on the left arm, and the distance between the wrist and the left index finger tip on the left arm.

## Data Extraction

Using the collected data, the pulse arrival time (PAT) to both the left and the right index fingertip was calculated by automated algorithm as the time delay between each R-wave peak on the ECG waveform and the first positive inflection on the plethysmograph tracing for both the left and the right side.

## Calculations

PWV for both the left (Equation 1) and right (Equation 2) sides were determined using the measured hemi-span (sternal notch to tip of the index finger) lengths divided by the PAT.

$$PWV_{Left} = \frac{d_{wingspan}}{2PAT_{Left}} \quad (1)$$

$$PWV_{Right} = \frac{d_{wingspan}}{2PAT_{Right}} \quad (2)$$

We also calculated the difference in PAT values (ΔPAT) between the left and right side and the difference in PWV (ΔPWV) between the left and right side at each position keeping right arm at the level of the heart (Equations 3 and 4).

$$\Delta PAT = PAT_{Left} - PAT_{Right} \quad (3)$$

$$\Delta PWV = PWV_{Left} - PWV_{Right} \quad (4)$$

The hydrostatic blood pressure changes were quantified by multiplying the density of blood ($\rho$ = 1,060 kg/m3), gravity related acceleration ($g = 9.81$ m/s$^2$), and the height of the fluid column *(d)* (Equation 5). To convert the hydrostatic pressure from Pascals to mmHg, the obtained value was multiplied by a conversion factor of 0.0075 (Butlin et al., 2015).

$$Hydrostatic\ pressure = 0.0075\rho gd \quad (5)$$

For our analysis, we quantified the maximum pressure change at the tip of the finger. Hydrostatic pressures calculated for the up positions (A1 and A2) were defined as negative; those calculated for the down positions (B1 and B2) were positive. To calculate the total blood pressure (accounting for both systemic and hydrostatic pressure), the mean arterial pressure (MAP), defined by Equation (6), was added to the hydrostatic pressure (Equation 7).

$$MAP = DBP + ([SBP - DBP]/3) \quad (6)$$

$$Calculated\ pressure = Hydrostatic\ pressure + MAP \quad (7)$$

## Statistical Analysis

Based on the results of the previous study, we estimated that a sample of 3 subjects would provide adequate power [80% power for a mean (SD) difference of 42.7 ms (11.0 ms)] for the change in PAT between horizontal and up arm position at an alpha level of 0.05 in a two-sided paired *t*-test (Foo et al., 2005). Based on the results of our previous study, we estimated that a sample of 18 subjects would provide adequate power [80% power for a mean (SD) difference of 8.78 ms (12.40 ms)] for the change in PAT between horizontal and down arm position at an alpha level of 0.05 in a two-sided paired *t*-test (Obata et al., 2017).

Paired *t*-tests were used to compare the PATs for each arm between the initial horizontal position (position A0) and the horizontal position after arm raise (position B0) and to compare the PAT and PWV values measured at different left arm positions to the respective values of the right arm, which was constantly kept at the level of the heart. A repeated measure one-way analysis of variance (ANOVA) test was used with the Dunnett's multiple comparisons test to check for differences between PAT, ΔPAT, PWV and ΔPWV at each position. We performed a non-linear regression model to assess the relationship between hydrostatic blood pressure change at the tip of the finger and the resultant change in PAT between left and right arm (ΔPAT), the relationship between the calculated blood pressure at the tip of the finger and the ΔPAT, and the relationship between the calculated blood pressure at the tip of the finger and ΔPWV. These analyses were performed with GraphPad Prism version 6.0 (GraphPad Software, San Diego, California, USA). All tests were two-sided. A *p*-value less than 0.05 was considered to be statistically significant.

To detect the point of inflection of ΔPAT or ΔPWV vs. calculated pressure at the left fingertip relationship, we first created a smoothed curve by applying a LOESS (locally weighted scatter-plot smoother)-smoothed filter to all observed data points. The inflection point of the curve is the point which is maximally distant from the line connecting the curve's ends (Lepeschkin and Surawicz, 1953). The method is robust with respect to the observations' perturbations and is invariant with respect to scaling of the axes. We used the standard LOESS function from the R package (R foundation for Statistical Computing, Vienna, Austria) with values of the span parameter 0.2, 0.4, and 0.75.

To detect the limits of autoregulation we compared the distribution of ΔPAT and ΔPWV observations in ±10 mmHg moving windows to the respective distribution within a known autoregulation range and to the right of the inflection point by the two-sided Mann-Whitney test. To confirm that the empirically chosen control range of calculated blood pressure is in fact within the limits of autoregulation, we calculated the linear regression slope and checked to see if the slope was statistically different from 0. Slopes not different from 0 indicate that the data points within control range are within the autoregulation limit as they show consistent PWV values despite changes in blood pressure. The relationship between the *p*-values of a Mann-Whitney test and blood pressure at the fingertip was plotted. The pressure values at which the plots cross the *p*-value of 0.05 (5% level) were considered to be the lower and higher limits of autoregulation.

# RESULTS

Demographic characteristics and blood pressure values are summarized in **Table 1**. Each position's average PAT of the left and right arm, ΔPAT, and PWV is summarized in **Table 2**. The

mean age of the volunteers was approximately 32 years and ranged from 18 to 42 years. At rest, the average systolic blood pressure (SBP) was 115.3 ± 24.5 mmHg and the average diastolic blood pressure (DBP) was 68.6 ± 14.5 mmHg.

## PAT Analysis

The PAT at positions A0 and B0 were compared using a *t*-test to determine if they were significantly different between the two horizontal readings. The average left PAT values at position A0 were not significantly different from the average left PAT values at position B0 ($p = 0.508$); similarly, the average right PAT at position A0 was not significantly different from the average right PATs at position B0 ($p = 0.064$).

The left PATs for each position were compared to their respective horizontal right PATs (Supplementary Figure 1). Left-sided PATs were significantly higher than right-sided PATs at position A1 ($p = 0.0002$), position A2 ($p < 0.0001$), and position B0 ($p = 0.0003$).

Left PATs at each position were compared to the left PAT at position A0 (Supplementary Figure 2A). Relative to the left PAT at position A0, the left PAT values were significantly higher at position A1 ($p = 0.005$) and position A2 ($p = 0.0001$) and significantly lower at position B2 ($p = 0.003$). The right PAT values were compared to the right PATs at position A0 (Supplementary Figure 2B). The right PATs were significantly higher at position A2 than those at position A0 ($p = 0.023$), despite only minimal changes. ΔPATs at each position were compared to the ΔPAT values at position A0 (Supplementary Figure 2C). Relative to the ΔPAT at position A0, the ΔPAT values were significantly higher at position A1 ($p = 0.005$) and position A2 ($p = 0.0001$).

**TABLE 1 |** Cohort demographics summary (Mean ± SD).

| | **Mean ± SD ($n = 18$)** |
|---|---|
| Age [years] | 32.2 ± 6.9 |
| Weight [kg] | 66.7 ± 14.0 |
| Height [cm] | 169.9 ± 6.9 |
| SBP [mmHg] | 115.3 ± 24.5 |
| DBP [mmHg] | 68.6 ± 14.5 |
| MAP [mmHg] | 84.1 ± 17.2 |
| Wingspan [cm] | 170.7 ± 8.4 |
| Half wingspan [cm] | 85.3 ± 4.2 |
| $d_{sternalnotch-fingertip}$ [left; cm] | 85.3 ± 4.2 |
| $d_{sternalnotch-axilla}$ [left; cm] | 20.1 ± 1.7 |
| $d_{axilla-elbow}$ [left; cm] | 22.8 ± 2.0 |
| $d_{elbow-wrist}$ [left; cm] | 24.3 ± 2.0 |
| $d_{wrist-fingertip}$ [left; cm] | 18.1 ± 1.8 |

*SD, Standard deviation; SBP, Systolic blood pressure; DBP, Diastolic blood pressure; MAP, Mean arterial pressure.*

## PWV Analysis

Left-sided PWV values for each position were compared to their respective horizontal right-sided PWV values (Supplementary Figure 3). Left-sided PWVs were significantly lower than the right-sided values at position A1 ($p < 0.0001$), position A2 ($p < 0.0001$), and position B0 ($p = 0.0003$).

PWV values on the left were compared to the left PWV values at position A0 (Supplementary Figure 4A). The left side PWV values at position A0 were significantly higher than the left side PWV values at position A1 ($p = 0.002$) and position A2 ($p = 0.0001$). The left side PWV values at position A0 were significantly lower than the left side PWV values at position B2 ($p = 0.002$). Right side PWV values were compared to right side PWV values at position A0 (Supplementary Figure 4B). The right values at position A0 were significantly higher than those at position A2 ($p = 0.011$). ΔPWV values were compared to ΔPWVs at position A0 (Supplementary Figure 4C). Relative to those at position A0, ΔPWV was significantly lower at position A1 ($p = 0.004$) and position A2 ($p = 0.0001$).

## Pressure Analysis

The hydrostatic pressure was calculated using (Equation 5) (**Table 3**). The convention implemented for hydrostatic pressure was such that if the left arm was either in position A1 or A2—that is, half-up or fully up—then the hydrostatic pressures were considered to be negative; conversely, if the left arm was in position B1 or B2, in the half-down or complete down position, then the hydrostatic pressures were considered to be positive. The pressure at the fingertip for each position was calculated

**TABLE 2 |** Measured and calculated data summary (Mean ± SD).

| | **A0** | **A1** | **A2** | **B0** | **B1** | **B2** |
|---|---|---|---|---|---|---|
| $PAT_{Left}$ [ms] | 218.6 ± 24.2 | 229.5 ± 26.4 | 264.8 ± 37.6 | 220.0 ± 21.1 | 215.5 ± 22.7 | 209.4 ± 22.6 |
| $PAT_{Right}$ [ms] | 214.8 ± 24.1 | 215.6 ± 24.8 | 211.5 ± 24.3 | 212.7 ± 23.5 | 213.2 ± 24.4 | 212.2 ± 24.1 |
| ΔPAT [ms] | 3.8 ± 9.1 | 14.1 ± 12.4 | 53.8 ± 22.8 | 7.2 ± 6.8 | 2.4 ± 7.2 | −1.9 ± 9.5 |
| $PWV_{Left}$ [m/s] | 3.9 ± 0.4 | 3.8 ± 0.5 | 3.3 ± 0.5 | 3.9 ± 0.3 | 4.0 ± 0.4 | 4.1 ± 0.4 |
| $PWV_{Right}$ [m/s] | 4.0 ± 0.4 | 4.0 ± 0.4 | 4.1 ± 0.4 | 4.0 ± 0.4 | 4.0 ± 0.4 | 4.1 ± 0.4 |
| ΔPWV [m/s] | −0.1 ± 0.2 | −0.2 ± 0.2 | −0.8 ± 0.3 | −0.1 ± 0.1 | 0.0 ± 0.1 | 0.0 ± 0.1 |

*SD, Standard deviation; $PAT_{Left}$, pulse arrival time at the left index finger; $PAT_{Right}$, pulse arrival time at the right index finger; ΔPAT, difference between the pulse arrival time at the left index finger and right index finger; $PWV_{Left}$, pulse wave velocity at the left index finger; $PWV_{Right}$, pulse wave velocity at the right index finger; position A0, baseline horizontal control position; position A1, left forearm extended vertically toward ceiling (half-up); position A2. left forearm and upper-arm extended vertically toward ceiling (up); position B0, horizontal position in the middle of the trial; position B1, left forearm extended vertically toward floor (half-down); position B2, left forearm and upper-arm extended vertically toward floor (down); ms, milliseconds; m/s, meters per second.*

**TABLE 3 |** Pressure data summary (Mean ± SD).

| Position | Hydrostatic pressure [mmHg] | Actual pressure [mmHg] |
|---|---|---|
| A0 | 0.0 ± 0.0 | 84.1 ± 17.2 |
| A1 | −33.1 ± 2.0 | 51.0 ± 17.2 |
| A2 | −50.8 ± 2.9 | 33.3 ± 16.9 |
| B0 | 0.0 ± 0.0 | 84.1 ± 17.2 |
| B1 | 33.1 ± 2.9 | 117.2 ± 17.5 |
| B2 | 50.8 ± 2.9 | 134.9 ± 18.0 |

*SD, Standard deviation; Position A0, baseline horizontal control position; position A1, left forearm extended vertically toward ceiling (half-up); position A2, left forearm and upper-arm extended vertically toward ceiling (up); position B0, horizontal position in the middle of the trial; position B1, left forearm extended vertically toward floor (half-down); position B2, left forearm and upper-arm extended vertically toward floor (down).*

using Equation (6) (**Table 3**) and the resulting values were plotted against ΔPAT (**Figure 1A**). The average pressure values at the fingertips were then calculated and plotted against the average ΔPAT values (**Figure 1B**). A non-linear one-phase regression model was generated for the average pressure at the fingertips vs. ΔPAT, yielding (Equation 8). The regression model had a coefficient of determination of 0.98, indicating a strong fit for the data.

$$\Delta PAT = 6.78 \times 10^2 \times e^{(-0.08 \times \textit{ pressure at the fingertips})} + 2.14 \quad (8)$$

The ΔPWV values were also compared to the calculated pressure at the fingertips (**Figure 1C**); the average ΔPWVs were plotted against the average pressure at the fingertips at their respective positions (**Figure 1D**). A non-linear one-phase regression model was generated, yielding Equation (9). This regression model had a coefficient of determination of 0.96.

$$\Delta PWV = -7.58 \times e^{(-0.07 \times \textit{ pressure at the fingertips})} - 0.03 \quad (9)$$

## Estimation of the Inflection Point

The inflection point for ΔPAT over pressure relationship was detected at 70.67, 70.26, and 71.36 mmHg for the LOESS function span parameter of 0.2, 0.4, and 0.75 respectively (**Figure 2A**). The inflection point for ΔPWV over the pressure relationship was detected at 70.55, 69.02, and 70.61 mmHg for the LOESS function span parameter of 0.2, 0.4, and 0.75 respectively (**Figure 2B**). This means that the window with the lowest regression slope within the autoregulation limit will be located at pressures above 70–71 mmHg.

## Estimation of the Control Blood Pressure Window within the Limits of Autoregulation

We chose a ±10 mmHg window to the right of the inflection point, empirically choosing 75–95 mmHg. The estimated regression slope for all data points within the 75–95 mmHg window was 0.097 with $p = 0.69$, indicating that it is not statistically different from the regression slope 0 and the 75–95 mmHg window is in fact within limits of autoregulation. We chose a second window of 80–100 mmHg, with the estimated regression slope for all data points within this window being 0.25 with $p = 0.36$, indicating that it is not statistically different from a regression slope 0 and the 80–100 mmHg window is within the limits of autoregulation.

## Estimation of the Limits of Regional Autoregulation

The ΔPAT data within a ±10 mmHg moving window compared to the ΔPAT data within a control window ranging from 75 to 95 mmHg was significant when blood pressures were below 56 mmHg or above 110 mmHg (**Figure 3A**). Similarly the ΔPWV data within ±10 mmHg moving window compared to the ΔPWV data within a control window ranging from 75 to 95 mmHg was significant when blood pressure was below 57 mmHg and above 112 mmHg. (**Figure 3B**). Changing the control window from 75–95 mmHg to 80–100 mmHg did not change the results. Hence, the lower limit of autoregulation was detected at 56 mmHg with the *p*-value graph derived from ΔPAT over the calculated blood pressure at the tip of finger relationship (**Figure 3A**) and at 57 mmHg for the *p*-value graph derived from ΔPWV over blood pressure at the tip of finger relationship (**Figure 3B**). The upper limit of autoregulation was detected at 110 mmHg on the *p*-value graph derived from ΔPAT over the pressure relationship (**Figure 3A**) and at 112 mmHg on the *p*-value graph derived from ΔPWV over the pressure relationship (**Figure 3B**).

# DISCUSSION

In our study, we confirmed that changes in hydrostatic pressure due to changes in arm position significantly affect peripheral PWV and PAT in healthy subjects. In addition, our data suggests the existence of autoregulation in the peripheral arteries of the arm. The average calculated MAP in the study subjects was 84 mmHg. The average length of the arm was 85 cm, which corresponds to an average 66 mmHg decrease in pressure due to hydrostatic effects when the arm is up. Hence, the effective distending pressure at the tip of the fingers is 18 mmHg (84 mmHg – 66 mmHg) in the arm up position and 150 mmHg (84 mmHg + 66 mmHg) in arm down position. As blood pressure at the tip of finger drops below 56 mmHg, we found sudden changes in both ΔPAT or ΔPWV compared to ΔPAT or ΔPWV at a known autoregulation range of 75–95 mmHg, which is consistent with the theory that the vasculature operates on distending pressures below the lower limit of autoregulation. We chose a control distending blood pressure window on the horizontal part of the ΔPAT/ΔPWV vs. blood pressure at left fingertip graph, to the right of the inflection point, which was 70 mmHg. A range of 75–95 mmHg was chosen based on published data on the lower limits of autoregulation in the brain and the kidneys (Carlström et al., 2015; Scheeren and Saugel, 2017). We performed the same analysis using different ranges (e.g., 80–100 mmHg) and observed the same results for the limits of autoregulation. Furthermore, if a particular range of distending blood pressures is within the limits of autoregulation, the specific range should have a slope close to 0. The slope of the regression

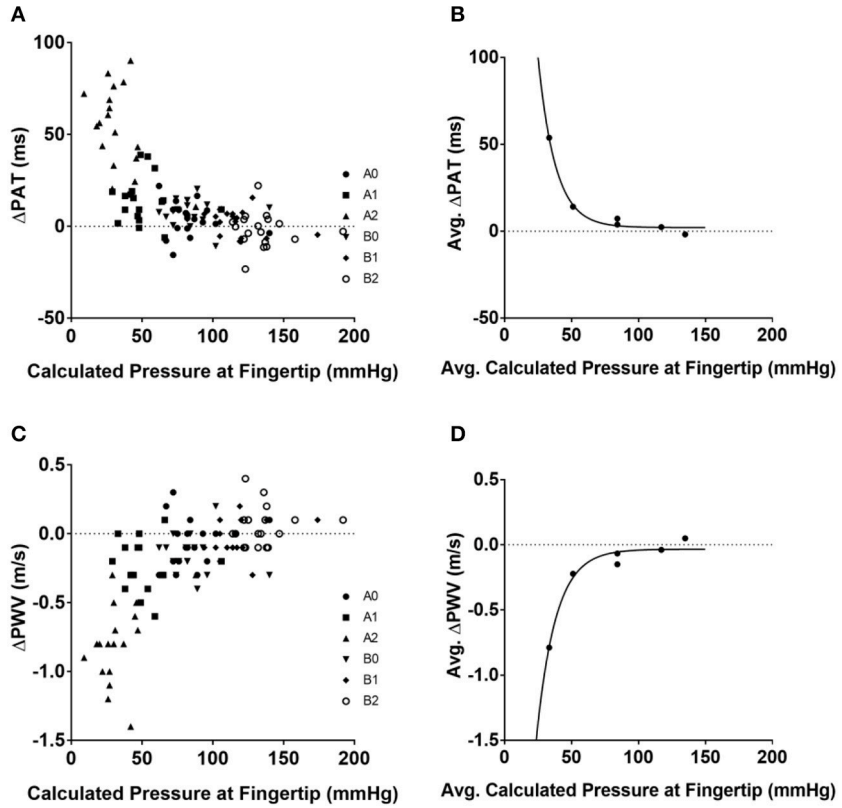


**FIGURE 1 |** Relationships between blood pressure at the tip of finger and ΔPAT and ΔPWV. Calculated pressure values compared to ΔPAT and ΔPWV values. **(A)** Calculated blood pressure at the tip of finger for each individual subject at each position and ΔPAT. **(B)** Average blood pressure at the tip of finger and average ΔPAT values with the generated non-linear regression model. **(C)** Calculated blood pressure at the tip of finger for each individual subject at each position and ΔPWV values. **(D)** Average blood pressure at the tip of finger and average ΔPWV values with the generated non-linear regression model. ΔPAT, difference between the pulse arrival time at the left index finger and right index finger; ΔPWV, difference between the pulse wave velocity at the left index finger and right index finger; ms, milliseconds; m/s, meters per second.

analysis for the 75–95 mmHg range was 0.097 ($p = 0.69$) and for the 80–100 mmHg range 0.25 ($p = 0.36$). As blood pressure at the tip of finger increased above 112 mmHg, we saw changes in both ΔPAT and ΔPWV compared to those at a known autoregulation range of 75-95 mmHg, which is consistent with the theory that the vasculature operates on distending pressures above the upper limit of autoregulation. Using our noninvasive approach, we were able to establish PWV based limits of peripheral artery autoregulation (56–112 mmHg) in human peripheral arteries of the upper extremity. Intriguingly they are very close to the known blood flow based limits of autoregulation described for the brain and kidneys. Thus, the peripheral arteries of the arm could potentially be used as a window into non-invasive assessment of responses in the arterial system to changes in blood pressure and establishing at least the lower limit of autoregulation in individual subjects.

From our data, it is evident that a low distending pressure results in a profound decrease in peripheral arteries PWV in healthy individuals. Interestingly, a notable change in the slope of both ΔPAT and ΔPWV over the distending blood pressure occurs at 70 mmHg. We did not observe such a notable change in the slope at high blood pressures, likely as lowering the arm cannot result in pressures high enough to overcome the upper limit of autoregulation in all subjects.

In an elegant study using ultrasonographic and Doppler techniques, Eiken and Kölegård, showed that indeed changes in intravascular pressure in the range of 75–275 mmHg lead to significant changes in arterial stiffness of peripheral arteries as evident by changes in flow and diameter (Eiken and Kölegård, 2004). Notably, they found that there were greater changes in the flow of the arm arteries compared to the arteries of the leg for the same changes in pressures above 160 mmHg. This indicates that the peripheral arterioles especially in the arm are sensitive to changes in distending pressure and present autoregulation behavior. The blood flow at the lowest pressure in their experiment (70 mmHg) did not change from the flow at 160 mmHg suggesting that they were not able to detect the lower limit of autoregulation in the experiments.

A study by Foo et al. examined pulse transit time (PTT) at different limb positions (Foo et al., 2005). They found that there were significant PTT changes in the limb that underwent positional change, relative to a baseline control value. When

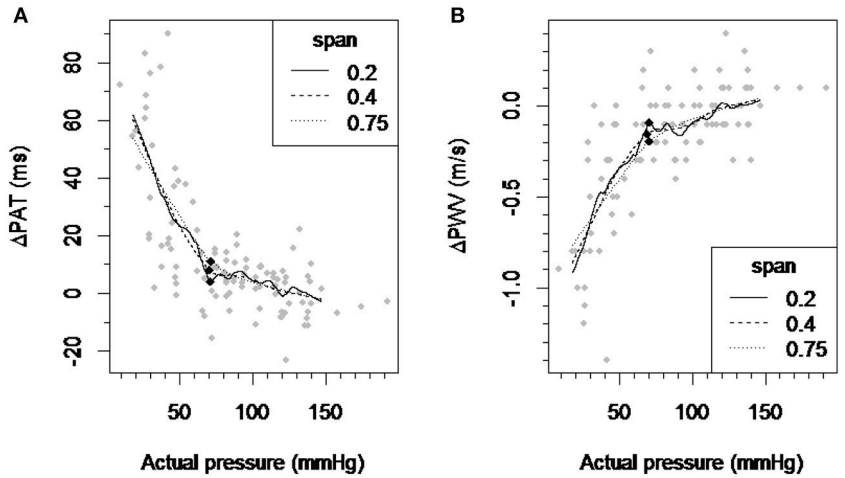


**FIGURE 2 |** Detection of the inflection point of the ΔPAT and ΔPWV over pressure relationship. **(A)** A scatter plot of ΔPAT vs. pressure and smoothed curves by applying the LOESS-smoothed filter to all observations with the span parameter values of 0.2, 0.4, and 0.75. **(B)** A scatter plot of ΔPWV vs. pressure and smoothed curves by applying the LOESS-smoothed filter to all observations with the span parameter values of 0.2, 0.4, and 0.75. Each black square indicates the inflection point which maximally distant from the line connecting the curve's ends. ΔPAT, difference between the pulse arrival time at the left index finger and right index finger; ΔPWV, difference between the pulse wave velocity at the left index finger and right index finger; ms, milliseconds; m/s, meters per second.

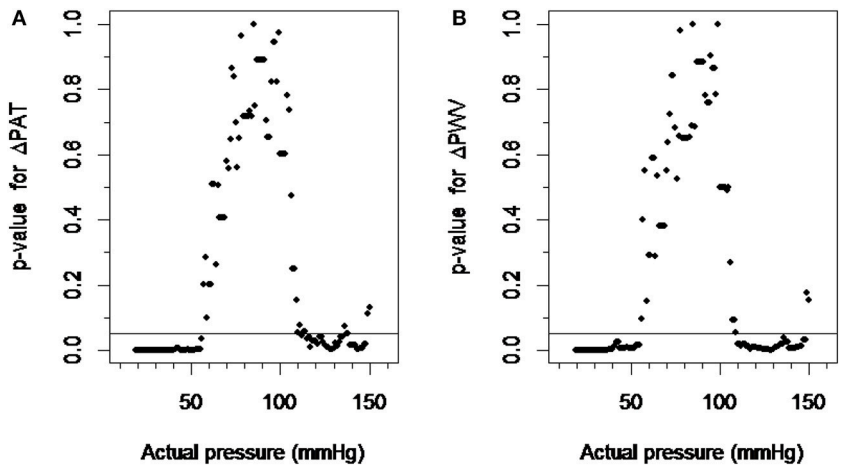


**FIGURE 3 |** Detection of the limits of autoregulation. **(A)** The scatter plot between *p*-values derived from ΔPAT over pressure relationship and actual pressure. **(B)** The scatter plot between *p*-values derived from ΔPWV over pressure relationship and actual pressure. The pressure values at which the plots cross the *p*-value of 0.05 were considered the lower and higher limits of autoregulation. ΔPAT, difference between the pulse arrival time at the left index finger and right index finger; ΔPWV, difference between the pulse wave velocity at the left index finger and right index finger.

the limb was vertically raised, PTT increased; this is consistent with our data. The authors attributed this increase in PTT to changes in hydrostatic pressure and regulation mechanisms within the limbs. They concluded that PTT is indicative of local circulatory responses, suggesting the existence of an autoregulatory mechanism within the arteries of the arm.

In our previous study, we showed that PAT changes significantly depend on the site of measurement (ear lobe, index finger, or big toe) (Obata et al., 2017). In that study, the volunteers changed their positions from supine to sitting to standing. Changing position from supine to standing introduces hydrostatic pressure gradients in the thoracic, abdominal, and peripheral arteries of the lower extremities. However, the observed changes in PAT and PWV did not allow to distinguish hydrostatic effects between the central and peripheral circulation. Moreover, changing the entire body position from supine to standing introduces significant global hemodynamic effects (such as heart rate and blood pressure changes) which affected arterial wall tension and PWV independent of hydrostatic blood pressure changes. This did not allow us to distinguish hydrostatic blood pressure changes from hemodynamically induced changes in the arterial wall.

The current study design enabled us to assess the effect of hydrostatic blood pressure changes specifically on peripheral arteries and to minimize the global changes in the hemodynamic state. Changing the position of only one arm introduced minimal hemodynamic effects compared to postural changes of the whole body. The right arm was consistently kept at the level of the heart to serve as an intrinsic control, canceling out any potential systemic hemodynamic effects. Thus, we quantified the relationship between distending pressure (MAP plus hydrostatic pressure changes due to changes in arm position) and ΔPAT with ΔPWV. Importantly, it allowed us to calculate the limits of autoregulation in a peripheral artery in a simple and non-invasive way. It would be intriguing to see if there is a correlation between limits of autoregulation in a peripheral artery and the brain.

### Limitations

Our study has several limitations. For MAP, we used only one single baseline blood pressure reading at position A0. There is a possibility that MAP would change with changes in the arm position. However, we believed that those changes will be minimal. Inflating the blood pressure cuff itself will induce local changes by squeezing the arm arteries, which we wanted to avoid. We used the peak of the R-wave on the ECG as the reference point for PAT and substituted pulse transit time with PAT for PWV calculations. The pre-ejection phase in healthy subjects is about 35 ms (Biering-Sørensen et al., 2016), whereas the PAT is in range of 150–300 ms, thus PAT overestimates true pulse transit time by 15%. However, we calculated ΔPAT between the left and right arm, which would cancel out the pre-ejection time and the time pulse wave spend in central aorta. To determine the limits of autoregulation, we used each position data point for every subject; this means, however, that there were a limited number of data points for each subject. Data points at angle increments for each subject would be more adequate in order to generate a smoother and more comprehensive model, which would yield more precise limits of autoregulation in individual subjects. Finally, the limits of autoregulation in our experiments are based on PWV instead of flow velocity. Without simultaneous measurements of Doppler flow velocity we cannot guarantee that PWV based limits of autoregulation are same as flow velocity based.

## CONCLUSIONS

In conclusion, our study shows that changes in hydrostatic pressure due to positional changes of the arm significantly affects peripheral arterial stiffness. This allows us to estimate the limits of regional autoregulation based on PWV.

## AUTHOR CONTRIBUTIONS

VB conceived the study and developed the protocol; AT, YO, NA, and VB collected data; AT, YO, PR, NA, and VB analyzed and interpreted the data; AT, YO, PR, DB, JS, and VB drafted and revised the manuscript. All authors read and approved the final version of the manuscript.

## FUNDING

This work was supported by StAAR (Stimulating and Advancing ACCM Research) grant to VB from the Department of Anesthesiology and Critical Care Medicine, The Johns Hopkins University.

## SUPPLEMENTARY MATERIAL

The Supplementary Material for this article can be found online at: https://www.frontiersin.org/articles/10.3389/fphys.2017.00855/full#supplementary-material

## REFERENCES

Biering-Sørensen, T., Mogelvang, R., de Knegt, M. C., Olsen, F. J., Galatius, S., and Jensen, J. S. (2016). Cardiac time intervals by tissue doppler imaging M-mode: normal values and association with established echocardiographic and invasive measures of systolic and diastolic function. *PLoS ONE* 11:e0153636. doi: 10.1371/journal.pone.0153636

Bramwell, J. C., and Hill, A. V. (1922). The velocity of the pulse wave in man. *Proc. R. Soc. Lond. B* 93, 298–306. doi: 10.1098/rspb.1922.0022

Butlin, M., Hathway, P. J., Kouchaki, Z., Peebles, K., and Avolio, A. P. (2015). A simplified method for quantifying the subject-specific relationship between blood pressure and carotid-femoral pulse wave velocity. *Conf. Proc. IEEE Eng. Med. Biol. Soc.* 2015, 5708–5711. doi: 10.1109/EMBC.2015.7319688

Carlström, M., Wilcox, C. S., and Arendshorst, W. J. (2015). Renal autoregulation in health and disease. *Physiol. Rev.* 95, 405–511. doi: 10.1152/physrev.00042.2012

Cupples, W. A., and Braam, B. (2007). Assessment of renal autoregulation. *Am. J. Physiol. Renal. Physiol.* 292, F1105–F1123. doi: 10.1152/ajprenal.00194.2006

Czosnyka, M., Brady, K., Reinhard, M., Smielewski, P., and Steiner, L. A. (2009). Monitoring of cerebrovascular autoregulation: facts, myths, and missing links. *Neurocrit. Care* 10, 373–386. doi: 10.1007/s12028-008-9175-7

Drew, B. J., Califf, R. M., Funk, M., Kaufman, E. S., Krucoff, M. W., Laks, M. M., et al. (2004). Practice standards for electrocardiographic monitoring in hospital settings: an American heart association scientific statement from the councils on cardiovascular nursing, clinical cardiology, and cardiovascular disease in the young: endorsed by the international society of computerized electrocardiology and the american association of critical-care nurses. *Circulation* 110, 2721–2746. doi: 10.1161/01.CIR.0000145144.56673.59

Eiken, O., and Kölegård, R. (2004). Comparison of vascular distensibility in the upper and lower extremity. *Acta Physiol. Scand.* 181, 281–287. doi: 10.1111/j.1365-201X.2004.01291.x

Foo, J. Y. A., Wilson, S. J., Williams, G. R., Harris, M.-A., and Cooper, D. M. (2005). Pulse transit time changes observed with different limb positions. *Physiol. Meas.* 26, 1093–1102. doi: 10.1088/0967-3334/26/6/018

Johnson, P. C. (1967). Autoregulation of Blood Flow in the Intestine. *Gastroenterology* 52, 435–441.

Lassen, N. A. (1959). Cerebral blood flow and oxygen consumption in man. *Physiol. Rev.* 39, 183–238.

Lepeschkin, E., and Surawicz, B. (1953). The duration of the Q-U interval and its components in electrocardiograms of normal persons. *Am. Heart J.* 46, 9–20. doi: 10.1016/0002-8703(53)90237-3

Meng, L., and Gelb, A. W. (2015). Regulation of cerebral autoregulation by carbon dioxide. *Anesthesiology* 122, 196–205. doi: 10.1097/ALN.0000000000000506

Obata, Y., Ong, Q. J., Magruder, J. T., Grichkevitch, H., Berkowitz, D. E., Nyhan, D., et al. (2017). Noninvasive assessment of the effect of position and exercise on pulse arrival to peripheral vascular beds in healthy volunteers. *Front. Physiol.* 8:47. doi: 10.3389/fphys.2017.00047

Pai, R. G., and Shah, P. M. (1999). Relationship between the pulse wave and the flow velocity wave and their propagation velocities in the arterial system: implications for the assessment of regional physical properties of the arterial beds. *Int. J. Angiol.* 8, 127–130. doi: 10.1007/BF01616831

Peterson, E. C., Wang, Z., and Britz, G. (2011). Regulation of cerebral blood flow. *Int. J. Vascular Med.* 2011, 1–8. doi: 10.1155/2011/823525

Scheeren, T. W. L., and Saugel, B. (2017). Journal of clinical monitoring and computing 2016 end of year summary: monitoring cerebral oxygenation and autoregulation. *J. Clin. Monit. Comput.* 31, 241–246. doi: 10.1007/s10877-017-9980-7

Steppan, J., Sikka, G., Jandu, S., Barodka, V., Halushka, M. K., Flavahan, N. A., et al. (2014). Exercise, vascular stiffness, and tissue transglutaminase. *J. Am. Heart Assoc.* 3:e000599. doi: 10.1161/JAHA.113.000599

Vogt, S., Venjakob, A. J., Stöckl, K., Tischer, T., Jost, P. J., Imhoff, A. B., et al. (2013). Evidence of an autoregulatory mechanism of regional bone blood flow at hypotension. *Arch. Orthop. Trauma Surg.* 133, 1233–1241. doi: 10.1007/s00402-013-1801-y

**Conflict of Interest Statement:** The authors declare that the research was conducted in the absence of any commercial or financial relationships that could be construed as a potential conflict of interest.

*Copyright © 2017 Tripathi, Obata, Ruzankin, Askaryar, Berkowitz, Steppan and Barodka. This is an open-access article distributed under the terms of the Creative Commons Attribution License (CC BY). The use, distribution or reproduction in other forums is permitted, provided the original author(s) or licensor are credited and that the original publication in this journal is cited, in accordance with accepted academic practice. No use, distribution or reproduction is permitted which does not comply with these terms.*

# Advantages of publishing in Frontiers

**OPEN ACCESS**
Articles are free to read for greatest visibility and readership

**FAST PUBLICATION**
Around 90 days from submission to decision

**HIGH QUALITY PEER-REVIEW**
Rigorous, collaborative, and constructive peer-review

**TRANSPARENT PEER-REVIEW**
Editors and reviewers acknowledged by name on published articles

**Frontiers**
Avenue du Tribunal-Fédéral 34
1005 Lausanne | Switzerland

**Visit us:** www.frontiersin.org
**Contact us:** info@frontiersin.org | +41 21 510 17 00

**REPRODUCIBILITY OF RESEARCH**
Support open data and methods to enhance research reproducibility

**DIGITAL PUBLISHING**
Articles designed for optimal readership across devices

**FOLLOW US**
@frontiersin

**IMPACT METRICS**
Advanced article metrics track visibility across digital media

**EXTENSIVE PROMOTION**
Marketing and promotion of impactful research

**LOOP RESEARCH NETWORK**
Our network increases your article's readership